

**Combining NMR spectroscopy and organic synthesis:
From small building blocks to large biomolecules**

Inauguraldissertation

zur

Erlangung der Würde eines Doktors der Philosophie

vorgelegt der

Philosophisch-Naturwissenschaftlichen Fakultät

der Universität Basel



von

Heiko Gsellinger

aus Stockmatt, Deutschland

Basel, 2014

Originaldokument gespeichert auf dem Dokumentenserver der Universität Basel
edoc.unibas.ch

Dieses Werk ist unter dem Vertrag „Creative Commons Namensnennung-Keine kommerzielle Nutzung-Keine Bearbeitung 3.0 Schweiz“ (CC BY-NC-ND 3.0 CH) lizenziert. Die vollständige Lizenz kann unter **creativecommons.org/licenses/by-nc-nd/3.0/ch/**



Namensnennung-Keine kommerzielle Nutzung-Keine Bearbeitung 3.0 Schweiz
(CC BY-NC-ND 3.0 CH)

Sie dürfen: Teilen — den Inhalt kopieren, verbreiten und zugänglich machen

Unter den folgenden Bedingungen:



Namensnennung — Sie müssen den Namen des Autors/Rechteinhabers in der von ihm festgelegten Weise nennen.



Keine kommerzielle Nutzung — Sie dürfen diesen Inhalt nicht für kommerzielle Zwecke nutzen.



Keine Bearbeitung erlaubt — Sie dürfen diesen Inhalt nicht bearbeiten, abwandeln oder in anderer Weise verändern.

Wobei gilt:

- **Verzichtserklärung** — Jede der vorgenannten Bedingungen kann **aufgehoben** werden, sofern Sie die ausdrückliche Einwilligung des Rechteinhabers dazu erhalten.
- **Public Domain (gemeinfreie oder nicht-schützbare Inhalte)** — Soweit das Werk, der Inhalt oder irgendein Teil davon zur Public Domain der jeweiligen Rechtsordnung gehört, wird dieser Status von der Lizenz in keiner Weise berührt.
- **Sonstige Rechte** — Die Lizenz hat keinerlei Einfluss auf die folgenden Rechte:
 - Die Rechte, die jedermann wegen der Schranken des Urheberrechts oder aufgrund gesetzlicher Erlaubnisse zustehen (in einigen Ländern als grundsätzliche Doktrin des **fair use** bekannt);
 - Die **Persönlichkeitsrechte** des Urhebers;
 - Rechte anderer Personen, entweder am Lizenzgegenstand selber oder bezüglich seiner Verwendung, zum Beispiel für **Werbung** oder Privatsphärenschutz.
- **Hinweis** — Bei jeder Nutzung oder Verbreitung müssen Sie anderen alle Lizenzbedingungen mitteilen, die für diesen Inhalt gelten. Am einfachsten ist es, an entsprechender Stelle einen Link auf diese Seite einzubinden.

Genehmigt von der Philosophisch-Naturwissenschaftlichen Fakultät

auf Antrag von

Prof. Dr. Andreas Pfaltz

PD. Dr. Daniel Häußinger

Prof. Dr. Catherine Housecroft

Basel, den 14.10.2014

Prof. Dr. Jörg Schibler

für Lena und meine Eltern

Zwei Dinge sind zu unserer Arbeit nötig:
Unermüdliche Ausdauer und die Bereitschaft,
etwas, in das man viel Zeit und Arbeit gesteckt hat,
wieder wegzuwerfen.

Albert Einstein

Acknowledgements

I am very grateful to my supervisor PD. Dr. Daniel Häußinger for the excellent mentoring and the outstanding support throughout the whole PhD studies. The working atmosphere was pleasant during the last 5 years. I thank you for giving me the opportunity to work on such diverse and challenging projects, your confidence and the freedom in all my projects. It was a pleasure to learn so much theoretical and practical aspects of NMR spectroscopy from you. The group trips and conferences eternize this period of my live for me.

I would like to thank Prof. Dr. Andreas Pfaltz for being my “Fakultätsverantwortlicher”.

I thank Prof. Dr. Catherine Housecroft for the co-examination of this thesis.

Sincere thank is given to Prof. Dr. Wolf-Dietrich Woggon for chairing this exam.

Collaborations with different groups made many aspects of this thesis possible. Therefore I really thank Prof. Dr. Marcel Mayor for the collaboration with many of your PhD students and especially for your helpful discussions and your confidence. More over I would like to thank Dr. Jürgen Rotzler for the synthesis of the biphenyl compounds, the help in the interpretation of the results, the useful discussions and mentoring during my studies.

I also would like to thank Markus Gantenbein and Dr. David Vonlanthen for the synthesis of biphenyls. Michel Rickhaus is acknowledged for the collaboration on the identification of the “Geländer-molecules”.

For all computational calculations I thank Prof. Dr. Willem Kloppers and Dr. Angela Bihlmeier from the KIT. It was a pleasure to work with both of you on this challenging project.

I would like to express my gratitude to Prof. Dr. Gennaro De Libero for the collaboration in the Lipid project. Especially Dr. Marco Lepore for the measurement of the immunological activation tests. Many thanks go to Dr. Gundimeda

Ramanjaneyulu, for the MS experiments of the natural sample and the purification of the synthetic mLPA sample by HPLC.

Especially I thank Dr. Jürgen Rotzler, Dr. Marco Lepore, Dr. Anne-Florence Tran Van and Alba Mascarin for proofreading this thesis.

I would really like to thank Kaspar Zimmermann for the excellent working atmosphere. I will miss the discussions in the lab and during the breaks. It was pleasant to work together with you for the last 5 years. I wouldn't have been such a great time without you.

I would like to thank the Group of Prof. Dr. Hermann Wegner for the great group seminars and the great time with your group members. It was pleasant to work with Dr. Anne-Florence Tran Van, Luca Schweighauser, Silas Götz and Patrick Wehrli in the Lab 023a/023b.

It was great to work with such highly motivated Master students. Therefore I thank Roche Walliser, Thomas Müntener and Florian Lüttin for the great work and the excellent working atmosphere.

I also would like to thank all the students (Pascal Eberle, Alexandra Wiessler, Johannes Wiest, Linda Bannwart, Veronica Hartmann, Max Klein, Raphael Vogt, Simone Grendelmeier, Fabian Brunner and Lucius Schmied) who did the "Abschlussversuch" with me.

I would also like to thank Prof. Dr. Helma Wennemers, especially with Dr. Roman Erdmann, Dr. Jörg Duchmalé and Robert Kastl for the great collaboration.

Sincere thank go to Liselotte Siegfried and Dominik Siefbrig for their support in maintaining the NMR spectrometers.

It's my pleasure to thank all students (Darja Kolbin, Paul Rempel, Florian Herren, Simone Grendelmeier, Ananth Rao, Davide Panighetti, Laura Luu, Serena Rigo, Raphael Vogt, Florian Lüttin, Silas Götz, Raphael Wyss, Thomas Müntener, Cathrin

Ertl, Simone Stratz, Roche Walliser, Martina Garni, Daniel Ris, Jonas Schätti, Severin Sigg, Martin Rother) who did their “Wahlpractica” in our group during the last five years.

Kaspar Zimmermann, Steffen Müller, Dr. Jonas Schönle, Roche Walliser, Cathrin Ertl, Dr. Gabriel Schneider, Annabell Bonn, Thomas Müntener, Simone Grendelmeier, Florian Lüttin, Sarah Keller and Alba Mascarini are very much acknowledged for the nice lunch/coffee-breaks.

Sincere thanks go to Bernadette Hammer Rotzler, Anna-Catherina Senn, Beat Amrein, Daniel Rösch, Steffen Müller, Andreas Buck, Michel Rickhaus and Kim von Allmen for the great learning sessions during the whole studies and for becoming such good friends! Also the team 2006 is acknowledged for the great time.

Dr. Heinz Nadig and PD. Dr. Ernst Gassmann (Novartis) are thanked for the measurement of HRMS-spectra.

Kiril Tishinov, Gero Harzmann, Dr. Nicolas Jenny and Dr. Sandro Gabutti are acknowledged for their maintenance of the ESI-MS machine.

The application team of Bruker especially Willy Scherer and Detlev Moskau are acknowledged for their support and for providing us with a 1.7 mm TXI probe head.

I would like to thank the whole technical staff and the secretaries for their help throughout the whole studies.

The Swiss National Science Foundation (SNF 200021_130263) is acknowledged for the financial support.

The department of Chemistry is also acknowledged for financial support.

Especially I want to thank my family for the support and love during my whole life. Most thanks go to Lena for the love and support during the last years.

I would also like to thank all my friends for their support and motivating words.

Abstract

Detailed knowledge of the structure of bio molecules with atomic resolution is essential for the understanding of their function. Moreover the identification and quantification of their dynamic processes are important, as they are the origin of molecular functionalities. Different spectroscopic methods like X-ray crystallography (limited to structure elucidation, no dynamics), mass spectroscopy, electron spin resonance (EPR) and nuclear magnetic resonance (NMR) spectroscopy can deliver this detailed structural information. Especially NMR spectroscopy has found its application in the identification of dynamic processes. This thesis was focused on the characterization of dynamic processes, the structure elucidation of natural products available in nanograms and the synthesis of lanthanide chelating tags for the study of protein-ligand and protein-protein interactions in solution.

The thesis is divided into three chapters addressing a specific task of the mentioned topic.

A: The influences of different donors and linkers on lanthanide chelating tags were investigated. A 4S-Tetramethylcyclen was used as enantiomerically pure core molecule. The side chains were based on enantiopure lactic acid derivatives. The carboxylic acids of lactic acid were transformed into different functional groups like thiols, nitrogens, and carbonyl. These different donor groups are expected to change the magnetic susceptibility tensor of the lanthanide cation in complex with the synthesized tags. Special protection protocols for the introduction of heteroatoms are presented. On this basis also two new linkers were introduced. These linkers bind in a selective way to cysteins on a protein surface as thioethers. The α -bromoketones are very selective for the coupling to cysteins, nevertheless they have a tendency to hydrolyse under Lewis acidic conditions. Vinylsulfones require harsher tagging conditions but they are much more stable against hydrolysis. All new tags were attached to proteins and tested as PCS reagents in protein NMR spectroscopy.

B: The effects of para-substituents on the rotation barrier of 2,2'-propyl and 2,2'-butyl-bridged biphenyls were studied by dynamic NMR spectroscopy and dynamic HPLC measurements. Gibbs free activation energies $\Delta G^\ddagger(T)$ of the rotation about the

central biphenyl bond were estimated by variable temperature $^1\text{H-NMR}$ experiments for the propyl bridged biphenyl. The resulting data were correlated to Hammett-parameters σ_{P} as a measure of electron donor and acceptor strength. It was demonstrated that the electronic effects influence the activation barrier significantly, whereas sterics had only minor influence. Rate constants were calculated from line shape analysis and analysed by Eyring plots to calculate the entropic and enthalpic contributions. Thermodynamic data for the butyl-bridged biphenyls were directly obtained from dynamic HPLC chromatograms. DFT calculations delivered different transition states for the two series of biphenyls. The calculation of the activation parameters showed a similar trend and therefore the model is validated. The differences in the enthalpic and entropic contributions between HPLC, NMR and DFT calculations are method dependent, which was proven by changes of the solvent in NMR experiments that led to alteration of these contributions.

C: The identification and total synthesis of a novel methylated lipid antigen (mLPA) was performed. The presented mLPA shows potent inhibition properties against human leukaemia. A combination of extraction protocols, activation essays and HPLC-MS measurements were used to identify the different antigen molecules from cell extracts. Three different candidates were identified. MS-MS experiments delivered structural insights, which were further confirmed by NMR spectroscopy and allowed the characterization of two of these structures. Total syntheses of the identified structures were performed in 6 linear steps. The high biological activity of the synthesized structures corroborated the identity of the active molecule.

Contents

Acknowledgements	I
Abstract	IV
Abbreviation	IX
A) Synthesis and characterization of DOTA based Lanthanide shift reagents	1
A.1 Introduction	1
A.1.1 Protein NMR spectroscopy	3
A.1.2 Historical background	3
A.1.3 Lanthanide metals.....	5
A.1.4 Paramagnetic shifts	6
A.1.5 The pseudocontact shift (PCS).....	7
A.1.6 Residual dipolar coupling (RDC).....	10
A.1.7 Paramagnetic relaxation enhancement (PRE).....	10
A.1.8 Development of lanthanide chelating tags	10
A.1.9 DOTA a strong lanthanide chelating tag	13
A.1.10 DOTA-M8: An extremely rigid, high-affinity lanthanide chelating tag.....	14
A.2 Research Goal	15
A.3 Methods and Materials.....	16
A.4 Synthetic strategy	18
A.4.1 Synthetic strategy for DOTA-M7 acetophenone (A1)	18
A.4.2 Synthetic strategy for DOTA-M7/8-thiovinylsulfone (B1, B1a)	20
A.4.3 Synthetic strategy for DOTA-M8- α,β -unsaturatedketone (C1).....	22
A.4.4 Synthetic strategy towards DOTA- M8-amino (D1).....	22
A.5 Results and Discussion.....	25
A.5.1 Investigation of acetophenone based linkers.....	25
A.5.2 Using a thiol as donor atom in the linker.....	33
A.5.3 Synthesis of the α,β -unsaturated target molecule C1	43
A.5.4 Synthesis towards amine based macrocycle D1.	45
A.5.5 Influence of different donor atoms to the anisotropy of the magnetic susceptibility tensor.....	47
A.5.6 Further developments	49
A.6 Conclusion	54
A.7 Outlook.....	55
A.8 Experimental Section	57

A.8.1	<i>Preparative HPLC purification</i>	57
A.8.2	<i>Experimental procedures</i>	57
A.9	<i>References</i>	113
B)	Thermodynamic studies of 4,4' substituted torsion angle restricted 2,2' alkyl-bridged biphenyl cyclophanes	119
B.1	<i>Research goal</i>	119
B.2	<i>Introduction</i>	120
B.2.1	<i>Dynamic NMR Spectroscopy (dNMR)</i>	120
B.2.2	<i>Historical development of dNMR</i>	122
B.2.3	<i>Biphenyls in dynamic NMR</i>	124
B.2.4	<i>Dynamic High Pressure Liquid Chromatography (DHPLC)</i>	129
B.2.5	<i>Applications of biphenyls</i>	130
B.3	<i>Methods and Materials</i>	131
B.3.1	<i>Dynamic NMR measurements and analysis</i>	131
B.3.2	<i>Dynamic HPLC measurements and fitting</i>	134
B.3.3	<i>Theoretical calculations</i>	134
B.3.4	<i>Synthesis</i>	135
B.4	<i>Results</i>	136
B.5	<i>Discussion</i>	152
B.6	<i>Conclusions</i>	167
B.7	<i>Outlook</i>	168
B.8	<i>Experimental</i>	169
B.8.1	<i>Temperature Calibration</i>	169
B.8.2	<i>Lanthanide shift reagents</i>	171
B.8.3	<i>Line shape analysis</i>	178
B.8.4	<i>Determination of the Standard Deviation for $\Delta H_{\text{Eyring}}^{\ddagger}$, $\Delta S_{\text{Eyring}}^{\ddagger}$, $\Delta G_{\text{Eyring}}^{\ddagger}$</i>	200
B.9	<i>References</i>	202
C)	Structure elucidation and Synthesis of a novel leukaemia- associated T cell lipid antigen	208
C.1	<i>Research Goal</i>	208
C.2	<i>Introduction</i>	208
C.3	<i>Methods and Materials</i>	211
C.3.1	<i>Cell extraction</i>	211
C.3.2	<i>LC-MS purification</i>	211
C.3.3	<i>NMR studies</i>	211
C.3.4	<i>Synthesis</i>	212

C.4	<i>Retrosynthetic analysis and synthetic strategy</i>	212
C.5	<i>Results</i>	214
C.6	<i>Discussion</i>	224
C.7	<i>Conclusion</i>	227
C.8	<i>Experimental</i>	228
C.8.1	<i>NMR spectra of the biological sample</i>	228
C.8.2	<i>Synthesis</i>	229
C.8.3	<i>NMR spectra of synthetic mLPA</i>	234
C.8.4	<i>LC-MS-data for the natural C-18 sample eluting at 19.9 min.</i>	236
C.9	<i>References</i>	237

Abbreviation

Å	Ångström
Ac	Acetyl
APC	Antigen presenting cell
B3LYP	Hybrid functional
Boc	<i>tert</i> -butyloxycarbonyl
BP86	Functional using gradient corrected methods
BRET	Bioluminescence resonance energy transfer spectroscopy
CD1	Cluster of differentiation 1
CID	Collision induced dissociation
COSY	Correlation spectroscopy
DCC	<i>N,N'</i> -Dicyclohexylcarbodiimide
DCM	Dichloromethane
DEER	Double electron-electron resonance
DFT	Density functional theory
dHPLC	Dynamic high performance liquid chromatography
DIC	<i>N,N'</i> -Diisopropylcarbodiimide
DIPEA	<i>N,N</i> -Diisopropylethylamine
DMAP	4-(Dimethylamino)pyridine
DMF	<i>N,N</i> -Dimethylformamide
dNMR	Dynamic nuclear magnetic resonance
DOTA	1,4,7,10-tetraazacyclododecane-1,4,7,10-tetraacetic acid
DOTA-M8	(2 <i>R</i> ,2' <i>R</i> ,2'' <i>R</i> ,2''' <i>R</i>)-2,2',2'',2'''-((2 <i>S</i> ,5 <i>S</i> ,8 <i>S</i> ,11 <i>S</i>)-2,5,8,11-tetramethyl-1,4,7,10-tetraazacyclododecane-1,4,7,10-tetrayl)tetrapropionic acid
DTPA	Diethylene triamine-pentaacetate
DTT	Dithiothreitol
EDTA	Ethylenediaminetetraacetic acid
EPR	Electron spin resonance
ESI-MS	Electrospray ionisation mass spectrometry
(fod) ₃	6,6,7,7,8,8,8-heptafluoro-2,2-dimethyl-3,5-octanedionate
(hfc) ₃	tris[3-(2,2,3,3,4,4,4-heptafluorohydroxymethylene)- <i>D</i> -camphorate

EWG	Electron withdrawing group
F	σ -field/inductive parameter
FRET	Förster energy transfer spectroscopy
GB1	Protein G: immunoglobulin binding protein
GGA	Generalized gradient approximation
HD	High definition
HMBC	Heteronuclear multiple bond coherence
HMQC	Heteronuclear multiple quantum coherence
HPLC	High performance liquid chromatography
HRMS	High resolution mass spectrometry
HSQC	Heteronuclear single quantum coherence
IC50	Inhibitory concentration 50
IR	Infrared spectroscopy
k	Rate constant
LC	Liquid chromatography
LC-MS	Liquid chromatography coupled to an mass detector
LSR	Lanthanide shift reagent
M4-cyclen	(2S,5S,8S,11S)-2,5,8,11-tetramethyl-1,4,7,10-tetraazacyclododecane
MALDI	Matrix assisted laser desorption/ionisation
Mes	Methanesulfonyl
MHC-I	Major histocompatibility complex I
mLPA	Methyl-lysophosphatidic acid
MRI	Magnetic resonance imaging
MS ²	Tadem mass spectrometry
MS ³	Triple stage mass spectrometry
MW	Microwave
NBS	N-bromo succinimide
NLO	Non linear optics
NMR	Nuclear magnetic resonance
NOE	Nuclear Overhauser enhancement
NOESY	Nuclear Overhauser Spectroscopy
OLED	Organic light emitting device
p-Ts	<i>Para</i> -toluenesulfonyl
PCS	Pseudocontact shift

Pd/C	Palladium on activated charcoal
Pd10	Disposable desalting column
pdb	Protein data base
PPTS	Pyridinium- <i>para</i> -toluenesulfonate
PRE	Paramagnetic relaxation enhancement
R	σ -resonance parameter
RDC	Residual dipolar coupling
react IR	Time dependent infrared spectroscopy
R _f	Retarding-front
SDBS	Integrated Spectral data base system for organic compounds
T	Temperature
TBDMS	<i>Tert</i> -butyldimethylsilane
TBME	<i>Tert</i> -butylmethylether
T _c	Coalescence temperature
TCEP	Tris(2-carboxyethyl)phosphine
THF	Tetrahydrofuran
THP	Tetrahydropyran
THP1-cells	Human monocytic cell line derived from an acute leukaemia patient
TLC	Thin layer chromatography
TMS	Tetramethylsilane (NMR standard)
TPSS	Hybrid functional
Triflate	Trifluoromethanesulfonyl
TROSY	Transverse relaxation optimized spectroscopy
UV-VIS	Ultra violet and visible light
VT-NMR	Variable temperature nuclear magnetic resonance
X-ray	X-radiation, Röntgen radiation
ΔG^\ddagger	Gibbs free activation energy
ΔH^\ddagger	Activation enthalpy
ΔS^\ddagger	Activation entropy
$\Delta\nu$	Chemical shift difference of two interchanging spins in slow exchange

A) Synthesis and Characterization of DOTA based Lanthanide shift reagents

A.1 Introduction

Structural biology is a part of molecular biology, biochemistry and biophysics. Molecular structures, their functionality and the origin of the functionality of proteins and nucleic acid are investigated in this field. The exact determination of molecular structures is necessary for rational design of drugs and understanding of protein functionalities. More and more applications of proteins in catalysis are described for which structural information is necessary. The investigation of proteins is extremely complex and thus gaining structural information required a long process of technical development. Classical protein sequence analysis was time consuming. The development of ESI-MS and MALDI assisted methods allowed an automated protein sequencing, which is much faster. However, knowledge of the sequence does not deliver any information about the functionality of a protein. The functionality of a

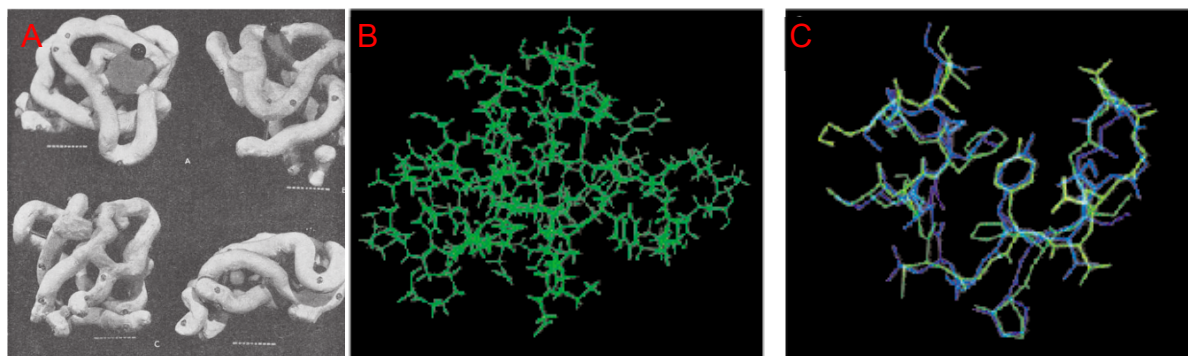


Figure A-1: Picture A shows the first protein X-ray structure (myoglobin) determined in 1958 by Kendrew et. al. Picture B represents the first protein NMR structure (proteinase inhibitor IIA from bull seminal plasma (BUSI IIA)) determined in 1982 by Wüthrich. Picture C shows the superimposed picture of the NMR and X-ray structures.

protein is mainly influenced by its 3D structure. Detailed 3D structural information are therefore unambiguously important to study their functionality. In 1958 Kendrew

published the first X-ray protein structure (Figure A-1).¹ This milestone in the characterization of proteins started a fast growing research field. In 1982 Wüthrich was able to determine the first 3D structure of a protein by NMR spectroscopy.² Protein structures determined by X-ray deliver a static picture, whereas the ones determined by NMR-spectroscopy deliver a more dynamic picture.

Figure A-2 (left) shows the comparison between the total numbers of 3D structures determined from 1990 to 2014 (black) and the number of structures determined each year (red) during this period (statistics of the published structures in the protein database (pdb)). By dividing the data into their spectroscopic origin, it becomes obvious that X-ray crystallography is the method that delivers by far the highest number of new structures per year with permanent increase. The number of new NMR structures remained constant during the last years. In many cases protein structures solved by X-ray crystallography were also determined by the complementary NMR method to identify flexible regions within the protein.

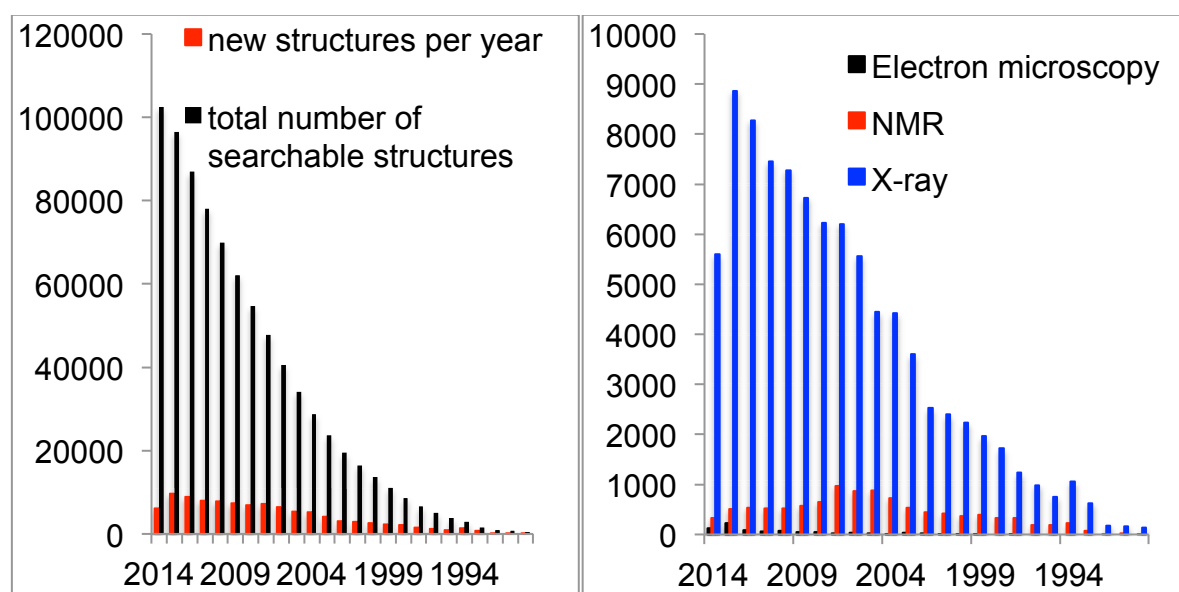


Figure A-2: Left graph: Statistic representation of the sum of 3D protein structures determined since 1975 (black) and the structure elucidation per year (red) (data obtained from pdb (15.08.2014)). Right graph: Separation of the structures elucidated per year by their spectroscopic origins.

Investigation of the active sites of proteins remains still challenging. Only a few spectroscopic methods can deliver such information. X-ray as main source of 3D protein structures delivers only static information even when an inhibitor is crystalized within a protein. Nevertheless, useful information about interactions inside a protein can be gained and model compounds synthesized to proof the results. For drug design, knowledge of the binding mode is important but in many cases not enough. It is also necessary to know, how the inhibitor is delivered to the active site. Monitoring

of the binding event or differentiation between open and closed protein conformations are therefore required. Limitations of crystallography are reached when dynamic processes play a role. Solution NMR-spectroscopy can deliver useful information about dynamics within a protein structure. Changes of the experimental conditions can also mimic the situation within a cell to some degree. With the development of more and more sensitive NMR equipment in-cell measurements became possible.³ Besides the identification of dynamics within a single protein it is of great interest to gain information about protein-protein interactions. These interactions are responsible for a variety of functionalities in cellular processes. Protein-protein interactions can be studied by special NMR experiments using paramagnetic ions that deliver long-range information. Electron spin resonance (EPR)⁴ spectroscopy and especially double electron-electron resonance (DEER)⁴⁻⁶ are the most prominent methods for the measurements of distances in biomolecules so far. Other methods like Förster energy transfer spectroscopy (FRET)⁷ and Bioluminescence resonance energy transfer (BRET) showed their ability to determine protein-protein interactions recently.

A.1.1 Protein NMR spectroscopy

The fast growing amount of available proteins from different organisms and plants requires structural information to understand the behaviour of such proteins. Around one third of the total numbers of known proteins are metal binding proteins.⁸ NMR is a valid tool to study solution and solid-state structures of proteins. The determination of 3D NMR structures is still not a straightforward task. NOE data are the classical restrains for the 3D structure determination that allowed the identification of neighbouring amino acids that are in close contact through space. The main problem of NOE data is the short range of about 5 Å that can be observed as the NOE intensity decreases with $\frac{1}{r^6}$. It is therefore difficult to gain information about the distance of two strands in a protein when they are further away than 5 Å, which is quite usual in proteins.

A.1.2 Historical background

Experiments that deliver long-range information are required in order to resolve protein-protein interactions in high quality. Paramagnetic relaxation enhancement

(PRE), residual dipolar couplings (RDC) and pseudocontact shifts (PCS) can deliver such long-range information by NMR spectroscopy. The use of such experiments in protein NMR spectroscopy was established during the last 20 years. The theoretical fundamentals^{9,10} were investigated much earlier in the 1960's and first experiments with small molecules presented. In the 1970's several groups investigated the influence of paramagnetic metals in NMR spectroscopy.^{11,12} They showed that lanthanide shift reagents such as Europium complexes deliver distance dependent shifts allowing the resolution of complex 1D-proton spectra.^{13,14} The first more complex application was shown by Barry,¹⁵ who used paramagnetic lanthanide ions to determine the conformation of mononucleotides in solution. Line broadening due to paramagnetic relaxation enhancement was also obtained in measurement of metal-binding proteins containing paramagnetic metals. The paramagnetic metals obtained in natural metal-binding proteins are usually high-spin Fe^{2+} , Ni^{2+} , Cu^{2+} and Mn^{2+} . These metals show only weak pseudocontact shift but strong PRE effects leading to broad signals. Strong PRE effects cause more experimental problems than the small PCS can deliver beneficial ones. In the end of the 1990's the Bertini group showed several applications of lanthanides for the structure determination of proteins using PCS by changing natural occurring metals to lanthanide metals. This work was reviewed in a article by Bertini and Luchinat in 1999.¹⁶ The groups of Prestegard¹⁷ and Bax¹⁸ reported that liquid crystals can be used to gain distance and angular information through the measurement of RDC's. The limitation of PCS and PRE experiments to metal binding proteins was solved by the development of lanthanide chelating tags in the beginning of the century. First trials using zinc fingers¹⁹ and EF hands²⁰ attached to the C- or N-terminus of the protein delivered weak PCS and RDC values due to motional freedom. Lanthanide-binding peptides were prepared by Schwalbe^{21,22} and Otting^{23,24} with better results. Tags (even if they are rigid) attached to the C- or N-termini loosen their rigidity due to the flexibility of the protein in this region. The resulting PCS values were therefore averaged. The development of tags that can be attached to cysteine residues via a disulphide bridge²⁵⁻²⁹ allowed binding to protein regions with higher rigidity. The averaging of the PCS was mainly influenced by the design of the lanthanide chelating tag. An even more rigid attachment could be generated using tags that bind to two cysteine³⁰⁻³² residues on the protein surface. In both cases stronger PCS and RDC values were measured. Nevertheless, the resulting PCS are in most cases weaker than the ones obtained for

metal-binding proteins. Therefore, further investigation on the optimization of lanthanide chelating tags is a current research topic.

A.1.3 Lanthanide metals

Lanthanide metals are most stable as their M^{3+} -metal cations. The unique properties of lanthanides can be explained by the fact that the 4f-electrons are located in the inner core of the atoms and are therefore not accessible for reactions. The sizes of all lanthanides are quite similar. A slight decrease of radii along the series from Lanthanum (La = 188 pm; La^{3+} = 116 pm)

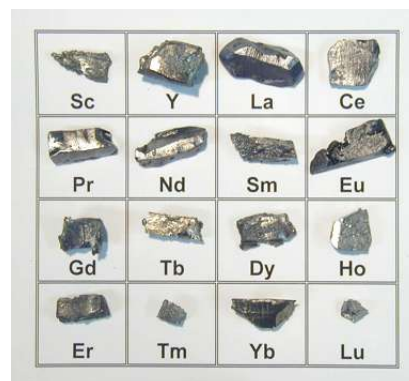


Figure A-3: Representation of the elemental forms of the lanthanide metals. (www.elementsales.com)

to Lutetium (Lu = 173 pm; Lu^{3+} = 98 pm) due to lanthanoid contraction is obtained. The comparable size and the identical oxidation states yield similar chemical and physical properties over the whole series.³³ Replacement of a lanthanide ion by another lanthanide ion within a tag does therefore not change the conformation of the resulting complex. In the series of lanthanides only lanthanum and lutetium are diamagnetic atoms all others are paramagnetic. Gadolinium has an isotropic χ -tensor leading to strong PRE effects but no PCS effects. These similarities of complexes obtained from different lanthanides are necessary to compare paramagnetic and diamagnetic complexes in a one to one manner. The paramagnetic properties of lanthanides are presented in Figure A-4. Lanthanides can be classified according to their PCS properties as weakly shifting: Cerium, Praseodymium, Neodymium, Samarium and Europium, the medium shifting: Erbium, Thulium, Holmium and Ytterbium and the strong shifting: Terbium and Dysprosium. The main advantage of paramagnetic lanthanides compared to other paramagnetic molecules is the fact that the unpaired electrons are located in the inner sphere of the atoms. Therefore contact shifts are very weak and only of importance for atoms that are located in the coordination sphere of the metal.

	f1	f2	f3	f5	f6	f7	f8	f9	f10	f11	f12	f13
	Cerium	Praseodymium	Neodymium	Samarium	Europium	Gadolinium	Terbium	Dysprosium	Holmium	Erbium	Thulium	Ytterbium
J	Ce	Pr	Nd	Sm	Eu	Gd	Tb	Dy	Ho	Er	Tm	Yb
$\Delta/10^{-32} \text{ m}^3$	5.6	11.4	11.4	0.6	~6	55.1	82.7	99.2	98.5	80.3	50.0	18.0
PRE												
	5 Å											
$\Delta\chi_{ax}/10^{-32} \text{ m}^3$	2.1	3.4	1.7	0.2	-2.3	0	42.1	34.7	18.5	-11.6	-21.9	-8.3
$\Delta\chi_{rh}/10^{-32} \text{ m}^3$	0.7	2.1	0.5	-0.1	-1.6	0	11.2	20.3	5.8	-8.6	-20.1	-5.8
PCS												
	5 Å											
τ_e/s	10^{-13}					10^{-8}	10^{-13}					

Figure A-4: "Paramagnetic properties of lanthanides. Only paramagnetic and nonradioactive lanthanides are included. The radii of the yellow spheres indicate the distance from metal ion where the ^1H nuclear magnetic resonance signals of a protein with rotational correlation time of 15 ns would be broadened by 80 Hz on an 800 MHz NMR spectrometer due to paramagnetic relaxation enhancement. The isotropic χ tensors were calculated by Bleaney (1972)³⁴ for a temperature of 25 °C. Representative isosurfaces for pseudocontact shifts of ± 5 ppm are plotted for $\Delta\chi$ tensors reported for calbindin D_{9k}.³⁵ Electronic relaxation times expected at 18.8 T are indicated at the bottom."^{28,29}

A.1.4 Paramagnetic shifts

Paramagnetic shifts consist of two different origins namely the contact and the pseudocontact contribution. Contact shifts are scalar interactions between the electron and the nuclear spin. They are strongly angular dependent and decay rapidly with increasing bond distance. The contact shift is described by Equation A-1

$$\delta^{CS} = \frac{A}{\hbar \mu_0} \frac{\chi}{Y_l g_e \mu_B}$$

Equation A-1: Formula for the calculation of the contact shift; A = contact coupling constant; \hbar = Planck constant; χ = magnetic susceptibility tensor; μ_0 = induced magnetic moment; Y_l = magnetogyric ratio; g_e = electron g-factor and μ_B = Bohr magneton.

where A is called the contact coupling constant. Contact couplings are strongly angular dependent. Contact shifts are quite difficult to determine as they are in the range where paramagnetic relaxation enhancement broadens the peaks. Contact shifts are more pronounced for paramagnetic substances having unpaired electrons in orbitals that can interact with the ligand. In the case of lanthanides the unpaired electrons are shielded and therefore these interactions can be more or less neglected. Indeed, all influenced atoms are located in the region where the shifts are

strongly broadened by PRE effects. The effects of contact shifts are usually smaller than PRE effects and much smaller than PCS shifts.

A.1.5 The pseudocontact shift (PCS)

One of the most useful data obtained from paramagnetic complexes are pseudocontact shifts. Paramagnetic atoms induce a magnetic moment due to their unpaired electrons. This magnetic moment orientates itself in an external magnetic field to yield a non-zero average, leading to an induced magnetic moment. This induced magnetic moment acts as a dipolar field influencing all nuclei located in this field. The strength of this interaction depends on the distances and angles of the influenced nuclei with respect to the paramagnetic ion. This induced magnetic moment can be averaged through rotational freedom of the paramagnetic ion. The magnetic moment of an electron consists of two different origins namely the spin and the orbital moment. Spin parts are isotropic, whereas orbit parts are anisotropic. This anisotropic contribution is the reason why the magnetic susceptibility tensor can become anisotropic within an external magnetic field. If this interaction is not averaged to zero, the resulting dipolar field induces a magnetic field that induces a chemical shift difference of the influenced nuclei, described by the following equation.

$$\Delta\delta^{PCS} = \frac{1}{12\pi r^3} [\Delta\chi_{ax}(3\cos^2\theta - 1) + 1.5 \Delta\chi_{rh}\sin^2\theta\cos 2\Phi]$$

Equation A-2: Formula for the calculation of the pseudocontact shift $\Delta\delta^{PCS}$; r = distance between unpaired electron and nuclear spin; $\Delta\chi$ tensor components axial and rhombic; θ , Φ = polar angles.

This formula highlights the r^{-3} in contrast to r^{-6} for NOE experiments. PCS deliver therefore long-range information. The pseudocontact shift is strongly dependent on the polar coordinates r, θ and Φ of the nuclear spin with respect to the χ tensor of the paramagnetic metal ion. However, the pseudocontact shift does not depend on the total χ tensor. The influences of anisotropic parts of the χ tensor, namely the axial and rhombic components are required for pseudocontact shifts. "For the definition of the χ tensor of a lanthanide ion the protein surface eight parameters are required: Three parameters that describe the metal position with respect to the protein; three parameters describing the orientation of the χ tensor with respect to the molecular coordinates (Euler-angles: α , β , γ) and two parameters that describe the axial and the rhombic components ($\Delta\chi_{ax}$, $\Delta\chi_{rh}$) are necessary".³⁶

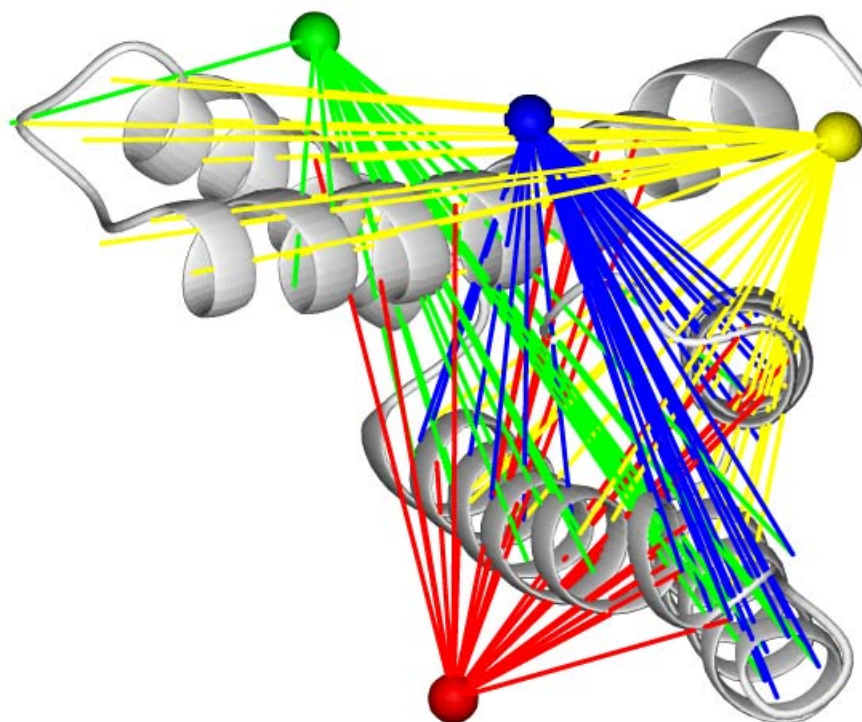


Figure A-5: Model of a protein determined by PCS NMR spectroscopy. The different positions of the lanthanide chelating tags are represented by the green, red, blue and yellow dots. The lines show schematically the interaction of unpaired electrons with the nuclear spin.³⁷

It is worth to mention that the measurement of only one set of PCS cannot determine the position of a nucleus.³⁷ To determine the position of the nucleus, different possibilities are available. The exchange of the paramagnetic ion by another will deliver different pseudocontact shifts, as the χ tensor is different for each ion. The main problem of this method is the fact that different ions are not completely linear independent from each other. This method is therefore mainly used for metal-binding proteins where only one position for the metal ion is accessible. For tags that are attached to the surface of the protein with a disulphide bridge the situation is different. Point mutations are performed on different positions of the protein and therefore the same tag with the same lanthanide ion can be used to deliver independent sets of PCS data. The resulting independent tensors led to much more precise results in this method.

- "Pseudocontact shifts can be predicted when the tensor components and the polar coordinates of the molecule are known.
- Tensor components can be calculated from known coordinates and pseudocontact shifts.
- However atomic coordinates cannot be calculated from one single set of pseudocontact shifts and tensor components.

- It is a valid tool to refine structures that have been determined with other methods.”⁸

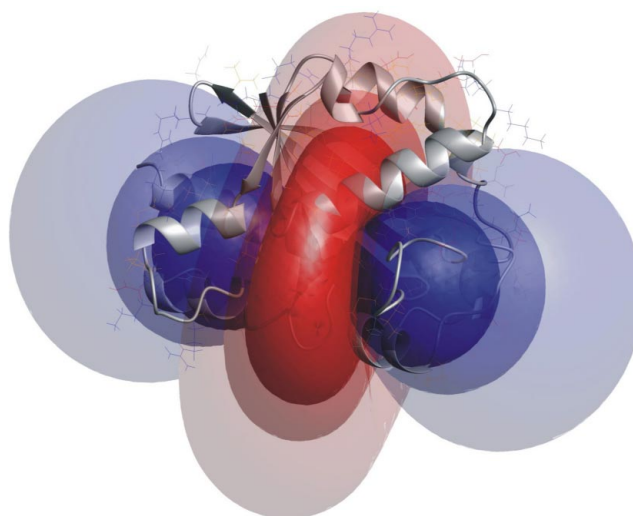


Figure A-6: Isosurfaces representing the positions that show the same pseudocontact shift.³⁸

Isosurfaces³⁸ are a quite informative representation of PCS as shown on the protein structure in a superimposed manner (Figure A-6). This is a good model for visualizing the χ tensor of the lanthanide ion.

Pseudocontact shifts are used to refine structures that were determined before with classical restraints. But more important are applications for the investigation of protein-ligand and protein-protein interactions as these interactions are quite difficult to study by other methods. These interactions are the key to understand biological activities and are of main interest for the pharmaceutical industry. The improvement of this method is urgently necessary for structural biology.

For most proteins investigated by PCS a crystal or NMR structure is already available. This allows the use of selectively isotope labelled proteins. This reduced number of resonances reduces the overlaps drastically. For the investigation of ligand positions or to calculate distances to a second protein only the tensors and not all residues have to be known. Therefore selective protein labelling allows a much faster assignment.³⁶ The assignment of paramagnetic shifts is quite easy when the diamagnetic reference signals are assigned, as in an HSQC spectra a 45° angle between paramagnetic and diamagnetic reference is obtained.²⁹ The measurement of a diamagnetic reference has therefore two main goals. First it allows comparison to the wild type protein to see if the tag (or in metal binding proteins the different ion) has an effect on the protein structure. But more important, it allows the calculation of the chemical shift difference of the two species and therefore the determination of the tensor parameters.

A.1.6 Residual dipolar coupling (RDC)

Residual dipolar coupling is obtained when dipolar couplings are not averaged due to rotational motion of the molecule in a magnetic field. These couplings can be introduced using liquid crystalline solvents for the measurements as they induce a partial alignment of the molecules inside the solution. The same effect can be obtained when a paramagnetic ion is placed on the molecular surface as it induces partial alignment of the unpaired electron with respect to the atomic coordinates of the other nucleus, similar to PCS. The formula for the calculation of RDCs is therefore quite similar and both effects are obtained simultaneously.

$$D^{res} = -\frac{B_0^2}{15kT} \left(\Delta\chi_{ax}(3\cos^2\theta - 1) + \frac{3}{2}\Delta\chi_{rh}\sin^2\theta\cos 2\Phi \right)$$

Equation A-3: Formula for the calculation of the residual couplings D^{res} ; $\Delta\chi$ tensor components axial and rhombic; θ , Φ = polar coordinates.

Residual dipolar couplings are distance independent. They depend only on the anisotropic parts of the axial and rhombic χ tensor and on the polar coordinates with respect to the χ tensors. In contrast to PCS measurements protein structures have been exclusively calculated from RDC restraints without the use of any NOE constraints.

A.1.7 Paramagnetic relaxation enhancement (PRE)

In all previously presented systems paramagnetic relaxation enhancement was obtained simultaneously. PRE measurements deliver long-range information in the range of 10-25 Å. PREs decay with r^{-6} which is similar to the NOE decay, but the effect is much stronger and therefore much more long-range. The precision of PRE measurements is less accurate than NOE measurements due to line broadening but distance restraints from PRE experiments became extremely useful in structural biology.

A.1.8 Development of lanthanide chelating tags

Several research groups have reported a variety of lanthanide-chelating tags in the last 20 years. Griessinger reviewed in 2006²⁹ the most important considerations for the synthesis of lanthanide-chelating tags. The first trials of tagging non metal-binding proteins used zinc fingers¹⁹ to couple the lanthanide ion to the protein. In this approach only weak PCS and RDC values in the order of 0.05 ppm or 1 Hz could be

measured. EF-hands delivered stronger RDC couplings up to 8 Hz after optimization of the linker.²⁰ Another approach using metal binding peptides delivered reasonable RDC couplings of 8 Hz but weak PCS of only 0.05 ppm.³⁹ The main problems of these tags are the high molecular weight and the low affinity towards lanthanide ions. Schwalbe developed a 17 amino acids containing tag, which showed high lanthanide affinity and delivered reasonable RDC and PCS values.²¹ However, these tags are limited to the functionalization of the C- and N-terminus. Only two different datasets for each tag and metal can be recorded, which limits this method drastically.

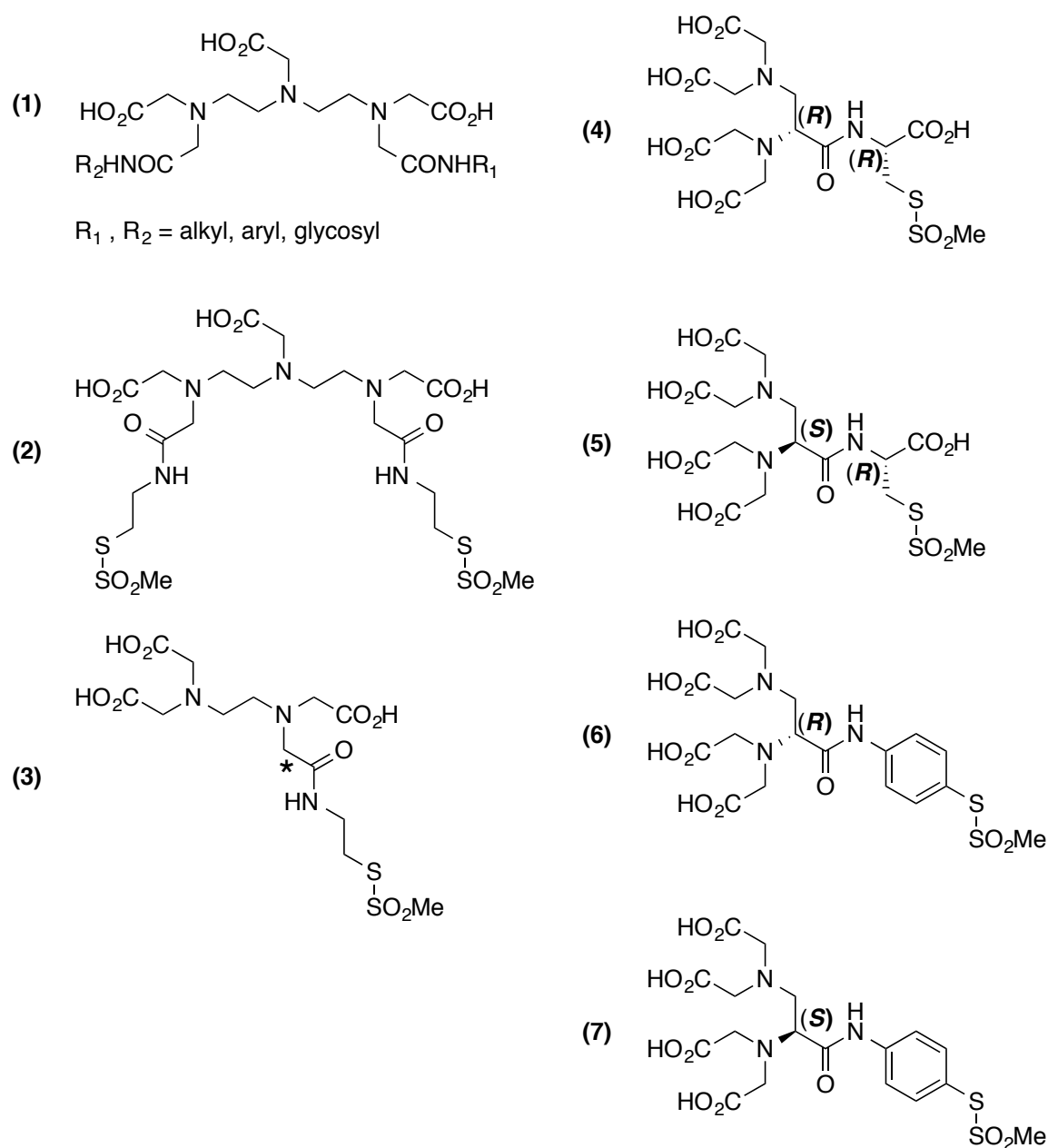


Figure A-7: Lanthanide chelating tags: (1) DTPA amide tag, (2) tag used by Ubbink³⁰ with two binding sides, (3) tag used by Griessinger, Byrd and Gaponenko,^{19,26-28} (4)-(7) optimized systems from Griessinger that showed reduced numbers of isomers.

Diethylenetriamine-pentaacetate (**DTPA**, **1**) was the first small molecular tag. It showed tremendously increased affinity to lanthanide binding ($K_d = 10^{-21}$ M) and the molecular weight of the tagged protein was only increased slightly. The first DTPA was tagged to the N-terminus of the protein. It turned out that the resulting complex existed in two different diastereomeric forms with different alignment tensors.⁴⁰

Ubbink used **DTPA** (**2**) (Figure A-7) as tag to address two cysteine residues on the surface of a protein. Nevertheless, five different diastereoisomers with different alignment tensors were recorded. All diastereoisomers were in slow exchange with each other. As different populations of signals were obtained, an assignment for some of the species was possible, but in many cases where the shift differences were really weak overlap of all signals was observed.³⁰

To avoid formation of so many diastereoisomers, the Griessinger²⁸ and Byrd²⁶ groups used the less stereochemically demanding **EDTA** based tag (**3**) (Figure A-7) for their investigations. This tag was attached to a protein surface using a single disulphide bridge. Nevertheless, they obtained two sets of signals, as the nitrogen marked in Figure A-7 became stereogenic after attachment to the protein surface. This demonstrates the huge importance of the formation of a single isomer on the protein surface in order to avoid signal multiplication.

The first step towards this goal was presented by a series of **EDTA**-based tags (**4-7**), which did not introduce any new chirality during the coupling process. They showed an extreme high affinity towards lanthanides and were successfully attached to protein surfaces. The application of this tags for RDC measurements was good but the **EDTA** complex were still not rigid enough so that PCS remained weak.^{28,29,41}

A.1.9 DOTA a strong lanthanide chelating tag

DOTA-Gd³⁺-derivatives are used in magnetic resonance imaging (MRI) for about 30 years.⁴² These gadolinium complexes were chosen due to their strong PRE effects to allow sufficient water suppression. Many studies have shown that DOTA complexes have more potential than DTPA complexes due to their higher thermodynamic and kinetic stability under physiological conditions.⁴² In MRI experiments the stability of gadolinium complexes is of utmost importance as free gadolinium is highly toxic.

Table A-1: Examples of MRI contrast agents.

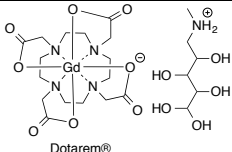
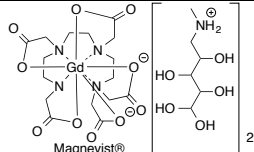
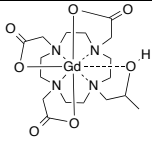
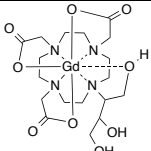
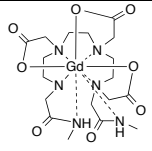
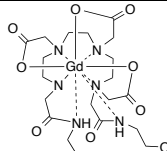
	Macrocyclic		Open chain	
Ionic	 Dotarem®		 Magnevist®	
Non ionic	 ProHance®	 Gadovist®	 Omniscan®	 OptiMARK®

Table A-2: $-\log K_d$ for the different MRI contrast agents. K_{d1} represents the thermodynamic dissociation constant, whereas K_{d2} represents the stability of the complex under physiological conditions (other metals are present under these conditions leading to competition reactions).

	Dotarem®	ProHance®	Gadovist®	Magnevist®	Omniscan®	OptiMARK®
K_{d1}	25.6	23.8	21.8	22.1	16.9	16.6
K_{d2}	19.3	17.1	14.7	17.7	14.9	15.0

These results inspired the NMR community to test DOTA as candidate for RDC and PCS measurements. Several groups used DOTA based tags successfully. Results showed increased PCS properties depending on the rigidity of the DOTA backbone used.^{24,31,36,43}

The greater stability of DOTA under physiological conditions compared to DTPA is of huge importance, especially for applications in in-cell NMR measurements. For NMR measurements even higher stabilities are required as the experimental time is usually longer compared to MRI.

A.1.10 DOTA-M8: An extremely rigid, high-affinity lanthanide chelating tag

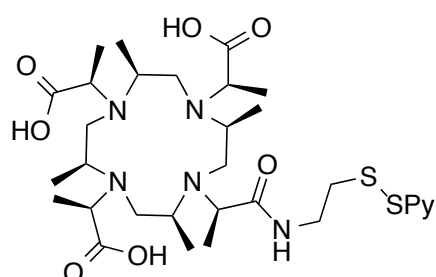


Figure A-8: (4*R*,4*S*)-DOTA-M8-SPy

The Häußinger group developed an extremely sterically demanding DOTA derivative.²⁵ The cyclen core was in this case four times stereospecifically methylated to yield (4*S*)-M4-cyclen. The use of natural *L*-lactic acid yielded an (4*R*,4*S*)-DOTA-M8 tag whereas the unnatural *D*-lactic acid led to a (8*S*)-DOTA-M8 tag. The introduction of this steric bulk

was performed in order to deliver one single stereoisomer. For DOTA molecules four different stereoisomers were obtained which were formed due to side arm rotation (Λ , Δ) and ring inversion (λ , δ) yielding $\Lambda_{\lambda\lambda\lambda\lambda}$, $\Lambda_{\delta\delta\delta\delta}$, $\Delta_{\lambda\lambda\lambda\lambda}$, $\Delta_{\delta\delta\delta\delta}$ complexes. The tag was attached with a single disulphide bridge to a cysteine residue (single point mutation) located on the protein surface. This DOTA derivative contains therefore a strongly hydrophilic as well as a strongly hydrophobic part.

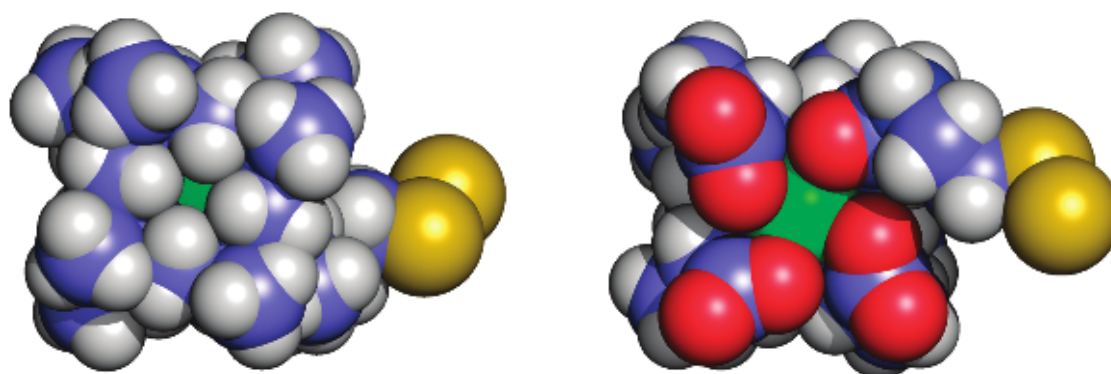


Figure A-9: Representation of DOTA-M8 hydrophobic side (left) and hydrophilic side (right).

Depending on the protein surface one of the two sides of the tag can induce stronger interactions and therefore binds with this specific side. This tag showed strong PCS and RDC values and is therefore a good starting point for further investigations.

Nevertheless, it should be mentioned that also in this case two species with different populations were detected. A cis/trans isomerization of the amide linker is the most likely explanation for this phenomenon.

A.2 Research Goal

The structural analysis of proteins and their inhibitor complexes remains still complicated. Measurements of protein-protein complexes by X-ray give information about the interaction site. However, the description of cellular activity remains inaccurate in the absence of physiological conditions. Measurements like FRET are quite useful for fluorescent proteins or fluorescently labelled proteins. NMR spectroscopy is one of the methods that can deliver high molecular resolution under conditions close to the physiological ones. The elucidation of protein-protein or protein-ligand interactions requires long-range information. In most cases long-range information is the limiting factor for accurate structure determinations. NOESY^{44,45} experiments deliver powerful information of distances through space, but their fast decay (r^{-6}) allows only investigations up to 5 Å. In many cases this is not enough to determine inter-protein interactions and therefore other techniques are required. Pseudocontact shifts (PCS) can offer such information as their intensity decays slower (r^{-3}) and distances up to 60 Å become accessible. To measure PCS a paramagnetic metal has to be placed on the surface of the molecule investigated in a rigid and specific way. DOTA frameworks especially DOTMA based metal chelating tags can deliver such rigid building blocks.

For all so far reported DOTA complexes the side chain donors were oxygen atoms from carboxylic acids or amides. The donors are therefore quite symmetric and deliver similar electron density to the metal core. Changing the side chain donor atoms could influence the χ -tensor anisotropy, as different electron densities are transferred to the metal from different fixed positions. Measurements of biological active molecules should be performed in native conditions to avoid structural changes. The PCS measurements presented so far were performed in buffered solutions. This environment is close to the native but still differences were present. Under physiological conditions a strong reduction potential is obtained which would cleave the disulphide bridge used to attach the tag on the protein surface. Only one case, using click chemistry to bind the tag on the protein surface, matches this stability problem.⁴⁶ The main problem of this technique is the use of an unnatural amino acid, which limits the preparation of the protein. The high affinity and the kinetic inertness of DOTA-M8 compared to DOTA-M0 make them better candidates for *in vivo* measurements as no metal release is expected.

The goal of this thesis was therefore to improve the previously reported DOTA-M8²⁵ tag. The development of a linker suitable for measurement under physiological conditions without using unnatural amino acids in the protein sequence to allow the investigation of PCS in living cells should be developed. This would, indeed, represent the first possibility to use NMR spectroscopy to investigate protein-protein or protein-ligand interactions *in vivo*.

A.3 Methods and Materials

Chemicals were used as purchased and used without further purification if not stated differently. Technical dichloromethane was distilled prior to use. For purification of cyclen derivatives only HPLC grade solvents were used.

All NMR data were acquired on Bruker NMR spectrometer using an Avance III console. The 250 MHz NMR data were recorded on a BBFO⁺ 5 mm probe head with Z-gradients. For carbon experiments the delay *d1* was set to 2 seconds. 400 MHz NMR data were recorded on a BBFO⁺ 5 mm probe head with Z-gradients. 500 MHz NMR data were recorded on a BBI 5 mm probe head. 600 MHz NMR data for cyclen derivatives and side chains were recorded on a BBFO⁺ 5 mm probe head. Metal complexes were measured in D₂O using a shigemitsu tube. For protein NMR measurements a TXI inverse 5 mm probe head was used.

Protein samples were additionally measured on a 600 MHz Avance III HD spectrometer using a cryogenic QCI probe head.

All protein samples were measured in 100 mM phosphate buffer in shigemitsu tubes. The pH was adjusted to values stated in the experimental section. The protein GB1 (T53C) was used as test-protein for the new lanthanide chelating tags. The purified protein was received from Dr. François-Xavier Theillet (FMP Berlin).

A NMR structure of GB1 was available from the SDBS-database allowing the chemical shift assignments by comparison.

HCAII mutants obtained from the group of Prof. Tom Ward in Basel were also used for the identification of linker candidates.

ESI-MS spectra were recorded on a Bruker Daltonics esquire 300 plus spectrometer. Solutions of concentration between 1-10 µg/mL in methanol, acetonitrile or acetonitrile/water/TFA mixtures were introduced to the spectrometer with a flow rate of 1µL/min.

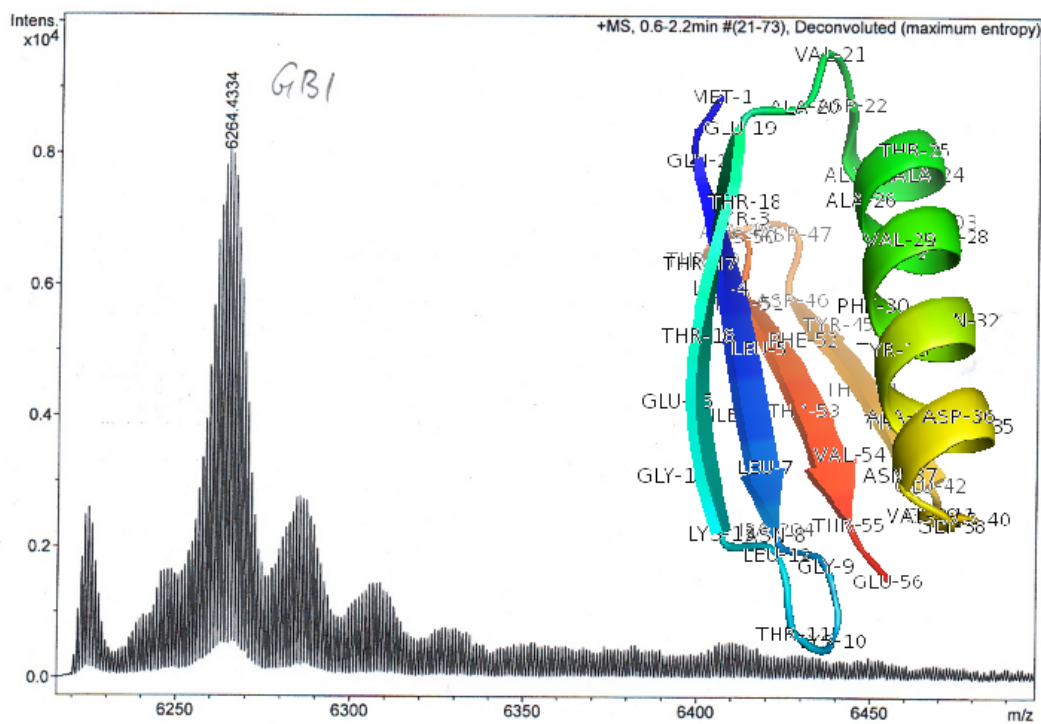


Figure A-10: ESI-MS-spectrum and structure of GB1 used for the investigations of new lanthanide chelating tags.

A.4 Synthetic strategy

A.4.1 Synthetic strategy for DOTA-M7 acetophenone (A1)

The title compound **A1** can be synthesized starting from (4S)-M4-cyclen. First introduction of protected lactic acid based side chains allows the selective introduction of the linker on the unfunctionalized M4-cyclen nitrogen.

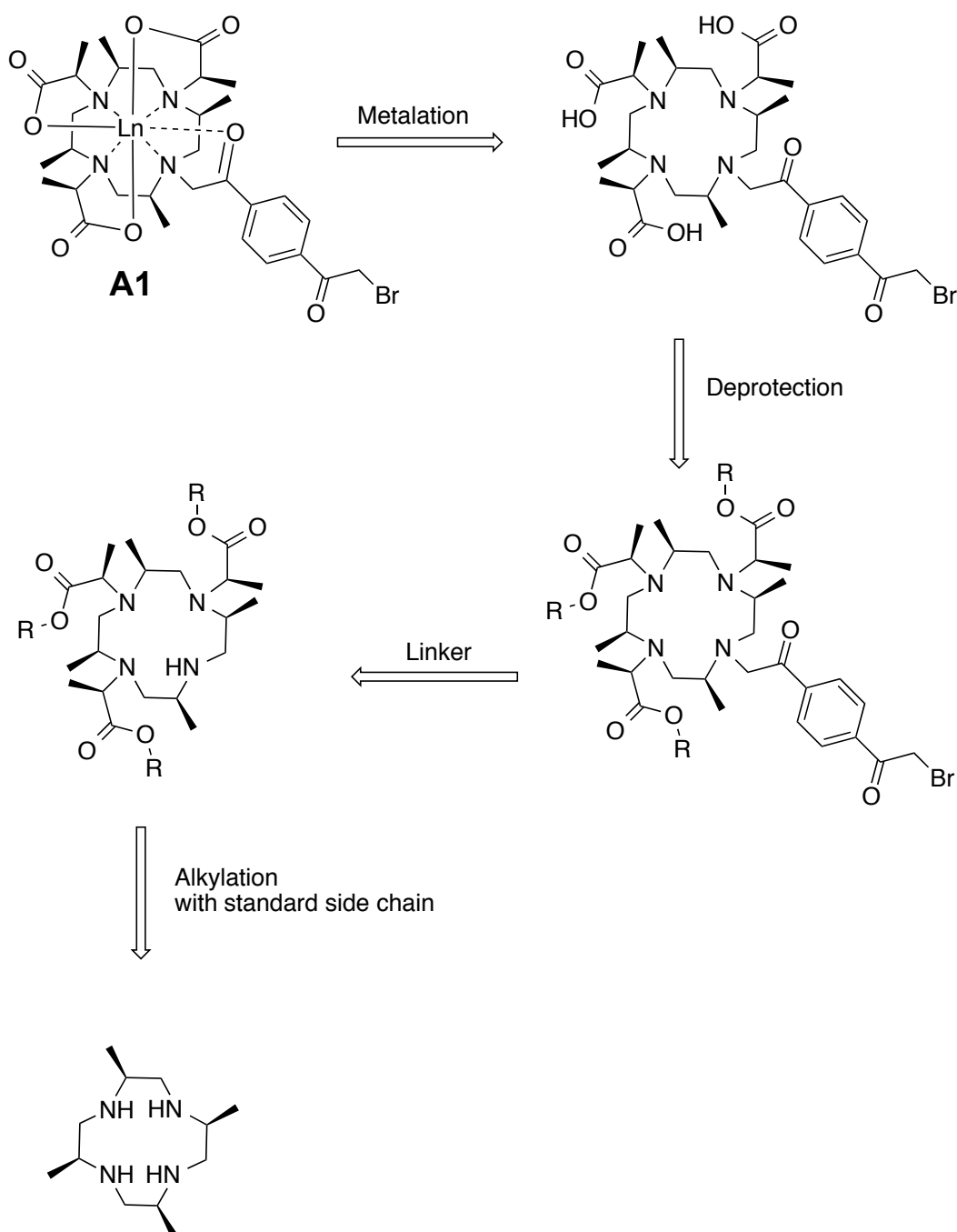


Figure A-11: Retrosynthetic analysis of DOTA-M7-acetophenone (**A1**).

The introduction of the linker has to be performed as last alkylation step due to the two reactive sites of the linker. The remaining free nitrogen is also less reactive. This

fact, in combination with the present steric bulk prevents side reactions like dimerization. Acid deprotection is performed, allowing the introduction of the lanthanide ion to form complex **A1**. Different possibilities for the synthesis of the acetophenone-based linker are presented in Figure A-12. The synthetic route shown in black delivers the symmetric 1,1'-(1,4-phenylene)bis(2-bromoethan-1-one) as precursor.

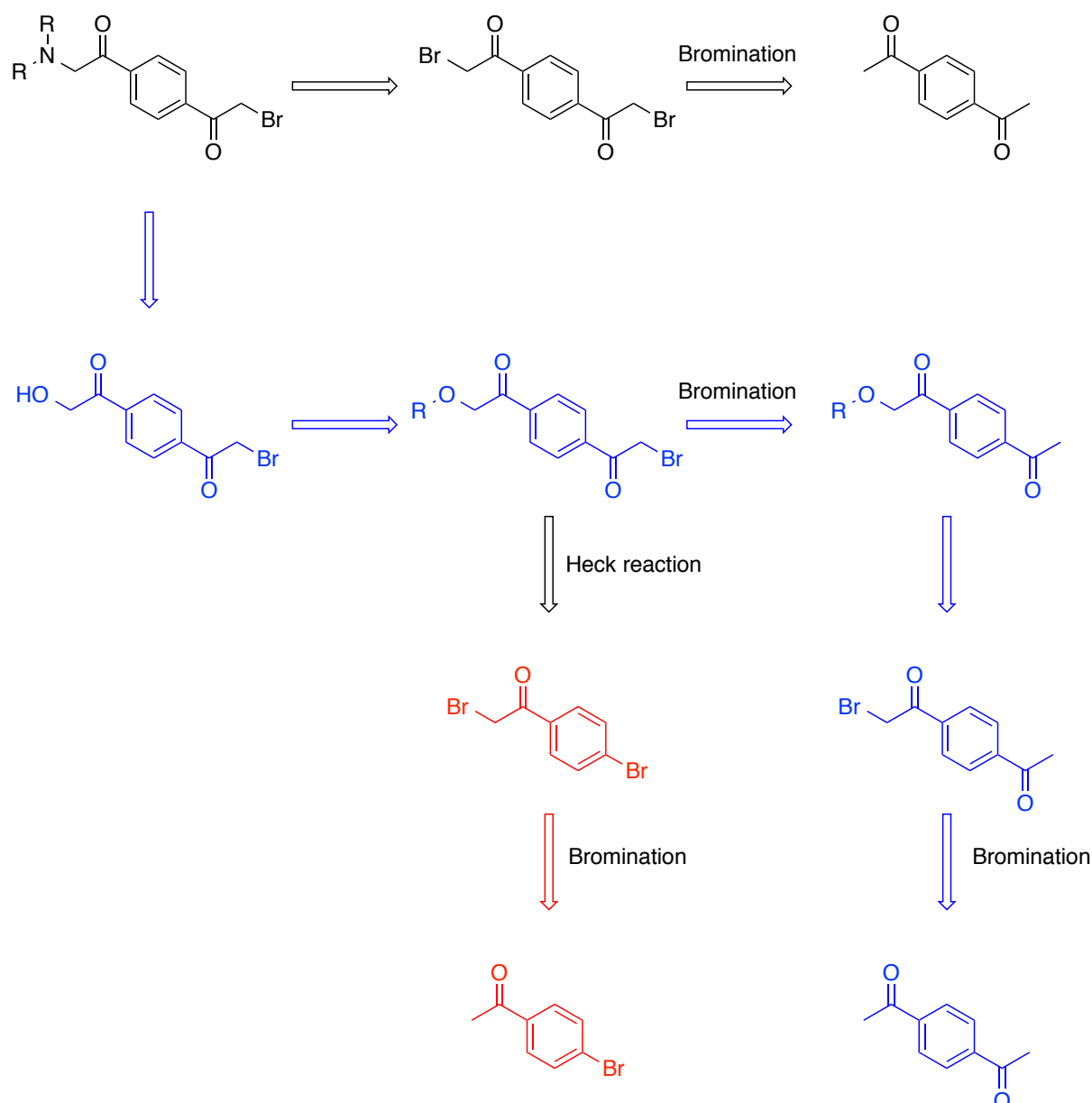


Figure A-12: Retrosynthetic analysis of an acetophenone based linker, on top symmetric precursor 1,1'-(1,4-phenylene)bis(2-bromoethan-1-one) followed by two different more selective ways presented on the bottom. In blue, a more selective route is shown. A hydroxyl moiety is introduced followed by bromination on the other side allowing selective coupling to the cyclen moiety. In red, an even more selective way is presented which allows the use of Heck reactions before or after addition to the cyclen moiety.

The advantage of this strategy is the reduced number of steps and the easy preparation. The use of a statistical reaction for the coupling to the DOTA-M7 and the possible dimer formation leading to unwanted side products is the main disadvantage of this strategy.

The strategy presented in blue shows a more selective way that allows the introduction of a better leaving group such as triflate, tosylate or mesylate. On the other hand it would also be possible to protect the hydroxyl group and therefore allow the selective reaction with the M4-cyclen. This strategy permits the introduction of this linker in the first step where the reactivity of the nitrogen is enlarged and less steric bulk present. The reaction sequence in red allows also selective coupling to the M4-cyclen moiety. All pathways can be performed in a similar way for 1,3 instead of 1,4 di-substituted aromatic rings delivering different geometries of the linker.

A.4.2 Synthetic strategy for DOTA-M7/8-thiovinylsulfone (B1, B1a)

For the synthesis of DOTA-M7/8 the retrosynthetic analysis is presented in Figure A-13. In this case, the introduction of the linker side chain can be performed in the first step as the thiol can be introduced in a protected way preventing side reactions. The acid labile protecting-group allows the removal of all protecting groups in a single step. Alternatively, the introduction of orthogonal protecting groups on the different side chains leads to selective cleavages. The introduction of the vinyl sulfone is thiol specific and requires therefore no special considerations.

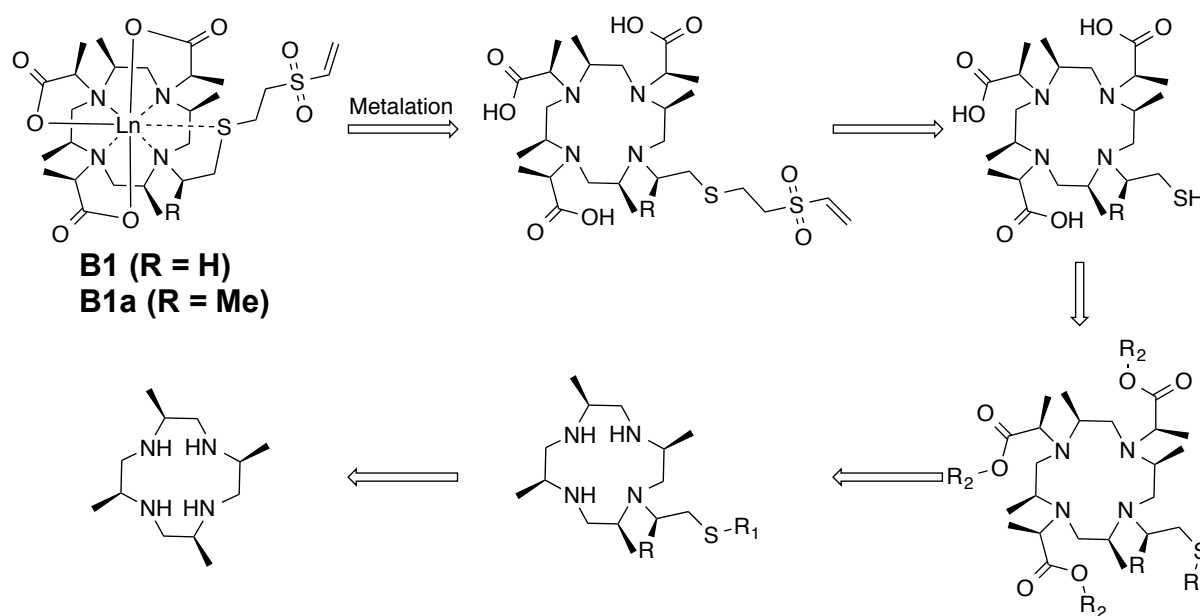


Figure A-13: Retrosynthetic analysis of DOTA-M7/8-thiovinylsulfone.

Different synthetic pathways for the introduction of the thiol containing side chain are shown in Figure A-14. Simple introduction of a thiol in a statistical reaction of potassium thioacetate with 1,2-dibromoethane delivers the side chain precursor.

For the synthesis of the M8-macrocyle **B1a** the situation is more complicated. There are three possible routes presented. The one shown in black presents a similar reaction pathway than used for the synthesis of **B1**. The complete side chain is synthesized before it is attached to the M4-cyclen core. The synthetic strategy presented in red is performed mainly on the macrocycle. The reaction sequence is quite similar to the one shown in black but less protecting groups are required. The number of steps is therefore drastically reduced. The synthetic strategy drawn in blue counts the most steps. The introduction of a protected alcohol allows the introduction of all other side chains before the sulphur is introduced. This is the main advantage to the strategy drawn in red where the alcohol has to be modified on the macrocycle before the other side chains can be introduced. The free alcohol can be easily converted into a good leaving group. Different nucleophiles can be introduced to the system in a late stage, leading to a highly flexible synthetic strategy.

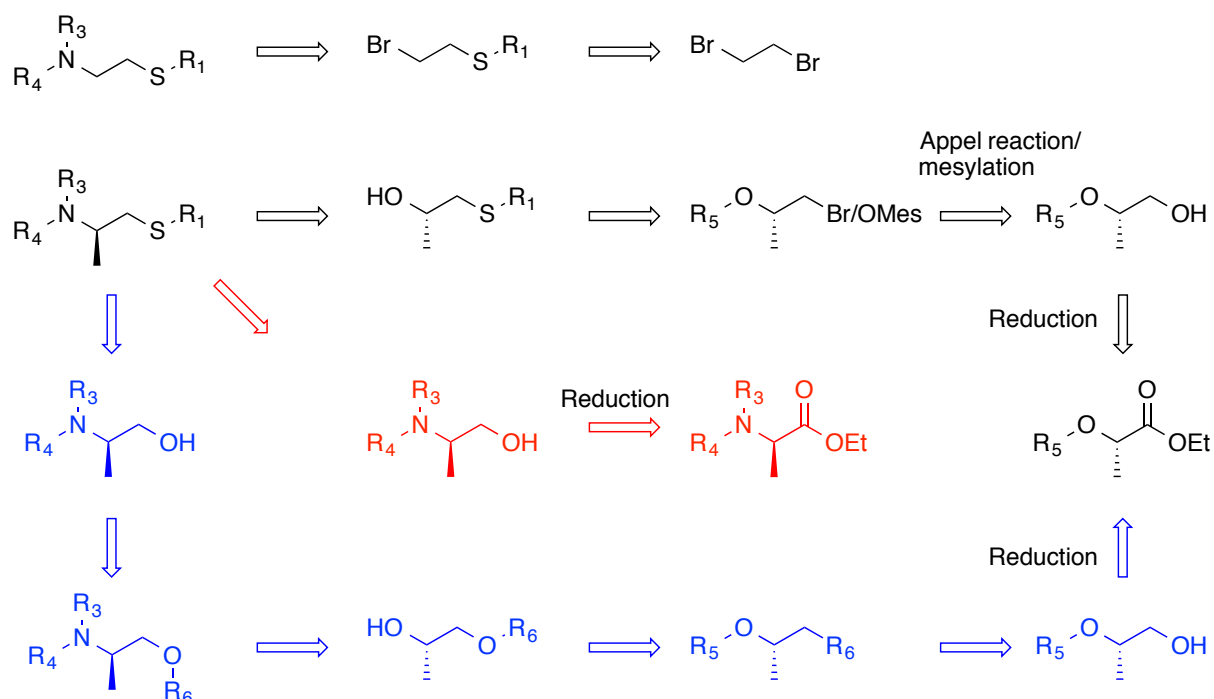


Figure A-14: Retrosynthetic analysis of side chains required for the synthesis of **B1** and **B1a**.

A.4.3 Synthetic strategy for DOTA-M8- α,β -unsaturated ketone (C1)

The synthesis towards an α,β -unsaturated side chain can be performed in two principle reaction pathways as shown in Figure A-15.

Classical Weinreb chemistry is shown in black. Grignard reagents are used to selectively introduce the vinyl moiety. A statistical approach is drawn in blue. The symmetric DOTA-M8 is functionalized with one equivalent of the nucleophile in a statistic manner. The main advantage of the blue strategy is the reduction of synthetic steps.

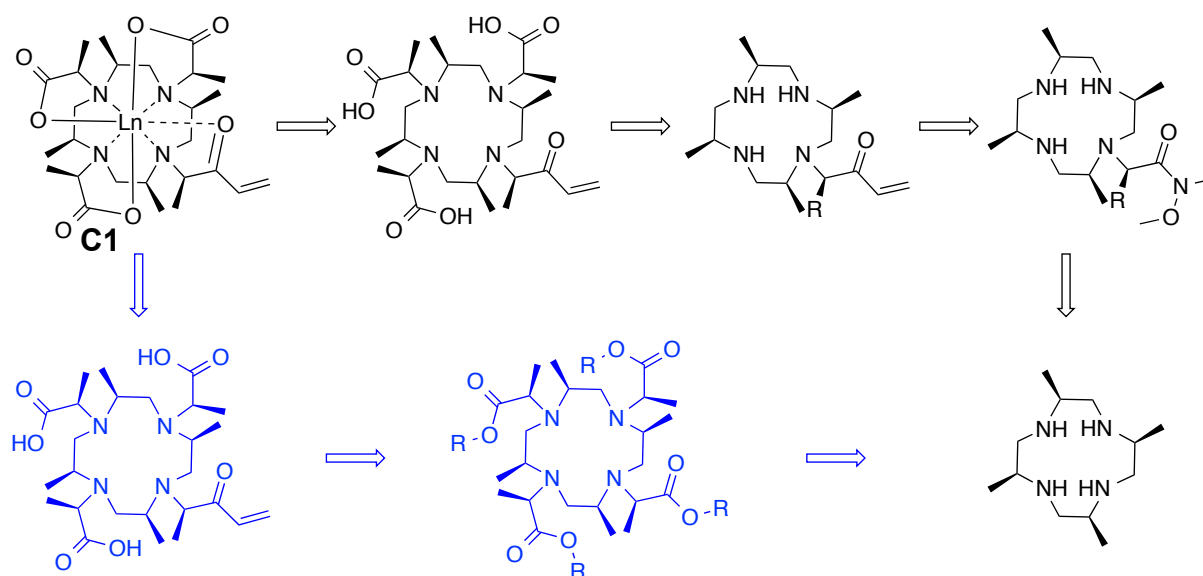


Figure A-15: Retrosynthetic analysis of DOTA-M8- α,β -unsaturated ketone.

The formation of the Weinreb amide can be performed in one single step starting from commercially available *L*-lactic acid ethyl ester.

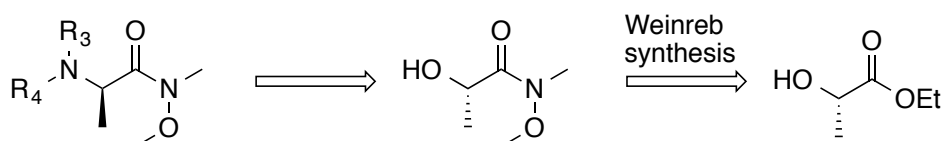


Figure A-16: Retrosynthetic analysis of the Weinreb side chain.

A.4.4 Synthetic strategy towards DOTA- M8-amino (D1)

The strategy towards the synthesis of a side chain containing a nitrogen atom as donor is similar to the DOTA-M8 synthesis reported earlier with the difference that the amide nitrogen and not the amid oxygen forms the five membered ring by coordination to the lanthanide metal.

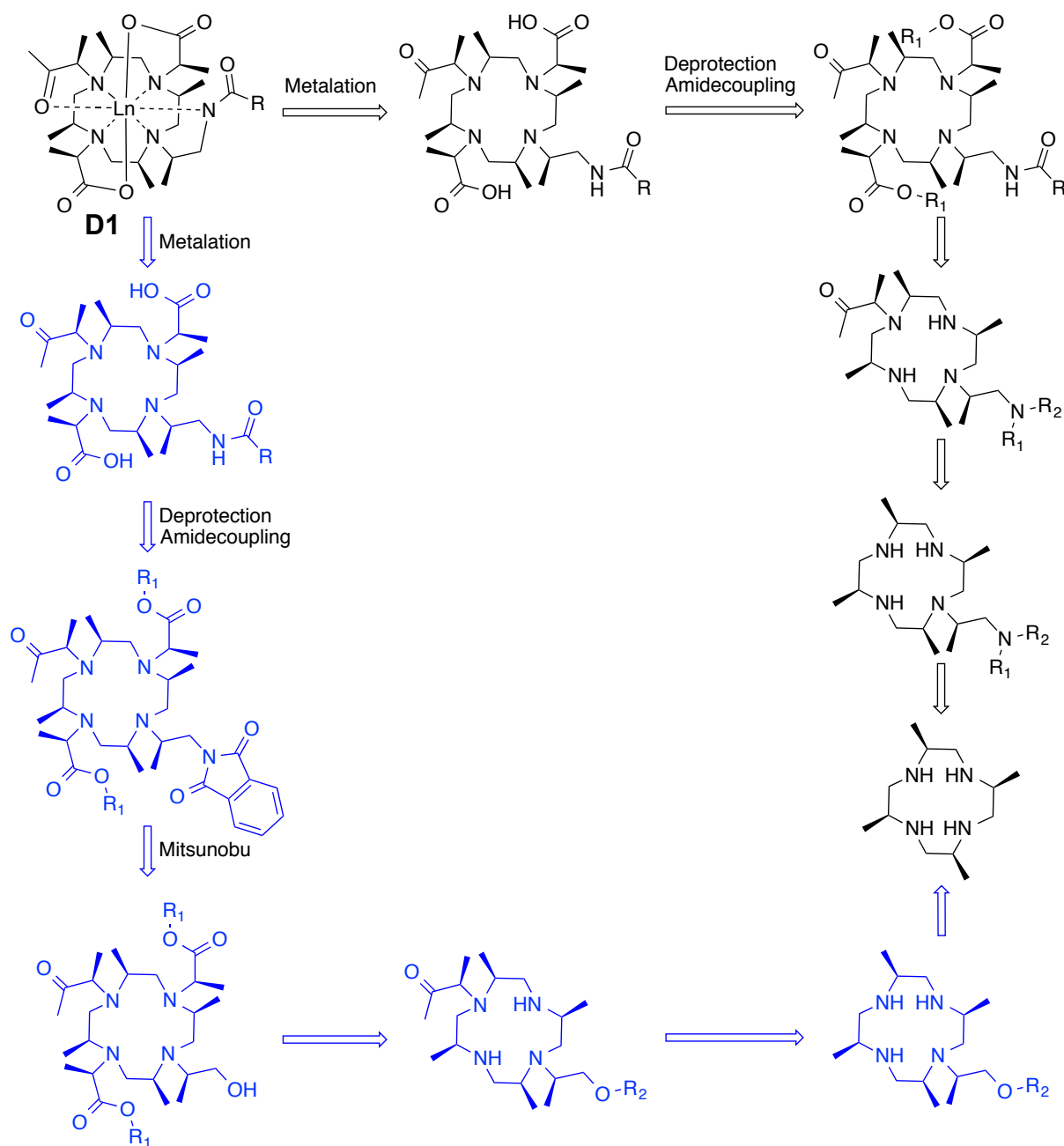


Figure A-17: Retrosynthetic analysis of DOTA-M8-amino.

On the other hand an amine linker can be created instead of an amide linker by the reaction with an alkyl halide. The route drawn in black allows the conversion of the amine to the linker in a late stage of the reaction pathway. Compared to the so far presented macrocycles, three different side chains are required to prevent the formation of a charged metal complex. For this reason a ketone in place of a carboxylic acid is used. In Figure A-17 only the complex where the amine and ketone functionality are *para* to each other is drawn. In general, both different *ortho* complexes are possible and accessible in a similar way.

The amine functionality is added in a protected way in the first step (black route) followed from the keto-side chain. This led to the formation of the *para* complex as main product (steric and electronic effects). Another possibility is again the introduction of an protected alcohol functionality. The nitrogen can be introduced after deprotection of the alcohol using Mitsunobu coupling conditions. All other steps are similar to the black route.

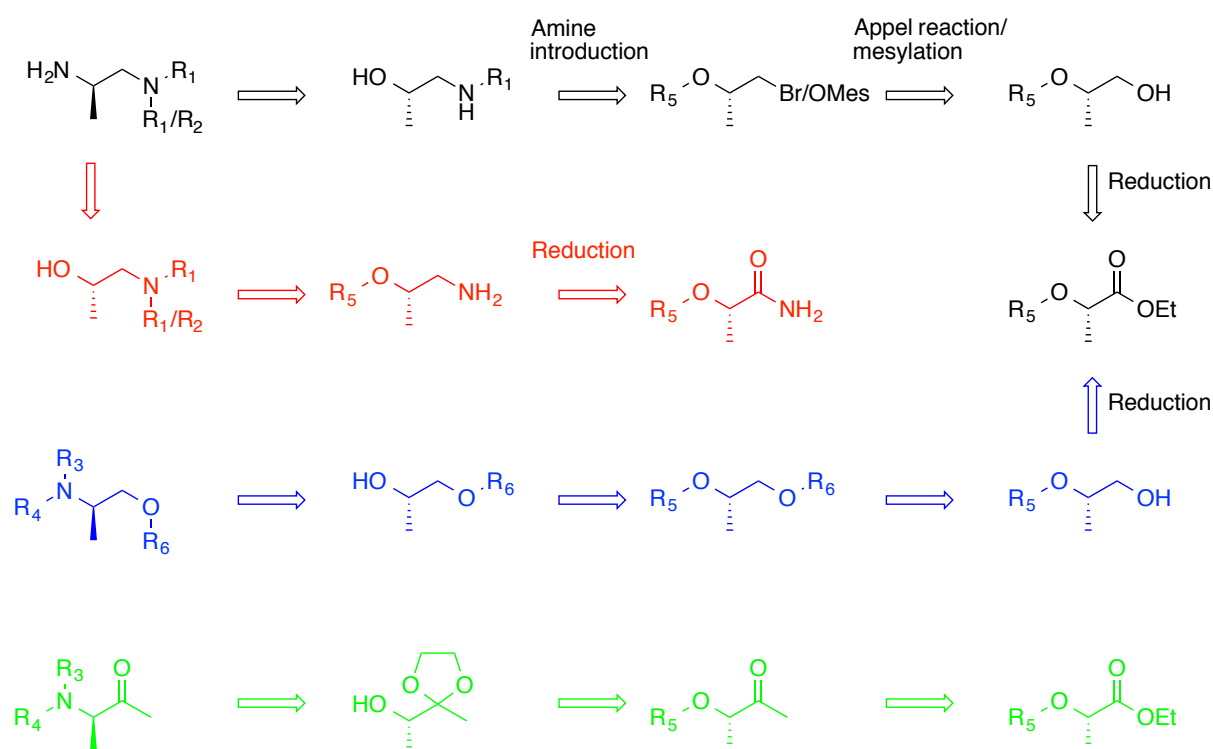


Figure A-18: Retrosynthetic analysis of the side chains required for DOTA-M8-amino.

The different synthetic strategies towards the side chains for **C1** are presented in Figure A-18. The black route illustrates the synthesis starting from *L*-lactic acid ethyl ester, which is an inexpensive precursor. After reduction to the alcohol a leaving group has to be generated. Appel reactions transforming the alcohol into bromide are useful in this case. Unfortunately, they are not atom efficient. An alternative would be the use of mesylate, tosylate or triflate as good leaving groups. They can easily react with different types of amine nucleophiles. The protected amine is then attached to the M4-cyclen moiety. The route drawn in red shows a more elegant way to synthesize the amine side chain starting from *L*-Lactamide. The reduction of reaction steps makes this route attractive. The route drawn in blue deals with a similar protocol as shown for DOTA-M8-thiovinyl. The introduction of the protected alcohol requires functionalization of the alcohol on the cyclen moiety.

A.5 Results and Discussion

Four target molecules **A1**, **B** (**B1**, **B1a**), **C1** and **D1** (Figure A-19) were suggested as alternative to DOTA-M8. These molecules have linkers that are stable under reductive conditions. All form a thioether through the reaction with a single cysteine on the protein surface.

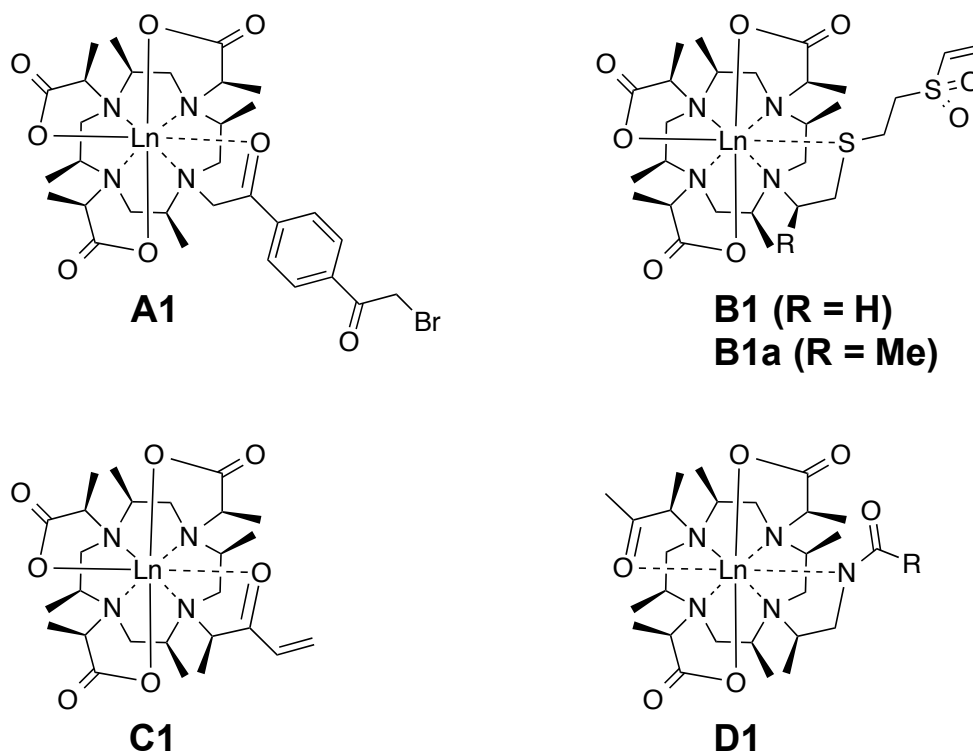


Figure A-19: Target molecules as candidates for PCS reagents using a reductive stable linker and different heteroatoms as donors.

A.5.1 Investigation of acetophenone based linkers.

Target molecule **A1** was synthesized in two different forms, namely DOTA-M0-acetophenone and DOTA-M7-acetophenone. The M0 version was synthesized as model molecule to test the linker for its ability to bind to the protein surface and to optimize the reaction conditions. Nevertheless, huge differences in the reactivity between M0 and M7 were obtained due to steric effects that made substitution reactions for M7 more challenging. Therefore, these reactions were not performed for all other target molecules, as the M0 version was not suitable for PCS measurements (formation of $\Lambda_{\lambda\lambda\lambda}$, $\Lambda_{\delta\delta\delta}$, $\Delta_{\lambda\lambda\lambda}$, $\Delta_{\delta\delta\delta}$ complexes) as the high flexibility of the backbone led to averaging of the PCS. Nevertheless, the M0-analogue could be successfully attached to GB1-T53C as shown in Figure A-20. The resulting ^{15}N - ^1H -

HSQC-spectrum (Figure A-21) shows that some of the peaks are doubled. The origin of these two species is most likely the formation of a Λ - and a Δ - form of the complex.

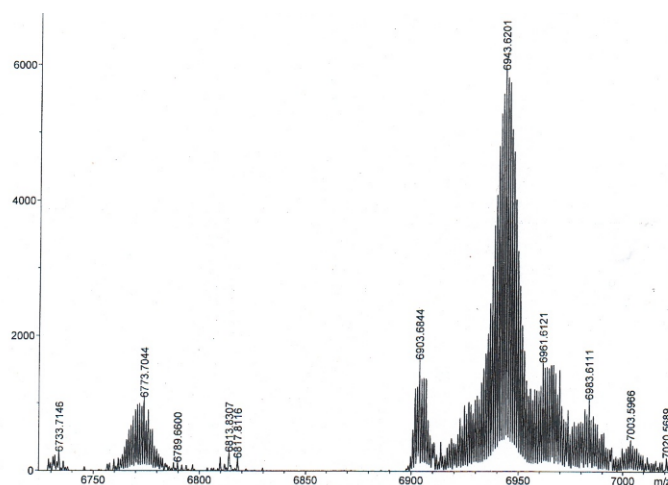


Figure A-20: ESI-MS spectra of Lu-DOTA-M0-acetophenone with GB1-T53C.

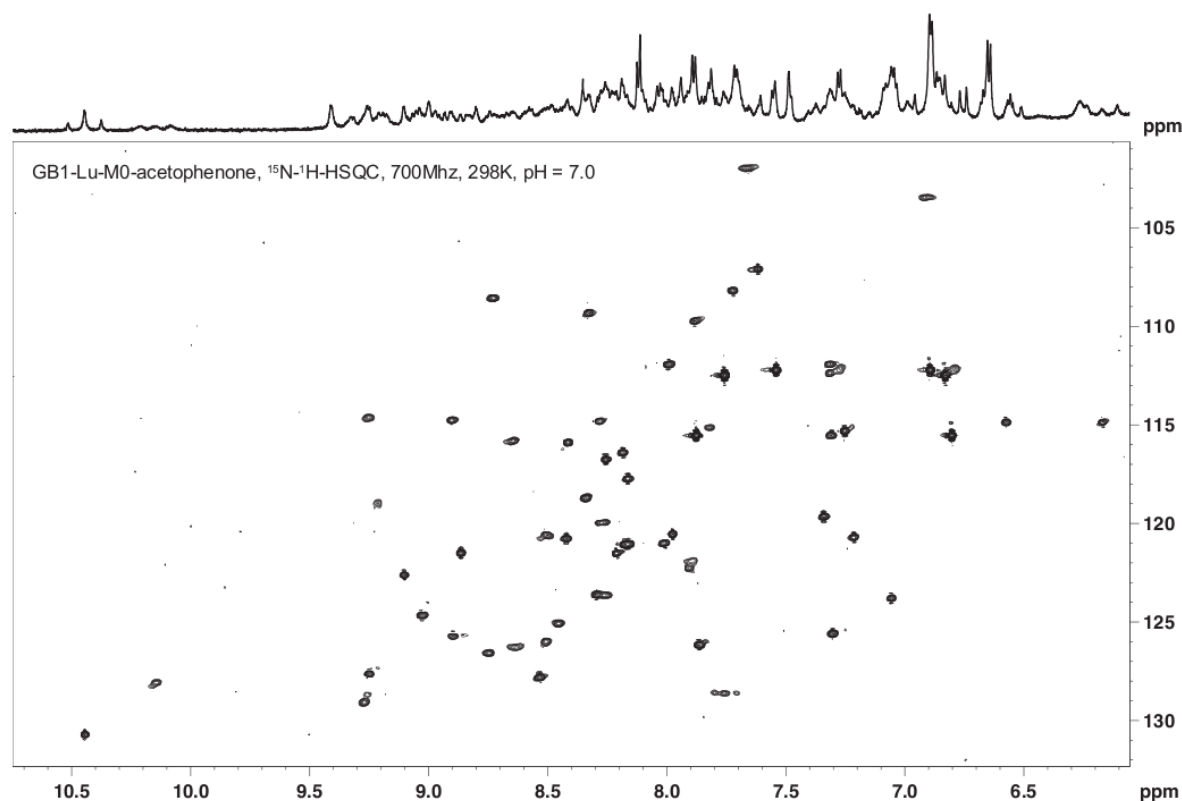


Figure A-21: ^{15}N - ^1H -HSQC spectra of GB1-T53C in complex with Lu-DOTA-M0-acetophenone.

The synthesis of **A1** was performed according to the retrosynthetic analysis (Figure A-12) in different ways. The optimized scheme is presented in Figure A-22. Molecule **A2** can be synthesized efficiently using dichloromethane as solvent, this stopped the reaction after the addition of three side chains. Some of the starting material contained two side chains. Separation of these two macrocycles was performed

successfully. Different protecting groups namely *tert*-butyl and benzyl were tested. As low yields were obtained for the deprotection of the *tert*-butyl protecting group, benzyl protection was preferred. The deprotection using palladium on carbon under 5 bar H₂-pressure (used for DOTA-M8) removed the protecting-groups quantitatively but also reduced one of the keto-groups to a CH₂-group.

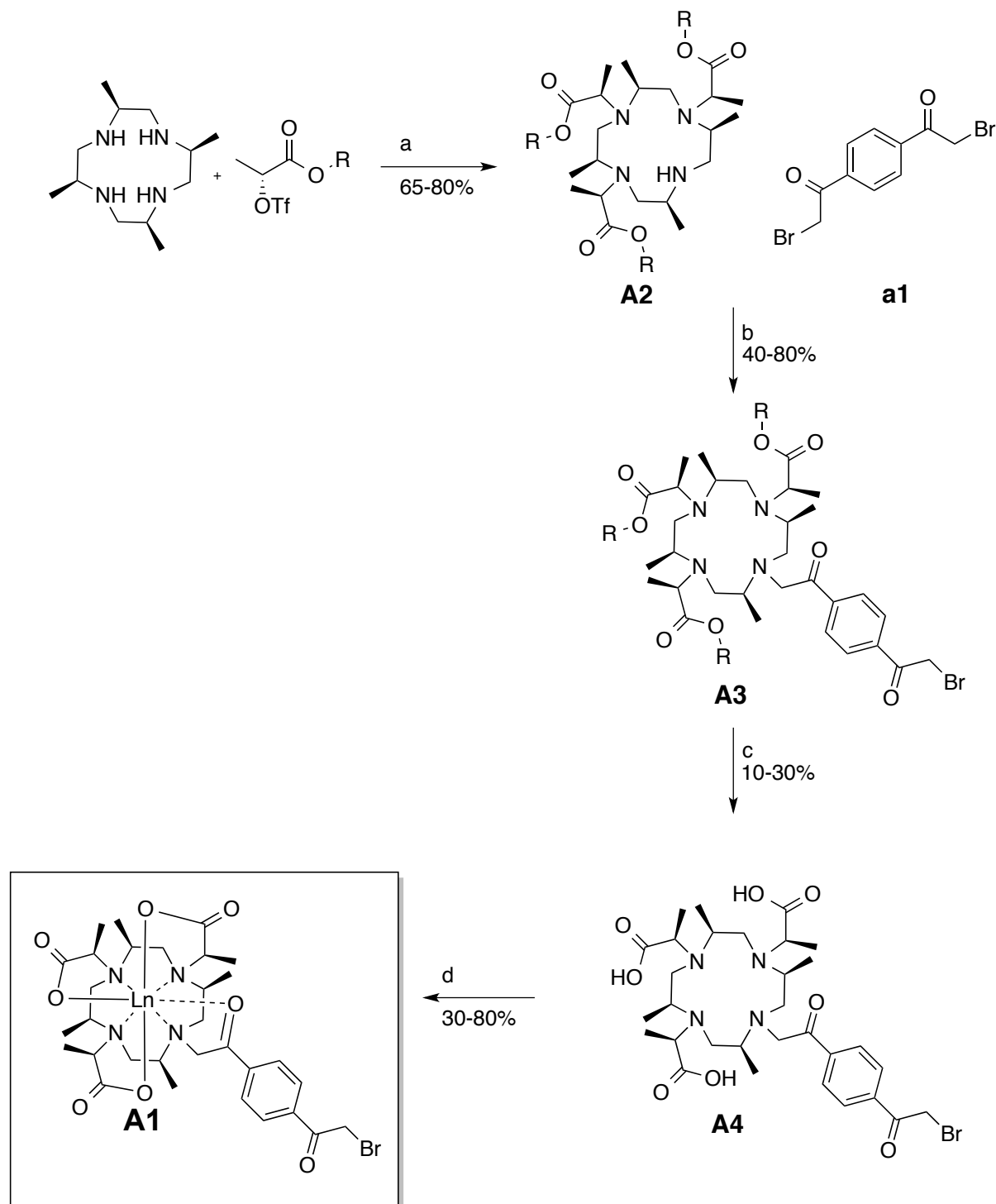


Figure A-22: Synthesis of macrocycle A1: a) K₂CO₃, DCM, rt, 28h (65% for R = Bn, 80 % for R = ^tBu); b) NaH (60%), MeCN, 40 °C, 3h (40% for R = Bn, 80 % for R = ^tBu); c) R = ^tBu => TFA, rt, 3h, 10-30 %; R = Bn => Pd/C, EtOH, 5 bar, 2h 0%; d) TmBr₃, DIPEA, H₂O, rt, 1h.

The two reactive sites of the linker made its introduction to the macrocycle challenging. To prevent bridging, the three other side chains were introduced first. Introduction of the linker to the M0-derivative worked well using potassium carbonate as base. However, the attachment of the linker to DOTA-M7 using potassium carbonate as base delivered low yields. Therefore four different bases were tested as shown in Table A-3.

Table A-3: Base screening for the attachment of the acetophenone linker to DOTA-M7.

Base	Reaction temperature	Yield
K ₂ CO ₃	rt. - 40 °C	30%
Cs ₂ CO ₃	40 °C	32%
NaHCO ₃	40 °C	65%
NaH (60 %)	40 °C	40-90%

The base screening showed clearly that sodium hydride and sodium bicarbonate improved the yield. Nevertheless, the reproducibility of the reaction was bad and therefore other reactions were tested to introduce the side chain more efficiently. The easiest way to get a better leaving group is to replace the bromide (**a1**) by an iodide (**a2**) using a simple Finkelstein reaction, which was successfully performed in 80 % yield. Test reactions of the di-iodo compound (**a2**) showed that the iodine moiety was not selective for the coupling to a free cysteine moiety.

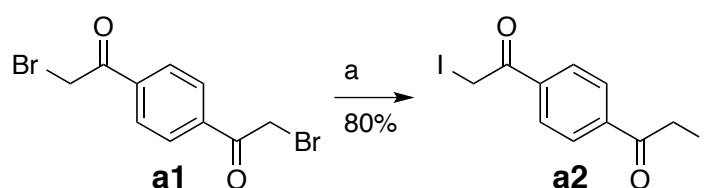


Figure A-23: Finkelstein reaction: a) NaI, tetrabutylammonium bromide, H₂O, rt, 2h.

Further attempts to develop an asymmetric linker were performed. For instance, a hydroxyl group on one side and a bromide on the other side should allow the formation of a better leaving group such as tosyl or triflate. The synthesis of these compounds was challenging. The literature reported α -hydroxylations did not work in our case, therefore a mono bromination was done. Microwave conditions were used to transform the bromide selectively into a hydroxyl group. Selective bromination on the other side failed in the case where the hydroxyl group was protected and without protection the hydroxyl group was transformed back to a bromide. The reaction of **a1**

with a hydroxyl nucleophile in a statistical reaction delivered the desired asymmetric compound in poor yield. Tosylation was performed in moderate yield, however, the reaction with the DOTA-M7 (**A2**) was not successful. The steric bulk of the tosyl group probably blocked the reaction. The more reactive triflates were not stable.

The steric bulk of DOTA-M7 (**A2**) in combination with the low reactivity of the α -bromo ketones towards nitrogen concluded that the linker should be attached first. The strategy drawn in red (Figure A-12) allows the introduction of the linker in the first reaction step. This is favourable as the reactivity of the unfunctionalized M4-cyclen is much higher. Therefore different test reactions were performed to explore the synthesis of compounds **a5** and **a6**. Unfortunately, no suitable reaction conditions for the Heck reaction could be found.

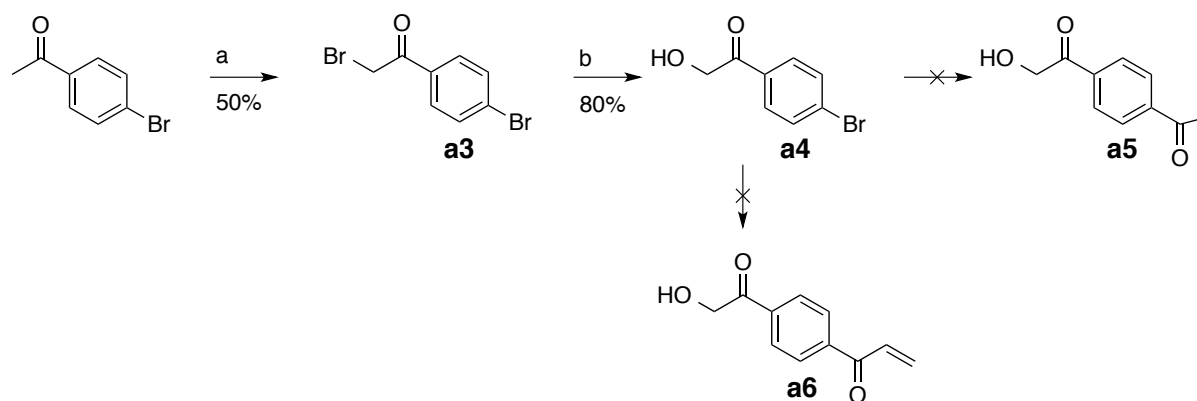


Figure A-24: Synthetic trials for the introduction of an asymmetric highly reactive linker to allow selective coupling reactions. a) Bromine, AcOH, 95 °C, 1h; b) H₂O, microwave, 125 °C (5bar) 25 min.

The influence of the hydroxyl group in the Heck reaction was investigated by changing the starting material to the bromine and the unfunctionalized starting material. In none of the investigated molecules suitable reaction conditions could be found. The potential linker was also coupled to morpholine to mimic the cyclen moiety but also in this case the Heck coupling did not work.

Another possible pathway is shown in Figure A-25. The introduction of the hydroxyl functionality was performed in a statistical reaction. The synthesis of compound **a7** as benzoyl and acetyl protected alcohol were performed in low yields of about 15-30%. One way would be the introduction of this linker to the unfunctionalized cyclen, but in this case the hydroxyl functionality has to be exchanged to the bromine on the final compound, which is a quite challenging task (already unsuccessful tested for the final compound). On the other hand the hydroxyl functionality can be converted into a good leaving group. The formation of the triflate **a9** was not successful. A synthesis

of the tosyl analogue could be performed but the reactivity was too low for functionalization of **A2**.

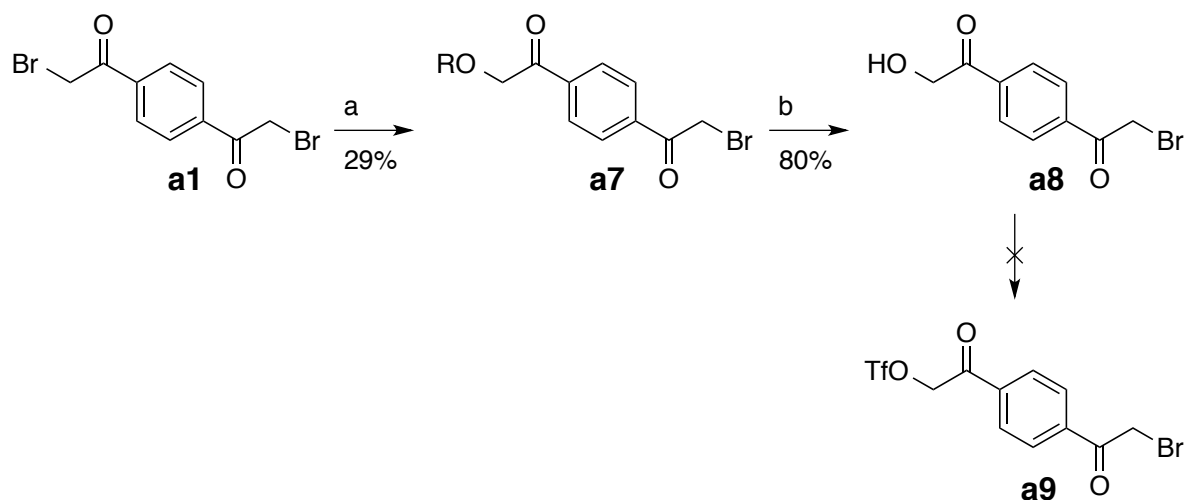


Figure A-25: Synthetic trials for the introduction of a single hydroxyl functionality in a statistical reaction. Conditions are presented for the benzoyl protection protocol: a) Benzoic acid, sodium, acetone, reflux, 5h; b) HCl (1M, aq.), ethanol, reflux, 5h.

Therefore, these asymmetric reaction pathways were abandoned and further reactions were performed using **a1** as linker. The cleavage of the *tert*-butyl protecting group using trifluoro acetic acid (TFA) yielded **A4** in 31% after HPLC purification. Different deprotection methods like sulphuric acid, hydrochloric acid have been tried with no improvement. Metalation of **A4** has been tried under standard conditions using $\text{LnCl}_3 \cdot 6\text{H}_2\text{O}$ in water, buffered with DIPEA to pH 8. Using this metalation procedure no product could be isolated. ESI-MS and HRMS indicated the formation of hydrolysed compound **A1a** and the chloro compound **A1b** as shown in Figure A-26. The Lewis acidity of the Lanthanide ion led to these side reactions. Reaction conditions were changed to $\text{Ln}(\text{OTf})_3 \cdot 6\text{H}_2\text{O}$ in dry acetonitrile to prevent high water concentrations, nevertheless the hydrolysed metal complex and only traces of the product were obtained. The fact that LnCl_3 delivered a 4:1 (**A1a/A1b**) ratio led us to the use of $\text{LnBr}_3 \cdot 6\text{H}_2\text{O}$ in water (LnBr_3 is insoluble in acetonitrile). The reaction time was cut down to 1 hour and the SepPak purification was performed as fast as possible to remove excess metal ions in order to prevent side reactions. The exchange of the hydrolysed linker back the brominated species using an Apple reaction was not performed successfully.

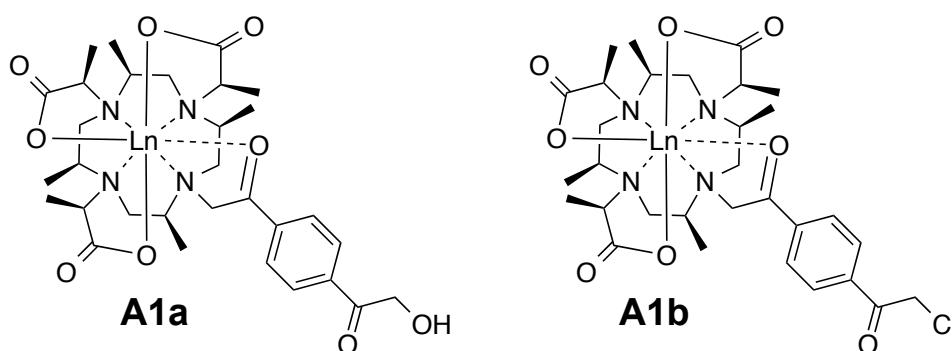


Figure A-26: Structure A1a hydrolysed linker, whereas structure A1b presents the exchange from bromine to chlorine.

The synthesis of the target molecule **A1** could be achieved in moderate yields. The standard side chain was synthesized in four linear steps (Figure A-54) as presented earlier.²⁵ The linker was synthesized in one step in moderate yield. The coupling conditions could be optimized for the linker by variation of the base. The macrocycle **A1** was synthesized in four linear steps using the two different side chains and standard deprotection procedure. The metalation was optimized to reduce hydrolysis side reactions.

The reaction of the metal complex in 10 μ M phosphate buffer at pH 7.0 with GBI was performed overnight in quantitative yield. Excess lanthanide chelating tag was removed by centrifugation using a 3 kDa cut off filter. The protein was washed with 50 μ M phosphate buffer and the pH was adjusted to 7.0 before NMR experiments were performed.

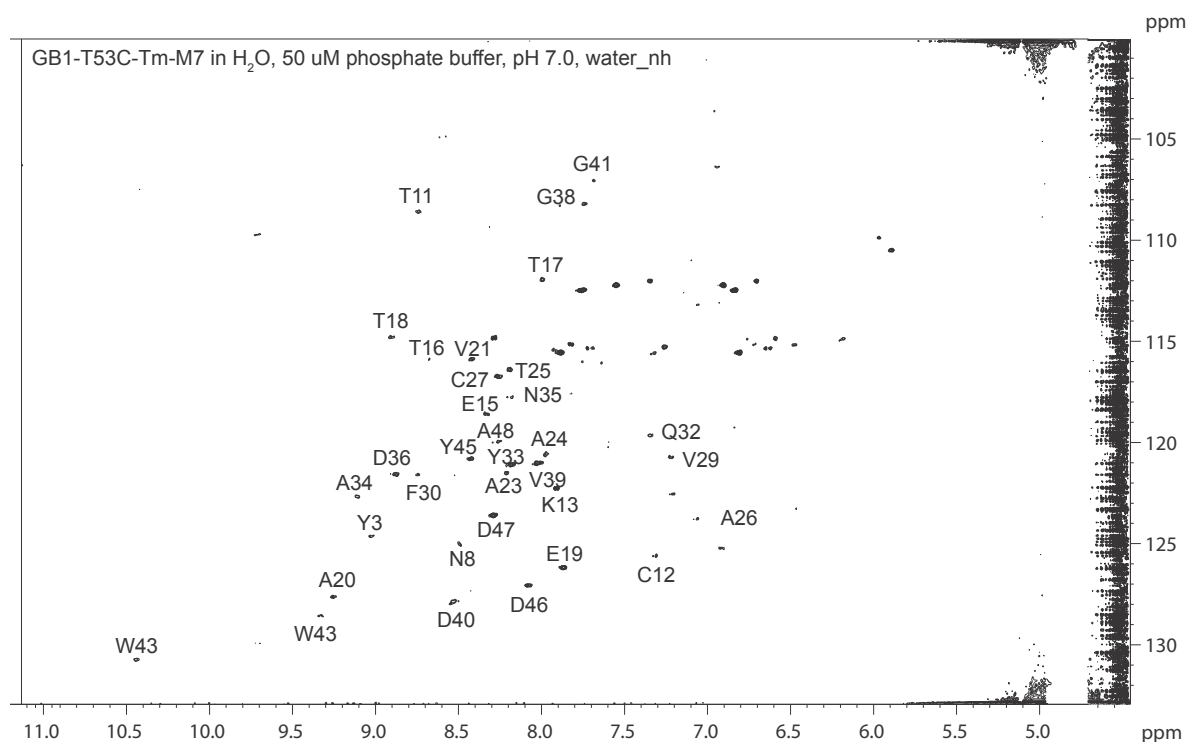


Figure A-27: GB1-T53C-Tm-M7 $^{15}\text{N}^1\text{H}$ -HSQC spectrum.

Figure A-27 shows the $^{15}\text{N}^1\text{H}$ -HSQC spectrum of GB1-DOTA-M7-Tm-acetophenone (GB1-A) and Figure A-28 shows the comparison of GB1-A with untagged GB1-T53C. Some resonances are bleached in the paramagnetic sample due to PRE effects. These resonances are close in space to the lanthanide chelating tag. The PCS obtained for the other resonances are quite weak. This means the flexibility of the tag is large and therefore averaging of the PCS can occur. It is possible that a linear linker is not flexible enough and prevents coordination of the tag with its hydrophilic or hydrophobic side to the protein surface.

All peaks are separated into two different signals (Figure A-27). The difference between the two signals is proportional to the distance from the tag to the influenced nucleus. This means that there are two stable conformers of this tag in solution. Different origins of this phenomenon are possible. One possibility is that the length of the tag is so long that interactions on two different sides become possible or that the tag itself forms two different isomers as one methyl group is missing. Too low PCS data give strong evidence that the complex itself forms two different stereoisomers and that the linker is too long leading to averaged signal intensity.

GB1-T53C-Tm-M7 (HEG-309) in H₂O, 50 μ M, phosphate, pH 7.0, water_nh

GB1-T53C in H₂O, 240 μ M, 2 mM DTT, pH 6.97, oneone, water_nh

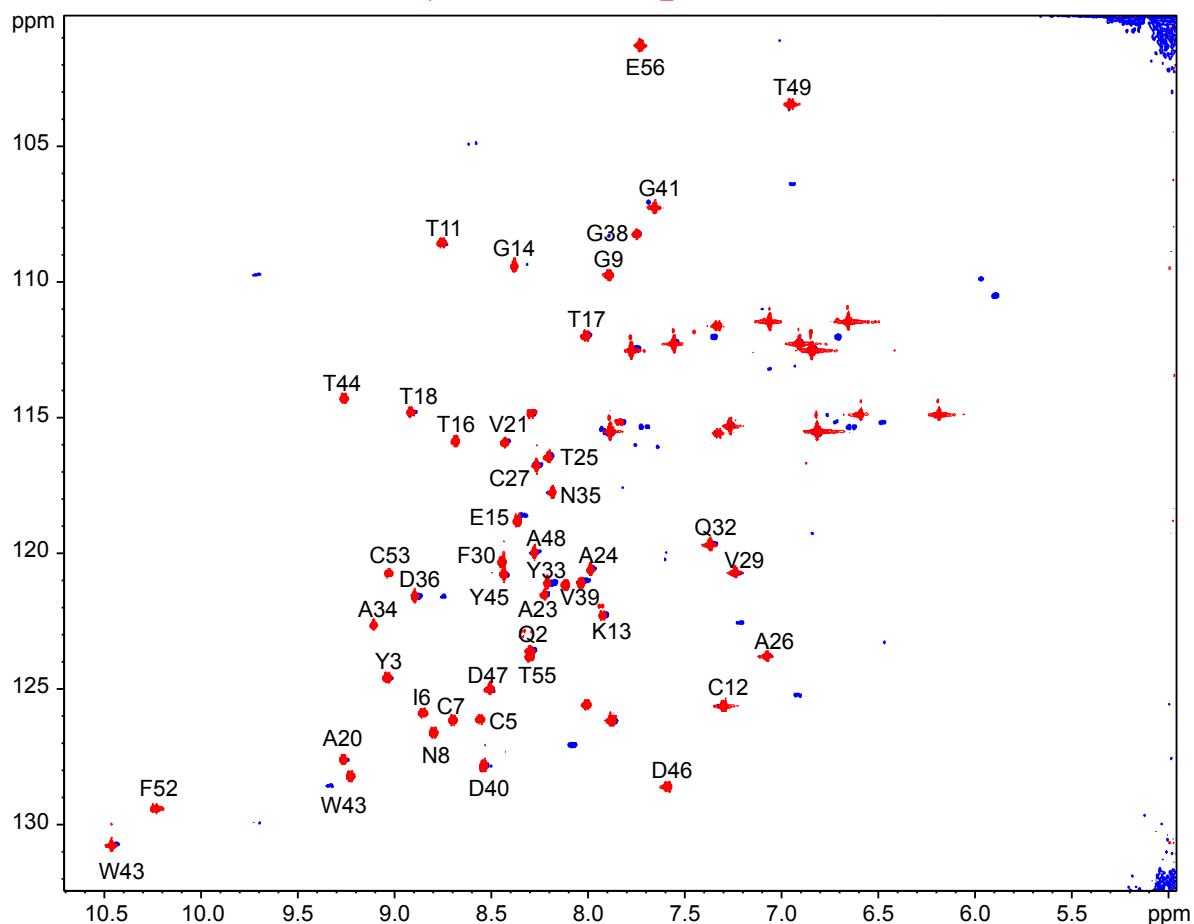


Figure A-28: Superimposed representation of GB1 with Tm-tag (blue) and without tag (red).

A.5.2 Using a thiol as donor atom in the linker.

Target molecule **B1** was synthesized in two different ways. The required sulphur side chain **b1** was synthesized in one single step using 1,2-dibromoethane and potassium thioacetate in a statistical reaction (Figure A-29). For reactions with DOTA-M7 a Finkelstein reaction was performed to increase the reactivity of the side chain (**b2**).

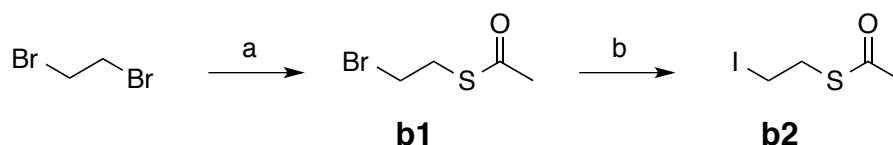


Figure A-29: Synthesis of sulphur side chain, a) KSAc, THF, reflux, 7h, 46%; b) NaI, acetone, rt, 2h, 80%.

The sulphur side chain (**b2**) was attached to DOTA-M7 (**A2**) in moderate yields of about 50% (starting materials could be recovered). Selective removal of the thiol protecting group was achieved using sodium thiomethoxide in methanol. ESI-MS

analysis showed dimer formation and S-SMe formation. To remove the resulting disulphide a huge excess of TCEP (2 mL (in 350 mM KOH)) was added to afford the free thiol. Simply boiling **B3** with divinylsulfone in ethanol delivered complex **B4**.

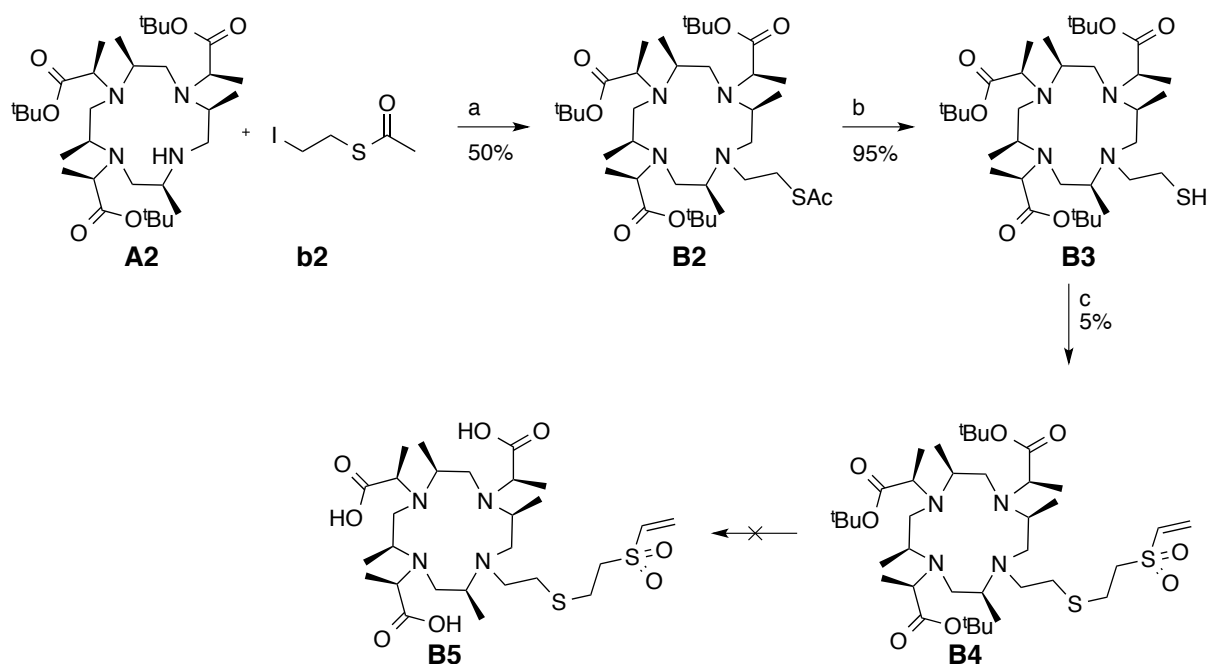


Figure A-30: Synthesis towards DOTA-M7 thiovinyl; a) NaH (60% in paraffin oil), MeCN, rt, 7h; b) NaSAc, MeOH, rt, 1.5h, TCEP; c) divinylsulfone, EtOH, reflux, 1h.

Full conversion was detected by ESI-MS without any side products. Nevertheless, purification by silica gel column chromatography using chloroform/ethanol (9:1 to 1:1) as eluent delivered only 5% of the desired macrocycle **B4**. The low yield is explained by the formation of macrocycle **B4a** (Figure A-31) where the double bond reacted with ethanol. This species is strong ionizing in the ESI-MS and therefore it is obvious that this side product was not formed during the reaction in boiling ethanol. Therefore the interaction with silica gel must have catalysed this reaction. Therefore, this purification method was avoided for further investigations of this type of molecules. Deprotection using TFA, degraded the macrocyclic molecule **B5** completely.

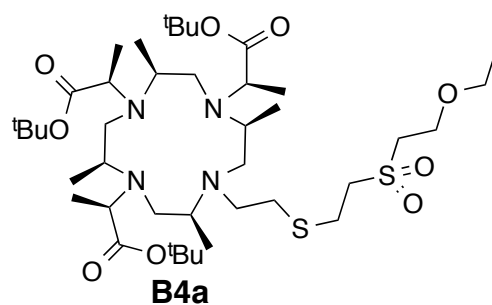


Figure A-31: Side product obtained after silica gel column chromatography.

The synthesis strategy was slightly changed to improve the yields of the reactions. The sulphur containing side chain was attached to M4-cyclen leading to an improved yield of the reaction. Addition of the standard side chain to form the fully alkylated macrocycle caused some problems. No full conversion was achieved under standard conditions. Addition of more starting material to the crude mixture was not successful. Intermediates that contained only two lactic acid side chains could be isolated and had to be reacted a second time to deliver the desired product. This increased the overall yield of this step up to 80%. Instead of the selective cleavage of the thiol protecting group all protecting groups were removed in one single step using boiling aqueous hydrochloric acid (1M, 1h). This deprotection worked in good yields of 80%. No dimer formation was obtained under these reaction conditions.

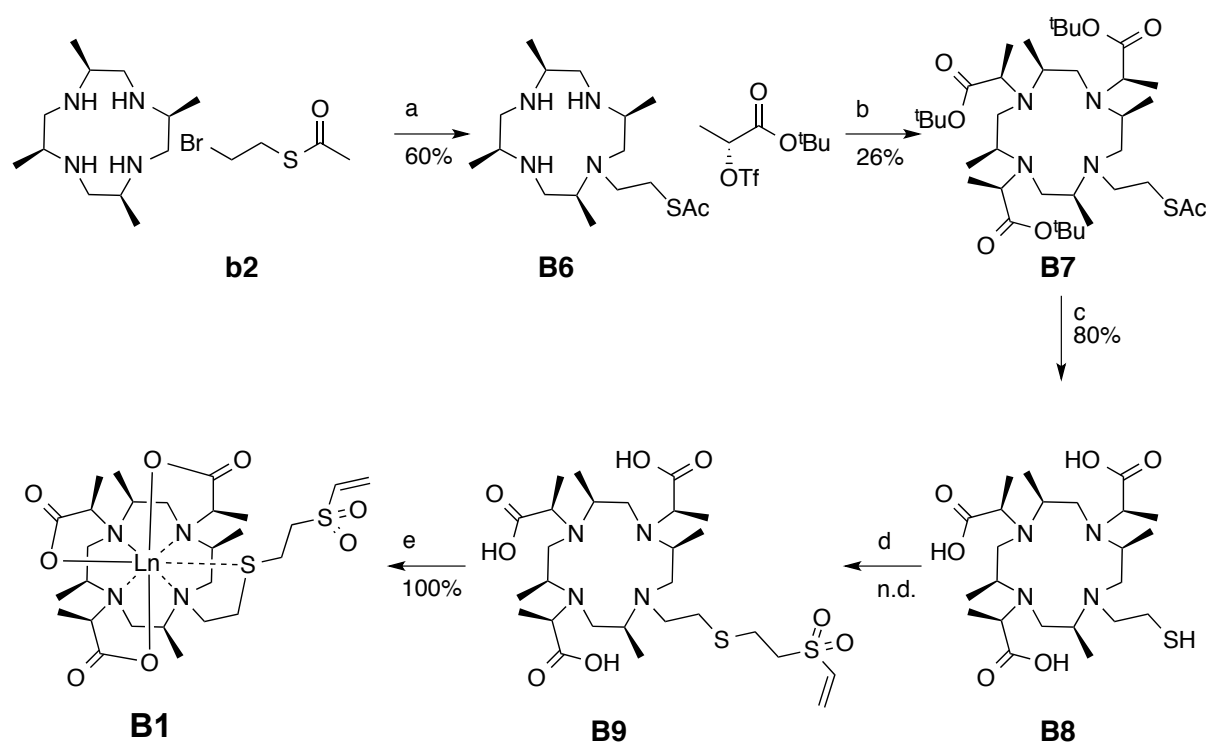


Figure A-32: Synthesis of DOTA-M7-thiovinylsulfone (B1); a) NaH (60% in paraffin oil), rt, 20h; b) K_2CO_3 , MeCN, rt, overnight; c) HCl (1M, aq), reflux, 60 min; d) divinylsulfone, EtOH, reflux, 1h; e) $LnCl_3 \cdot 6H_2O$, pH = 7.0 ammonium acetate buffer (100 mM, aq), H_2O , 75 °C, overnight

The reaction with divinylsulfone worked in very good yield and purification using preparative HPLC delivered exclusively the desired product. Metalation of complex **B9** under standard conditions worked in quantitative yield to deliver the desired macrocycle **B1**. Contrarily to macrocycle **A1** no chlorination or hydroxylation of the double bond were observed. Reaction of the vinylsulfone, was reported in literature to react fast even at low pH of around 6.5. In our case no full conversion was

obtained at this pH. Adjusting the pH stepwise to 8.0 delivered a full conversion after 48 hours.

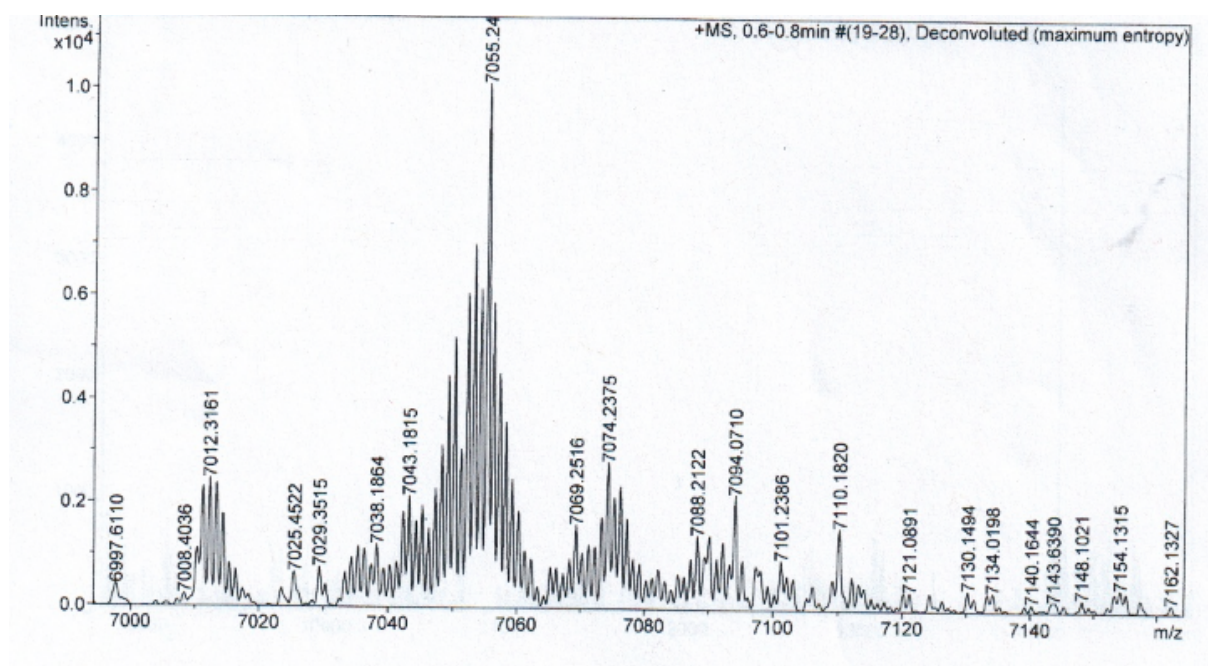


Figure A-33: ESI-MS spectrum of GB1-T53C-DOTA-M7-Tm-thio.

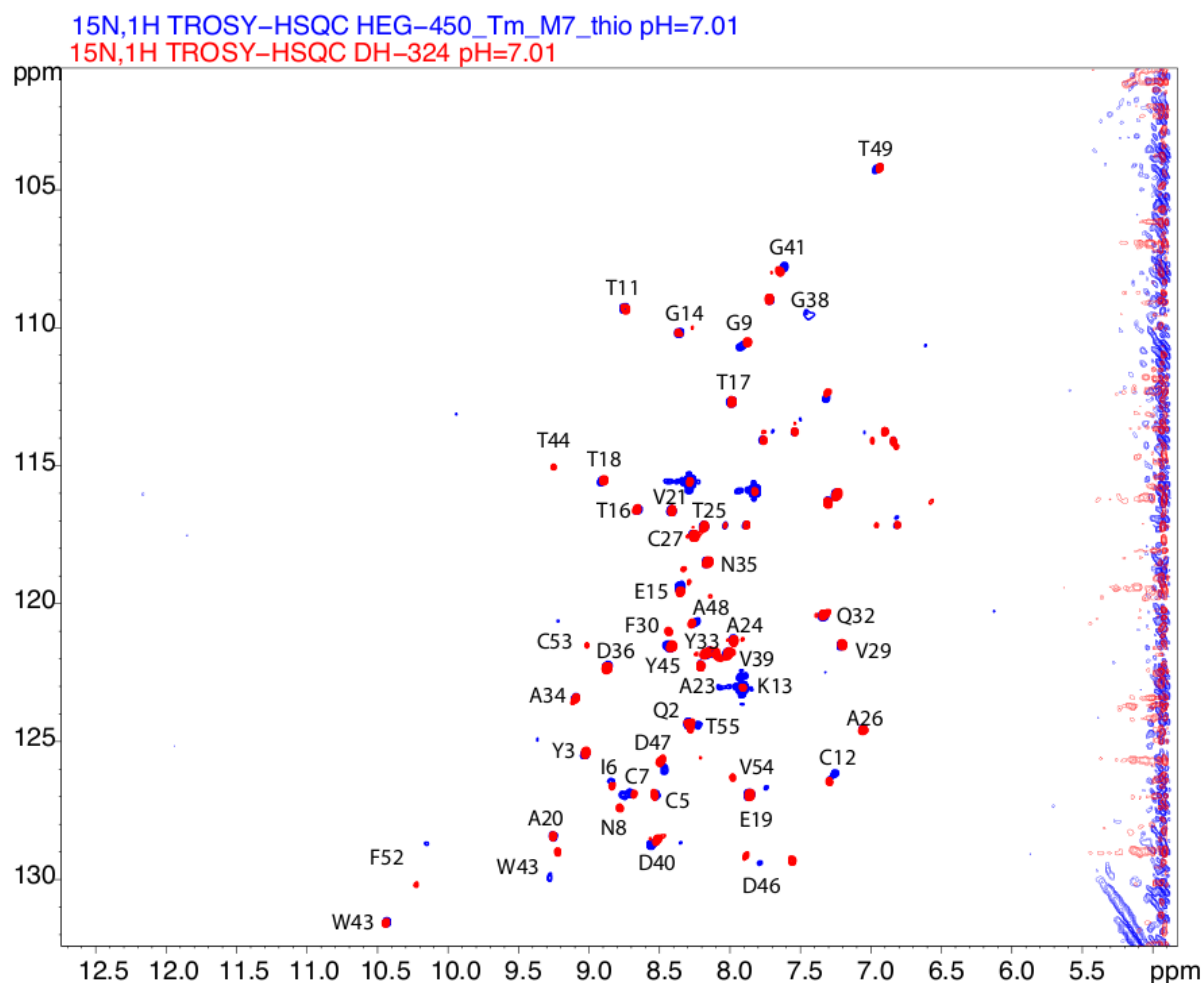


Figure A-34: Comparison of the TROSY-HSQC spectrum of GB1-T53C (red) and GB1-T53C-DOTA-M7-Tm-thio (blue).

The comparison of the two TROSY-HSQC spectra shows PRE effects of the resonances in close proximity to the paramagnetic ion. The obtained PRE effect is comparable to DOTA-M7-Tm-acetophenone. For the thiovinyl sample one single set of signals was observed. Nevertheless, the PCS are weak and indicate that the tag must be still flexible.

Two explanations for the low PCS of DOTA-M7-divinylsulfone (**B1**) are predicted. Either the linker is too long if the oxygen in the side chain is not coordinated to the lanthanide allowing a greater flexibility and therefore led to PCS averaging. On the other hand there are no data available showing the influence of one missing stereospecific side chain in the backbone. Therefore, synthetic strategies towards an M8-version (**B1a**) were developed. Attachment of the stereospecific side chain has to be performed in a similar way as presented for standard side chains. Modifications of the lactic acid backbone were performed as discussed in the synthetic strategy.

Commercially available *L*-lactic acid ethyl ester was used as starting point for these investigations. In a first trial, a benzyl protecting group (**b3**) was introduced before reduction of the ester to the alcohol (**b4**). Both reactions worked in good yields. The free hydroxyl group was converted into a good leaving group using tosylchloride in pyridine (**b5**). The reaction of **b5** with potassium thioacetate delivered **b6** in moderate yield. Starting material could be recovered after purification. The removal of the benzyl-protecting group using Pd/C was not successful even under high catalyst loading, high pressure (20 bar) and extended reaction time (24 h). Therefore, a similar protocol was tested using a THP protecting group instead of the benzylprotecting group.

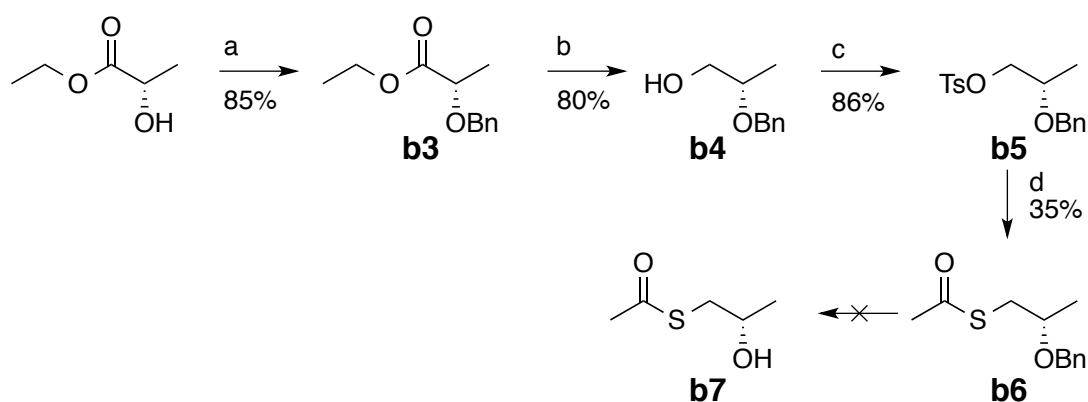


Figure A-35: Functionalization of the lactic acid side chain: a) benzyl bromide, NaH, DCM, -10 °C – rt, overnight; b) LiAlH₄, THF, 0 °C – reflux, overnight; c) p-TsCl, pyridine, rt, overnight; d) KSAc, THF, reflux, 3h.

The THP-protecting group was introduced in moderate yield. The product **b8** was obtained as mixture of two diastereoisomers (*S-S*, *S-R*) because an additional stereogenic centre was introduced in a racemic way. The two diastereoisomers are only partially separated by silica gel column chromatography. All further reactions were performed with a mixture of these two diastereoisomers. Reduction to compound **b9** could be achieved in quantitative yield. Extending the reaction time for the formation of **b11** doubled the yield compared to the synthesis **b6**. Deprotection under mild conditions worked in moderate yield. Purification of compound **b7** was challenging as the hydrolysed THP-protecting group showed similar properties as the free alcohol. After two silica gel column chromatographies using different eluents the compound could be isolated as pure product.

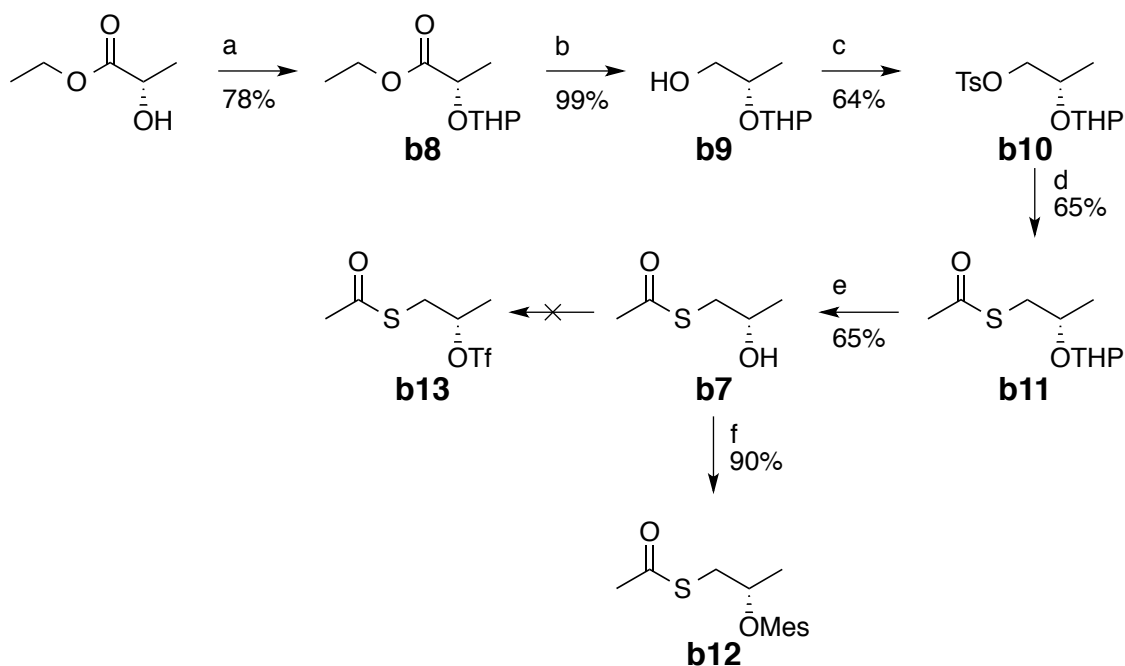


Figure A-36: Functionalization of the side chain using THP-protection: a) *p*-TsOH, 2*H*-dihydropyran, CHCl_3 , 4°C – rt, 3h; b) LiAlH_4 , Et_2O , reflux, 2h; c) *p*-TsCl, pyridine, DCM, 0°C – rt, overnight; d) KSAc, THF, reflux, overnight; e) $\text{AcOH}/\text{THF}/\text{H}_2\text{O}$ (4:2:1), 45 °C, 4h; f) methanesulfonyl chloride, NEt_3 , THF, 0°C – rt, 2h.

Formation of the triflate **b13** failed under different reaction conditions as presented in in Table A-4. Therefore, the less reactive mesyl compound **b12** was synthesized.

Table A-4: Different conditions tested for the synthesis of triflate **b13**.

Reagent	Temperature	Reaction time	Workup temp.	Yield
Tf_2O	-10 °C	30 min	rt	0-5 % not pure
Tf_2O	-50 °C	30 min	0 °C	Decomposition
Tf_2O	-50 °C	30 min	-20 °C	No conversion
TfCl	-20 °C	30 min	0 °C	Decomposition

Compound **b12** was synthesized in high yields and was much more stable than **b13**. Nevertheless, coupling reactions of **b12** to the M4-cyclen failed as the reactivity of the mesyl compound was not high enough to allow substitution on this sterically bulky molecule. It was therefore obvious that only a molecule as reactive as a triflate can be used as candidate to attach the side chain stereospecifically.

The introduction of an orthogonally protected alcohol should allow the attachment of the thiol group to the side chain on the macrocycle selectively. The strategy towards a benzyl protected side chain (**b15**) is shown in Figure A-37.

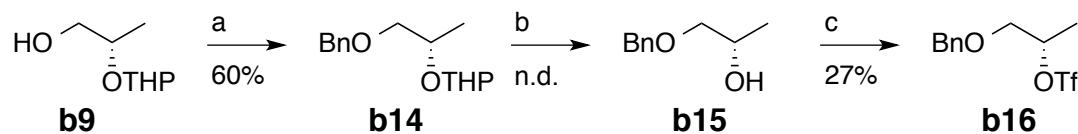


Figure A-37: Synthesis of the benzyl protected side chain **b16**: a) benzyl bromide, NaH (60% in paraffin oil), DMF, rt, 2h; b) AcOH/THF/H₂O (4:2:1); 45 °C, 8h; c) Tf₂O, pyridine, DCM, -78 °C, rt, 10 min.

High purity of compound **b15** was achieved after two purifications by silica gel column chromatography. The reaction of the alcohol **b15** to triflate **b16** worked in moderate yield and high purity was reached after filtration over silica gel. Mono-alkylation using **b16** to form **B10** worked only in poor yields, but the starting material (M4-cyclen) could be recovered.

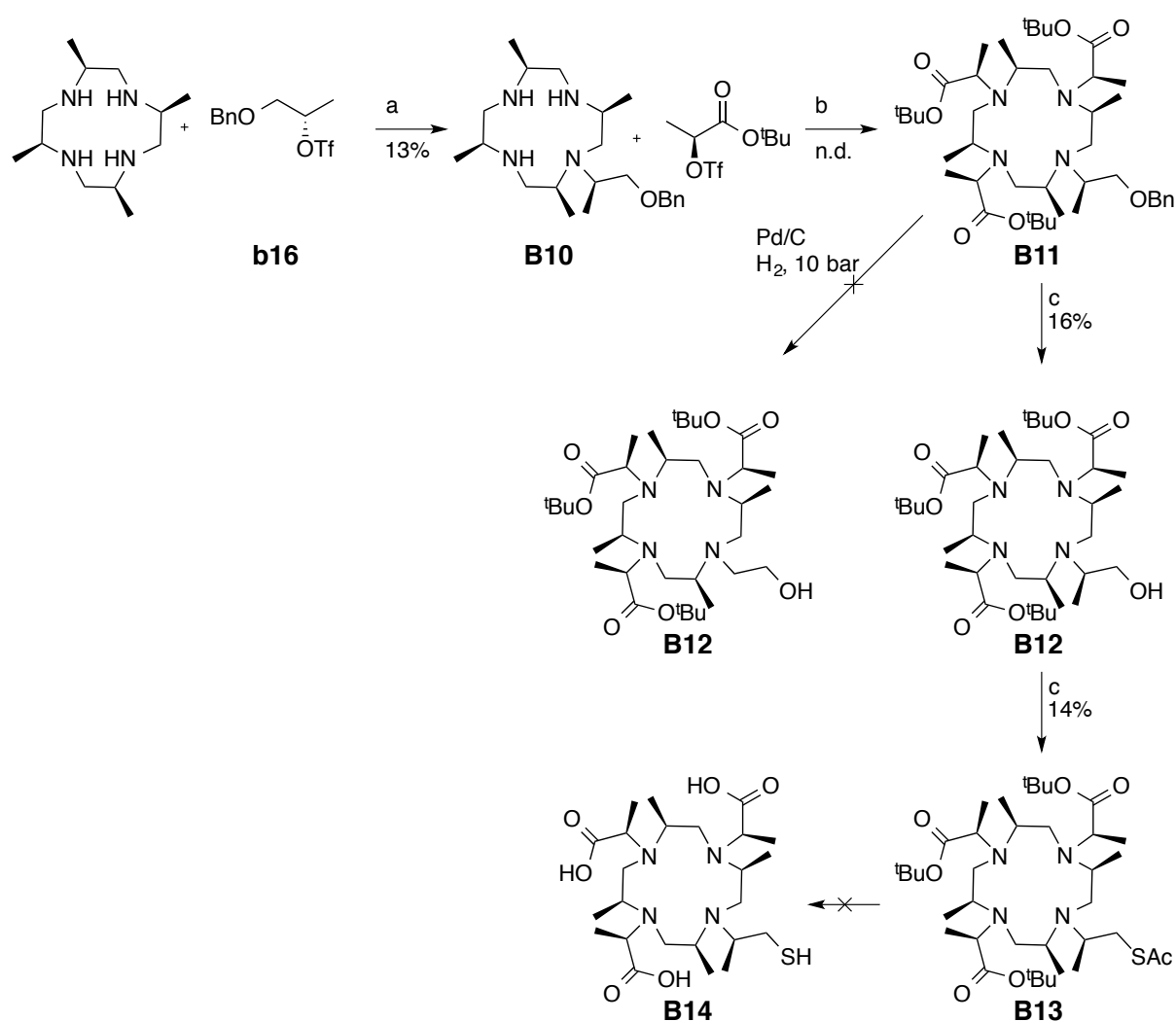


Figure A-38: DOTA-M8 introduction of a sulphur side chain: a) NaH (60% in paraffin oil), DCM, rt, 48h; b) NaH (60% in paraffin oil), MeCN, rt – 50 °C overnight; c) liquid ammonia, Na, -78 °C, 120 min; d) MesCl, 0°C – rt, 2h, KSAc, reflux, 6h.

Alkylation using sodium hydride as base was not ideal, as different side products were formed. Therefore, carbonate is the base of choice to obtain better yields for

this alkylation reactions. Selective removal of the benzyl-protecting group was much more challenging than expected. Standard conditions using Pd/C or Pd(OH)/C under different hydrogen pressures did not deliver any deprotected intermediates. Therefore, harsh Birch conditions were applied affording **B12** in low yields. Scaling up of this reaction failed. The low quantities available and the high amount of impurities are the main reason for the low conversion of this reaction. Deprotection conditions used for **B7** did not work similar for **B13** most like due to the large number of impurities in this reaction mixture. The main problem of this synthetic strategy is the hard removal of the benzyl protecting group.

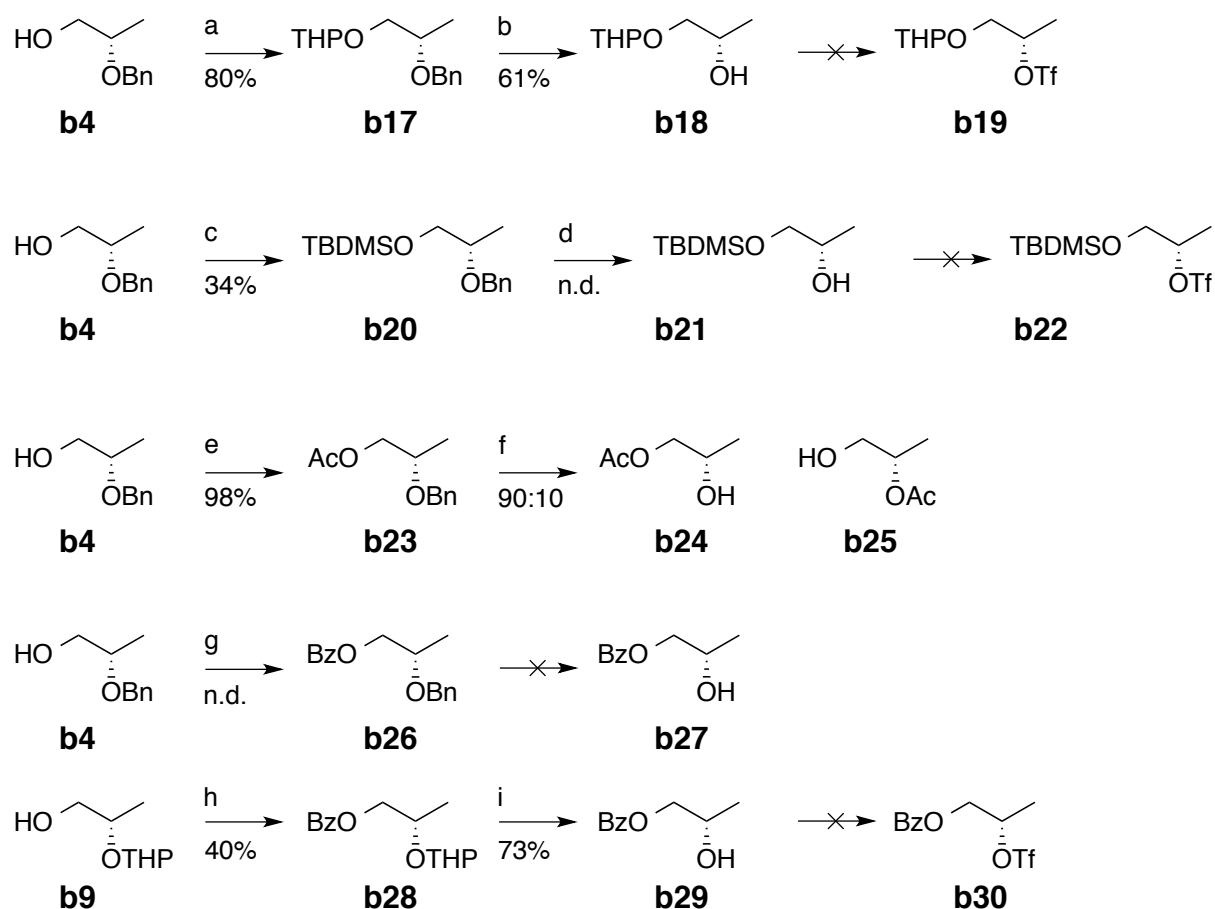


Figure A-39: Preparation of different orthogonally protected side chains: a) 3,4-dihydro-2*H*-pyrane, *p*-TsOH, CHCl₃, rt, 3h; b) Pd/C, H₂ (5 bar), EtOH, rt, overnight; c) TBDMSCl, 1*H*-imidazole, DMF, rt, overnight; d) Pd/C, H₂ (10 bar), EtOH, rt, 2h; e) acetylchloride, THF, rt, overnight; f) Pd/C, H₂ (10 bar), EtOH, rt, overnight; g) benzoylchloride, NEt₃, DMAP, toluene, rt, 4h; h) benzoylchloride, NEt₃, DMAP, toluene, rt, 3h; i) AcOH/THF/water (4:2:1), 45 °C, 4h.

Other protection protocols with similar orthogonality but milder deprotection conditions were developed. Protection protocols using THP, Benzoyl, Acetyl and TBDMS were tested as shown in Figure A-39. THP, Benzoyl and TBDMS were not stable under the reaction conditions required for the triflate synthesis. The acetyl-

protecting group moved in polar solvents and was obtained as mixture of 1 and 2 protected alcohol **b24** and **b25**. Separation of these two isomers by silica gel column chromatography was not possible under various conditions. Attaching such isomer mixtures to the M4-cyclen moiety would cause major problems. Separation after attachment to the M4-cyclen would be complicated, owing to similar polarity of the two molecules. The main surprise in this series was the fact that the benzoyl-protecting group was removed under these conditions, as benzoyl is known to be an acid stable protecting group removable under basic conditions.

Selective introduction of an orthogonally protected alcohol side chain, easily removable remained therefore unsolved. Another possibility would be the introduction of a standard side chain, which would be reduced on the macrocycle. Such a route is presented in Figure A-40. The free amines were protected with a benzyl protecting group. The benzyl protecting group was chosen, as it is stable under the reducing conditions necessary to form compound **B16**.

The introduction of the mesyl group was difficult and hard to monitor. As a range of isomers were obtained on TLC, making TLC control too complicated. This intermediate was not ESI-MS active and therefore only consumption of starting material could be detected. Test reactions on small scale (4 mg) were performed, ESI-MS showed full conversion but after reaction with potassium thioacetate, a mixture containing mainly starting material and only traces of product was isolated.

In previously presented strategies, removal of the benzyl protecting group was problematic when a thiol was in close proximity. Also in this case deprotection using Pd/C at 8 bar hydrogen pressure did not work. Birch conditions were applied but the products were degraded under these harsh conditions. Attempts to protect the free amine with TMS and THP remained unsuccessful. This opens new possibilities as the alcohol can probably be selective protected with THP on the macrocycle. The standard side chain can be attached to the M5-intermediate, the THP selective deprotected and the thiol introduced.

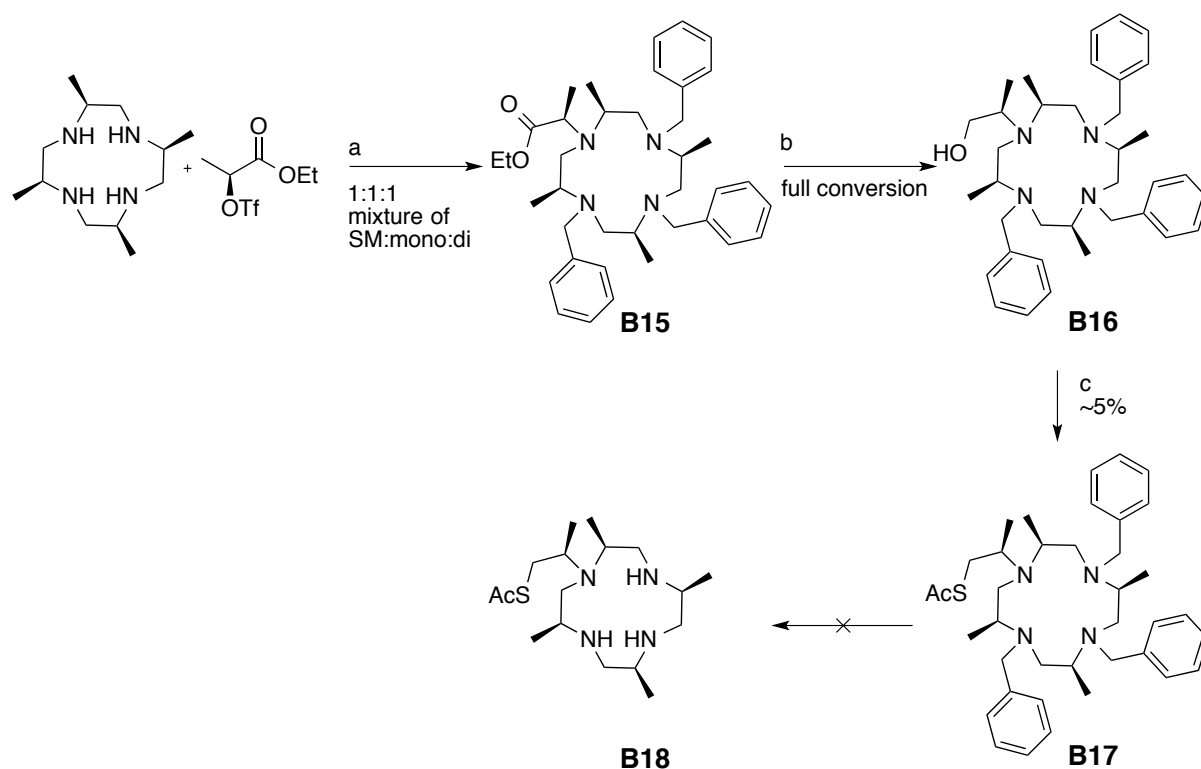


Figure A-40: Reduction of the side chain on the macrocycle: a) 1.) sodium hydride, dichloromethane, rt, 3h, 2.) benzyl bromide, sodium hydride, THF/DMF (2:1), -10 °C – 50 °C, 3h; b) LiAlH₄, diethylether, 0°C – reflux, overnight; c) 1.) methanesulfonyl chloride, THF, 0°C – rt, 5h, 2.) potassium thioacetate, THF, reflux, 7h.

A.5.3 Synthesis of the α,β -unsaturated target molecule C1

The synthesis of target molecule **C1** was developed as shown in Figure A-41. The formation of a Weinreb amide (**c2**) was obtained in moderate yields from the TBDMS protected lactic acid ethyl ester (**c1**). This approach allows selective introduction of a single vinyl moiety using Grignard reagents (vinylmagnesium bromide). When Grignard reagents are reacting with an ester a second vinyl moiety is added, as the ketone intermediate is even more reactive than the ester. Removal of the amine is performed under acidic conditions to deliver the target molecule (**c3**) in moderate yield. Molecule **c3** was synthesized as test molecule. Removal of the protecting group followed by triflate synthesis was not performed as an alkylation reaction is expected to be unselective.

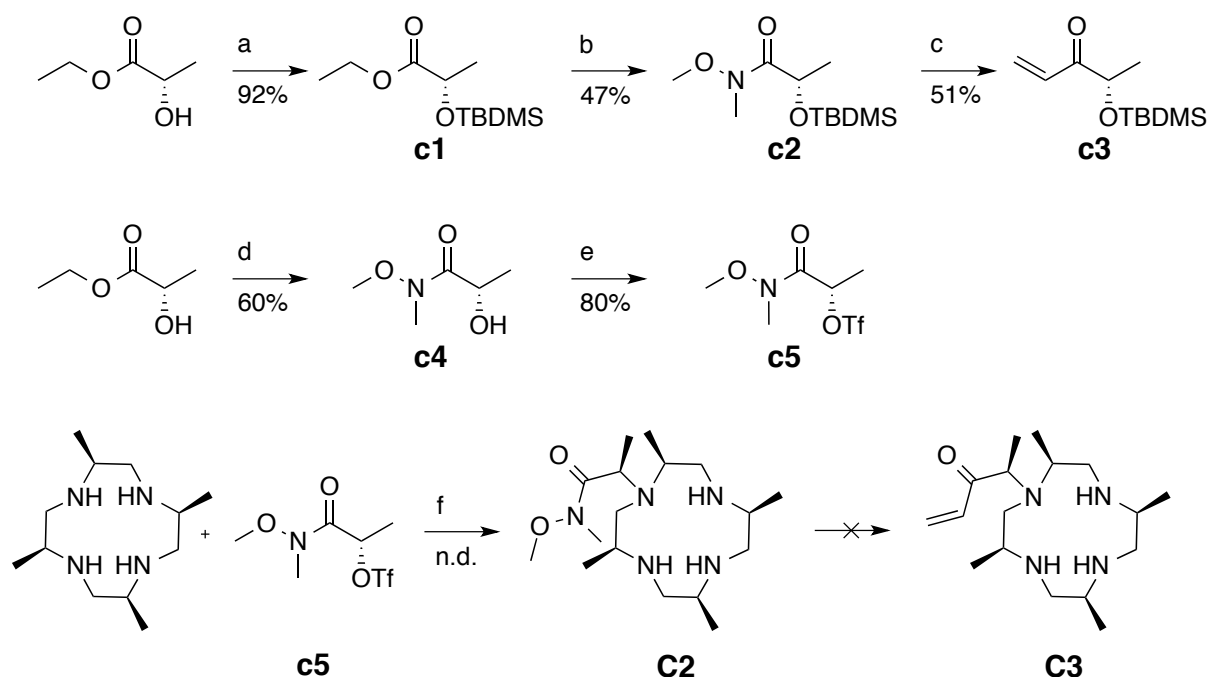


Figure A-41: Synthetic strategy towards **C1**: a) TBDMSCl, 1*H*-imidazole, DMF, 0°C, 48h; b+d) *N,O*-dimethylhydroxylamine hydrochloride, isopropyl magnesium chloride, THF, -20 °C – 5°C, 3h; c) vinylmagnesium bromide, THF, -15 °C – rt, 5h; e) Tf₂O, pyridine, -78 °C – rt, 1h; f) NaH, 0 °C – rt, overnight.

Therefore, the stable Weinreb intermediate **c5** was attached to the cyclen moiety to form macrocycle **C2**. The Grignard reaction performed from **c2** to **c3** did not work in a similar way for the transformation of **C2** to **C3**. ESI-MS analysis showed that the amine and the vinyl group are located on the macrocycle. This means the reaction stops at the intermediate. Several attempts to remove the amine remained unsuccessful.

Other reaction conditions were therefore tested as shown in Figure A-42. Introduction of the vinyl moiety at extremely low temperatures (-105 °C) was tested. Addition of vinylmagnesium bromide yielded exclusively the bis-vinyl alcohol **c7**. Vinyl lithium delivered the desired vinylketone in 25% yield. Vinyl lithium is unstable at temperatures above -78 °C and requires in situ preparation. The concentration was only estimated as titration experiments at rt. delivered several different concentrations. Using vinyl lithium at mono alkylated macrocycles would require a special *N*-protection protocol. This is necessary as lithium compounds are strong bases.

The symmetric macrocycle **C4** was therefore synthesized. Molecule **C4** can be transformed via statistical reaction into **C5**. Dilute conditions and slow addition of vinyl lithium can help driving the reaction towards **C5**.

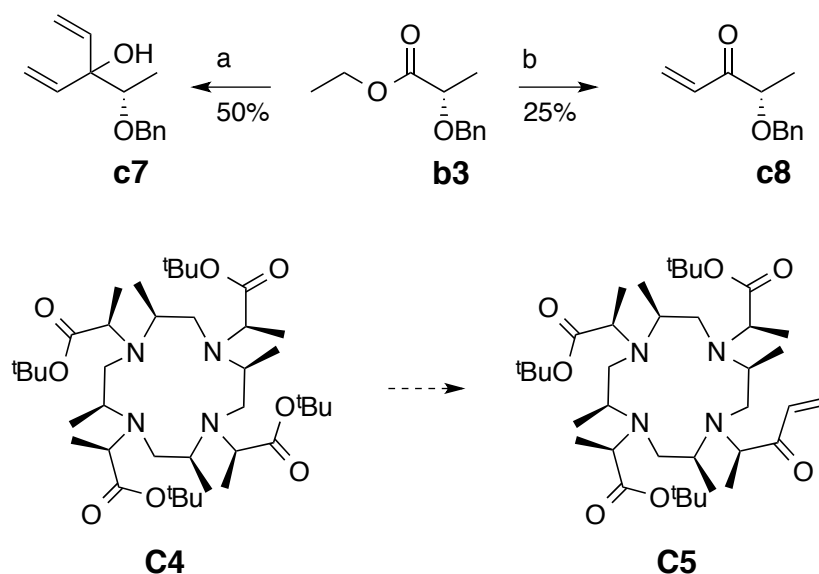


Figure A-42: Test reactions towards intermediate **C5**: a) vinylmagnesium bromide, TMSCl, THF, $-105\text{ }^{\circ}\text{C}$, 30min; b) Vinylolithium, TMSCl, THF, $-105\text{ }^{\circ}\text{C}$, 30 min.

A.5.4 Synthesis towards amine based macrocycle **D1**.

To keep an amine based metal complex neutral, a neutral side chain has to be introduced. A methyl ketone was chosen instead of the carboxylic acid. The synthetic route is described in detail in Figure A-43. The selective introduction of the methyl group was performed in a similar way as for **c8**. Two different reaction pathways for the introduction of an amine side chain are presented. Starting from **b9** the hydroxyl group was transformed to bromine (**d1**) in an Appel reaction. The amine was introduced using benzyl amine to form **d2**, which was further protected using benzyl bromide to yield the bis-benzyl protected amine. The bis benzyl-protected compound **d3** was selectively deprotected on the hydroxyl function leading to compound **d4** in good yield. Unfortunately, formation of the triflate was again not successful. The lone pair of the bis-benzyl protected amine was probably too reactive causing trouble in the reaction.

Therefore, another pathway using intermediate **b9** in a Mitsunobu reaction to introduce phthalimide is presented in Figure A-43. The reaction worked in moderate yield. In this case, the reactivity of the nitrogen lonepair should be tremendously reduced because of the partial double bond. The THP deprotection works well and the compound could be satisfyingly purified by silica gel column chromatography.

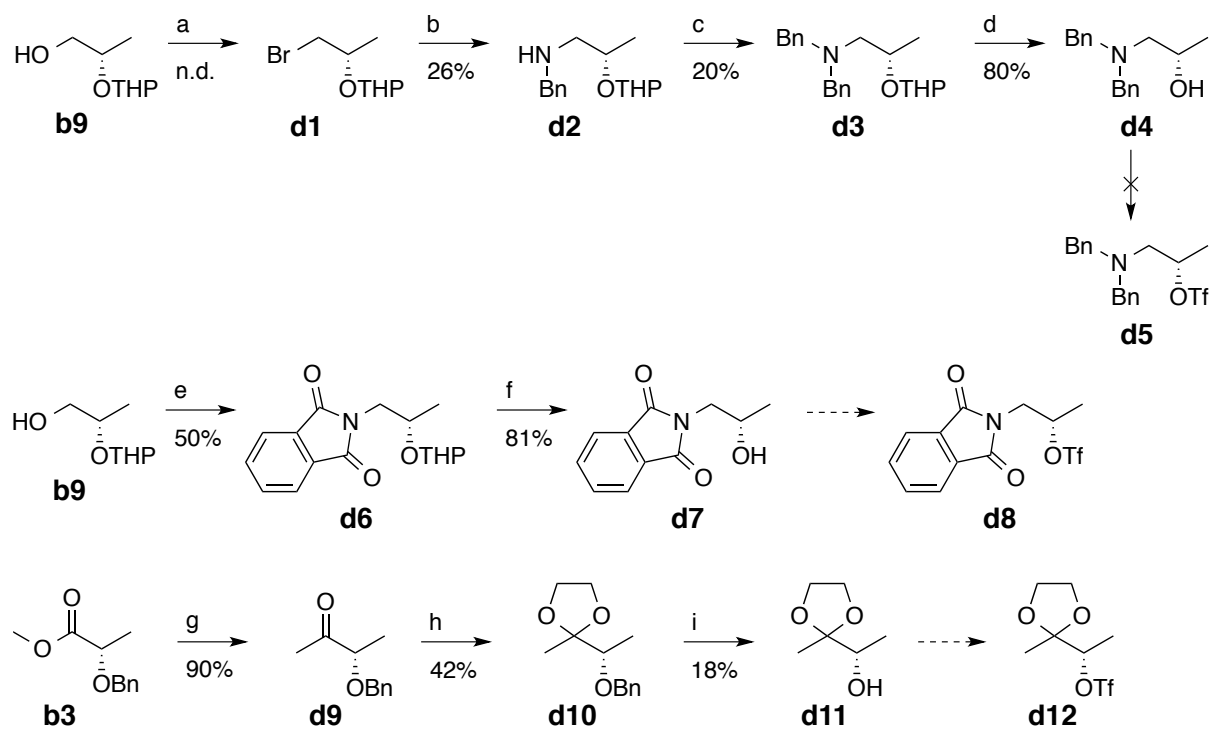


Figure A-43: Synthetic routes towards amine based side chains: a) CBr_4 , triphenylphosphine, triethylamine, dichloromethane, 0°C , 18h; b) benzyl amine, THF, rt, 2h; c) benzyl bromide, sodium hydride, THF/DMF (2:1), $-10^\circ\text{C} - 50^\circ\text{C}$, 2h; d+f) acetic acid/THF/water (4:2:1), 45°C , 4h; e) DEAD, triphenylphosphine, phthalimide, THF, $0^\circ\text{C} - \text{rt}$, overnight; g) methyl lithium, TMSCl, THF, $-110^\circ\text{C} - \text{rt}$, 1h; h) ethylene glycol, *p*-TsOH, toluene, reflux, 30h; i) Pd/C, hydrogen 10 bar, methanol, 3h.

A.5.5 Influence of different donor atoms to the anisotropy of the magnetic susceptibility tensor.

The ^1H -NMR spectra of DOTA-M8-Lu, DOTA-M8-Sm, DOTA-M8-SSP-Lu, DOTA-M8-SSPy-Sm, DOTA-M7-thio-Lu and DOTA-M7-thio-Sm were compared. The symmetric DOTA-M8 shows only six different chemical shifts that could be easily assigned for the diamagnetic and paramagnetic metal ion. The sharp lines obtained for the paramagnetic samarium sample gave strong evidence that the metal ion is fixed in one position inside the complex and does not show any motional freedom.

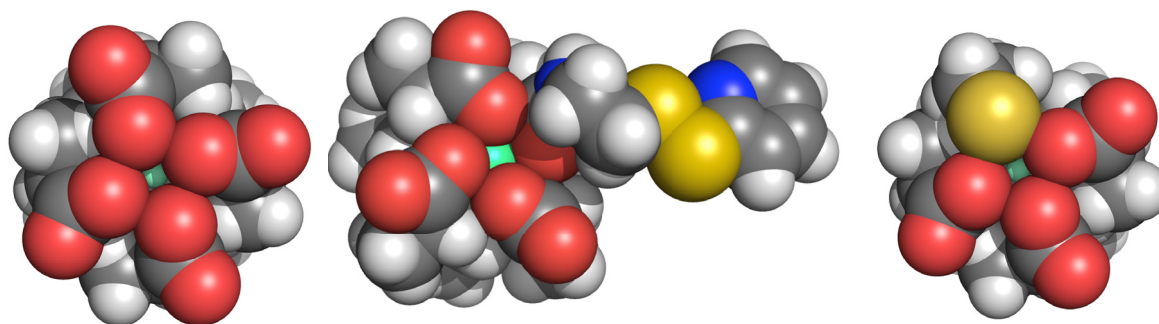
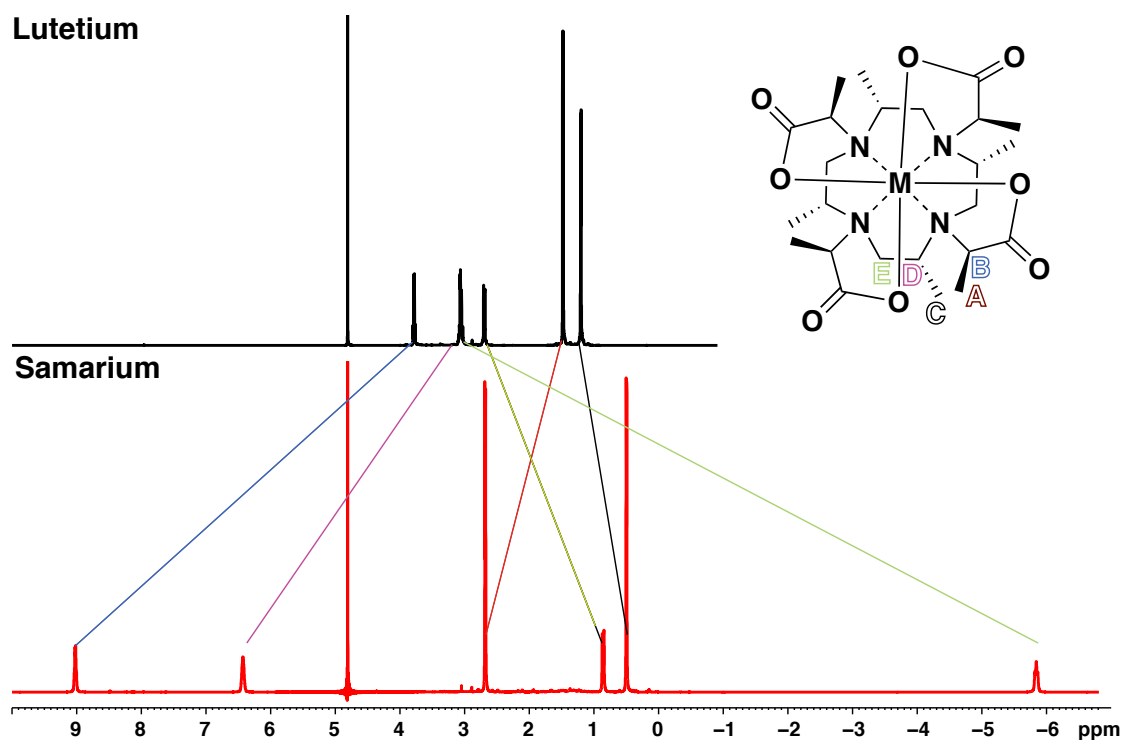
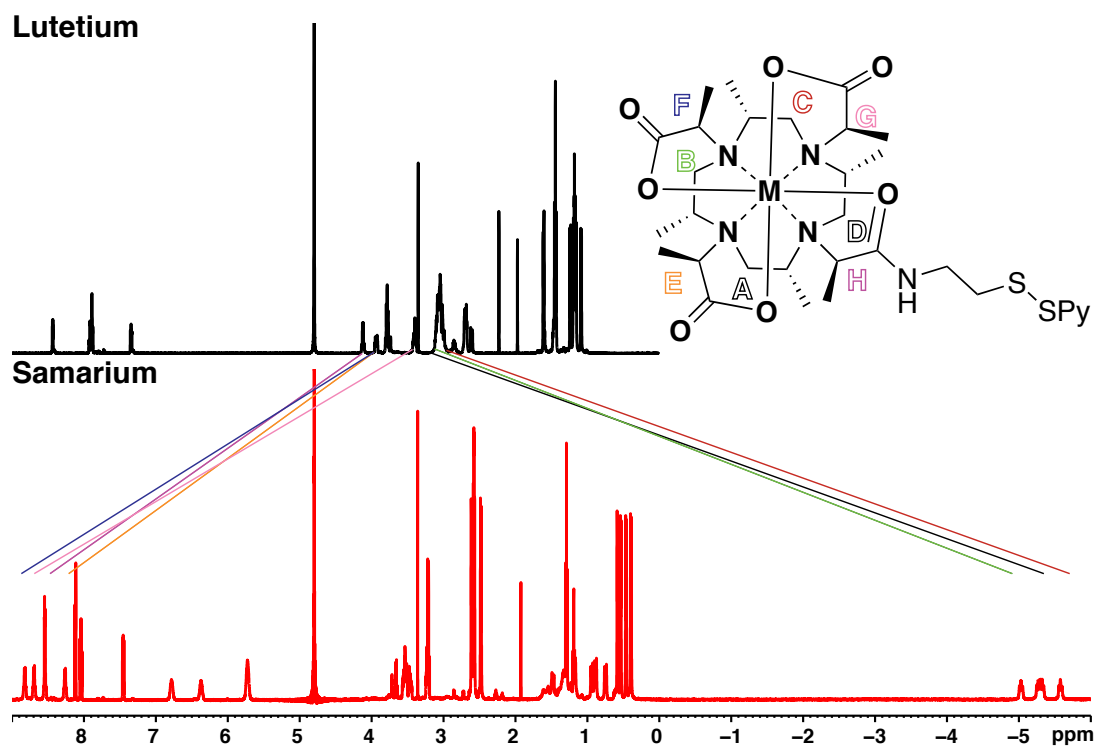


Figure A-44: Space filling representation of DOTA-M8 (left), DOTA-M8-SSPy (middle), DOTA-M7-thio (right).

The asymmetric DOTA-M8-SSPy delivered 32 NMR signals. The assignment of the lutetium sample was complicated but possible. Also some resonances could be assigned in the samarium sample as shown in Figure A-46. In this case the distances between the paramagnetic centre and side chains should be similar for all and comparable to DOTA-M8. If the change of donor (carboxylic acid to amide) does not influence the anisotropy of the magnetic susceptibility tensor then no shift dispersion should be observed. Figure A-46 shows nicely that small shift dispersion occurred and therefore a measurable influence could be detected. But it was also visible that the PCS was slightly smaller in this case.

Figure A-45: $^1\text{H-NMR}$ spectra of DOTA-M8 as Lutetium and Samarium complex.Figure A-46: $^1\text{H-NMR}$ spectra of DOTA-M8 with standard linker as Lutetium and Samarium complex.

The analysis of DOTA-M7-thio shows that the lines are slightly broader than determined for the two DOTA-M8 complexes. This means that this complex is not as rigid as the others. The main question is whether this is because of the missing methyl group in the side chain or the S-metal binding strength. Anyway one can see that the chemical shift dispersion is much larger, indicating an influence on the anisotropy of the magnetic susceptibility factor. Also, in this case the PCS are slightly decreased for all chemical shifts.

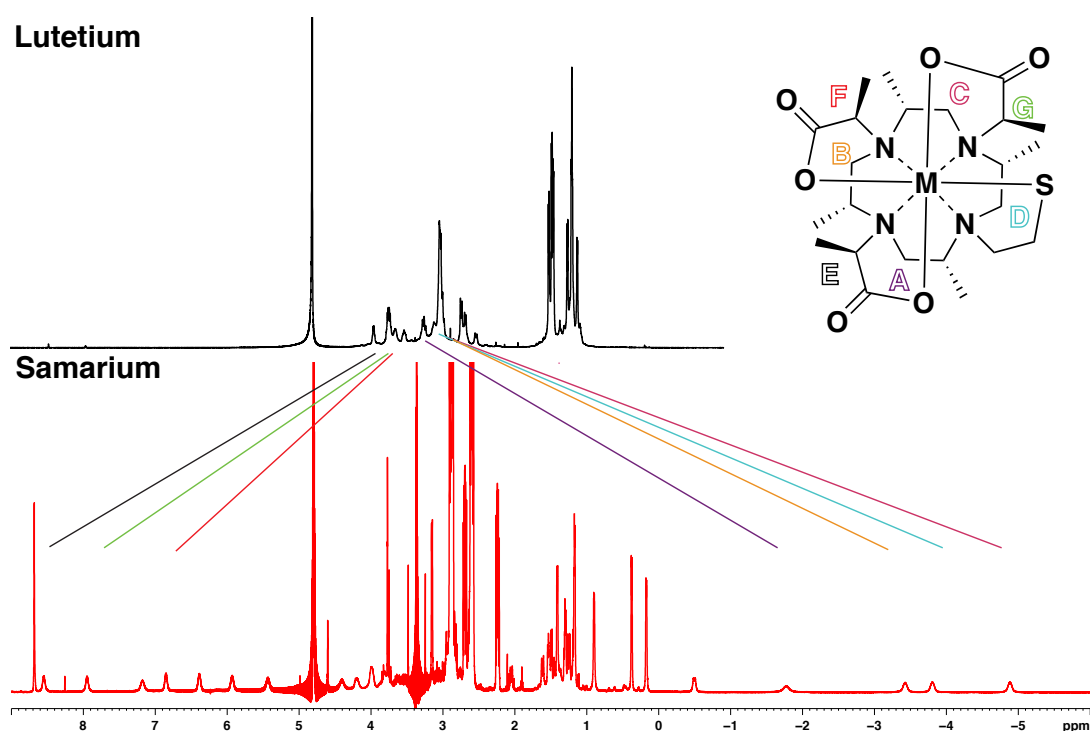


Figure A-47: ¹H-NMR spectra of DOTA-M7-thio as Lutetium and Samarium complex.

A.5.6 Further developments

Besides the so far presented target molecules other macrocycles were investigated. These target molecules show strong similarities to the so far presented ones. Also combinations of the standard side chain and the new ones are presented. The synthesis of these molecules was discarded in an early stage. Problems in the synthetic sequence were the main reason for this. They were development to gain deeper insights on the influence of the geometry of the linker to the obtained PCS.

E1, **F1** and **H1** are analogues of **A1**, all of them have a linear aromatic linker. The

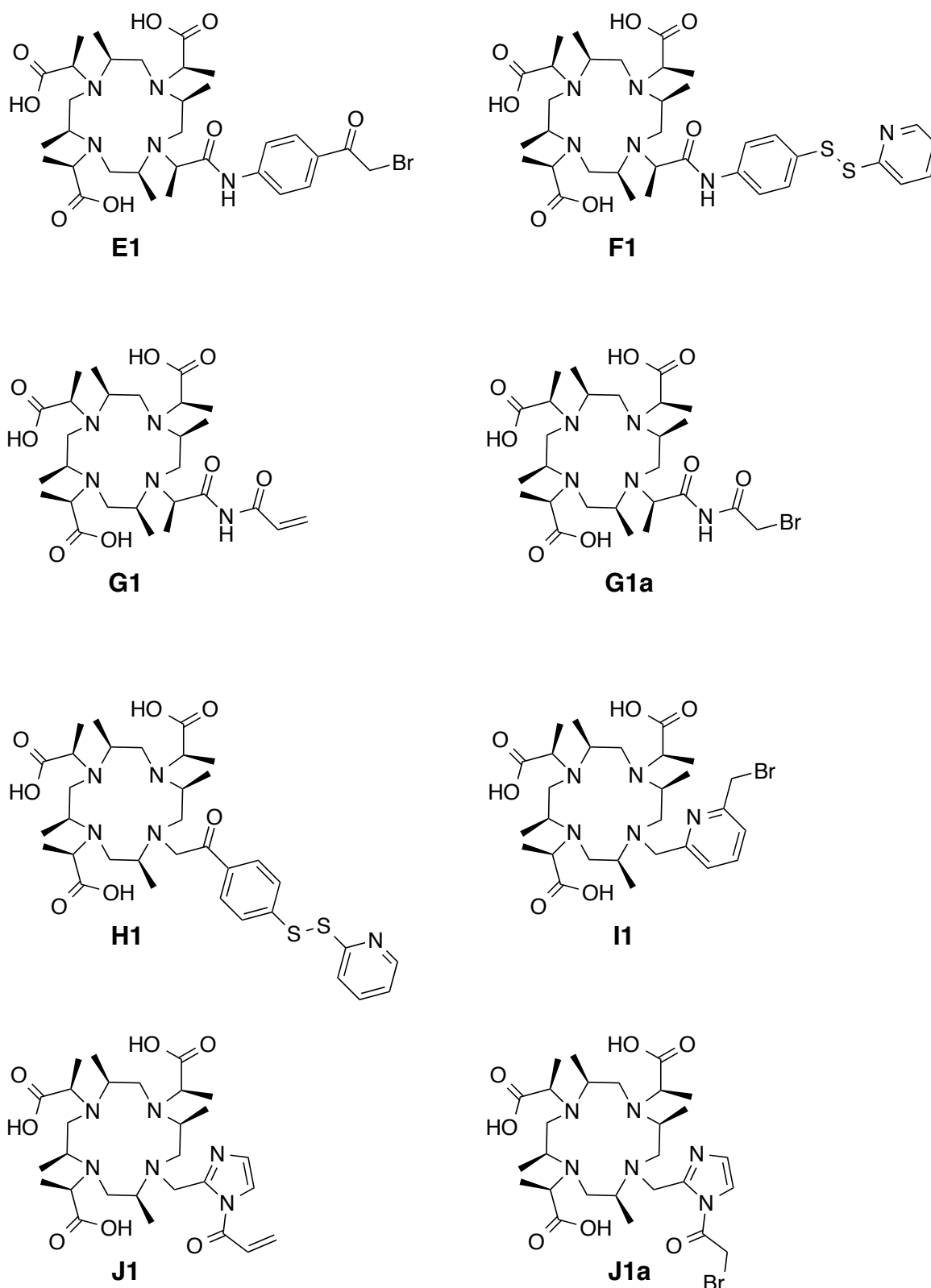


Figure A-48: Target molecules inspired by or as inspiration for the so far presented molecules.

length and bond type for the attachment to the protein varies in this study. Target molecules **G1**, **G1a**, **J1** and **J1a** show huge similarities to **C1**. These two sets are amide based linkers and shown in two different reactive forms. A special case is

target molecule **I1**. This linker is extremely short and has a fixed geometry when the pyridine nitrogen is coordinated to the lanthanide ion. In the following section the challenges and achievements towards the synthesis of these target molecules are discussed. Some special reactions are also presented in the experimental section.

The synthesis of the amine precursors for **E1** was much more challenging than predicted. Bromination procedures known from literature did not work in our case. We tried therefore different protection protocols to avoid bromination of the aromatic core. Even with the use of amine protecting groups many side products were generated. The amide coupling using different coupling reagents showed no conversion.

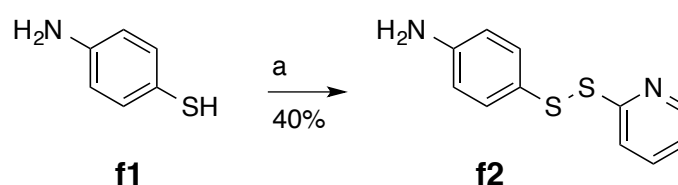


Figure A-49: Synthesis of the activated disulphide **f2**: a) 2,2'-dipyridinyldisulfid, ethanol/acetic acid (20:1), rt., 1h.

The precursor molecule **f2** could be synthesized as *para* and *meta* version. Nevertheless, we could not find conditions that allowed the amide coupling. For both aromatic amines the main problem was the low reactivity of the nitrogen that prevented a successful preparation of the target molecule. Mitsunobu conditions for the preparation of the amine analogue instead of the amide were not tested so far.

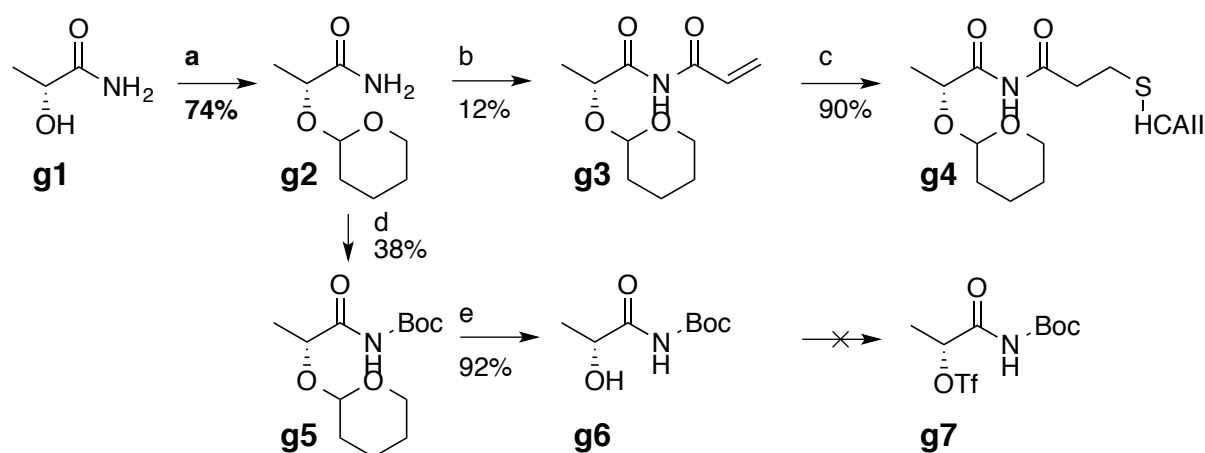


Figure A-50: Synthesis of an acetamide based side chain: a) 3,4-dihydro-2H-puran, PPTS, DCM, rt., 5h; b) acryloylchloride, NaH, THF, rt., 3.5h; c) wasser, pH7 (phosphate buffer), HCAII, rt., overnight; d) Boc₂O, NEt₃, DMAP, rt., overnight; e) acetic acid/THF/water, 45°C, 4h.

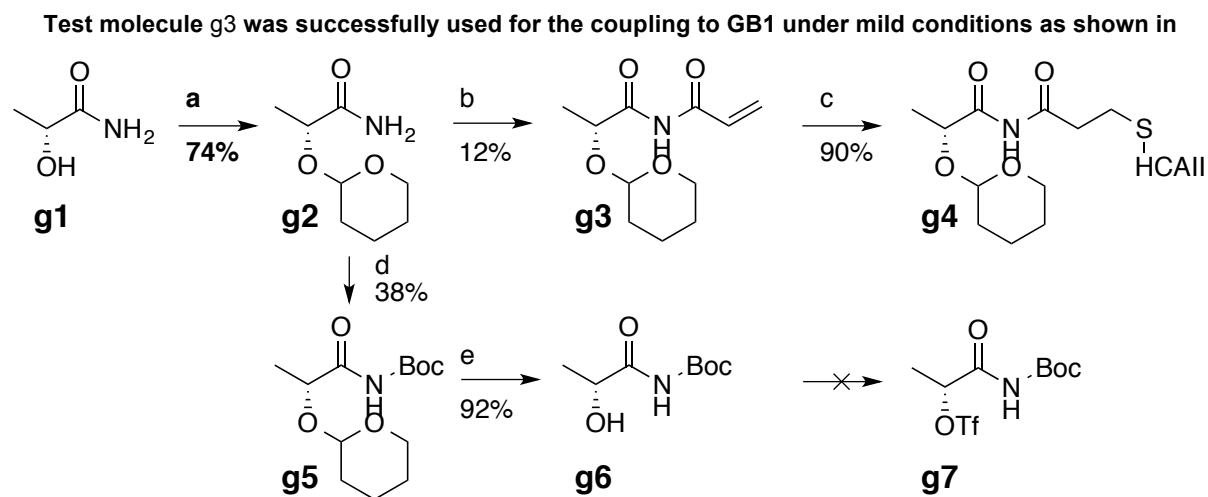


Figure A-50. Numerous efforts towards the synthesis of **G1** were therefore undertaken. Nevertheless, the introduction of such a side chain remains extremely challenging. Formation of the boc-protected amide was performed, but the triflate synthesis was not successful. The unsuccessful reactions performed in this case led to the synthesis of target molecule **C1**, which was presented earlier.

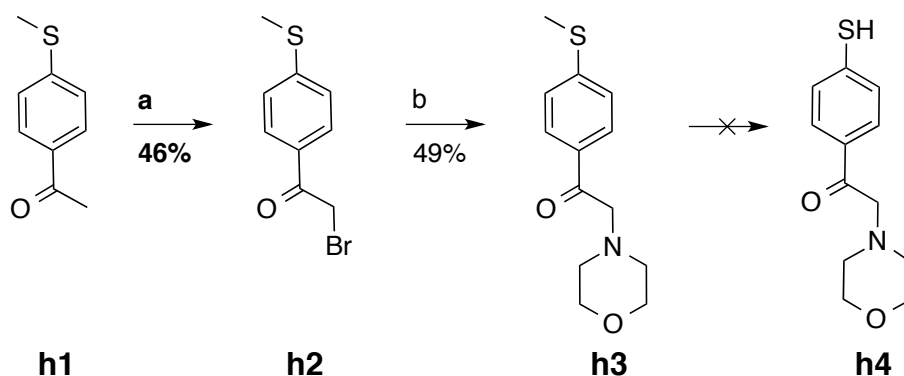


Figure A-51: Synthesis of the side chain towards target molecule **H1**: a) NBS, ammonium acetate, diethylether, rt., overnight; b) morpholine, NaH, THF, reflux, 3h.

Target molecule **A1** delivered several problems, namely the hydrolysis of the α -bromo-ketone and the formation of two species in the protein NMR spectra. Target molecule **H1** is a combination of **A1** and the standard linker using the ketone as donor and the disulphide as linker to the protein. The removal of the methyl-thioether protection group could not be achieved successfully at the modified molecule at different stages. One possibility to overcome this problem would be a change of the protection group before other transformations are performed. The combination of the synthetic problems and the experience from **A1** led to the conclusion that other target molecules should be investigated in more detail than **H1**.

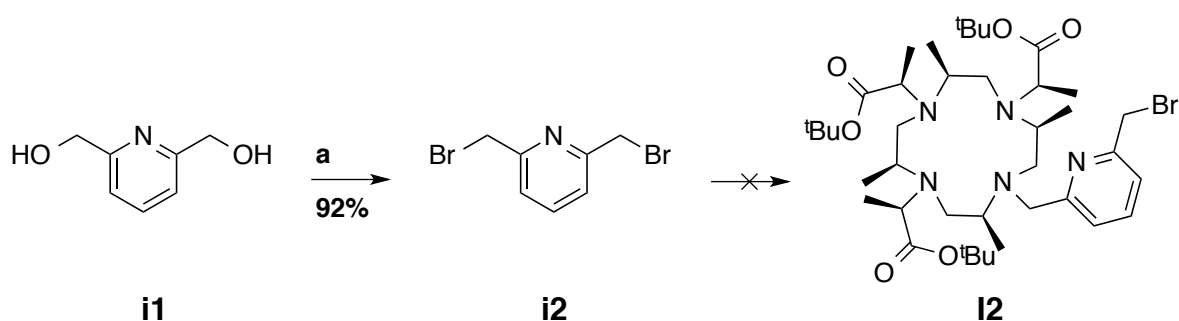


Figure A-52: Synthesis towards **I2**: a) HBr (48%, aq.), 125°C, 6h.

The synthesis of **I2** was developed to have an extremely short linker that should exclude most motion of the tag on the protein surface. The bis functionality of this linker led to the same problems detected for **A1**. The precursor **i2** could be easily synthesized in good yields but good coupling conditions were not found and only conversions below 5% reached. Reaction scales in the 100 mg range (high costs of precursors) are useless with such low yields, when two more steps are required to reach the target molecule, especially when the yield of the ^tBu deprotection is known to be low as well.

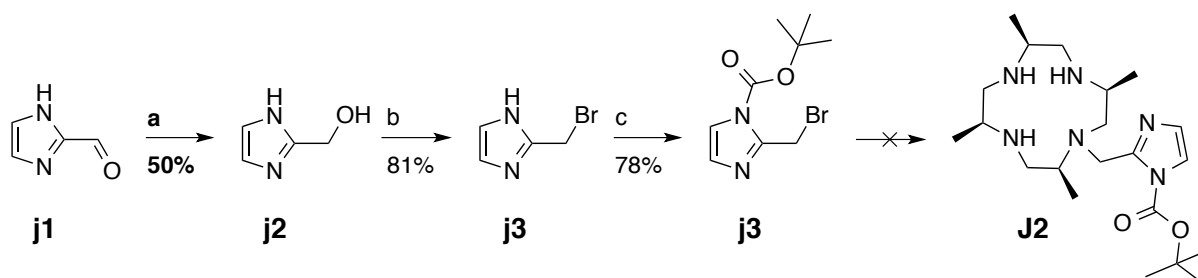


Figure A-53: Synthetic trials towards an imidazole based linker/side chain: a) NaBH₄, ethanol, rt., 2h; b) HBr (33% in AcOH), 100 °C, 4h; c) Boc₂O, NEt₃, DMAP, rt., 2h.

An extremely interesting target molecule is **J2**. Imidazole-based molecules have the advantage that they can be used as neutral side chain, as charged side chain and as linker. The synthesis of this compound was therefore investigated several times under different conditions. Purification by column chromatography does not work for these molecules. The low solubility represents a challenge for the synthesis and purification. The investigation of a suitable protection protocol was quite difficult. The formation of amides works quite well but the removal has to be performed under harsh conditions. The use of Boc is probably also not perfect as the resulting steric bulk decreases the reactivity of the bromine further. Triflate formation was not possible and the mesyl compound again not reactive enough. The formation of the iodo compound is part of on-going research.

A.6 Conclusion

The successful synthesis of three different macrocycles DOTA-M0-acetophenone, DOTA-M7-acetophenone (**A**) and DOTA-M7-thiovinylsulfone (**B**) was achieved. DOTA-M0-acetophenone showed high flexibility, which was predicted for this type of DOTA complexes. Special metalation conditions had to be developed as under standard conditions defunctionalisation of the bromo-functionality was obtained. The high affinity of this linker towards a single cysteine on the protein surface was proven. Fast uptake and a high selectivity were obtained for this complex. The moderate yields obtained for this reaction could not be reproduced for DOTA-M7-acetophenone complexes. The increased steric bulk of the core molecules decrease the reactivity of the 4th nitrogen tremendously. Nevertheless, with the use of sodium hydride we could attach the linker to the macrocycle in about 50% conversions. Recovering of the starting materials was possible. The optimized metalation conditions could be directly applied and worked similar. The weak PCS obtained from NMR experiments compared to DOTA-M8 limit the application of this tag in protein NMR spectroscopy. The fixed geometry of the linker seems to be unfavourable and therefore the tag can no longer interact with the protein surface with its hydrophilic and hydrophobic part. The resulting motion of the tag on the protein surface averages the influence of the paramagnetic ion with respect to the nuclear spins and leads to weak pseudocontact shifts.

A synthetic route towards DOTA-M7-thiovinylsulfone (**B1**) was presented. The metalation works in this case, under standard conditions and no hydrolysed intermediates are obtained. The attachment to the protein surface works much slower for the vinylsulfone than for the disulphides and the α -bromo ketones. Changing to slightly basic conditions could deliver a complete tagging anyway. The obtained PCS are much weaker than the ones obtained for DOTA-M8 and DOTA-M7-acetophenone (**A**). The linker is in this case much longer and has therefore increased flexibility. We further studied the influence of the sulphur atom to the magnetic susceptibility tensor. The comparison of the ¹H-NMR spectra of the Sm-DOTA-M8-SSPy with Sm-DOTA-M7-thio, shows that the dispersion of the shifts is bigger for the complex using a thiol as donor. Nevertheless the absolute shift is stronger for DOTA-M8. It is obvious that the line width is increased for DOTA-M7, this means also that the freedom of the metal ion in the complex is higher for this molecule. The synthesis of DOTA-M8-thiovinyl (**B1**) is still in progress. It is therefore

still unclear if the introduction of an additional methyl group can help to induce stronger PCS. A variety of experiments have been performed and to obtain **B1** and this research may set the basis for further investigations. In general the performed reactions delivered the bases for the introduction of different heteroatoms as donors. The syntheses of macrocycles **C** and **D** are also not finished completely. Many trials have been performed and the latest experimental setup seems to be quite promising for the successful synthesis of these macrocycles.

The studies of different heteroatoms showed, that the tensor can be influenced but it become also obvious that this 8-stereospecific methyl groups are required for an extremely rigid system at rt. It is therefore unambiguous that synthetic routes towards 8 times methylated macrocycles have to be designed. With the studies of the different protection protocols we delivered the bases towards this synthetic challenges.

A.7 Outlook

The synthesis of macrocycles **B1**, **C** and **D** will be finished in the near future. For macrocycle **B1** several ways are possible. The removal of the benzyl protection group using Pd/C has to be performed once again and catalytic amounts of Pd/C exchanged to stoichiometric amounts. On the other hand, it was shown that the amine functionalities couldn't be protected with THP ether. Reduction of mono alkylated species is possible and can be followed by a selective THP protection of the resulting alcohol. The introduction of the missing side chains can than be performed and the alcohol selectively deprotected. This should allow the selective introduction of a thiol moiety. The comparison of Sm-M7 (**B1**) and Sm-M8 (**B1a**) will be performed to see if the line shape become more sharp and to see if the dispersion of the signal has its origin in the change of the tensor and not only in the movement of the metal ion.

For macrocycle **C1** the formation of the triflates has to be tested. The reduced reactivity of the amide nitrogen compared to the amine nitrogen should help to prevent side reactions. The introduction of the keto side chain is also a challenging task. It is so far unclear whether the acetal protection group is stable under these conditions. The usage of a keto-protection group is required as the unprotected ketone is volatile and could not be purified without loss of the molecule. The use of a nitrogen donor opens the way for the introduction of the linker even on the

methylated macrocycle as the nitrogen should be accessible for reactions. Therefore, also highly reactive α -bromo-ketones or α,β -unsaturated systems could be introduced.

The introduction of an α,β -unsaturated ketone is one of the most challenging tasks. Macrocycle **D1** has an extremely short linker and would deliver a thio ether which is stable under physiological conditions. The introduction of the vinyl moiety using vinyl-lithium has to be tested. We hope that dilute conditions allow this introduction in a selective way.

Also further investigations in **J1** should be performed, as this molecule offers a huge variety of possibilities. Nevertheless this molecule has the main disadvantage that a synthesis of an M8 analogue is incredibly difficult. Experiments must show if this is a huge problem or not.

A.8 Experimental Section

A.8.1 Preparative HPLC purification

A Waters Prep LC 4000 system equipped with a Waters 2487 dual λ absorbance detector and a Waters 740 data module was used.

The HPLC solvents were used as followed: Solvent A = water + 0.1 % TFA; Solvent B = 90 % acetonitrile + 10 % water + 0.085 % TFA. The HPLC method started with 2 min 90 % A and 10 % B followed by a gradient over 20 minutes from 90:10 to 50:50. These conditions were kept constant for 3 minutes before changed to 100 % B over 10 minute and flushed for additional 10 minutes.

A.8.2 Experimental procedures

The synthesis of the standard side chain was slightly modified. Also a one-pot synthesis was carried out but the overall yield was below the three-step synthesis.

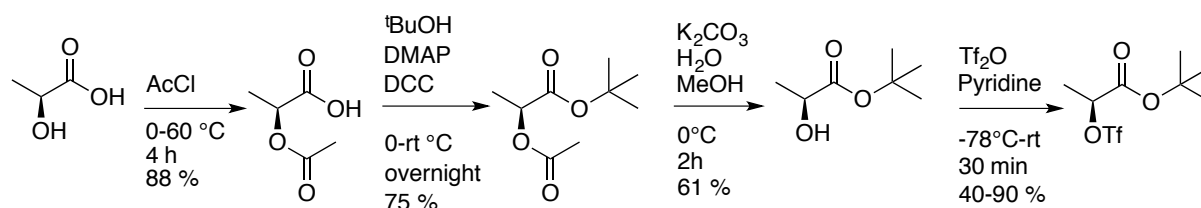


Figure A-54: Synthesis of the standard side chain.

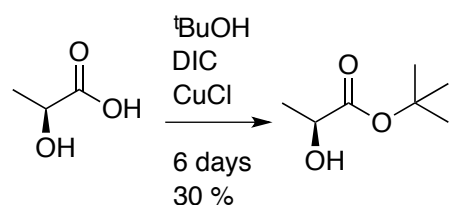
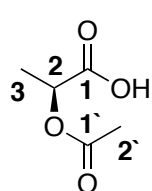


Figure A-55: One pot synthesis for the ^tBu protected lactic acid side chain.

Synthesis of (S)-2-acetoxypropionic acid



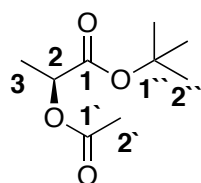
L-lactic acid (5.0 g, 55.5 mmol, 1.0 eq) was dissolved in acetyl chloride (20 mL) at 0 °C. The resulting solution was stirred for 10 min at 0 °C, warmed to rt over 20 min before refluxed (60 °C) for 4 hours. Acetyl chloride was removed under reduced pressure and the crude mixture purified by silica gel column chromatography using chloroform/ethyl acetate (9:1) as eluent to yield 88 % pure product.²⁵

TLC: (SiO₂, chloroform/ethyl acetate (9:1)): **R_f** = 0.27.

$^1\text{H-NMR}$ (400 MHz, 298 K, CDCl_3 , δ in ppm): 7.20 (s, 1H, OH); 5.11 (q, $^3J_{\text{HH}} = 7.1$ Hz, 1H, H2); 2.14 (s, 3H, H2); 1.54 (d, $^3J_{\text{HH}} = 7.1$ Hz, 1H, H3).

$^{13}\text{C-NMR}$ (101 MHz, 298 K, CDCl_3 , δ in ppm): 16.8 (1C, C3); 20.6 (1C, C2'); 68.2 (1C, C2); 170.6 (1C, C1'); 176.2 (1C, C1).

Synthesis of (S)-tert-butyl 2-acetoxypropionate

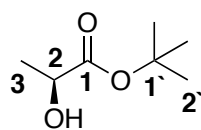


S-2-acetoxypropionate (25.8 g, 196 mmol, 1.0 eq), DMAP (7.9 g, 65 mmol, 0.33 eq) and *tert*-butanol (43.7 g, 589 mmol, 3.0 eq) were dissolved in dichloromethane (560 mL). *N,N'*-dicyclohexylcarbodiimide (60.7 g, 294 mmol, 1.5 eq) dissolved in dichloromethane (200 mL) was added dropwise at 0 °C. The reaction mixture was warmed to rt. and stirred overnight. The resulting precipitate was removed by filtration over celite and washed with dichloromethane. The combined organic layer was washed with water (3 x 250 mL), dried over sodium sulphate and the solvent removed under reduced pressure. The crude mixture was purified by distillation (45°C, 0.5 mbar) and (S)-*tert*-butyl 2-acetoxypropionate (27.8 g, 75%) obtained as colorless liquid.²⁵

Boiling point: 45 °C at 0.5 mbar.

$^1\text{H-NMR}$ (400 MHz, 298 K, CDCl_3 , δ in ppm): 4.95 (q, $^3J_{\text{HH}}=7.2$ Hz, 1H, H2); 2.12 (s, 3H, H2); 1.47 (s, 9H, H2'); 1.45 (d, $^3J_{\text{HH}}=7.2$ Hz, 3H, H3).

Synthesis of (S)-tert-butyl-2-hydroxypropionate



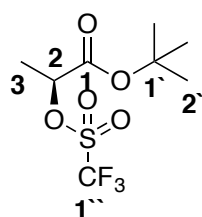
Potassium carbonate (61.0 g, 441 mmol, 3.0 eq) was dissolved in water/methanol (300 mL, 3:2) and a solution of (S)-*tert*-butyl-2-acetoxypropionate (27.8 g, 147 mmol, 1.0 eq) in methanol (15 mL) was added dropwise at 0 °C and further stirred at 0 °C for 2 hours. Dichloromethane (200 mL) was added, the layers separated and the aqueous layer extracted with dichloromethane (2 x 200 mL). The combined organic layer was dried over sodium sulphate and the solvent removed under reduced pressure. The crude mixture was purified by silica gel column chromatography (cyclohexane/ethyl acetate 8:1) to obtain (S)-*tert*-butyl-2-hydroxypropionate (13.2 g, 61 %) as white crystals.⁴⁷

TLC: (SiO_2 , cyclohexane/ethyl acetate (8:1)): $R_f = 0.23$.

$^1\text{H-NMR}$ (250 MHz, 298 K, CDCl_3 , δ in ppm): 4.95 (dq, $^3J_{\text{HH}}=6.9$ Hz, $^3J_{\text{HH}}=4.9$ Hz, 1H, H2); 2.84 (d, $^3J_{\text{HH}}=4.9$ Hz, OH); 1.49 (s, 9H, H2'); 1.37 (d, $^3J_{\text{HH}}=6.9$ Hz, 3H, H3).

$^{13}\text{C-NMR}$ (63 MHz, 298 K, CDCl_3 , δ in ppm): 20.7 (1C, C3); 28.1 (3C, C2'); 67.1 (1C, C2); 82.4 (1C, C1'); 174.2 (1C, C1).

Synthesis of *tert*-butyl (S)-2-(((trifluoromethyl)sulfonyl)oxy)propanoate



Trifluoromethanesulfonic anhydride (7.18 mmol, 1.19 mL, 1.05 eq) was dissolved in dichloromethane (20 mL) under an atmosphere of argon and cooled to $-78\text{ }^\circ\text{C}$. Pyridine (7.87 mmol, 0.64 mL, 1.15 eq) was added and a white precipitate was formed rapidly. *S*-^tBu-lactic acid (1.0 g, 6.84 mmol, 1.0 eq) was dissolved in dichloromethane

(6mL) and added dropwise to the solution. The mixture was stirred at $-78\text{ }^\circ\text{C}$ for 10 minutes before warming to rt. over 10 min and stirred for additional 10 min. The solvent was removed under reduced pressure (water bath cooled to $0\text{ }^\circ\text{C}$). The resulting waxy solid was purified by silica gel column chromatography using a cooled column ($15 - 20\text{ }^\circ\text{C}$, 1.0 cm diameter, 4-5 cm filled) and dichloromethane/hexane (4:1) as eluent. The product (57 %) was isolated (under cooled conditions as described before) as colourless oil. (The reaction was performed several times and yields between 40 and 90 % achieved.)²⁵

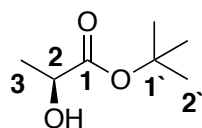
TLC: (SiO_2 , dichloromethane/hexane (4:1)): $R_f = 0.9$.

$^1\text{H-NMR}$ (400 MHz, 298 K, CDCl_3 , δ in ppm): 5.10 (q, $^3J_{\text{HH}}=7.0\text{ Hz}$, 1H, H2); 1.67 (d, $^3J_{\text{HH}}=7.0\text{ Hz}$, 3H, H3); 1.51 (s, 9H, H2).

$^{19}\text{F-NMR}$ (376 MHz, 298 K, CDCl_3 , δ in ppm): -75.4 (s, 3F, CF_3).

$^{13}\text{C-NMR}$ (101 MHz, 298 K, CDCl_3 , δ in ppm): 18.0 (1C, C3), 27.8 (1C, C2'), 80.6 (1C, C2), 84.3 (1C, C1'); 166.4 (1C, C1).

Synthesis of (S)-*tert*-butyl-2-hydroxypropanoate



Tert-butanol (28.8 mL, 305 mmol, 1.1 eq) was added dropwise to a solution of diisopropylcarbodiimide (DIC, 35 g, 43.2 mL, 277 mmol, 1.0 eq) and CuCl (549 mg, 5.5 mmol, 0.02 eq) under inert conditions.

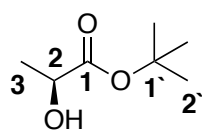
The resulting mixture was stirred for 4 days in the dark to form the activated complex. The activated complex (3.17 mL, 11.1 mmol, 3.5 mol/L, 1.0 eq) was added dropwise to a suspension of *L*-Lactic acid (1.0 g, 11.1 mmol, 1.0 eq) in dichloromethane (20 mL) at $0\text{ }^\circ\text{C}$ over 30 min. The resulting solution was warmed to rt and stirred overnight. Acetic acid (1.4 mL) was added over 20 min and stirred for additional 30 min. The resulting solid diisopropyl urea was removed by filtration and washed with cold dichloromethane (20 mL). Ice-cold water (20 mL) was added and the pH

adjusted to about 8 using solid NaHCO_3 under vigorous stirring. The resulting solid material was removed by filtration. The mixture was extracted and the aqueous layer extracted with DCM (2 X 10 mL) the combined organic layers were washed with NaHCO_3 (sat., aq, 10 mL), water (10 mL) and brine (10 mL). The organic layer was dried over sodium sulphate and the solvent removed under reduced pressure at 10 °C! (The product is easily sublimated). To the resulting oil was added heptane (8 mL) the resulting precipitate filtered off and the filtrate stored at -20 °C overnight. The resulting crystalline product was filtered off and (*S*)-*tert*-butyl-2-hydroxyproponate (31%) obtained as white crystals.⁴⁸

¹H-NMR (600 MHz, 298 K, CDCl_3 , δ in ppm): 4.95 (q, $^3J_{\text{HH}}=6.9$ Hz, $^3J_{\text{HH}}=4.9$ Hz, 1H); 2.84 (d, $^3J_{\text{HH}}=4.9$ Hz, OH); 1.49 (s, 9H); 1.37 (d, $^3J_{\text{HH}}=6.9$ Hz, 3H).

¹³C-NMR (63 MHz, 298 K, CDCl_3 , δ in ppm): 20.7 (1C, C3); 28.1 (3C, C2'); 67.1 (1C, C2); 82.4 (1C, C1'); 174.2 (1C, C1).

Synthesis of (*S*)-*tert*-butyl-2-hydroxyproponate



Tert-butanol (28.8 mL, 305 mmol, 1.1 eq) was added dropwise to a solution of dicyclohexylcarbodiimide (DCC, 57.2 g, 277 mmol, 1.0 eq) and CuCl (549 mg, 5.5 mmol, 0.02 eq) under inert conditions.

The resulting mixture was stirred for 4 days in the dark to form the activated complex. The activated complex (3.17 mL, 11.1 mmol, 3.5 mol/L, 1.0 eq) was added dropwise to a suspension of *L*-Lactic acid (1.0 g, 11.1 mmol, 1.0 eq) in dichloromethane (20 mL) at 0 °C over 30 min. The resulting solution was warmed to rt and stirred overnight. Acetic acid (1.4 mL) was added over 20 min and stirred for additional 30 min. The resulting solid diisopropyl urea was removed by filtration and washed with cold dichloromethane (20 mL). Ice-cold water (20 mL) was added and the pH adjusted to about 8 with solid NaHCO_3 and stirred vigorously. The resulting solid material was removed by filtration. The mixture was extracted and the aqueous layer extracted twice with DCM (10 mL) the combined organic layers were washed with NaHCO_3 (sat., aq, 10 mL), water (10 mL) and brine (10 mL). The organic layer was dried over sodium sulphate and the solvent removed under reduced pressure at 10 °C (The product is easily sublimated). To the resulting oil was added heptane (8 mL) the resulting precipitate filtered off and the filtrate stored at -20 °C overnight. No crystals were formed, therefore the solvent removed and the crude mixture purified by silica gel column chromatography using cyclohexane/ethyl acetate 8:1 as eluent

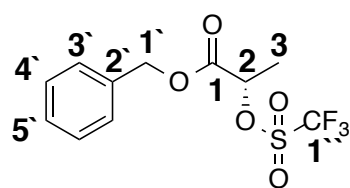
yielding (*S*)-*tert*-butyl-2-hydroxypropanoate (19 %) as white crystals.⁴⁸

TLC: (SiO₂, cyclohexane/ethyl acetate (8:1)): **R_f** = 0.23.

¹H-NMR (600 MHz, 298 K, CDCl₃, δ in ppm): 4.95 (dq, ³J_{HH}=6.9 Hz, ³J_{HH}=4.9 Hz, 1H, H₂); 2.84 (d, ³J_{HH}=4.9 Hz, OH); 1.49 (s, 9H, H₂′); 1.37 (d, ³J_{HH}=6.9 Hz, 3H, H₃).

¹³C-NMR (63 MHz, 298 K, CDCl₃, δ in ppm): 20.7 (1C, C₃); 28.1 (3C, C₂′); 67.1 (1C, C₂); 82.4 (1C, C₁′); 174.2 (1C, C₁).

Synthesis of benzyl (*S*)-2-(((trifluoromethyl)sulfonyl)oxy)propanoate



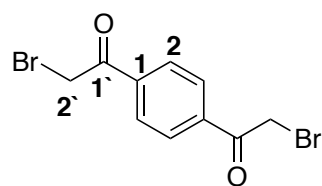
Trifluoromethanesulfonic anhydride (422 μL, 2.54 mmol, 1.15eq) was dissolved in dichloromethane (10 mL) and cooled to -40 °C and pyridine (188 μL, 2.32 mmol, 1.05eq) was added. After a white precipitate was formed the addition of benzyl-2-hydroxy-propanoate (400 mg, 2.22 mmol, 1.0 eq) in dichloromethane (5 mL) was started. The mixture was allowed to warm to rt. and the solvent removed under reduced pressure at 0 °C. The mixture was purified by silica gel column chromatography 1.5 X 3 cm using DCM/hexane (4:1) as eluent.²⁵

TLC: (SiO₂, dichloromethane/hexane (4:1)): **R_f** = 0.88.

¹H-NMR (400 MHz, 298 K, CDCl₃, δ in ppm): 7.34-7.41 (m, 5 H, H₃′-H₅′); 5.23-5.29 (m, 3H, H₂, H₁′); 1.71 (d, ³J_{HH}=7.3 Hz, 3H, H₃).

¹⁹F-NMR (376 MHz, 298 K, CDCl₃, δ in ppm): -75.2 (s, 3F, CF₃).

Synthesis of 1,1'-(1,4-phenylene)bis(2-bromoethan-1-one) (a1)



1,4-diacetylbenzene (324 mg, 2.0 mmol, 1.0 eq), NBS (747 mg, 4.2 mmol, 2.05 eq) and ammonium acetate (30.8 mg, 0.04 mmol, 0.1 eq) were stirred in diethyl ether (10 mL) (suspension). The resulting reaction was stirred for 2 hours before ethyl acetate (10 mL) was added and the resulting mixture washed with water. The organic layer was dried over sodium sulphate and the solvent removed under reduced pressure. The resulting solid was purified by silica gel column chromatography using cyclohexane/ethyl acetate (3:2) as eluent. The pail yellow solid was obtained in 40 % yield.⁴⁹

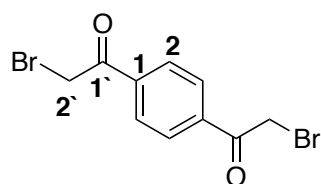
TLC: (SiO₂, cyclohexane/ethyl acetate (3:2)): **R_f** = 0.33

¹H-NMR (400 MHz, 298 K, CDCl₃, δ in ppm): 8.10 (m, 4H, H₂); 4.46 (s, 4H, H₂′).

¹³C-NMR (101 MHz, 298 K, CDCl₃, δ in ppm): 30.9 (2C, C₂′); 129.8 (4C, C₂); 138.1

(2C, C1); 191.1 (2C, C1').

Synthesis of 1,1'-(1,4-phenylene)bis(2-bromoethan-1-one) (a1)

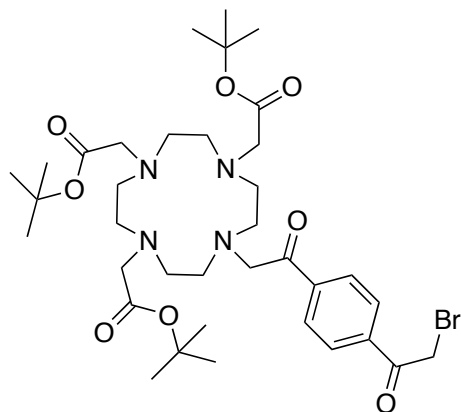


1,4-diacetylbenzene (800 mg, 4.9 mmol, 1.0 eq) was dissolved in glacial acetic acid and bromine (0.5 mL, 9.8 mmol, 2.0 eq) in glacial acetic acid (6 mL) was added dropwise over 20 min at rt. The resulting brownish reaction mixture was heated to 95 °C for 90 min. The reaction mixture was poured into ice-cold water and the resulting precipitate was filtered. The resulting mixture of mono, di and tri brominated species were recrystallized from glacial acetic acid and only the di-brominated species crystallized. The crystallization was performed two times, but the crystals still were not completely white (643 mg, 40 %) (still some contaminations from bromine left).⁵⁰

¹H-NMR (400 MHz, 298 K, CDCl₃, δ in ppm): 8.10 (m, 4H, H₂); 4.46 (s, 4H, H₂').

¹³C-NMR (101 MHz, 298 K, CDCl₃, δ in ppm): 30.9 (2C, C2'); 129.8 (4C, C2); 138.1 (2C, C1); 191.1 (2C, C1').

Synthesis of tri-*tert*-butyl 2,2',2''-(10-(2-(4-(2-bromoacetyl)phenyl)-2-oxoethyl)-1,4,7,10-tetraazacyclododecane-1,4,7-triyl)triacetate; (A3-M0)

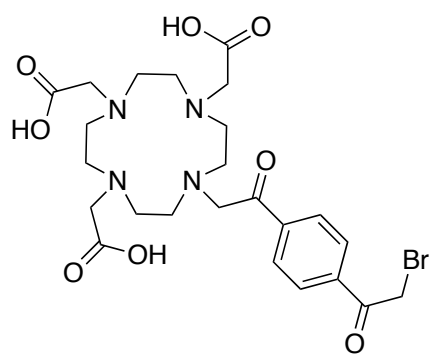


1,2,7-tris(*tert*-butyloxycarbonyl)1,4,7,10-tetraazacyclododecane (50 mg, 0.1 mmol, 1.0 eq) was dissolved in acetonitrile and powdered potassium carbonate (17 mg, 0.12 mmol, 1.12 eq) was added. The resulting solution was heated to 60 °C for 20 minutes before 1,1'-(1,4-phenylene)-bis(2-bromoethan-1-one) (160 mg, 0.5 mmol, 5.0 eq) was added. The resulting reaction mixture was heated to 90 °C for 18 hours, analysed by ESI-MS and a 1:1 mixture of starting material to product determined. Further heating for 24 hour did not deliver any progress and therefore the reaction mixture cooled to rt. and filtered. The solvent was removed under reduced pressure and the crude mixture was purified by silica gel column chromatography using methanol/chloroform (1:10) as eluent. 10 mg (0.013 mmol, 13%) of the desired product were isolated as red solid compound. NMR analysis of the compound could only indicate the introduction of the linker as the

characteristic sharp singlets at 4.50 ppm for the CH₂Br, the CH₂N at 2.01 ppm and the aromatic multiplet between 8.05-8.09 ppm could be identified. A sharp singlet for the *tert*-butyl groups at 1.44 ppm was also identified. All other signals are broad due to conformational changes. The product could be validated by ESI-MS and the bromine pattern could be easily identified.⁵¹

ESI-MS: calc. 753.3 (M+1), 755.3 (M+1); measured 753.5 (M+1); 755.4 (M+1); 775.5 (M+Na), 777.4 (M+Na).

**Synthesis of 2,2',2''-(10-(2-(4-(2-bromoacetyl)phenyl)-2-oxoethyl)-1,4,7,10-tetraazacyclododecane-1,4,7-triyl)triacetic acid;
(DOTA-M0-bromoacetophenone, A4-M0)**



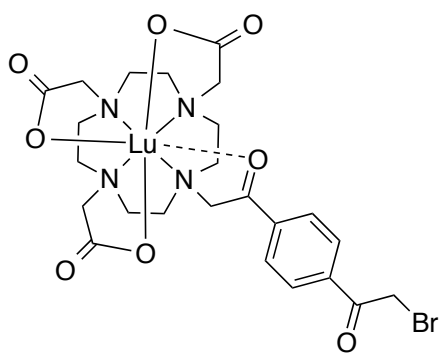
Tri-*tert*-butyl-2,2',2''-(10-(2-(4-(2-bromoacetyl)phenyl)-2-oxoethyl)-1,4,7,10-tetraazacyclododecane-1,4,7-triyl)triacetate (10 mg, 0.01 mmol, 1.0 eq) was dissolved in the deprotection mixture containing TFA/thioanisol/water (9.2:0.6:0.2 v/v, 10 mL) and stirred at rt. The reaction was monitored by ESI-MS.

A steady state between mono and di protected species was determined and an increase of the product. After about 4.5 hours the reaction was finished and the reaction mixture extracted with dichloromethane. The crude mixture was redissolved in acetonitrile/water (1:1, 8 mL) and purified by preparative HPLC under standard HPLC conditions. The desired product (2 mg, 0.003 mmol, 30 %) was obtained as waxy solid.²⁵

ESI-MS: calc. 585.1 (M+1), 587.1 (M+1); measured 585.2 (M+1); 587.2 (M+1).

Retention time: 19.6-20.8 min (A to B, 63:37-62:38)

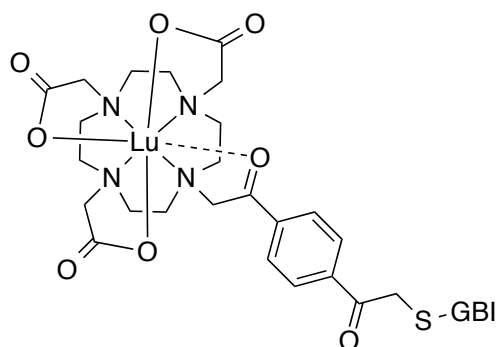
Synthesis of DOTA-M0-Lutetium-bromoacetophenone; (A1-M0)



DOTA-M0-bromoacetophenone (**A4-M0**) (4 mg, 0.007 mmol, 1.0 eq) was dissolved in water (2 mL) and $\text{LuCl}_3 \cdot 6\text{H}_2\text{O}$ (10.6 mg, 0.028 mmol, 4.0 eq) in water (2 mL) was added. To keep the pH slightly basic 3.0 eq of DIPEA were added and the solution was heated to 40 °C for 8 hours. A ESI spectra was measured and in negative mode the desired

product 755^- , 757^- , the hydroxyl-compound 693^- and the chloro-compound 711^- were obtained. Therefore the access of lutetium was removed by a sepag C18 column. The resulting metal complexes were isolated in the MeOH/ H_2O phase. The pH of the hydroxyl-compound was adjusted to about 12 to crash out the metall. After an additional sepag column no more hydroxyl-compound was obtained.²⁵

Synthesis of DOTA-M0-Lutetium-GBI



GB1-T53C (240 μM , in phosphate pH=7, 2 mM DTT). Removal of DTT is needed to react GB1 with the TAG. A exchange column PD MiniTrap G-25 (GE-Healthcare) was used for the removal of DTT. For the elution the Gravity protocol was used.

1.) Open the top and bottom cap to remove the column storage solution.

2.) Fill up the column with equilibration buffer and allow the equilibration buffer to enter the packed bed completely (Phosphate buffer pH = 7.001) A total volume of 8 mL were used for equilibration.

3.) Add 0.5 mL of the sample to the column if less sample is available fill it up to 0,5 mL with buffer.

4.) Elute the sample with exact 1 mL buffer.

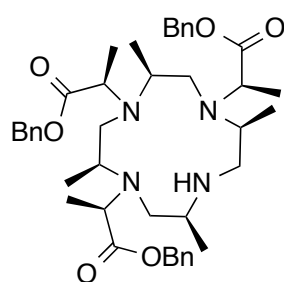
After removing most DTT the protein was labelled with DOTA-M0-Lutetium (chloro- and bromo-compound). Therefore 250 μL (100 μM) GB1 was mixed with 30 μL (1mg/300 μL) of DOTA-M0-Lutetium solution. The mixture was stirred for 1 hour until a full conversion to the protein-tag complex was obtained by ESI-MS.

The protein was purified with an Amicon Ultra Centrifugal Filter (Ultracel - 3K). The Membrane was equilibrated with 3.5 mL phosphate buffer (PO_4^{3-} , 10 mM) (7490 rpm, 15 min). The protein was added and the volume enlarged to 3.5 mL with phosphate buffer and centrifuged. This process was repeated 4 times. Finally the centrifugal time was enlarged to result in a volume of about 200 μL . The protein was taken of the membrane and the membrane washed with 2x35 μL phosphate buffer. The pH was adjusted to 7.002 and 5% D2O was added. The resulting about 300 μL were transferred to a shigemi tube and NMR spectra measured on a Bruker[®] Ascend NMR-700 equipped with cryo probe head.

2 Species were obtained in the ^{15}N - ^1H -HSQC-NMR spectra.

ESI-MS data are presented in the Result section.

Synthesis of tribenzyl 2,2',2''-((2S,5S,8S,11S)-2,5,8,11-tetramethyl-1,4,7,10-tetraazacyclododecane-1,4,7-triyl)(2R,2'R,2''R)-tripropionate; (M7-Bn₃-(3R,4S)-,



A3Bn)

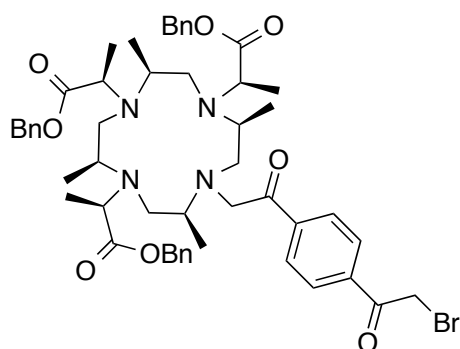
M4-cyclen (100 mg, 0.44 mmol, 1.0 eq) was dissolved in dichloromethane (20 mL, dry) under inert conditions and freshly powdered potassium carbonate (220 mg, 2.19 mmol, 5.0 eq) was added. (*L*)-Bn-lactate triflate (400 mg, 1.23 mmol, 2.9 eq) in dichloromethane (6 mL, dry) was added dropwise

over 1.5 hours. The reaction was stirred overnight and quenched with triethylamine (3 mL). The crude mixture was filtered and washed with dichloromethane before the solvent was removed under reduced pressure and purified by silica gel column chromatography using chloroform/ethanol/triethylamine (3:1:0.15) as eluent. Fractions were analysed by ESI-MS and the product isolated as brownish oil in 65 % yield.²⁵

ESI-MS: calc. 715.4 (M+1); measured 715.5 (M+1).

Synthesis of tribenzyl 2,2',2''-((2*S*,5*S*,8*S*,11*S*)-10-(2-(4-(2-bromoacetyl)phenyl)-2-oxoethyl)-2,5,8,11-tetramethyl-1,4,7,10-tetraazacyclododecane-1,4,7-

triyI)(2*R*,2'*R*,2''*R*)-tripropionate; (M7-Bn₃-(3*R*,4*S*)-bromoacetophenone, A4Bn)



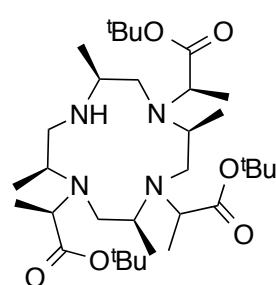
M7-Bn₃ (**A3Bn**) (90 mg, 0.13 mmol, 1.0 eq) was dissolved in acetonitrile (5 mL, dry) under inert conditions and freshly powdered potassium carbonate (20 mg, 0.15 mmol, 1.2 eq) was added and heated to 60 °C for 20 min. 1,1'-(1,4-phenylene)bis(2-bromoethan-1-one) (200 mg, 0.63 mmol, 5.0 eq) in acetonitrile (2 mL, dry) was added

and stirred for additional 8 hours at 60 °C. The reaction mixture was cooled to rt., filtered and the solvent removed under reduced pressure. The reaction mixture was purified by silica gel column chromatography using chloroform/ethanol/triethylamine (3:1:0.15) as eluent. The product was obtained as waxy yellowish solid in 40 % yield.⁵¹ (Benzyl deprotection using Pd/C, 1 bar H₂ pressure delivered no conversion and with an pressure increase to 4 bar also one of the keto groups was reduced to a CH₂-group).

ESI-MS: calc. 953.4 (M+1); 955.4 (M+1); measured 953.4 (M+1); 955.4 (M+1).

Synthesis of di-*tert*-butyl 2,2'-((2*S*,5*S*,8*S*,11*S*)-4-(1-(*tert*-butoxy)-1-oxopropan-2-yl)-2,5,8,11-tetramethyl-1,4,7,10-tetraazacyclododecane-1,7-diyl)(2*R*,2'*R*)-dipropionate

(M7-tri-*tert*butyl, A2^tBu)

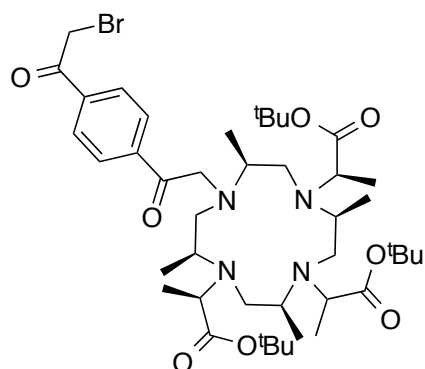


M4-cyclen (100 mg, 0.438 mmol, 1.0 eq) was dissolved in dry dichloromethane (20 mL) under an atmosphere of argon and *tert*-butyl (S)-2-(((trifluoromethyl)sulfonyl)oxy)propanoate (380 mg, 1.37 mmol, 2.85 mmol) in dichloromethane (6 mL) was added over 10 minutes. The solution was stirred at rt. ESI-MS showed formation of mono and bis alkylated species after 1 hour. ESI-MS after 14 hours showed major bis alkylated, some mono and some tri alkylated species. Therefore K₂CO₃ (100 mg) was added to push the equilibrium to the tri alkylated species. Additional two hours of stirring later another 80 mg of *tert*-butyl (S)-2-(((trifluoromethyl)sulfonyl)oxy)propanoate was added. Even after 28 hours no full conversion was obtained therefore acetonitrile (5 mL, 20 %) was added. After

60 hour reaction time the desired product was formed as mayor product. The reaction was quenched wit triethylamine (300 μ L) and stirred for 30 minutes. The reaction mixture was filtered over celite and the solvent removed under reduced pressure. The crude mixture was purified by silica gel column chromatography using chloroform/ethanol/triethylamine (95:5:1 -> 80:20:1) to yield 80 % off the desired product.²⁵

ESI-MS: calc. 613.5 (M+1); measured 613.5 (M+1).

Synthesis of di-*tert*-butyl 2,2'-((2*S*,5*S*,8*S*,11*S*)-4-(2-(4-(2-bromoacetyl)phenyl)-2-oxoethyl)-10-(1-(*tert*-butoxy)-1-oxopropan-2-yl)-2,5,8,11-tetramethyl-1,4,7,10-tetraazacyclododecane-1,7-diyl)(2*R*,2'*R*)-dipropionate (M7-tri-*tert*butyl-bromoacetophenone, A3^tBu)

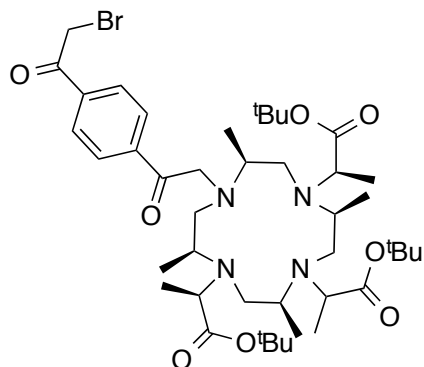


M7-tri-*tert*butyl (**A2^tBu**) (40 mg, 0.065 mmol, 1.0 eq) was dissolved in acetonitrile (7 mL) and K₂CO₃ (4.5 mg, powdered) was added. The mixture was heated to 60 °C and 1,1'-(1,4-phenylene)bis(2-bromoethan-1-one) (**a1**) (83 mg, 0.26 mmol, 4.0 eq) in acetonitrile (5 mL) was added in one shot. The reaction was monitored by ESI-MS, every 30 minutes. After 3

hours the reaction mixture was filtered and the solvent removed under reduced pressure. The crude reaction mixture was purified by silica gel column chromatography using chloroform/ethanol (9:1 -> 9:2 -> ethanol with 1 % triethylamine). Starting materials could be recovered and 30% of the desired product was isolated.⁵¹

ESI-MS: calc. 851.5 (M+1); 853.5 (M+1) measured 851.5 (M+1); 853.5 (M+1).

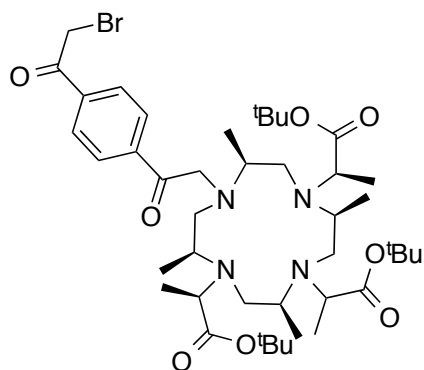
Synthesis of di-*tert*-butyl 2,2'-((2*S*,5*S*,8*S*,11*S*)-4-(2-(4-(2-bromoacetyl)phenyl)-2-oxoethyl)-10-(1-(*tert*-butoxy)-1-oxopropan-2-yl)-2,5,8,11-tetramethyl-1,4,7,10-tetraazacyclododecane-1,7-diyl)(2*R*,2'*R*)-dipropionate (M7-tri-*tert*butyl-bromoacetophenone, A3^tBu)



M7-tri-*tert*butyl (40 mg, 0.065 mmol, 1.0 eq) was dissolved in acetonitrile (7 mL) and Cs₂CO₃ (43 mg, powdered, 4.0 eq) was added. The mixture was heated to 40 °C and 1,1'-(1,4-phenylene)bis(2-bromoethan-1-one) (**a1**) (83 mg, 0.26 mmol, 4.0 eq) in acetonitrile (5 mL) was added in one shot. The reaction was monitored by ESI-MS, every 30 minutes. After 3 hours the reaction mixture was filtered and the solvent removed under reduced pressure. The crude reaction mixture was purified by silica gel column chromatography using chloroform/ethanol (9:1 → 9:2 → ethanol with 1 % triethylamine). Starting materials could be recovered and 32% of the desired product was isolated.⁵¹

ESI-MS: calc. 851.5 (M+1); 853.5 (M+1) measured 851.5 (M+1); 853.5 (M+1).

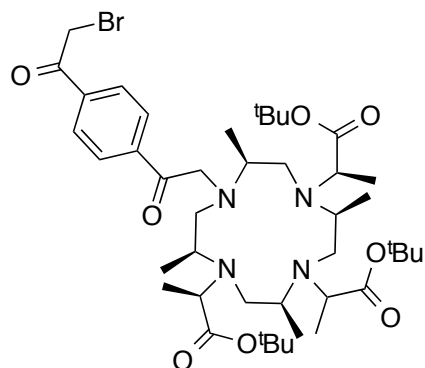
Synthesis of di-*tert*-butyl 2,2'-((2*S*,5*S*,8*S*,11*S*)-4-(2-(4-(2-bromoacetyl)phenyl)-2-oxoethyl)-10-(1-(*tert*-butoxy)-1-oxopropan-2-yl)-2,5,8,11-tetramethyl-1,4,7,10-tetraazacyclododecane-1,7-diyl)(2*R*,2'*R*)-dipropionate



(M7-tri-*tert*butyl-bromoacetophenone, A3^tBu)
M7-tri-*tert*butyl (40 mg, 0.065 mmol, 1.0 eq) was dissolved in acetonitrile (7 mL) and NaHCO₃ (166 mg, powdered, 8.0 eq) was added. The mixture was heated to 40 °C and 1,1'-(1,4-phenylene)bis(2-bromoethan-1-one) (**a1**) (83 mg, 0.26 mmol, 4.0 eq) in acetonitrile (5 mL) was added in one shot. The reaction was monitored by ESI-MS, every 30 minutes. After 3 hours the reaction mixture was filtered and the solvent removed under reduced pressure. A conversion of 65% was determined from ESI-MS analysis.⁵¹

ESI-MS: calc. 851.5 (M+1); 853.5 (M+1) measured 851.5 (M+1); 853.5 (M+1).

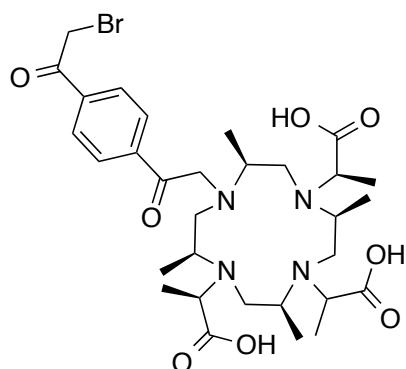
Synthesis of di-*tert*-butyl 2,2'-((2*S*,5*S*,8*S*,11*S*)-4-(2-(4-(2-bromoacetyl)phenyl)-2-oxoethyl)-10-(1-(*tert*-butoxy)-1-oxopropan-2-yl)-2,5,8,11-tetramethyl-1,4,7,10-tetraazacyclododecane-1,7-diyl)(2*R*,2'*R*)-dipropionate (M7-tri-*tert*butyl-bromoacetophenone, A3^tBu)



M7-tri-*tert*butyl (50 mg, 0.082 mmol, 1.0 eq) was dissolved in acetonitrile (7 mL) and NaH (4.8 mg, 0.2 mmol, 2.5 eq, 60%) was added. The mixture was heated to 40 °C for 40 min before 1,1'-(1,4-phenylene)bis(2-bromoethan-1-one) (104 mg, 0.33 mmol, 4.0 eq) in acetonitrile (5 mL) was added in one shot. The reaction was monitored by ESI-MS, every 30 minutes. After 3 hours the reaction mixture was filtered and the solvent removed under reduced pressure. A conversion of 80-90% was determined from ESI-MS analysis. No purification was performed.⁵¹

ESI-MS: calc. 851.5 (M+1); 853.5 (M+1) measured 851.5 (M+1); 853.5 (M+1).

Synthesis of (2*R*,2'*R*)-2,2'-((2*S*,5*S*,8*S*,11*S*)-4-(2-(4-(2-bromoacetyl)phenyl)-2-oxoethyl)-10-(1-carboxyethyl)-2,5,8,11-tetramethyl-1,4,7,10-tetraazacyclododecane-1,7-diyl)dipropionic acid (M7-tri-acid-bromoacetophenone, A4)

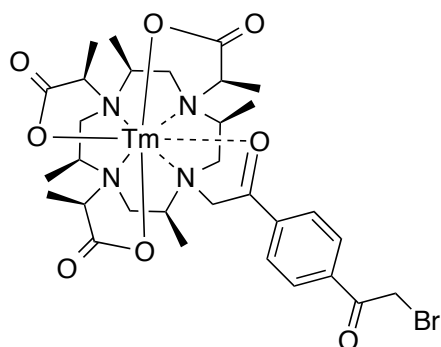


M8-tri-*tert*butyl-bromoacetophenone (60 mg, 0.07 mmol, 1.0 eq) was dissolved in trifluoroacetic acid. The resulting reaction mixture was stirred at rt. for 3 hours. Trifluoroacetic acid was removed under reduced pressure. The resulting mixture was redissolved in water and the pH adjusted to 7 using ammonium acetate. The resulting neutral compound was purified by prep HPLC under standard conditions to yield 15 mg (31%) of the desired product.⁵²

Retention time: 16.3-18.1 min (45 – 47% B).

ESI-MS: calc. 683.3 (M+1); 685.3 (M+1) measured 683.3 (M+1); 685.3 (M+1).

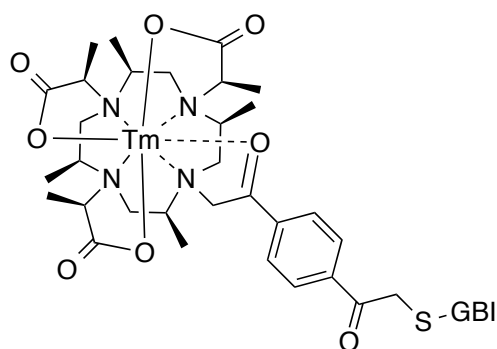
Synthesis of DOTA-M7-Thulium-bromoacetophenone (TmA1)



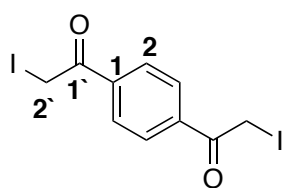
M7-tri-acid-bromoacetophenone (2.0 mg, 0.003 mmol, 1.0 eq) was dissolved in water (2 mL) and TmBr_3 (4.8 mg, 0.012 mmol, 4.0 eq) was added. The pH was adjusted with DIPEA to 8 and the solution was stirred at rt. for 1 hour (Short reaction time to avoid strong defunctionalisation). The crude mixture was purified by SepPak column chromatography (Elution with water removes excess Tm salt, whereas a mixture of water/methanol 2:8 elutes the metal complex). The solvent mixture was removed under reduced pressure and the title compound obtained as a 2:1 mixture of bromo to hydrolysed metal complex.²⁵

ESI-MS: calc. 849.2 (M+1); 851.2 (M+1) measured 849.2 (M+1); 851.2 (M+1); 871.2 (M+Na); 8.73.2 (M+Na); 787.3 (OH, M+1); 809.3 (OH, M+Na).

Synthesis of DOTA-M7-Thulium-acetophenone-GBI

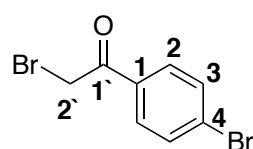


DOTA-M7-Thulium-bromoacetophenone (2.5 mg) was dissolved in 100 μL phosphate buffer (PO_4^{3-} , 10 mM) and GBI (124 μL , 10 μM) in phosphate buffer was added. The reaction was performed over night. The protein was purified with a Amicon Ultra Centrifugal Filter (Ultracel - 3K). The Membrane was equilibrated with 3.5 mL phosphate buffer (PO_4^{3-} , 10 mM) (7490 rpm, 15 min). The protein was added and the volume enlarged to 3.5 mL with phosphate buffer and centrifuged. This process was repeated 4 times. Finally the centrifugal time was enlarged to result in a volume of about 200 μL . The protein was taken of the membrane and the membrane washed with 2*35 μL phosphate buffer. The pH was adjusted to 7.002 and 5% D_2O was added. The resulting about 300 μL were transferred to a shigemi tube and the NMR measurements were performed on a Bruker Ultra Shield 600 MHz NMR-spectrometer using a TXI-probehead. The correct mass-pattern was obtained by ESI-MS analysis.

Synthesis of 1,1'-(1,4-phenylene)bis(2-iodoethan-1-one) (a2)

1,1'-(1,4-phenylene)bis(2-bromoethan-1-one) (20 mg, 1.0 eq) dissolved in acetone (3 mL) and sodium iodide (120 mg, 3.0 eq) in acetone (2 mL) was added over 5 min. The resulting reaction mixture was stirred for 5 hours and the resulting precipitate was filtered off. The solvent was removed under reduced pressure. The desired product was obtained in quantitative yield as reddish solid.

$^1\text{H-NMR}$ (400 MHz, 298 K, CDCl_3 , δ in ppm): 8.09 (m, 4H, H₂); 4.39 (s, 4H, H_{2'}).

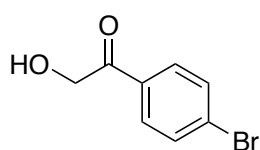
Synthesis of 2-bromo-1-(4-bromophenyl)ethan-1-one (a3)

4-bromoacetophenone (1.0 g, 5.0 mmol, 1.0 eq) was dissolved in water (2.5 mL) and hydrobromic acid (0.29 mL, 2.5 mmol, 0.5 eq) was added. The resulting mixture was stirred at rt. in the dark for 5 min before hydrogen peroxide (0.26 mL, 2.5 mmol, 0.5 eq) was added and stirred for additional 2 hours. Another 0.5 eq of hydrobromic acid and hydrogen peroxide were added and stirred for another 2 hours before the procedure was repeated once again and the resulting mixture stirred overnight at rt.. The reaction was quenched with hexane/ethyl acetate (10:1; 10 mL) and Na_2SO_3 (2g). The reaction mixture was filtered over sodium sulphate and washed with 20 mL dichloromethane. The solvent was removed under reduced pressure and the crude mixture purified by silica gel column chromatography using cyclohexane/dichloromethane (1:1) as eluent. Nice white crystalline product (700 mg, 2.5 mmol, 50 %) was obtained.⁵³

TLC: (SiO_2 , cyclohexane/dichloromethane (1:1)): $R_f = 0.46$.

$^1\text{H-NMR}$ (400 MHz, 298 K, CDCl_3 , δ in ppm): 7.84-7.87 (m, 2H, H₂); 7.64-7.66 (m, 2H, H₃); 4.40 (s, 2H, H_{2'}).

$^{13}\text{C-NMR}$ (63 MHz, 298 K, CDCl_3 , δ in ppm): 30.4 (1C, C_{2'}); 129.5 (1C, C₁); 130.6 (2C, C₃); 132.4 (2C, C₂); 132.8 (1C, C₄); 190.6 (1C, C_{1'}).

Synthesis of 2-bromo-1-(4-bromophenyl)ethan-1-one (a4)

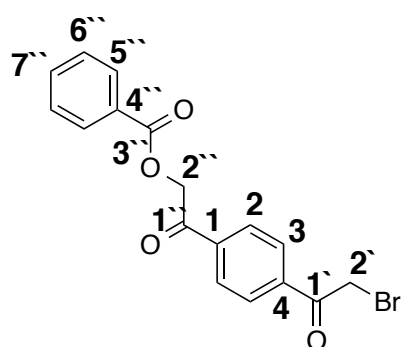
2-bromo-1-(4-bromophenyl)ethan-1-one (500 mg, 2.3 mmol, 1.0 eq) was dissolved in water (3 mL) irradiated with microwave in a sealed tube to 125 °C (5 bar) for 25 minutes. Diethylether (30 mL) was added and the phases separated. The organic layer

was washed with sodium thiosulphate (2 X 2 mL) and brine (2 X 2 mL) and finally water (2 X 2 mL). The organic layer was dried over sodium sulphate and the solvent removed under reduced pressure. The crude mixture was purified by silica gel column chromatography using cyclohexane/ethyl acetate (4:1) as eluent yielding the desired product as yellow solid (90-95 %).⁵⁴

TLC: (SiO₂, cyclohexane/ethyl acetate (4:1)): **R_f** = 0.13.

¹H-NMR (400 MHz, 298 K, CDCl₃, δ in ppm): 7.78-7.80 (m, 2H, H₂); 7.65-7.67 (m, 2H, H₃); 4.84 (d, ³J_{HH}=4.0 Hz, 2H, H_{2'}); 3.43 (t, ³J_{HH}=4.0 Hz, 1H, OH).

Synthesis of 2-(4-(2-bromoacetyl)phenyl)-2-oxoethyl benzoate a7



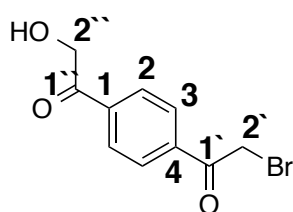
Benzoic acid (135 mg, 0.938 mmol, 1.0 eq) was dissolved in acetone (20 mL) and sodium (1.0 eq) was added. The solution was stirred until all sodium had reacted. 1,1'-(1,4-phenylene)bis(2-bromoethan-1-one) (300 mg, 0.938 mmol, 1.0 eq) was dissolved in acetone (20 mL) and added at rt. The reaction was stirred at rt. overnight. The mixture was heated to

reflux for further 5 hours. The reaction was checked by TLC cyclohexane/ethyl acetate (7:3). Heating did not deliver any progress. The solvent was removed under reduced pressure and the crude mixture redissolved in dichloromethane. The organic layer was washed with water three times and dried over sodium sulphate. The solvent was removed and the mixture was purified by silica gel column chromatography cyclohexane/ethyl acetate (9:1 -> 8:2) to yield 100 mg (29 %) of the title compound.⁵⁵

TLC: (SiO₂, cyclohexane/ethyl acetate (9:1)): **R_f** = 0.07.

¹H NMR (400 MHz, 298 K, CDCl₃, δ in ppm): 8.07-8.15 (m, 6H, H₂, H₃, H_{5''}); 7.60-7.64 (m, 1H, H_{7''}); 7.46-7.50 (m, 2H, H_{6''}); 5.58 (s, 2H, H_{2''}); 4.47 (s, 2H, H_{2'}).

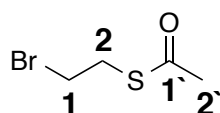
¹³C NMR (101 MHz, 298 K, CDCl₃, δ in ppm): 30.6 (1C, 2'); 66.7 (1C, C_{2''}); 128.43 (2C, C₃); 128.67 (2C, C₂); 129.27 (1C, C_{7''}); 129.6 (2C, C_{5''}); 130.1 (2C, C_{6''}); 133.7 (1C, C_{4''}); 137.8 (1C, C₄); 138.2 (1C, C₁); 166.1 (1C, C_{3''}); 190.8 (1C, C_{1'}); 191.8 (1C, C_{1''}).

Synthesis of 2-bromo-1-(4-(2-hydroxyacetyl)phenyl)ethan-1-one a8

2-(4-(2-bromoacetyl)phenyl)-2-oxoethyl acetate (crude mixture containing (25%) mono and di protected species) (500 mg, 1.94 mmol, 1.0 eq) were dissolved in ethanol (10 mL) and HCl (1M aq, 5mL) was added. The yellowish mixture was heated to reflux and the reaction progress was monitored by TLC cyclohexane/ethyl acetate (7:3). The pure product (80%) was obtained after silica gel column chromatography using cyclohexane/ethyl acetate (7:3) as eluent.⁵²

TLC: (SiO₂, cyclohexane/ethyl acetate (7:3)): **R_f** = 0.19.

¹H NMR (400 MHz, 298 K, CDCl₃, δ in ppm): 8.02-8.13 (m, 4H, H₂, H₃); 4.92 (d, ³J_{HH} = 4.6 Hz, H_{2''}); 4.71 (s, 2H, H_{2'}); 3.39 (t, ³J_{HH} = 4.6 Hz, OH).

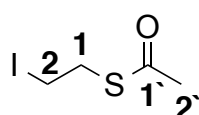
Synthesis of 1-bromo-2-thioacetate-ethane (b1)

1,2-dibromomethane (3 mL, 35.0 mmol, 2.0 eq) and potassium thioacetate (2.0 g, 17.5 mmol, 1.0 eq) were dissolved in THF (dry, 40 mL) and heated to reflux for 7 hours. KBr was removed by filtration and the solvent of the filtrate was removed under reduced pressure. The crude mixture was pre-purified by silica gel column chromatography using ethyl acetate/cyclohexane (1:10) as eluent, followed by a second silica gel column using cyclohexane/dichloromethane (9:1) as eluent. The title compound (1.48 g, 8.1 mmol, 46%) was obtained as colourless oil.⁵⁶

TLC: (SiO₂, cyclohexane/dichloromethane (9:1)): **R_f** = 0.29

¹H-NMR (400 MHz, 298 K, CDCl₃, δ in ppm): 3.42 – 3.47 (m, 2H, H₁); 3.28 – 3.32 (m, 2H, H₂); 2.35 (s, 3H, H_{2'}).

¹³C-NMR (101 MHz, 298 K, CDCl₃, δ in ppm): 30.1 (1C, C_{2'}); 30.7 (1C, C₁); 31.4 (1C, C₂); 194.7 (1C, C_{1'}).

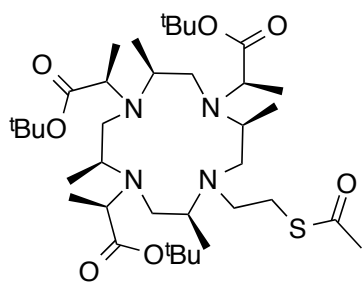
Synthesis of 1-iodo-2-thioacetate-ethane (b2)

1-bromo-2-thioacetate-ethane (180 mg, 0.98 mmol, 1.0 eq) was dissolved in acetone (5 mL, dry) and sodium iodide (1.18 mmol, 177 mg, 1.2 eq) was added. The resulting reaction mixture was stirred at rt. for 2 hours, filtered and the precipitate washed with ethyl acetate. The solvent was removed under reduced pressure and the crude mixture containing 80% iodo and 20% bromo was used without further purification.⁵⁶

$^1\text{H-NMR}$ (400 MHz, 298 K, CDCl_3 , δ in ppm): 3.30-3.37 (m, 2H, H1); 3.21-3.29 (m, 2H, H1); 2.35 (s, 3H, H2').

$^{13}\text{C-NMR}$ (101 MHz, 298 K, CDCl_3 , δ in ppm): 2.2 (1C, C2); 30.7 (1C, C2'); 32.2 (1C, C1); 194.6 (1C, C1').

Synthesis of tri-*tert*-butyl 2,2',2''-((2*S*,5*S*,8*S*,11*S*)-10-(2-(acetylthio)ethyl)-2,5,8,11-tetramethyl-1,4,7,10-tetraazacyclododecane-1,4,7-triyl)(2*R*,2'*R*,2''*R*)-

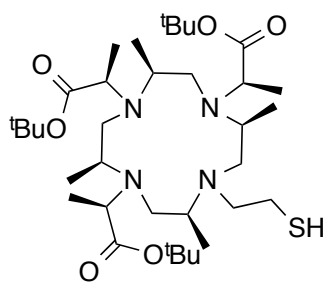


tripropionate; (DOTA-M7-(3*R*,4*S*)-thioacetate, (B2))

DOTA-M7-(3*R*,4*S*) (A2) (50 mg, 0.08 mmol, 1.0 eq) was dissolved in acetonitrile (10 mL, dry) under inert conditions and sodium hydride (60 % in mineral oil, 15 mg, excess) was added. 1-iodo-2-thioacetate-ethane (56 mg, 0.25 mmol, 3.0 eq) was added. The reaction was stirred at rt. for 7 hours. A maximum of about 50 % conversion was achieved even after reflux overnight.

ESI-MS: calc. 715.5 (M+1); measured 715.5 (M+1) + starting material 613.5 (M+1).

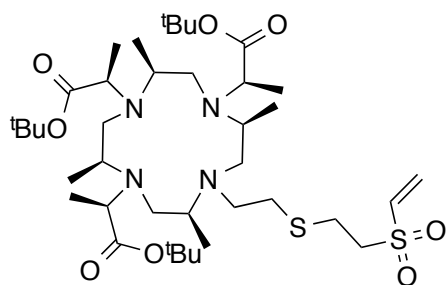
Synthesis of tri-*tert*-butyl 2,2',2''-((2*S*,5*S*,8*S*,11*S*)-10-(2-mercaptoethyl)-2,5,8,11-tetramethyl-1,4,7,10-tetraazacyclododecane-1,4,7-triyl)(2*R*,2'*R*,2''*R*)-
tripropionate; (DOTA-M7-(3*R*,4*S*)-thio, (B3))



To a solution of (DOTA-M7-(3*R*,4*S*)-thioacetate) (12 mg, 0.02 mmol, 1.0 eq) in methanol (1 mL) under inert conditions was added sodium thiomethoxide (1.0 eq, 1M, in MeOH). The reaction mixture was stirred for 1.5 hours. The reaction was quenched using hydrochloric acid (2mL, 0.1 M) and extracted with dichloromethane (2 X 5 mL). The combined organic layer was washed with brine, dried over sodium sulphate and the solvent removed under reduced pressure. ESI-MS showed dimer and RS-SMe formation therefore an excess of TCEP (2 mL (in 350 mM KOH)) was added and stirred overnight. A full conversion to free thiol was determined by ESI-MS.⁵²

ESI-MS: calc. 673.5 (M+1); measured 673.5 (M+1).

Synthesis of tri-*tert*-butyl 2,2',2''-((2*S*,5*S*,8*S*,11*S*)-2,5,8,11-tetramethyl-10-(2-((2-(vinylsulfonyl)ethyl)thio)ethyl)-1,4,7,10-tetraazacyclododecane-1,4,7-triyl)(2*R*,2'*R*,2''*R*)-tripropionate; (DOTA-M7-(3*R*,4*S*)-thiovinylsulfone, (B4))

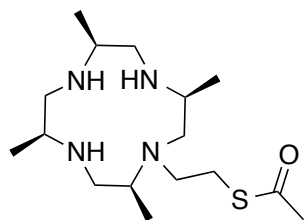


(DOTA-M7-(3*R*,4*S*)-thio) (10 mg, 0.015 mmol, 1.0 eq) and divinyl sulfone (7.0 mg, 0.06 mmol, 4.0 eq) were dissolved in ethanol (5 mL, dry) and heated to reflux for 60 minutes. Full conversion was obtained by ESI. Unfortunately purification with silica gel column chromatography using chloroform/ethanol

9:1 → 1:1 led to by-product formation where ethanol was attached to the vinyl group. This fact was quite strange as formation of the divinyl sulfone to the thiol was performed in boiling ethanol without formation of any by-products. A yield from about 5% was therefore determined out of the mixture.^{57,58}

ESI-MS: calc. 791.5 (M+1); measured 791.6 (M+1).

Synthesis of S-(2-((2*S*,5*S*,8*S*,11*S*)-2,5,8,11-tetramethyl-1,4,7,10-tetraazacyclododecan-1-yl)ethyl) ethanethioate; (DOTA-M4-(4*S*)-thioacetate (B6))



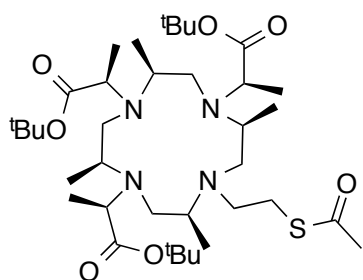
Cyclen-M4 (300 mg, 1.31 mmol, 1.0 eq) was dissolved in dichloromethane (20 mL, dry) under inert conditions and sodium hydride (63 mg, 1.58 mmol, 1.2 eq, 60% in mineral oil) was added and stirred for 20 min at rt. 1-bromo-2-thioacetate-ethane (240 mg, 1.31 mmol, 1.0 eq) was added

and stirred at rt. for 20 hours. The statistical reaction delivered 20 % starting material, 60 % product and 20 % of the bis-alkylated species. The crude mixture was used without further purification.

ESI-MS: calc. 331.3 (M+1); measured 331.2 (M+1).

(ESI-MS: bis alkylated calc. 433.3 (M+1); measured 433.2 (M+1).)

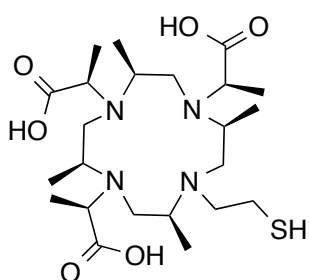
Synthesis of tri-*tert*-butyl 2,2',2''-((2*S*,5*S*,8*S*,11*S*)-10-(2-(acetylthio)ethyl)-2,5,8,11-tetramethyl-1,4,7,10-tetraazacyclododecane-1,4,7-triyl)(2*R*,2'*R*,2''*R*)-tripropionate; (DOTA-M7-(3*R*,4*S*)-thioacetate, (B7))



(DOTA-M4-(4*S*)-thioacetate) (433 mg crude mixture, 1.0 eq) was dissolved in acetonitrile (20 mL) and potassium carbonate (724 mg, 5.24 mmol, 4.0 eq) was added under inert conditions. A solution of *tert*-butyl (*S*)-2-(((trifluoromethyl)sulfonyl)oxy)propanoate in acetonitrile was added slowly and the resulting reaction mixture was stirred at rt. overnight. The crude mixture was purified by silica gel column chromatography using chloroform/ethanol/triethylamine (9:1:0.01) as eluent and the desired product (250mg, 26%) was obtained as yellowish waxy oil.²⁵

ESI-MS: calc. 715.5 (M+1); measured 715.5 (M+1).

Synthesis of (2*R*,2'*R*,2''*R*)-2,2',2''-((2*S*,5*S*,8*S*,11*S*)-10-(2-mercaptoethyl)-2,5,8,11-tetramethyl-1,4,7,10-tetraazacyclododecane-1,4,7-triyl)tripropionic acid; (DOTA-M7-(4*S*,3*R*)-OH-thiol, (B8))

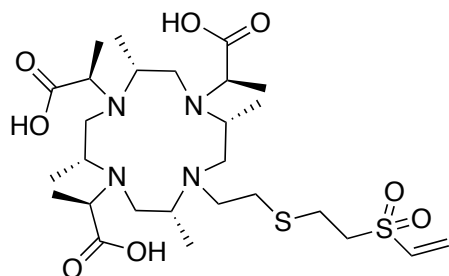


(DOTA-M7-(3*R*,4*S*)-thioacetate) (50 mg, 0.07 mmol, 1.0 eq) was dissolved in hydrochloric acid (1M, 20 mL) and heated to reflux for 60 minutes. The pH was adjusted to 7.0 using potassium hydroxide. The volume was reduced to 10 mL and the crude mixture purified by preparative HPLC under standard conditions. The product was obtained as colourless waxy solid in 80% yield.⁵²

Retention time: 13.2-14 min.

ESI-MS: calc. 505.3 (M+1); measured 505.3 (M+1).

Synthesis of (2*R*,2'*R*,2''*R*)-2,2',2''-((2*R*,5*R*,8*R*,11*R*)-2,5,8,11-tetramethyl-10-(2-((2-(vinylsulfonyl)ethyl)thio)ethyl)-1,4,7,10-tetraazacyclododecane-1,4,7-triyl)tripropionic acid; (DOTA-M7-(4*S*,3*R*)-OH-thiovinylsulfone, (B9))

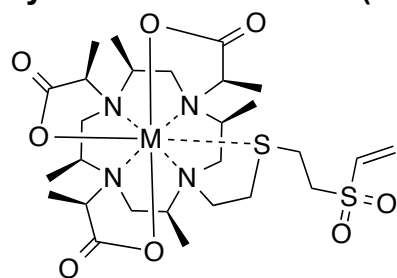


under standard conditions.^{57,58}

Retention time: 16.3-17.4 min.

ESI-MS: calc. 623.3 (M+1); measured 623.4 (M+1).

Synthesis of DOTA-M7-(4*S*,3*R*)-metal-thiovinylsulfone, (B1)



DOTA-M7-(4*S*,3*R*)-OH-thiovinylsulfone (4.0 mg, 0.006 mmol, 1.0 eq) and metal chloride hexahydrate (4.0 eq) were dissolved in aqueous ammonium acetate (100 mM, aq) and the pH adjusted to 7.0. The resulting reaction mixture was heated to 75 °C overnight and excess metal was removed by a single use SepPak C18 column on an peristaltic pump using water to water/methanol (2:8) as eluent. The complex was further purified by preparative HPLC under standard conditions.²⁵

Retention time: 11.8-12.2 min.

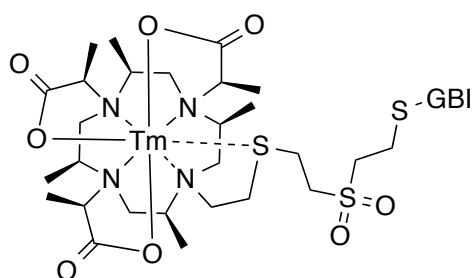
ESI-MS: Lutetium: calc. 795.2 (M+1); measured 795.2 (M+1).

ESI-MS: Samarium: calc. 772.2 (M+1); measured 772.2 (M+1) (Samarium pattern identified).

ESI-MS: Thulium: calc. 789.2 (M+1); measured 789.6 (M+1); 811.6 (M+Na); 827.6 (M+K).

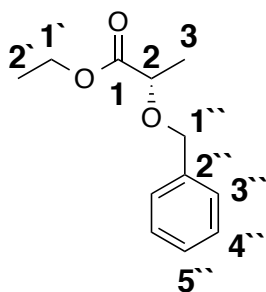
HRMS: Thulium: calc. 788.2177 (M); measured 789.2250 (M+H) C₂₇H₄₈N₄O₈S₂Tm; 811.2070 (M+Na) C₂₇H₄₈N₄NaO₈S₂Tm

Synthesis of DOTA-M7-(4*S*,3*R*)-thulium-GBI



GBI was treated with TCEP (10.0 eq, in 10 mM phosphate buffer pH = 6.5) to break the disulphide bridges of the dimer. The protein was purified using an Amicon Ultra Centrifugal Filter (Ultracel -3K). The membrane was equilibrated with 3.5 mL phosphate buffer (PO_4^{3-} , 10 mM) (7490 rpm, 15 min). The protein was added and the volume enlarged to 3.5 mL with TCEP in phosphate buffer and centrifuged. This process was repeated 4 times. The protein was taken of the membrane and the membrane washed with phosphate buffer to a total volume of 1mL. The protein was further purified on a Pd 10 cartridge. The resulting solution with a pH of 6.5 was added to DOTA-M7-(4*S*,3*R*)-metal-thiovinylsulfone (2 mg, in 100 μL (10 mM phosphate buffer)) and shaken at 25 °C overnight. No full conversion was obtained therefore the pH was stepwise enlarged to 8, which speeded up the reaction and delivered after 48 hours a full conversion. NMR data and ESI-MS spectra are shown in the results section.

Synthesis of ethyl (S)-2-(benzyloxy)propanoate (b3)



L-lactate ethyl ester (20.0 g, 169 mmol, 1.0 eq) was added dropwise to a suspension of benzyl bromide (31.9 g, 186 mmol, 1.1 eq), sodium hydride (6.8 g, 169 mmol, 60 %) in dry THF/DMF (2:1, 160/80 mL) at -10 °C. The reaction mixture was stirred for 1 hour before warmed to rt. and stirred for additional 30 min before heated to 50 °C for 2 hours. The resulting mixture was poured into a mixture of water (250 mL) and petrol ether (150 mL). The organic layer was separated and the aqueous layer extracted with ether (2 X 50 mL). The combined organic layer was washed with water, brine and dried over sodium sulphate. The solvent was removed under reduced pressure and the crude mixture purified by silica gel column chromatography pentane/*tert*-butyl methyl ether (9:1) as eluent yielding the title product (30.0 g, 144 mmol, 85%) as colourless oil.⁵⁹

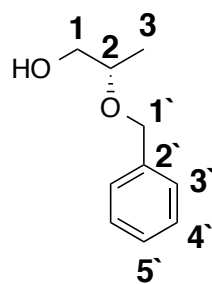
TLC: (SiO_2 , pentane/TBME (9:1.5)): R_f = 0.73.

$^1\text{H-NMR}$ (400 MHz, CDCl_3 , TMS, δ in ppm): 7.23 - 7.41 (m, 5H, $\text{H}3''$ - $\text{H}5''$); 4.70 (d, $^2J_{\text{HH}} = 11.6$ Hz, 1H, $\text{H}1''$); 4.47 (d, $^2J_{\text{HH}} = 11.6$ Hz, 1H, $\text{H}1''$); 4.22 (m, 2H, $\text{H}1'$); 4.05

(q, $^3J_{\text{HH}} = 6.9$ Hz, 1H, H2); 1.44 (d, $^3J_{\text{HH}} = 6.9$ Hz, 3H, H3); 1.29 (t, $^3J_{\text{HH}} = 7.1$ Hz, 3H, H2').

$^{13}\text{C-NMR}$ (151 MHz, CDCl_3 , TMS, δ in ppm): 14.4 (1C, C2'); 18.9 (1C, C3); 61.0 (1C, C1'); 72.2 (1C, C1''); 74.3 (1C, C2); 128.0 (1 C, C5''); 128.2 (2C, C3''); 128.6 (2C, C4''); 137.8 (1C, C2''); 173.5 (1C, C1).

Synthesis of (S)-2-(benzyloxy)propanoic acid (b4)



Ethyl (S)-2-(benzyloxy)propanoate (**b3**) (32.0 g, 154 mmol, 1.0 eq) in diethylether (30 mL, dry) was added dropwise to a suspension of lithium aluminium hydride (5.83 g, 154 mmol, 1.0 eq) in diethylether (300 mL) at 0 °C. The resulting suspension was warmed slowly to rt. before heated to reflux overnight. The reaction mixture was quenched under cooling with water, sodium hydroxide (15 %, aq)

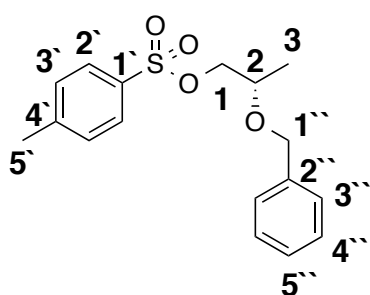
and a second portion of water. The precipitate was filtered over HYFLO and washed with ether. The combined organic layer was dried over sodium sulphate and the solvent removed under reduced pressure. The crude mixture was purified by silica gel column chromatography using pentane/*tert*-butyl methyl ether (4:1) as eluent. The title compound was obtained in (80-95%) yield as colourless oil.

TLC: (SiO_2 , pentane/TBME (4:1)): $R_f = 0.31$

$^1\text{H-NMR}$ (400 MHz, CDCl_3 , TMS, δ in ppm): 7.26-7.39 (m, 5H, H3'-H5'); 4.66 (d, $^2J_{\text{HH}} = 11.6$ Hz, 1H, H1'); 4.49 (d, $^2J_{\text{HH}} = 11.6$ Hz, 1H, H1''); 3.66-3.73 (m, 1H, H2); 3.62 (ddd, $^2J_{\text{HH}} = 11.4$ Hz, $^3J_{\text{HH}} = 8.0$ Hz, $^3J_{\text{HH}} = 3.4$ Hz, 1H, H1); 3.51 (ddd, $^2J_{\text{HH}} = 11.4$ Hz, $^3J_{\text{HH}} = 7.1$ Hz, $^3J_{\text{HH}} = 4.4$ Hz, 1H, H1); 2.05 (dd, $^3J_{\text{HH}} = 8.0$ Hz, $^3J_{\text{HH}} = 4.4$ Hz, 1H, OH); 1.19 (d, $^3J_{\text{HH}} = 6.2$ Hz, 3H, H3).

$^{13}\text{C-NMR}$ (63 MHz, 298 K, CDCl_3 , δ in ppm): 16.0 (1C, C3); 66.6 (1C, C1); 71.0 (1C, C1'); 75.7 (1C, C2); 127.9 (3C, C3', C5'); 128.6 (2C, C4'); 138.6 (1C, C2').

Synthesis of (S)-2-(benzyloxy)propyl 4-methylbenzenesulfonate (b5)



(S)-2-(benzyloxy)propanol (900 mg, 5.41 mmol, 1.0 eq) was dissolved in pyridine (8 mL) and *p*-TsCl (para-toluenesulfonyl chloride) (2.06 g, 10.8 mmol, 2.0 eq) was added. The resulting mixture was stirred overnight. After addition of water and extraction with dichloromethane the combined organic layers were

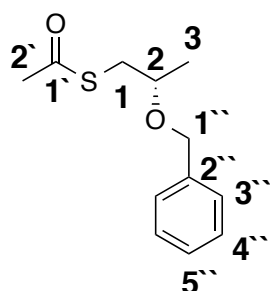
washed with 18% HCl aq. twice and brine, dried over sodium sulphate and the solvent removed under reduced pressure. The desired product (1.49 g, 4.65 mmol, 86%) was obtained as colourless oil without further purification.

TLC: (SiO₂, pentane/TBME (2:1)): **R_f** = 0.73

¹H-NMR (400 MHz, CDCl₃, TMS, δ in ppm): 7.68-7.90 (m, 2H, H2''); 7.22-7.38 (m, 7H, H3', H3''-H5''); 4.53 (d, ²J_{HH} = 11.7 Hz, 1H, H1''); 4.48 (d, ²J_{HH} = 11.7 Hz, 1H, H1''); 3.94-4.05 (m, 2H, H1); 3.76 (m, 1H, H2); 2.43 (s, 3H, H5'); 1.16 (d, ³J_{HH} = 6.3 Hz, 3H, H3).

¹³C-NMR (101 MHz, CDCl₃, TMS, δ in ppm): 16.8 (1C, C3); 21.7 (1C, C5'); 71.3 (1C, C1''); 72.4 (1C, C1); 72.7 (1C, C2); 127.6 (2C, C3''); 127.7 (1C, C5''); 128.0 (2C, C2'); 128.4 (2C, C4''); 129.8 (2C, C3'); 133.0 (1C, C2''); 138.1 (1C, C4'); 144.8 (1C, C1').

Synthesis of (S)-S-(2-(benzyloxy)propyl) ethanethioate (b6)



(S)-2-(benzyloxy)propyl 4-methylbenzenesulfonate (**b5**) (500 mg, 1.56 mmol, 1.0 eq) was dissolved in tetrahydrofuran (20 mL) and potassium thioacetate (364 mg, 3.12 mmol, 2.0 eq) was added. The resulting reaction mixture was refluxed for 3 hours. The precipitate was filtered off and washed with additional 20 mL THF. The solvent was removed under reduced

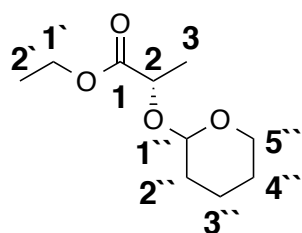
pressure and the crude mixture purified by silica gel column chromatography using pentane/*tert*butyl methyl ether (9:1) as eluent to yield the title compound (35%) as colourless oil.⁵⁶

TLC: (SiO₂, pentane/TBME (9:1)): **R_f** = 0.34

¹H-NMR (400 MHz, CDCl₃, TMS, δ in ppm): 7.26-7.35 (m, 5H, H3''-H5''); 5.58 (dd, ²J_{HH} = 14.5 Hz, ⁴J_{HH} = 4.9 Hz, 1H, H1''); 5.54 (dd, ²J_{HH} = 14.5 Hz, ⁴J_{HH} = 2.5 Hz, 1H, H1''); 3.65 (ddq, ³J_{HH} = 6.2 Hz, ³J_{HH} = 5.7 Hz, ³J_{HH} = 5.2 Hz, 1H, H2); 3.11 (dd, ²J_{HH} = 14.0 Hz, ³J_{HH} = 5.7 Hz, 1H, H1); 3.05 (dd, ²J_{HH} = 14.0 Hz, ³J_{HH} = 5.2 Hz, 1H, H1); 2.34 (s, 3H, H2'), 1.25 (d, ³J_{HH} = 6.2 Hz, 3H, H3).

¹³C-NMR (101 MHz, CDCl₃, TMS, δ in ppm): 19.5 (1C, C3); 30.7 (1C, C2'); 35.0 (1C, C1); 71.0 (1C, C1''); 73.9 (1C, C2); 127.7 (1C, C5''); 127.8 (2C, C3''); 130.0 (2C, C4''); 138.6 (1C, C2''); 195.8 (1C, C1').

Synthesis of ethyl (2S)-2-((tetrahydro-2H-pyran-2-yl)oxy)propanoate (b8)



L-Lactic acid ethyl ester (10.0 g, 84.7 mmol, 1.0 eq) was dissolved in chloroform (90 mL) and p-TsOH (288 mg, 1.7 mmol, 0.02 eq) was added. The resulting suspension was cooled to 4 °C and 2H-dihydropyran (10.8 mL, 119 mmol, 1.4 eq) was added dropwise. After completion of the addition the

reaction was stirred for another 5 min before warmed to rt. for 3 hours. The resulting reaction mixture was extracted with 0.2N KOH (2*150 mL). The organic phase was dried over sodium sulphate and the crude mixture purified by silica gel column chromatography using pentane/*tert*butyl methyl ether (95:5 -> 8:1) as eluent yielding the title compound (13.5 g, 66.7 mmol, 78%) as colourless oil as a mixture of two diastereoisomers.⁶⁰

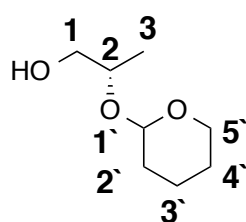
TLC: (SiO₂, pentane/TBME (9:1)): R_f = 0.58; 0.69.

Diastereoisomer 1: **¹H-NMR** (500 MHz, CDCl₃, TMS, δ in ppm): 4.69 (t, ³J_{HH} = 3.7 Hz, 1H, H1''); 4.40 (qd, ³J_{HH} = 7.0 Hz, ⁴J_{HH} = 1.4 Hz, 1H, H2); 4.12-4.24 (m, 2H, H1'); 3.80-3.88 (m, 1H, H5''); 3.47-3.54 (m, 1H, H5''); 1.82-1.90 (m, 1H, H4''); 1.72-1.80 (m, 2H, H2''); 1.63-1.71 (m, 2H, H3''); 1.49-1.62 (m, 1H, H4''); 1.44 (dd, ³J_{HH} = 7.0 Hz, ⁵J_{HH} = 0.5 Hz, 3H, H3); 1.24-1.30 (m, 3H, H2').

Diastereoisomer 2: **¹H-NMR** (500 MHz, CDCl₃, TMS, δ in ppm): 4.71 (t, ³J_{HH} = 3.6 Hz, 1H, H1''); 4.12-4.24 (m, 3H, H2, H1'); 3.88-3.96 (m, 1H, H5''); 3.42-3.47 (m, 1H, H5''); 1.82-1.90 (m, 1H, H4''); 1.72-1.80 (m, 2H, H2''); 1.63-1.71 (m, 2H, H3''); 1.49-1.62 (m, 1H, H4''); 1.39 (dd, ³J_{HH} = 7.0 Hz, ⁵J_{HH} = 0.5 Hz, 3H, H3); 1.24-1.30 (m, 3H, H2').

Diastereoisomer 1: **¹³C-NMR** (126 MHz, CDCl₃, TMS, δ in ppm): 14.35 (1C, C1'); 18.9 (1C, C3); 19.3 (1C, C4''); 25.6 (1C, C3''); 30.6 (1C, C2''); 60.94 (1C, C1'); 62.6 (1C, C5''); 70.1 (1C, C2); 97.4 (1C, C1''); 173.5 (1C, C1).

Diastereoisomer 2: **¹³C-NMR** (126 MHz, CDCl₃, TMS, δ in ppm): 14.29 (1C, C1'); 18.2 (1C, C3); 19.25 (1C, C4''); 25.4 (1C, C3''); 30.8 (1C, C2''); 60.86 (1C, C1'); 62.4 (1C, C5''); 72.6 (1C, C2); 98.4 (1C, C1''); 173.4 (1C, C1).

Synthesis of (2S)-2-((tetrahydro-2H-pyran-2-yl)oxy)propan-1-ol (b9)

(2S)-2-((tetrahydro-2H-pyran-2-yl)oxy)propanoate (**b8**) (10.0 g, 49.4 mmol, 1.0 eq) in diethylether (30 mL, dry) was added dropwise to LiAlH₄ (1.88 g, 49.4 mmol, 1.0 eq) in diethylether (100 mL) at 0 °C. The resulting reaction mixture was warmed to rt. before refluxed for 2 hours. The reaction was quenched under

cooling with water (2 mL), NaOH (15%, aq, 2 mL) and again water (6 mL). The precipitate was filtered over HYFLO and washed with ether. The combined organic layer was dried over sodium sulphate and the solvent removed under reduced pressure.

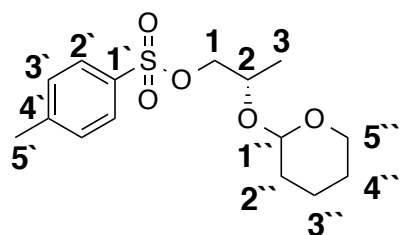
Diastereoisomer 1: **¹H-NMR** (500 MHz, CDCl₃, TMS, δ in ppm): 4.72 (dd, ³J_{HH} = 5.2 Hz, ³J_{HH} = 2.8 Hz, 1H, H1'); 3.90-3.96 (m, 1H, H5'); 3.87 (ddq, ³J_{HH} = 10.0 Hz, ³J_{HH} = 6.6 Hz, ³J_{HH} = 3.3 Hz, 1H, H2); 3.55-3.61 (m, 1H, H1); 3.47-3.54 (m, 1H, H5'); 3.42-3.49 (m, 1H, H1); 2.20 (dd, ³J_{HH} = 7.4 Hz, ³J_{HH} = 5.1 Hz, 1H, OH); 1.79-1.88 (m, 1H, H3'); 1.69-1.82 (m, 1H, H2'); 1.52-1.62 (m, 1H, H2'); 1.50-1.52 (m, 2H, H4'); 1.48-1.57 (m, 1H, H3'); 1.21 (d, ³J_{HH} = 6.6 Hz, 3H, H3).

Diastereoisomer 2: **¹H-NMR** (500 MHz, CDCl₃, TMS, δ in ppm): 4.51-5.56 (m, 1H, H1'); 3.99-4.02 (m, 1H, H5'); 3.78-3.83 (m, 1H, H2); 3.50-3.57 (m, 1H, H5'); 3.44-3.54 (m, 2H, H1); 2.13-2.17 (m, 1H, OH); 1.79-1.88 (m, 1H, H3'); 1.69-1.82 (m, 1H, H2'); 1.52-1.62 (m, 1H, H2'); 1.50-1.52 (m, 2H, H4'); 1.48-1.57 (m, 1H, H3'); 1.12 (d, ³J_{HH} = 6.5 Hz, 3H, H3).

Diastereoisomer 1: **¹³C-NMR** (126 MHz, CDCl₃, TMS, δ in ppm): 17.8 (1C, C3); 20.2 (1C, C3'); 25.5 (1C, C4'); 31.2 (1C, C2'); 63.3 (1C, C5'); 66.3 (1C, C1); 75.1 (1C, C2); 99.2 (1C, C1').

Diastereoisomer 2: **¹³C-NMR** (126 MHz, CDCl₃, TMS, δ in ppm): 17.4 (1C, C3); 21.1 (1C, C3'); 25.2 (1C, C4'); 31.7 (1C, C2'); 64.7 (1C, C5'); 67.4 (1C, C1); 77.9 (1C, C2); 100.1 (1C, C1').

Synthesis of (2S)-2-((tetrahydro-2H-pyran-2-yl)oxy)propyl 4-methylbenzenesulfonate (b10)



To a solution *p*-TsCl (9.5 g, 50.0 mmol, 2.0 eq) in dichloromethane (100 mL, dry) was added (2S)-2-((tetrahydro-2H-pyran-2-yl)oxy)propan-1-ol (**b9**) (4.0 g, 25.0 mmol, 1.0 eq) and pyridine (6.5 mL, 79.9 mmol, 3.2 eq) at 0 °C. The resulting reaction mixture was

stirred at rt. overnight before quenched with HCl (2M, aq., 100 mL) and extracted with dichloromethane (3 X 50 mL). The crude reaction mixture was purified with silica gel column chromatography using pentane/tert-butylmethylether (9:1 → 1:1) as eluent to yield the title compound (5.05 g, 16.1mmol, 64%) as colourless oil (mixture of two diastereoisomers).

TLC: (SiO₂, pentane /TBME (9:1)): **R_f** = 0.15.

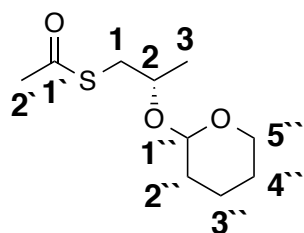
Diastereoisomer 1: **¹H-NMR** (500 MHz, CDCl₃, TMS, δ in ppm): 7.76-7.82 (m, 2H, H2'); 7.33-7.36 (m, 2H, H3'); 4.63 (t, ³J_{HH} = 3.9 Hz, 1H, H1''); 3.95-4.03 (m, 1H, H2); 3.90-3.98 (m, 2H, H1); 3.82-3.87 (m, 1H, H5''); 3.44-3.50 (m, 1H, H5''); 2.45 (s, 3H, H5'); 1.68-1.79 (m, 1H, H3''); 1.58-1.69 (m, 1H, H2''); 1.45-1.57 (m, 2H, H4''); 1.44-1.52 (m, 1H, H3''); 1.42-1.52 (m, 1H, H2''); 1.18 (d, ³J_{HH} = 5.1 Hz, 3H, H3).

Diastereoisomer 2: **¹H-NMR** (500 MHz, CDCl₃, TMS, δ in ppm): 7.76-7.82 (m, 2H, H2'); 7.33-7.36 (m, 2H, H3'); 4.67 (t, ³J_{HH} = 3.5 Hz, 1H, H1''); 4.07-4.11 (m, 1H, H1); 3.95-3.99 (m, 1H, H2); 3.92-3.95 (m, 1H, H1); 3.75-3.82 (m, 1H, H5''); 3.39-3.49 (m, 1H, H5''); 2.45 (s, 3H, H5'); 1.68-1.79 (m, 1H, H3''); 1.58-1.69 (m, 1H, H2''); 1.45-1.57 (m, 2H, H4''); 1.44-1.52 (m, 1H, H3''); 1.42-1.52 (m, 1H, H2''); 1.12 (d, ³J_{HH} = 6.2 Hz, 3H, H3).

Diastereoisomer 1: **¹³C-NMR** (126 MHz, CDCl₃, TMS, δ in ppm): 18.3 (1C, C3); 19.75 (1C, C3''); 21.8 (1C, C5'); 25.4 (1C, C4''); 30.8 (1C, C2''); 62.9 (1C, C5''); 70.7 (1C, C2); 72.9 (1C, C1); 99.1 (1C, C1''); 128.1 (2C, C2'); 130.0 (2C, C3'); 133.1 (1C, C4'); 149.0 (1C, C1').

Diastereoisomer 2: **¹³C-NMR** (126 MHz, CDCl₃, TMS, δ in ppm): 16.3 (1C, C3); 19.73 (1C, C3''); 21.75 (1C, C5'); 27.1 (1C, C4''); 30.78 (1C, C2''); 62.1 (1C, C5''); 69.2 (1C, C2); 73.3 (1C, C1); 96.3 (1C, C1''); 128.1 (2C, C2'); 130.0 (2C, C3'); 133.1 (1C, C4'); 149.0 (1C, C1').

Synthesis of *S*-((2*S*)-2-((tetrahydro-2*H*-pyran-2-yl)oxy)propyl) ethanethioate (b11)



(2*S*)-2-((tetrahydro-2*H*-pyran-2-yl)oxy)propyl 4-methylbenzene-sulfonate (**b10**) (4.0 g, 12.7 mmol, 1.0 eq) was dissolved in THF (dry, 100mL), potassium carbonate (5.3 g, 38.2 mmol, 3.0 eq) and potassium thioacetate (2.2 g, 19.1 mmol, 1.5 eq) were added. The reaction mixture was heated

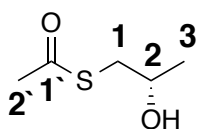
to reflux overnight. The resulting precipitate was filtered off over HYFLO, washed with THF and solvent removed under reduced pressure. The crude mixture purified by silica gel column chromatography using pentane/*tert*butyl methyl ether (9:1) as eluent yielding the title compound (1.8 g, 8.24 mmol, 65%) as colourless oil.⁵⁶

TLC: (SiO₂, pentane/TBME (9:1)): **R_f** = 0.5.

The product was obtained as a 9:1 mixture of two diastereoisomers. The shifts of the two diastereoisomers are only separated for H3 and therefore not presented as separate spectra.

¹H-NMR (400 MHz, CDCl₃, TMS, δ in ppm): 4.70-4.77 (m, 1H, H1''); 3.83-3.97 (m, 2H, H2, H5''); 3.46-3.52 (m, 1H, H5''); 2.96-3.11 (m, 2H, H1); 2.33 (b"s", 3H, H2'); 1.75-1.87 (m, 1H, H3''); 1.65-1.75 (m, 1H, H2''); 1.45-1.59 (m, 4H, H2'', H3'', H4''); 1.26 (1.17) (d, ³J_{HH} = 6.3 Hz, 3H, H3).

Synthesis of (*S*)-*S*-(2-hydroxypropyl) ethanethioate (b7)



S-((2*S*)-2-((tetrahydro-2*H*-pyran-2-yl)oxy)propyl) ethanethioate (**b11**) (1.0 g, 4.58 mmol, 1.0 eq) was dissolved in deprotection mixture acetic acid/THF/water (28 mL, 4:2:1). The resulting solution was

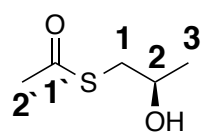
heated to 45 °C for 4 hours. The solvent were removed at 20 °C under reduced pressure. The resulting product was purified by silica gel column chromatography using pentane/TBME (95:5) as eluent. The title compound (400 mg, 2.98 mmol, 65%) was obtained as colourless oil in mixture with THP deprotection product.⁵²

TLC: (SiO₂, pentane/TBME (95:5)): **R_f** = 0.19.

¹H-NMR (400 MHz, CDCl₃, TMS, δ in ppm): 3.90-3.99 (m, 1H, H2); 3.11 (dd, ²J_{HH} = 14.0 Hz, ³J_{HH} = 4.1 Hz, 1H, H1); 2.90 (dd, ²J_{HH} = 14.0 Hz, ³J_{HH} = 7.1 Hz, 1H, H1); 2.38 (s, 3H, H2'); 1.26 (d, ³J_{HH} = 6.2 Hz, 3H, H3).

¹³C-NMR (101 MHz, 298 K, CDCl₃, δ in ppm): 22.4 (1C, C3); 30.7 (1C, C2'); 37.8 (1C, C1); 67.2 (1C, C2); 196.4 (1C, C1').

Synthesis of (*R*)-*S*-(2-hydroxypropyl) ethanethioate (**b7-R**)



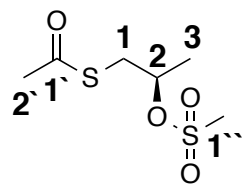
R-Propylene oxide (2.5 mL, 35.7 mmol, 1.0 eq) and thioacetic acid (2.8 mL, 39.3 mmol, 1.1 eq) were dissolved in water (30 mL) and stirred at rt. for 10 hours. The resulting mixture was extracted with EtOAc and washed with sodium carbonate (2M aq). The solvent was removed under reduced pressure and the crude mixture purified by silica gel column chromatography using pentane/TBME (95:5) as eluent. The title compound (2100 mg, 15.6 mmol, 43%) was obtained as colourless oil.⁶¹

TLC: (SiO₂, pentane/TBME (95:5)): R_f = 0.19.

¹H-NMR (400 MHz, CDCl₃, TMS, δ in ppm): 3.90-3.99 (m, 1H, H2); 3.11 (d, ²J_{HH} = 14.0 Hz, ³J_{HH} = 4.1 Hz, 1H, H1); 2.90 (d, ²J_{HH} = 14.0 Hz, ³J_{HH} = 7.1 Hz, 1H, H1); 2.38 (s, 3H, H2'); 1.26 (d, ³J_{HH} = 6.2 Hz, 3H, H3).

¹³C-NMR (101 MHz, 298 K, CDCl₃, δ in ppm): 22.4 (1C, C3); 30.7 (1C, C2'); 37.8 (1C, C1); 67.2 (1C, C2); 196.4 (1C, C1').

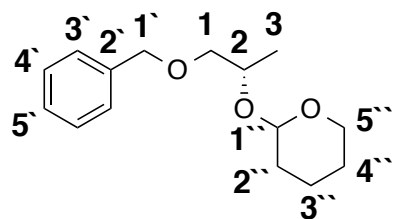
Synthesis of (*R*)-*S*-(2-((methylsulfonyl)oxy)propyl) ethanethioate (**b12-R**)



(*R*)-*S*-(2-hydroxypropyl) ethanethioate (**b7-R**) (500 mg, 3.73 mmol, 1.0 eq) was dissolved in THF (15 mL) and triethylamine (1.57 mL, 11.2 mmol, 3.0 eq) was added, cooled to 0 °C. Methanesulfonyl chloride (0.43 mL, 5.59 mmol, 1.5 eq) was

added dropwise over 5 minutes and stirred for additional 10 min at 0 °C before warmed to rt. for 2 hours. The reaction mixture was filtered over HyFlo and the solvent removed under reduced pressure. The crude mixture showed purity higher than 90% and was therefore used without further purification.

¹H-NMR (400 MHz, CDCl₃, TMS, δ in ppm): 4.81 (pd, ³J_{HH} = 6.3 Hz, ³J_{HH} = 5.5 Hz, 1H, H2); 3.09-3.21 (m, 2H, H1); 3.05 (s, 3H, H1'); 2.33 (s, 3H, H2'); 1.26 (d, ³J_{HH} = 6.3 Hz, 3H, H3).

Synthesis of 2-(((S)-1-(benzyloxy)propan-2-yl)oxy)tetrahydro-2H-pyran (b14)

(2S)-2-(((S)-1-(benzyloxy)propan-2-yl)oxy)tetrahydro-2H-pyran (**b9**)

(3.0 g, 18.7 mmol, 1.0 eq) was added to a suspension of sodium hydride (899 mg, 22.5 mmol, 1.2 eq, 60% in mineral oil) in DMF (10 mL). The resulting reaction mixture was stirred at rt. for 2 h before benzyl bromide (2.7 mL, 22.5 mmol, 1.2 eq) was added slowly and stirred for additional 15 hours. Ammonium chloride (sat., aq.) was added and the mixture extracted with diethylether two times. The combined organic layers were washed with brine, dried over sodium sulphate and the solvent removed under reduced pressure. The crude reaction mixture was purified with silica gel column chromatography using pentane/*tert* butylmethylether (4:1) as eluent to yield the title compound (2.8 g, 11.2 mmol, 60%) as colourless oil.⁵⁶

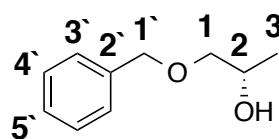
TLC: (SiO₂, pentane/TBME (4:1)): **R_f** = 0.74

Diastereoisomer 1: **¹H-NMR** (400 MHz, CDCl₃, TMS, δ in ppm): 7.27-7.38 (m, 5H, H3'-H5'); 4.80 (dd, ³J_{HH} = 4.8 Hz, ³J_{HH} = 2.8 Hz, 1H, H1''); 4.55 (s, 2H, H1'); 3.98-4.06 (m, 1H, H2); 3.88-3.96 (m, 1H, H5''); 3.47-3.55 (m, 1H, H5''); 3.40-3.47 (m, 2H, H1); 1.78-1.91 (m, 1H, H3''); 1.68-1.77 (m, 1H, H2''); 1.47-1.64 (m, 4H, H2'', H3'', H4''); 1.23 (d, ³J_{HH} = 6.5 Hz, 3H, H3).

Diastereoisomer 2: **¹H-NMR** (400 MHz, CDCl₃, TMS, δ in ppm): 7.27-7.38 (m, 5H, H3'-H5'); 4.95 (dd, ³J_{HH} = 5.0 Hz, ³J_{HH} = 2.8 Hz, 1H, H1''); 4.59 (s, 2H, H1'); 3.98-4.06 (m, 1H, H2); 3.85-3.89 (m, 1H, H5''); 3.58 (dd, ²J_{HH} = 9.9 Hz, ³J_{HH} = 5.6 Hz, 1H, H1); 3.47-3.55 (m, 1H, H5''); 3.40-3.47 (m, 1H, H1); 1.78-1.91 (m, 1H, H3''); 1.68-1.77 (m, 1H, H2''); 1.47-1.64 (m, 4H, H2'', H3'', H4''); 1.17 (d, ³J_{HH} = 6.3 Hz, 3H, H3).

Diastereoisomer 1: **¹³C-NMR** (101 MHz, CDCl₃, TMS, δ in ppm): 18.8 (1C, C3); 20.1 (1C, C3''); 25.66 (1C, C4''); 31.21 (1C, C2''); 62.9 (1C, C5''); 72.0 (1C, C2); 73.36 (1C, C1'); 74.5 (1C, C1); 98.8 (1C, C1''); 127.63 (2C, C3'); 127.66 (1C, C5'); 128.49 (2C, C4'); 138.6 (1C, C2').

Diastereoisomer 2: **¹³C-NMR** (101 MHz, CDCl₃, TMS, δ in ppm): 16.6 (1C, C3); 19.9 (1C, C3''); 25.61 (1C, C4''); 31.16 (1C, C2''); 62.4 (1C, C5''); 70.5 (1C, C2); 73.32 (1C, C1'); 74.4 (1C, C1); 96.2 (1C, C1''); 127.59 (1C, C5'); 127.73 (2C, C3'); 128.44 (2C, C4'); 138.8 (1C, C2').

Synthesis of (S)-1-(benzyloxy)propan-2-ol (b15)

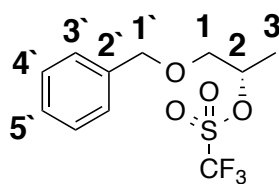
2-(((S)-1-(benzyloxy)propan-2-yl)oxy)tetrahydro-2*H*-pyran(**b14**) (2.8 g, 11.3 mmol, 1.0 eq) was dissolved in acetic acid/THF/water (4:2:1, 35 mL) and heated to 45 °C for 8 hours.

The solvents were removed under reduced pressure (20 °C) and purified by silica gel column chromatography using cyclohexane/ethyl acetate (4:1) as eluent.⁵²

TLC: (SiO₂, pentane/TBME (9:1)): **R_f** = 0.13.

¹H-NMR (400 MHz, CDCl₃, TMS, δ in ppm): 7.27-7.40 (m, 5H, H3'-H5'); 4.56 (s, 2H, H1'); 4.01 (dq, ³J_{HH} = 8.1 Hz, ³J_{HH} = 6.4 Hz, ³J_{HH} = 3.1 Hz, 1H, H2); 3.48 (dd, ²J_{HH} = 9.4 Hz, ³J_{HH} = 3.1 Hz, 1H, H1); 3.29 (dd, ²J_{HH} = 9.4 Hz, ³J_{HH} = 8.1 Hz, 1H, H1); 1.15 (d, ³J_{HH} = 6.4 Hz, 3H, H3).

¹³C-NMR (63 MHz, 298 K, CDCl₃, δ in ppm): 18.8 (1C, C3); 66.7 (1C, C1'); 73.5 (1C, C1); 76.0 (1C, C2); 127.88 (2C, C3'); 127.93 (1C, C5'); 128.6 (2C, C4'); 138.1 (1C, C2').

Synthesis of (S)-1-(benzyloxy)propan-2-yl trifluoromethanesulfonate (b16)

Triflic anhydride (0.25 mL, 1.51 mmol, 1.01 eq) was dissolved in dichloromethane (10 mL) and the resulting solution was cooled to -78 °C. Pyridine (0.12 mL, 1.49 mmol, 1.00 eq) was added and a white precipitate was formed rapidly.

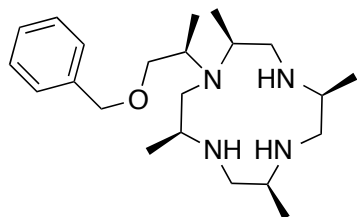
(S)-1-(benzyloxy)propan-2-ol (**b15**) (248 mg, 1.49 mmol, 1.00 eq) in dichloromethane (21 mL) was added slowly and the reaction mixture was allowed to warm to room temperature and stirred for another 10 min. The solvent was removed under reduced pressure at 0 °C and the crude mixture purified by filtration over silica gel (5X1.5 cm) (dichloromethane/hexane, 4:1). The title compound (120 mg, 0.4 mmol, 27%) was obtained as colourless oil and stored at -20 °C in solution with dichloromethane.²⁵

TLC: (SiO₂, dichloromethane/hexane (4:1)): **R_f** = 0.9.

¹H-NMR (400 MHz, CDCl₃, TMS, δ in ppm): 7.27-7.40 (m, 5H, H3'-H5'); 5.17 (pd, ³J_{HH} = 6.4 Hz, ³J_{HH} = 4.0 Hz, 1H, H2); 4.61 (d, ²J_{HH} = 13.8 Hz, 1H, H1'); 4.57 (d, ²J_{HH} = 13.8 Hz, 1H, H1'); 3.61-3.66 (m, 2H, H1); 1.50 (d, ³J_{HH} = 6.4 Hz, 3H, H3).

¹⁹F-NMR (376 MHz, CDCl₃, TMS, δ in ppm): -75.5 (s, 3F, CF₃).

Synthesis of (2*S*,5*S*,8*S*,11*S*)-1-((*R*)-1-(benzyloxy)propan-2-yl)-2,5,8,11-tetramethyl-1,4,7,10-tetraazacyclododecane (B10)



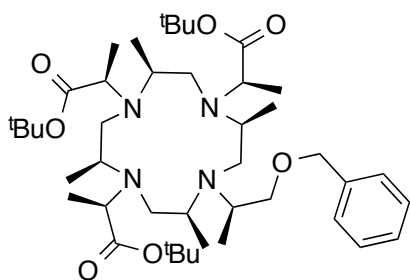
Cyclen (200 mg, 0.87 mmol, 1.0 eq) was dissolved in dichloromethane (20 mL) and sodium hydride (45.5 mg, 1.14 mmol, 1.3 eq, 60% in oil) was added under inert conditions. The resulting suspension was stirred for 5 min before (*S*)-1-(benzyloxy)propan-2-yl trifluoromethanesulfonate (235 mg, 0.96 mmol, 1.1 eq) in dichloromethane (10 mL) was added dropwise. The resulting reaction mixture was stirred at rt. over the weekend. The reaction was quenched with water (5 mL), extracted and reextracted twice with dichloromethane. The crude reaction mixture was purified by preparative HPLC to deliver the pure compound (42 mg, 0.11 mmol, 13%) as white waxy solid.²⁵

Retention time: 20-22 min (A/B = 54:46 -> 50:50)

ESI-MS: calc. 377.3 (M+1); measured 377.4 (M+1).

HRMS: 377.3275 (C₂₂H₄₁N₄O, 1+); 189.1674 (C₂₂H₄₁N₄O, 2+).

Synthesis of tri-*tert*-butyl 2,2',2''-((2*S*,5*S*,8*S*,11*S*)-10-((*R*)-1-(benzyloxy)propan-2-yl)-2,5,8,11-tetramethyl-1,4,7,10-tetraazacyclododecane-1,4,7-triyl)(2*R*,2'*R*,2''*R*)-tripropionate (B11)



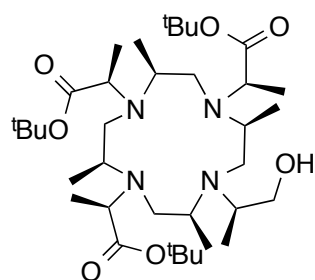
B10 (2*S*,5*S*,8*S*,11*S*)-1-((*R*)-1-(benzyloxy)propan-2-yl)-2,5,8,11-tetramethyl-1,4,7,10-tetraazacyclododecane (42 mg, 0.11 mmol, 1.0 eq) was dissolved in acetonitrile (10 mL) and sodium hydride (17.8 mg, 0.44 mmol, 4.0 eq, 60% in mineral oil) was added under inert conditions. The resulting suspension was stirred for 5 min before *tert*-butyl (*S*)-2-(((trifluoromethyl)sulfonyl)oxy)propanoate (**b16**) (124 mg, 0.44 mmol, 4.0 eq) in acetonitrile (10 mL) was added dropwise. The resulting reaction mixture was stirred at rt. overnight. No full conversion was obtained, therefore the reaction was warmed to 50 °C and additional triflate (2.0 eq) was added. The reaction was stirred for another 6 hours but no full conversion was obtained and a mixture of tri and tetra alkylated species obtained. The reaction was cooled to rt and quenched with water (5 mL), extracted and reextracted twice with dichloromethane. The crude reaction

mixture was purified by preparative HPLC to deliver the pure compound as white waxy solid.²⁵

ESI-MS: calc. 761.6 (M+1); measured 761.9 (M+1).

HRMS: 761.5787 (C₄₃H₇₇N₄O₇, 1+).

Synthesis of tri-*tert*-butyl 2,2',2''-((2*S*,5*S*,8*S*,11*S*)-10-((*R*)-1-hydroxypropan-2-yl)-2,5,8,11-tetramethyl-1,4,7,10-tetraazacyclododecane-1,4,7-triyl)(2*R*,2'*R*,2''*R*)-tripropionate (M8-tri-*tert*butyl-OH, B12)

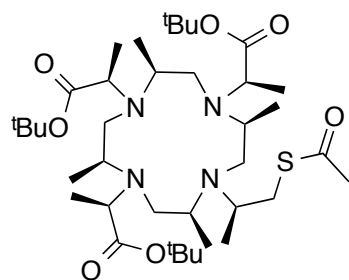


Ammoniak (30 mL) was condensed at -78 °C into a 2-necked flask. Sodium (106 mg, 4.59 mmol, 20 eq) was added and the resulting blue mixture was stirred for 10 min before **B11** (175 mg, 0.23 mmol, 1.0 eq) in THF (1 mL) was added and the reaction stirred for additional 120 min at -78 °C. NH₄Cl (50 mg) was added until the blue colour

disappeared. Ammoniak was removed with nitrogen and the resulting gas washed in 20% AcOH. The pure product (25 mg, 0.037, 16%) was obtained as white waxy solid.⁵²

ESI-MS: calc. 671.5 (M+1); measured 671.8 (M+1).

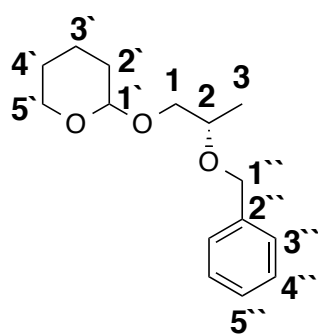
Synthesis of tri-*tert*-butyl 2,2',2''-((2*S*,5*S*,8*S*,11*S*)-10-((*R*)-1-(acetylthio)propan-2-yl)-2,5,8,11-tetramethyl-1,4,7,10-tetraazacyclododecane-1,4,7-triyl)(2*R*,2'*R*,2''*R*)-tripropionate (M8-tri-*tert*butyl-Sac, B13)



M8-tri-*tert*butyl-OH (**B12**) (25 mg, 0.037 mmol, 1.0 eq) was dissolved in dry THF (2 mL) and cooled to 0 °C. Methanesulfonylchloride (8 μL, 0.11 mmol, 3.0 eq) and triethylamine (31 μL, 0.224 mmol, 6.0 eq) were added and stirred for additional 10 min at 0 °C before warmed to rt and stirred until no more starting material was detected by

ESI-MS. Potassium thioacetate (21.7 mg, 0.19 mmol, 5.0 eq) was added and heated to reflux for 6 hours. The reaction mixture was filtered and the solvent removed under reduced pressure. The crude reaction mixture was purified by preparative HPLC to yield the title compound (4 mg, 0.005 mmol, 13.5%) as yellowish waxy solid.

ESI-MS: calc. 729.5 (M+1); measured 729.9 (M+1).

Synthesis of 2-((S)-2-(benzyloxy)propoxy)tetrahydro-2H-pyran (b17)

(S)-2-(benzyloxy)propan-1-ol (**b4**) (10g, 60.2, 1.0 eq) was dissolved in chloroform (30 mL) and p-TsOH (229 mg, 1.2 mmol, 0.02 eq) was added. The resulting suspension was cooled below 4 °C and 3,4-dihydro-2H-pyrane (7.7 mL, 84.2 mmol, 1.4 eq) was added dropwise and stirred for additional 5 min before warmed to rt. and stirred for additional 3 hours.

The crude mixture was purified by silica gel column chromatography to yield the title compound (80%) as colourless oil (one to one mixture of two diastereoisomers).⁶⁰

TLC: (SiO₂, pentane/TBME (9:1)): R_f = 0.37; 0.27.

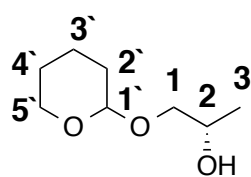
Diastereoisomer 1: **¹H-NMR** (400 MHz, CDCl₃, TMS, δ in ppm): 7.22-7.40 (m, 5H, H3''-H5''); 4.64 (s, 2H, H1''); 4.63-4.65 (m, 1H, H1'); 3.85-3.90 (m, 1H, H5'); 3.72-3.77 (m, 1H, H2); 3.70 (dd, ²J_{HH} = 10.4 Hz, ³J_{HH} = 4.4 Hz, 1H, H1); 3.50 (dd, ²J_{HH} = 10.4 Hz, ³J_{HH} = 6.7 Hz, 1H, H1); 3.48-3.55 (m, 1H, H5'); 1.80-1.93 (m, 1H, H4'); 1.69-1.76 (m, 1H, H2'); 1.57-1.65 (m, 2H, H2', H3'); 1.49-1.56 (m, 2H, H3', H4'); 1.19 (d, ³J_{HH} = 6.3 Hz, 3H, H3).

Diastereoisomer 2: **¹H-NMR** (400 MHz, CDCl₃, TMS, δ in ppm): 7.22-7.40 (m, 5H, H3''-H5''); 4.64 (s, 2H, H1''); 4.62-4.64 (m, 1H, H1'); 3.85-3.90 (m, 1H, H5'); 3.80 (dd, ²J_{HH} = 10.3 Hz, ³J_{HH} = 5.8 Hz, 1H, H1); 3.72-3.77 (m, 1H, H2); 3.48-3.55 (m, 1H, H5'); 3.41 (dd, ²J_{HH} = 10.3 Hz, ³J_{HH} = 4.5 Hz, 1H, H1); 1.80-1.93 (m, 1H, H4'); 1.69-1.76 (m, 1H, H2'); 1.57-1.65 (m, 2H, H2', H3'); 1.49-1.56 (m, 2H, H3', H4'); 1.22 (d, ³J_{HH} = 6.3 Hz, 3H, H3).

Diastereoisomer 1: **¹³C-NMR** (101 MHz, CDCl₃, TMS, δ in ppm): 17.46 (1C, C3); 19.61 (1C, C3'); 27.13 (1C, C4'); 30.79 (1C, C2'); 62.35 (1C, C5'); 71.17 (1C, C1''); 71.74 (1C, C1); 73.82 (1C, C2); 99.34 (1C, C1'); 127.52 (1C, C5''); 127.72 (2C, C3''); 128.43 (2C, C4''); 139.15 (1C, C2'').

Diastereoisomer 2: **¹³C-NMR** (101 MHz, CDCl₃, TMS, δ in ppm): 17.54 (1C, C3); 19.42 (1C, C3'); 25.63 (1C, C4'); 30.69 (1C, C2'); 62.06 (1C, C5'); 71.05 (1C, C1); 71.33 (1C, C1''); 74.45 (1C, C2); 98.68 (1C, C1'); 127.54 (1C, C5''); 127.74 (2C, C3''); 128.43 (2C, C4''); 139.17 (1C, C2'').

Synthesis of (2S)-1-((tetrahydro-2H-pyran-2-yl)oxy)propan-2-ol (b18)



2-((S)-2-(benzyloxy)propoxy)tetrahydro-2H-pyran (**b17**) (1.0 g, 3.99 mmol, 1.0 eq) was dissolved in EtOH (5 mL, dry) and Pd/C (56.1 mg, 0.0399 mmol, 0.01 eq) was added. 5bar hydrogen pressure was applied and the reaction mixture stirred vigorously

overnight in an autoclave. The crude mixture was filtered over HyFlo and washed with EtOH. The solvent was removed under reduced pressure and the crude mixture purified by silica gel column chromatography using pentane/*tert*butyl methyl ether (9:1 → 1:1) as eluent to yield (390 mg, 2.43 mmol, 61%) as colourless oil.⁵²

TLC: (SiO₂, pentane/TBME (9:1)): R_f = 0.27.

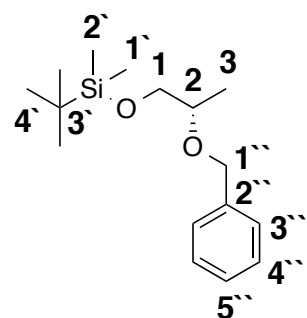
Diastereoisomer 1: ¹H-NMR (600 MHz, CDCl₃, TMS, δ in ppm): 4.56-4.59 (m, 1H, H1'); 3.85-4.02 (m, 2H, H2, H5'); 3.61 (dd, ²J_{HH} = 10.9 Hz, ³J_{HH} = 2.6 Hz, 1H, H1); 3.50-3.58 (m, 1H, H5'); 3.47 (dd, ²J_{HH} = 10.9 Hz, ³J_{HH} = 8.3 Hz, 1H, H1); 1.71-1.90 (m, 2H, H2', H4'); 1.49-1.65 (m, 4H, H2', H3', H4'), 1.14 (d, ³J_{HH} = 6.5 Hz, 3H, H3).

Diastereoisomer 2: ¹H-NMR (600 MHz, CDCl₃, TMS, δ in ppm): 4.56-4.59 (m, 1H, H1'); 3.85-4.02 (m, 2H, H2, H5'); 3.73 (dd, ²J_{HH} = 10.2 Hz, ³J_{HH} = 2.9 Hz, 1H, H1); 3.50-3.58 (m, 1H, H5'); 3.29 (dd, ²J_{HH} = 10.2 Hz, ³J_{HH} = 7.9 Hz, 1H, H1); 1.71-1.90 (m, 2H, H2', H4'); 1.49-1.65 (m, 4H, H2', H3', H4'), 1.16 (d, ³J_{HH} = 6.4 Hz, 3H, H3).

Diastereoisomer 1: ¹³C-NMR (151 MHz, CDCl₃, TMS, δ in ppm): 18.9 (1C, C3); 20.1 (1C, C3'); 25.5 (1C, C4'); 30.9 (1C, C2'); 63.2 (1C, C5'); 66.87 (1C, C2); 74.3 (1C, C1); 100.29 (1C, C1').

Diastereoisomer 2: ¹³C-NMR (151 MHz, CDCl₃, TMS, δ in ppm): 18.9 (1C, C3); 20.1 (1C, C3'); 25.5 (1C, C4'); 30.9 (1C, C2'); 63.2 (1C, C5'); 66.87 (1C, C2); 74.3 (1C, C1); 100.32 (1C, C1').

Synthesis of (S)-2-(benzyloxy)propoxy(*tert*-butyl)dimethylsilane (b20)



A solution of (S)-2-(benzyloxy)propan-1-ol (**b4**) (1.0 g, 6.02 mmol, 1.0 eq), 1*H*-imidazole (2.7 g, 39.7 mmol, 6.6 eq) and TBDMSCl (2.9 g, 19.3 mmol, 3.2 eq) in anhydrous DMF (8 mL) was stirred at rt. overnight. The reaction was quenched with MeOH (2 mL) and the solvent removed under reduced pressure. The crude mixture was purified by silica gel column

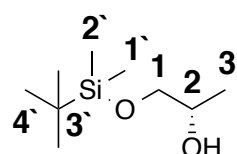
chromatography using pentane/*tert*butyl methyl ether (1:1) as eluent to yield the title compound (570 mg, 2.03 mmol, 34%) as colourless oil.⁵²

TLC: (SiO₂, pentane/TBME (1:1)): **R_f** = 0.95.

¹H-NMR (400 MHz, CDCl₃, TMS, δ in ppm): 7.30 - 7.37 (m, 4H, H3'', H4''); 7.24-7.29 (m, 1H, H5''); 4.62 ("s", 2H, H1''); 3.70 (dd, ²J_{HH} = 10 Hz, ³J_{HH} = 5.7 Hz, 1H, H1); 3.60 (ddq, ³J_{HH} = 6.2 Hz, ³J_{HH} = 5.7 Hz, ³J_{HH} = 5.3 Hz, 1H, H2); 3.52 (dd, ²J_{HH} = 10 Hz, ³J_{HH} = 5.3 Hz, 1H, H1); 1.17 (d, ³J_{HH} = 6.2 Hz, 3H, H3); 0.90 (s, 9H, H4'); 0.06 (broad s, 6 H, H1', H2').

¹³C-NMR (101 MHz, CDCl₃, TMS, δ in ppm): -5.23 (1C, C1'), -5.15 (1C, C2'), 17.7 (1C, C3), 18.5 (1C, C3'), 26.1 (3C, C4'), 67.4 (1C, C1), 71.4 (1C, C1''), 75.9 (1C, C2), 127.5 (1C, C5''), 127.7 (2C, C3''), 128.4 (2C, C4''), 139.2 (1C, C2'').

Synthesis of (S)-1-((*tert*-butyldimethylsilyloxy)propan-2-ol (b21)



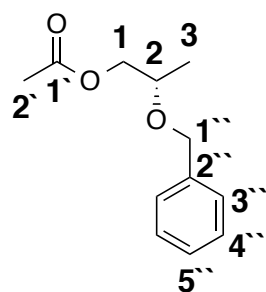
(S)-2-(benzyloxy)propoxy(*tert*-butyl)dimethylsilane (500 mg, 1.78 mmol, 1.0 eq) was dissolved in EtOH and Pd/C (13 mg, 0.009 mmol, 0.005 eq, 10%) was added. Hydrogenation was performed

in an autoclave with 10 bar H₂ pressure and stirred for 2 hours. The crude mixture was filtered over HYFLO and washed with ethanol and the solvent removed under reduced pressure.⁵²

¹H-NMR (400 MHz, 298 K, δ in ppm): 3.90 - 3.79 (m, 1H, H2); 3.61 (dd, ²J_{H,H} = 9.9 Hz, ³J_{H,H} = 3.4 Hz, 1H, H1); 3.36 (dd, ²J_{H,H} = 9.9 Hz, ³J_{H,H} = 7.8 Hz, 1H, H1); 2.48 (bs, 1H, OH); 1.13 (d, ³J_{H,H} = 6.3 Hz, 3H, H3); 0.93 (s, 9H, H4'); 0.095 (s, 3H, H1''); 0.093 (s, 3H, H2').

¹³C-NMR (63 MHz, 298 K, CDCl₃, δ in ppm): -5.22 (2C, C1', C2'); 18.33 (1C, C3); 25.8 (1C, C3'); 26.0 (3C, C4'); 68.06 (1C, C1); 68.67 (1C, C2).

Synthesis of (S)-2-(benzyloxy)propyl acetate (b23)



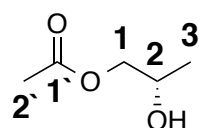
(S)-2-(benzyloxy)propan-1-ol (**b4**) (2.0 g, 12 mmol, 1.0 eq) was dissolved in THF (10 mL) and acetyl chloride (0.95 mL) 13.2 mmol, 1.1 eq) was added. The resulting reaction mixture was stirred overnight. The solvent was removed under reduced pressure and pure product (2.45 g, 11.8 mmol, 98%) was obtained without further purification.⁵²

¹H-NMR (400 MHz, 298 K, δ in ppm): 7.25 - 7.37 (m, 5H, H3''-H5''); 4.62 (d, ²J_{H,H} = 12.0 Hz, 1H, H1''); 4.57 (d, ²J_{H,H} = 12.0 Hz, 1H, H1''); 4.12 (dd, ²J_{H,H} = 11.6 Hz, ³J_{H,H}

= 4.4 Hz, 1H, H1); 4.08 (dd, $^2J_{H,H} = 11.6$ Hz, $^3J_{H,H} = 6.0$ Hz, 1H, H1); 3.72 - 3.79 (m, 1H, H2); 2.07 (s, 3H, H2'); 1.22 (d, $^3J_{H,H} = 6.4$ Hz, 3H, H3).

$^{13}\text{C-NMR}$ (101 MHz, CDCl_3 , TMS, δ in ppm): 17.0 (1C, C3); 21.1 (1C, C2'); 67.5 (1C, C1); 71.1 (1C, C1''); 72.7 (1C, C2); 127.75 (1C, C5''); 127.77 (2C, C3''); 128.51 (2C, C4''); 138.6 (1C, C2''); 171.1 (1C, C1').

Synthesis of (S)-2-hydroxypropyl acetate (b24)



(S)-2-(benzyloxy)propyl acetate (**b23**) (1.0 g, 4.8 mmol, 3.4 eq) was dissolved in EtOH (5 mL) and Pd/C (20 mg, 0.14 mmol, 0.1 eq) was added. Hydrogen (10 bar) was applied and stirred at rt. overnight.

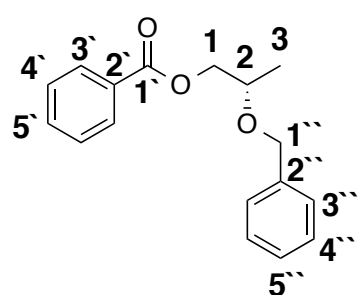
The reaction mixture was filtered over HYFLO and washed with ethanol (40 mL). The crude mixture was purified by silica gel column chromatography using pentane/tBME 2:1 as eluent. The product was obtained as 90:1 mixture of 1 and 2 protected product! Ethanol causes travelling of the acetyl group (about 10%), which cannot be removed by column chromatography.⁵²

TLC: (SiO_2 , pentane/TBME (2:1)): $R_f = 0.2$.

$^1\text{H-NMR}$ (400 MHz, CDCl_3 , 298 K, δ in ppm): 4.11 (dd, $^2J_{H,H} = 11.1$ Hz, $^3J_{H,H} = 3.0$ Hz, 1H, H1); 4.02-4.06 (m, 1H, H2); 3.92 (dd, $^2J_{H,H} = 11.1$ Hz, $^3J_{H,H} = 7.3$ Hz, 1H, H1); 2.10 (s, 3H, H2); 1.21 (d, $^3J_{H,H} = 6.4$ Hz, 3H, H3).

$^{13}\text{C-NMR}$ (101 MHz, CDCl_3 , 298 K, δ in ppm): 19.1 (1C, C3); 20.9 (1C, C2'); 66.1 (1C, C2); 69.7 (1C, C1); 171.1 (1C, C1').

Synthesis of (S)-2-(benzyloxy)propyl benzoate (b26)



(S)-2-(benzyloxy)propan-1-ol (**b4**) (4.0 g, 24.1 mmol, 1.0 eq) was dissolved in toluene (180 mL), benzoyl chloride (4.2 mL, 36.1 mmol, 1.5 eq), triethylamine (3.4 mL, 24.1 eq, 1.0 eq) and *N,N*-dimethylaminopyridine (294 mg, 2.41 mmol, 0.1 eq) were added and the resulting reaction mixture was stirred at rt. Rapidly a white precipitate was

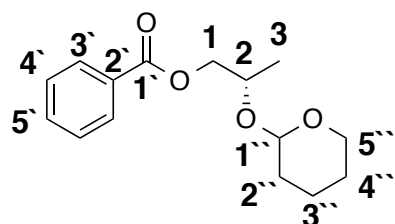
formed. TLC (pentane/TBME 9:1) indicated full conversion after 4 hours. The precipitate was filtered off and the solvent removed under reduced pressure. Filtration over silica (pentane/TBME 9:1) delivered pure product as pale yellow oil.⁶²

TLC: (SiO_2 , pentane/TBME (9:1)): $R_f = 0.76$.

¹H-NMR (400 MHz, CDCl₃, 298 K, δ in ppm): 8.02-8.08 (m, 2H, H3'); 7.64-7.71 (m, 1H, H5'); 7.41-7.47 (m, 2H, H4'); 7.23-7.39 (m, 5H, H3''-H5''); 4.67 (d, ²J_{H,H} = 12.0 Hz, 1H, H1''), 4.63 (d, ²J_{H,H} = 12.0 Hz, 1H, H1''), 4.29-4.40 (m, 2H, H1); 3.91 (pd, ³J_{H,H} = 6.3 Hz, ³J_{H,H} = 4.5 Hz, 1H, H2); 1.31 (d, ³J_{H,H} = 6.3 Hz, 3H, H3).

¹³C-NMR (101 MHz, CDCl₃, 298 K, δ in ppm): 17.2 (1C, C3); 68.0 (1C, C1); 71.2 (1C, C1''); 72.8 (1C, C2); 127.73 (1C, C5''); 127.78 (2C, C3''); 128.5 (4C, C4', C4''); 129.1 (1C, C2'); 129.8 (2C, C3'); 133.1 (1C, C5'); 135.4 (1C, C2''); 166.6 (1C, C1').

Synthesis of (2S)-2-((tetrahydro-2H-pyran-2-yl)oxy)propyl benzoate (b28)



(2S)-2-((tetrahydro-2H-pyran-2-yl)oxy)propan-1-ol (**b9**)

(3.1 g, 19.3 mmol, 1.0 eq) was dissolved in toluene (120 mL), benzoyl chloride (3.4 mL, 29.0 mmol, 1.5 eq), triethylamine (2.7 mL, 19.3 mmol, 1.0 eq) and *N,N*-dimethylaminopyridine (236 mg, 1.9 mmol, 0.1 eq)

were added and the resulting reaction mixture was stirred at rt. Rapidly a white precipitate was formed. After 3 hours the precipitate was filtered off and washed with toluene. The solvent was removed under reduced pressure and purified by silica gel column chromatography pentane/TBME (9:1) followed by a second column using cyclohexane/ethyl acetate (95:5 → 9:1) as eluent. The title compound (2.02 g, 7.64 mmol, 40%) was obtained as colourless oil.⁶²

TLC: (SiO₂, cyclohexane/ethyl acetate (95:5)): **R_f** = 0.28; 0.09.

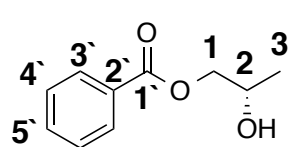
Diastereoisomer 1: **¹H-NMR** (600 MHz, CDCl₃, TMS, δ in ppm): 8.02-8.05 (m, 2H, H3'); 7.53-7.59 (m, 1H, H5'); 7.41-7.47 (m, 2H, H4'); 4.83 (dd, ³J_{HH} = 4.7 Hz, ³J_{HH} = 2.9 Hz, 1H, H1''); 4.34 (dd, ²J_{HH} = 11.4 Hz, ³J_{HH} = 4.2 Hz, 1H, H1); 4.25 (dd, ²J_{HH} = 11.4 Hz, ³J_{HH} = 6.5 Hz, 1H, H1); 4.12-4.20 (m, 1H, H2); 3.85-3.96 (m, 1H, H5''); 3.49-3.55 (m, 1H, H5''); 1.78-1.88 (m, 1H, H3''); 1.67-1.80 (m, 1H, H2''); 1.53-1.64 (m, 1H, H2''); 1.49-1.55 (m, 1H, H3''); 1.43-1.60 (m, 2H, H4''); 1.34 (d, ³J_{HH} = 6.4 Hz, 3H, H3).

Diastereoisomer 2: **¹H-NMR** (600 MHz, CDCl₃, TMS, δ in ppm): 8.05-8.09 (m, 2H, H3'); 7.53-7.59 (m, 1H, H5'); 7.41-7.47 (m, 2H, H4'); 4.80 (t, ³J_{HH} = 3.4 Hz, 1H, H1''); 4.40 (dd, ²J_{HH} = 11.2 Hz, ³J_{HH} = 6.4 Hz, 1H, H1); 4.30 (dd, ²J_{HH} = 11.2 Hz, ³J_{HH} = 4.6 Hz, 1H, H1); 4.12-4.20 (m, 1H, H2); 3.85-3.96 (m, 1H, H5''); 3.44-3.49 (m, 1H, H5''); 1.78-1.88 (m, 1H, H3''); 1.67-1.80 (m, 1H, H2''); 1.53-1.64 (m, 1H, H2''); 1.49-1.55 (m, 1H, H3''); 1.43-1.60 (m, 2H, H4''); 1.24 (d, ³J_{HH} = 6.3 Hz, 3H, H3).

Diastereoisomer 1: $^{13}\text{C-NMR}$ (101 MHz, CDCl_3 , 298 K, δ in ppm): 18.5 (1C, C3); 19.6 (1C, C3''); 25.40 (1C, C4''); 30.8 (1C, C2''); 62.8 (1C, C5''); 67.8 (1C, C1); 70.9 (1C, C2); 98.8 (1C, C1''); 128.3 (2C, C4'); 129.53 (2C, C3'); 130.2 (1C, C2'); 133.0 (1C, C5'); 166.4 (1C, C1').

Diastereoisomer 2: $^{13}\text{C-NMR}$ (101 MHz, CDCl_3 , 298 K, δ in ppm): 16.4 (1C, C3); 19.6 (1C, C3''); 25.40 (1C, C4''); 30.8 (1C, C2''); 61.9 (1C, C5''); 68.3 (1C, C1); 69.5 (1C, C2); 96.0 (1C, C1''); 128.3 (2C, C4'); 129.64 (2C, C3'); 130.2 (1C, C2'); 133.0 (1C, C5'); 166.4 (1C, C1').

Synthesis of (S)-2-hydroxypropyl benzoate (b29)



(2S)-2-((tetrahydro-2H-pyran-2-yl)oxy)propyl benzoate (**b28**)

(1.0 g, 3.78 mmol, 1.0 eq) was dissolved in acetic acid/THF/water (4:2:1, 55 mL) and heated to 45 °C for 4 hours.

The solvents were removed under reduced pressure (20 °C) and purified by silica gel column chromatography using pentane/tert-butylmethylether (4:1) followed by a second column using dichloromethane/ethyl acetate (9:1) as eluent to yield the title compound (500 mg, 2.77 mmol, 73%) as colourless oil.⁵²

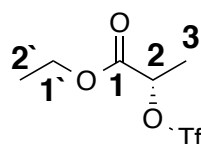
TLC: (SiO_2 , dichloromethane/ethyl acetate (9:1)): R_f = 0.33.

ESI-MS: calc. 203.1 (M+Na); measured 203.1 (M+Na).

$^1\text{H-NMR}$ (400 MHz, CDCl_3 , 298 K, δ in ppm): 8.02-8.10 (m, 2H, H3'); 7.52-7.62 (m, 1H, H5'); 7.41-7.50 (m, 2H, H4'); 4.30-4.40 (m, 1H, H1); 4.15-4.25 (m, 2H, H1, H2); 2.17 (d, $^3J_{\text{H,H}}$ = 3.8 Hz, 1H, OH); 1.30 (d, $^3J_{\text{H,H}}$ = 6.1 Hz, 3H, H3).

$^{13}\text{C-NMR}$ (101 MHz, CDCl_3 , 298 K, δ in ppm): 19.4 (1C, C3); 66.4 (1C, C2); 70.2 (1C, C3); 128.6 (2C, C4'); 129.8 (2C, C3'); 130.0 (1C, C2'); 133.3 (1C, C5'); 166.8 (1C, C1').

Synthesis of ethyl (S)-2-(((trifluoromethyl)sulfonyl)oxy)propanoate



Triflic anhydride (1.42 mL, 8.55 mmol, 1.01 eq) was dissolved in anhydrous dichloromethane (20 mL) and cooled (isopropanol/dry ice).

L-lactic acid ethyl ester (1.0 g, 0.97 mL, 8.47 mmol, 1.0 eq) and

Pyridine (0.69 mL, 8.47 mmol, 1.0 eq) were dissolved in

dichloromethane (10 mL) and added dropwise. The resulting reaction mixture was stirred for 10 min before warmed to rt. over 10 min. The solvent was removed under reduced pressure at 0 °C. The crude reaction mixture was filtered over silica gel (4

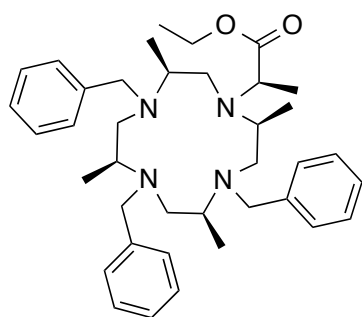
cm, water cooled column) using dichloromethane/hexane (4:1) as eluent. The solvent was removed under reduced pressure and the resulting product (60 %) stored at -20 °C in dichloromethane.²⁵

TLC: (SiO₂, dichloromethane/hexane (4:1)): **R_f** = 0.85.

¹H-NMR (400 MHz, CDCl₃, 298 K, δ in ppm): 5.22 (q, ³J_{H,H} = 7.0 Hz, 1H, H2); 4.30 (qd, ³J_{H,H} = 7.2 Hz, ²J_{H,H} = 2.0 Hz, 2H, H1`); 1.71 (d, ³J_{H,H} = 7.0 Hz, 3H, H3); 1.33 (t, ³J_{H,H} = 7.2 Hz, 3H, H2`).

¹⁹F-NMR (376 MHz, CDCl₃, 298 K, δ in ppm): -75.2 (3F, CF₃).

Synthesis of ethyl (*R*)-2-((2*S*,5*S*,8*S*,11*S*)-4,7,10-tribenzyl-2,5,8,11-tetramethyl-1,4,7,10-tetraazacyclododecan-1-yl)propanoate (**B15**)

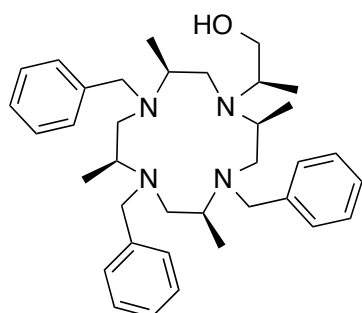


Cyclen (150 mg, 0.66 mmol, 1.0 eq) was dissolved in dichloromethane (20 mL) and sodium hydride (34 mg, 0.85 mmol, 1.3 eq, 60% in oil) was added and stirred for 5 min before ethyl (*S*)-2-(((trifluoromethyl)sulfonyl)oxy)propanoate (164 mg, 0.66 mmol, 1.0 eq) in dichloromethane (10 mL) was added dropwise. The resulting mixture of mono-, bis-functionalized cyclone and

starting material was quenched with water, extracted with dichloromethane, dried over sodium sulphate and the solvent removed under reduced pressure. The crude mixture was redissolved in dichloromethane (2 mL) and added dropwise to a suspension of benzyl bromide (291 μL, 2.4 mmol, 4.0 eq) and sodium hydride (97 mg (60%), 2.4 mmol, 4.0 eq) in dry THF/DMF (2:1, 12 mL) at -10 °C. The reaction mixture was stirred for 1 hour before warmed to rt. (30 min) and finally heated to 50 °C for 2 hours. The reaction mixture was poured into a mixture of water/pentane (2.5:1.5 (8 mL)). The organic layer was separated, washed with water, brine before dried over sodium sulphate. The solvent was removed under reduced pressure and the crude mixture purified by silica gel column chromatography using chloroform/ethanol (9:1) as eluent. Further purification was performed with preparative HPLC chromatography. The title compound was obtained as one to one mixture with the 4 times benzyl protected cyclen.

ESI-MS: calc. 599.4 (M+1); measured 599.7 (M+1).

Synthesis of (*R*)-2-((2*S*,5*S*,8*S*,11*S*)-4,7,10-tribenzyl-2,5,8,11-tetramethyl-1,4,7,10-tetraazacyclododecan-1-yl)propan-1-ol (**B15**)

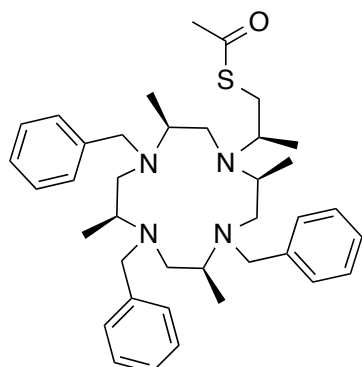


B15 (300 mg, 0.5 mmol, 1.0 eq) in diethylether (2 mL) was added dropwise to LiAlH_4 (28.5 mg, 0.751 mmol, 1.5 eq) in diethylether (10 mL) at 0 °C. The reaction mixture was warmed to rt. before heated to reflux overnight. The reaction was quenched with water, NaOH (15%). The precipitate was filtered off, washed with ether. The

combined organic layer was dried over sodium sulphate and the solvent was removed under reduced pressure. The title compound was used without further purification.

ESI-MS: calc. 557.4 (M+1); measured 557.7 (M+1).

Synthesis of *S*-((*R*)-2-((2*S*,5*S*,8*S*,11*S*)-4,7,10-tribenzyl-2,5,8,11-tetramethyl-1,4,7,10-tetraazacyclododecan-1-yl)propyl) ethanethioate (**B17**)

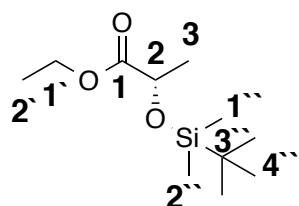


The crude mixture of **B16** (100 mg, 0.18 mmol, 1.0 eq) was dissolved in dry THF (4 mL) and cooled to 0 °C. Methanesulfonyl chloride (41 μL , 0.54 mmol, 3.0 eq) and triethylamine (151 μL , 1.08 mmol, 6.0 eq) were added slowly and stirred for additional 10 min at 0 °C before warmed to rt. and stirred until a high conversion was indicated by ESI-MS (disappearance of the starting

material peak). The reaction mixture was neutralized with 0.1 N HCl and extracted with chloroform. The combined organic layer was dried over sodium sulphate and the solvent removed under reduced pressure.

The crude reaction mixture was redissolved in THF (10 mL) and potassium thioacetate (92 mg, 0.79 mmol, 5.0 eq) was added and heated to reflux for 7 hours. The reaction mixture was quenched with water and extracted with chloroform, dried over sodium sulphate and the solvent removed under reduced pressure. Only traces of the desired product were obtained by ESI-MS.

ESI-MS: calc. 615.4 (M+1); measured 615.7 (M+1).

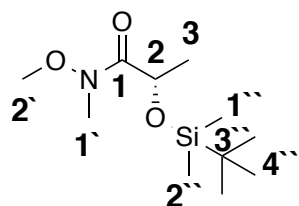
Synthesis of ethyl (S)-2-((*tert*-butyldimethylsilyl)oxy)propanoate (c1)

To a mixture of *L*-lactic acid ethyl ester (5.0 g, 42.3 mmol, 1.0 eq) and imidazole (3.46 g, 50.8 mmol, 1.2 eq) in DMF (20 mL) was added TBDMSCl (7.66 g, 50.8 mmol, 1.2 eq) at 0 °C. The reaction was warmed to rt. and stirred over the weekend. The reaction was quenched with water and the aqueous layer extracted with ether. The combined organic layer was washed with brine, dried over sodium sulphate and the solvent removed under reduced pressure. The crude mixture was purified with pentane/dichloromethane (2:1) to yield the title compound (9.01 g, 38.8 mmol, 92 %) as colourless oil.⁶³

TLC: (SiO₂, pentane/dichloromethane (2:1)): **R_f** = 0.93.

¹H-NMR (400 MHz, CDCl₃, 298 K, δ in ppm): 4.31 (q, ³J_{H,H} = 6.7 Hz, 1H, H₂); 4.06-4.25 (m, 2H, H_{1'}); 1.39 (d, ³J_{H,H} = 6.7 Hz, 3H, H₃); 1.27 (t, ³J_{H,H} = 7.1 Hz, 3H, H_{2'}); 0.90 (s, 9H, H_{4''}); 0.10 (s, 3H, H_{1''}); 0.07 (s, 3H, H_{2''}).

¹³C-NMR (101 MHz, CDCl₃, 298 K, δ in ppm): -5.1 (1C, C_{2''}); -4.8 (1C, C_{1''}); 14.3 (1C, C_{2'}); 18.5 (1C, C_{3''}); 21.5 (1C, C₃); 25.9 (3C, C_{4''}); 60.9 (1C, C_{1'}); 68.6 (1C, C₂); 174.3 (1C, C₁).

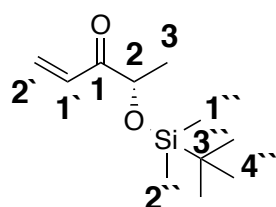
Synthesis of (S)-2-((*tert*-butyldimethylsilyl)oxy)-*N*-methoxy-*N*-methyl-propanamide (c2)

To a mixture of (S)-2-((*tert*-butyldimethylsilyl)oxy)propanoate (c1) (2.0 g, 8.61 mmol, 1.0 eq) and *N,O*-dimethylhydroxylamine hydrochloride (1.3 g, 13.3 mmol, 1.55 eq) in THF (60 mL) at -20 °C (the temperature was kept constant with a cryostat) under inert conditions was added isopropyl magnesium chloride (2M in THF, 12.9 mL, 25.8 mmol, 3.0 eq) over 1h under vigorous stirring. After 2h reaction the mixture was warmed to up to 5 °C over 1h. The cooling bath was removed and the slurry turned into a homogeneous solution. The reaction was quenched with saturated ammonium chloride solution and the aqueous layer extracted with diethylether. The combined organic layer was dried over sodium sulphate and the solvent removed under reduced pressure. The crude mixture was purified by silica gel column chromatography using pentane/*tert*butyl methyl ether (9:1 → 1:1 → 1:2) as eluent to yield the title compound (1.0 g, 4.04 mmol, 47%) as colourless oil.⁶³

TLC: (SiO₂, pentane/TBME (9:1)): **R_f** = 0.26

¹H-NMR (400 MHz, CDCl₃, 298 K, δ in ppm): 4.68 (q, ³J_{H,H} = 6.6 Hz, 1H, H2); 3.70 (s, 3H, H2''); 3.21 (s, 3H, H1''); 1.36 (d, ³J_{H,H} = 6.6 Hz, 3H, H3); 0.90 (s, 9H, H4''); 0.10 (s, 3H, H1''); 0.07 (s, 3H, H2'').

Synthesis of (S)-4-((*tert*-butyldimethylsilyloxy)pent-1-en-3-one (c3)



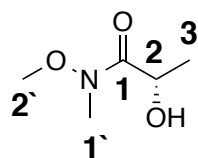
To a solution of (S)-2-((*tert*-butyldimethylsilyloxy)-*N*-methoxy-*N*-methylpropanamide (500 mg, 2.02 mmol, 0.5 eq) in THF (19 mL) was added vinylmagnesium bromide solution (1M in THF, 12 mmol, 12 mL, 3.2 eq) at -15 °C and the mixture was warmed to rt. over 5 hours. The reaction was quenched with NH₄Cl aq. and the resulting mixture was extracted with TBME. The combined organic layer was dried over sodium sulphate and the solvent removed under reduced pressure. The crude mixture was purified by silica gel column chromatography using pentane/*tert*-butyl methyl ether (9:1) as eluent and the title compound (220 mg, 1.03 mmol, 51%) was isolated as yellow oil.⁶³

TLC: (SiO₂, pentane/TBME (9:1)): **R_f** = 0.91.

¹H-NMR (400 MHz, CDCl₃, 298 K, δ in ppm): 6.86 (dd, ²J_{H,H} = 17.4 Hz, ³J_{H,H} = 10.6 Hz, 1H, H2'_{trans}); 6.40 (dd, ²J_{H,H} = 17.4 Hz, ³J_{H,H} = 1.9 Hz, 1H, H2'_{cis}); 5.76 (dd, ³J_{H,H} = 10.6 Hz, ³J_{H,H} = 1.9 Hz, 1H, H1'); 4.30 (q, ³J_{H,H} = 6.8 Hz, 1H, H2); 1.31 (d, ³J_{H,H} = 6.8 Hz, 3H, H3); 0.91 (s, 9H, H4''); 0.07 (s, 3H, H1''); 0.06 (s, 3H, H2'').

¹³C-NMR (101 MHz, CDCl₃, 298 K, δ in ppm): -4.83 (1C, C2''); -4.67 (1C, C1''); 21.1 (1C, C3); 25.9 (3C, C4''); 30.5 (1C, C3''); 74.4 (1C, C2); 129.6 (1C, C2'); 130.7 (1C, C1'); 202.0 (1C, C1).

Synthesis of (S)-2-hydroxy-*N*-methoxy-*N*-methylpropanamide (c4)



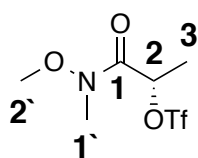
To a mixture of *L*-Lactic acid ethylester (2.95 g, 2.86 mL, 25 mmol, 1.5 eq) and *N*,*O*-dimethylhydroxylamine hydrochloride (4.06 g, 41.7 mmol, 2.50 eq) in THF (30 mL) at -20 °C (the temperature was kept constant with a cryostat) under inert conditions was added isopropyl magnesium chloride (2M in THF, 25 mL, 50 mmol, 3.0 eq) over 1h under vigorous stirring. After 2h reaction the mixture was warmed to up to 5 °C over 1h. The cooling bath was removed and the slurry turned into a homogeneous solution. The reaction was quenched with saturated ammonium chloride solution and the aqueous layer extracted with diethylether. The combined organic layer was dried over sodium

sulphate and the solvent removed under reduced pressure. The crude mixture was purified by silica gel column chromatography pentane/tert-butyl methyl ether (1:1 → 0:1) to yield the title compound (1.98 g, 14.9 mmol, 60%) as colourless oil.⁶³

TLC: (SiO₂, pentane/TBME (1:1)): **R_f** = 0.09.

¹H-NMR (400 MHz, CDCl₃, 298 K, δ in ppm): 4.49 (p, ³J_{H,H} = 6.9 Hz, 1H, H₂); 3.72 (s, 3H, H₂′); 3.34 (d, ³J_{H,H} = 6.9 Hz, 1H, OH); 3.25 (s, 3H, H₁′); 1.37 (d, ³J_{H,H} = 6.9 Hz, 3H, H₃).

Synthesis of (S)-1-(methoxy(methyl)amino)-1-oxopropan-2-yl trifluoromethanesulfonate (c5)



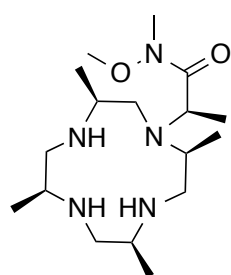
Triflic anhydride (312 μL, 1.88 mmol, 1.01 eq) was dissolved in dichloromethane (10 mL) and cooled to -78 °C. (S)-2-hydroxy-N-methoxy-N-methylpropanamide (**c4**) (250 mg, 1.88 mmol, 1.01 eq) and pyridine (150 μL, 1.86 mmol, 1.0 eq) were dissolved in dichloromethane (5 mL) and added dropwise. The resulting mixture was stirred at -78 °C for 10 min, warmed to rt. over 45 min, filtered over cooled silica using dichloromethane/hexane (4:1) as eluent to yield the title compound (400 mg, 1.51 mmol, 80%) as yellowish oil.²⁵

TLC: (SiO₂, dichloromethane/hexane (4:1)): **R_f** = 0.85.

¹H-NMR (400 MHz, CDCl₃, 298 K, δ in ppm): 5.58 (q, ³J_{H,H} = 6.8 Hz, 1H, H₂); 3.76 (s, 3H, H₂′); 3.25 (s, 3H, H₁′); 1.66 (d, ³J_{H,H} = 6.8 Hz, 3H, H₃).

¹⁹F-NMR (376 MHz, CDCl₃, 298 K, δ in ppm): -75.28 (3F, CF₃).

Synthesis of (R)-N-methoxy-N-methyl-2-((2S,5S,8S,11S)-2,5,8,11-tetramethyl-1,4,7,10-tetraazacyclododecan-1-yl)propanamide (C2)

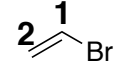


Cyclen (100 mg, 0.438 mmol, 1.0 eq) was dissolved in dichloromethane (10 mL) and sodium hydride (19.3 mg, 0.482 mmol, 1.1 eq) added. The resulting mixture was stirred for 5 min, cooled to 0 °C before **c5** (116 mg, 0.438 mmol, 1.0 eq) was added dropwise. After the addition the reaction mixture was warmed to rt. and stirred overnight. The solvent was removed under reduced pressure and the crude mixture purified by preparative HPLC. The pH of the resulting HPLC-fractions was adjusted to 7 with ammonium acetate and extracted with chloroform.

Retention time: 11-14 min.

ESI-MS: calc. 344.3 (M+1); measured 344.5 (M+1).

Synthesis of bromoethene

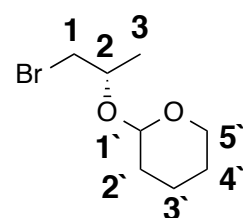
 Potassium hydroxide (9.38 g, 167 mmol, 1.57 eq) in ethanol (80 mL) was heated to reflux and 1,2-dibromoethane was added dropwise over 1 hour. The resulting vinyl bromide was distilled over N₂ stream (nitrogen is required to push the vinyl bromide to the condenser) and condensed in -70 °C cooling trap. The resulting mixture was washed with ice-cold water and dried over K₂CO₃. The resulting mixture was purified by distillation (50 °C) to yield a colourless oil, the slightly higher boiling substances contained ethanol as by-product.⁶⁴

Bp.: 50 °C (1bar)

¹H-NMR (400 MHz, CDCl₃, 298 K, δ in ppm): 6.38 (dd, ²J_{H,H} = 15.0 Hz, ³J_{H,H} = 7.2 Hz, 1H, H_{2trans}); 5.93 (dd, ³J_{H,H} = 7.2 Hz, ³J_{H,H} = 1.9 Hz, 1H, H₁); 5.80 (dd, ²J_{H,H} = 15.0 Hz, ³J_{H,H} = 1.9 Hz, 1H, H_{2cis}).

¹³C-NMR (101 MHz, CDCl₃, 298 K, δ in ppm): 114.1 (1C, C₁); 122.1 (1C, C₂).

Synthesis of 2-(((S)-1-bromopropan-2-yl)oxy)tetrahydro-2H-pyran (d1)



(2S)-2-((tetrahydro-2H-pyran-2-yl)oxy)propan-1-ol (6.0 g, 37.5 mmol, 1.0 eq) was dissolved in dichloromethane (160 mL), cooled to 0 °C and triphenylphosphine (29.5 g, 112 mmol, 3.0 eq), carbon tetrabromide (18.6 g, 56.2 mmol, 1.5 eq) and triethylamine (36.8 mL, 262 mmol, 7.0 eq) were added. The resulting reaction

mixture was stirred at 0 °C for 18 hours before water (240 mL) were added. The phases were separated and the aqueous layer was reextracted with dichloromethane three times. The combined organic layer was dried over sodium sulphate and the solvent removed under reduced pressure. The crude mixture was purified by silica gel column chromatography using pentane/TBME (9:1 -> 1:1) as eluent to yield the title compound as colourless oil.⁶⁵

TLC: (SiO₂, pentane/TBME (9:1)); **R_f** = 0.58.

Diastereoisomer 1: **¹H-NMR** (400 MHz, CDCl₃, 298 K, δ in ppm): 4.75 (dd, ³J_{H,H} = 4.6 Hz, ³J_{H,H} = 2.9 Hz, 1H, H_{1'}); 3.94-4.03 (m, 1H, H₂); 3.86-3.93 (m, 1H, H_{5'}); 3.47-3.56 (m, 1H, H₁); 3.33-3.41 (m, 2H, H₁, H_{5'}); 1.78-1.88 (m, 1H, H_{3''}); 1.67-1.80 (m, 1H,

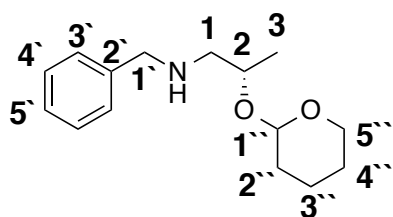
H2`); 1.53-1.64 (m, 1H, H2`); 1.49-1.55(m, 1H, H3`); 1.48-1.64 (m, 2H, H4`); 1.34 (d, $^3J_{H,H} = 6.4$ Hz, 3H, H3).

Diastereoisomer 2: $^1\text{H-NMR}$ (400 MHz, CDCl_3 , 298 K, δ in ppm): 4.71-4.74 (m, 1H, H1`); 3.94-4.03 (m, 2H, H2, H5); 3.47-3.56 (m, 2H, H1, H5`); 3.33-3.41 (m, 1H, H1); 1.78-1.88 (m, 1H, H3`); 1.67-1.80 (m, 1H, H2`); 1.53-1.64 (m, 1H, H2`); 1.49-1.55 (m, 1H, H3`); 1.48-1.64 (m, 2H, H4`); 1.27 (d, $^3J_{H,H} = 6.2$ Hz, 3H, H3).

Diastereoisomer 1: $^{13}\text{C-NMR}$ (101 MHz, CDCl_3 , 298 K, δ in ppm): 19.64 (1C, C3`); 20.4 (1C, C3); 25.41 (1C, C4`); 30.71 (1C, C2`); 36.6 (1C, C1); 62.71 (1C, C5`); 72.3 (1C, C2); 98.4 (1C, C1`).

Diastereoisomer 2: $^{13}\text{C-NMR}$ (101 MHz, CDCl_3 , 298 K, δ in ppm): 18.4 (1C, C3); 19.45 (1C, C3`); 25.42 (1C, C4`); 30.96 (1C, C2`); 37.5 (1C, C1); 62.52 (1C, C5`); 72.9 (1C, C2); 97.2 (1C, C1`).

Synthesis of (2S)-N-benzyl-2-((tetrahydro-2H-pyran-2-yl)oxy)propan-1-amine (d2)



Compound **d1** (3.5g, 15.7 mmol) in THF (10 mL) was added dropwise to benzylamine (3.8 mL, 34.5 mmol, 2.2 eq) in THF (25 mL) and stirred at rt. for 2 hours. The solvent was removed under reduced pressure and the crude mixture purified by silica gel column

chromatography to yield the title compound (1.0 g, 4.01 mmol, 26%) as colourless oil.

TLC: (SiO_2 , pentane:TBME (9:1)): $R_f = 0.12$; 0.04.

Diastereoisomer 1: $^1\text{H-NMR}$ (400 MHz, CDCl_3 , 298 K, δ in ppm): 7.29-7.36 (m, 4H, H3`, H4`); 7.23-7.28 (1H, H5`); 4.68 (t, $^3J_{H,H} = 2.6$ Hz, 1H, H1`); 3.85-3.97 (m, 2H, H5`); 3.77-3.83 (m, 2H, H1`); 3.43-3.55 (m, 1H, H2); 2.67 (dd, $^2J_{H,H} = 12.2$ Hz, $^3J_{H,H} = 4.3$ Hz, 1H, H1); 2.61 (dd, $^2J_{H,H} = 12.2$ Hz, $^3J_{H,H} = 4.3$ Hz, 1H, H1); 1.78-1.88 (m, 1H, H3`); 1.67-1.80 (m, 1H, H2`); 1.53-1.64 (m, 1H, H2`); 1.49-1.55 (m, 1H, H3`); 1.48-1.64 (m, 2H, H4`); 1.25 (d, $^3J_{H,H} = 6.3$ Hz, 3H, H3).

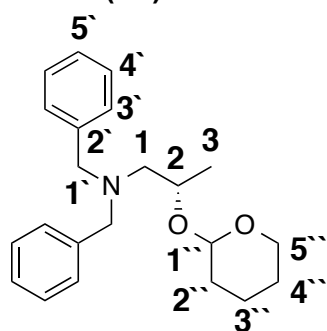
Diastereoisomer 2: $^1\text{H-NMR}$ (400 MHz, CDCl_3 , 298 K, δ in ppm): 7.29-7.36 (m, 4H, H3`, H4`); 7.23-7.28 (1H, H5`); 4.64-4.67 (m, 1H, H1`); 3.97-4.05 (m, 2H, H5`); 3.77-3.83 (m, 2H, H1`); 3.43-3.55 (m, 1H, H2); 2.62-2.74 (m, 2H, H1); 1.78-1.88 (m, 1H, H3`); 1.67-1.80 (m, 1H, H2`); 1.53-1.64 (m, 1H, H2`); 1.49-1.55 (m, 1H, H3`); 1.48-1.64 (m, 2H, H4`); 1.13 (d, $^3J_{H,H} = 6.2$ Hz, 3H, H3).

Diastereoisomer 1: $^{13}\text{C-NMR}$ (101 MHz, CDCl_3 , 298 K, δ in ppm): 20.19 (1C, C3); 20.28 (1C, C3`); 25.58 (1C, C4`); 31.38 (1C, C2`); 54.06 (1C, C1); 54.92 (1C, C1`);

63.2 (1C, C5''); 74.5 (1C, C2); 99.9 (1C, C1''); 127.0 (1C, C5'); 128.18 (2C, C3'); 128.52 (2C, C4'); 140.60 (1C, C2').

Diastereoisomer 2: ¹³C-NMR (101 MHz, CDCl₃, 298 K, δ in ppm): 18.01 (1C, C3); 20.44 (1C, C3''); 25.54 (1C, C4''); 31.50 (1C, C2''); 53.9 (1C, C1); 55.4 (1C, C1'); 63.4 (1C, C5''); 71.6 (1C, C2); 97.0 (1C, C1''); 126.89 (1C, C5'); 128.22 (2C, C3'); 128.45 (2C, C4'); 140.69 (1C, C2').

Synthesis of (2S)-N,N-dibenzyl-2-((tetrahydro-2H-pyran-2-yl)oxy)propan-1-amine (d3)



(2S)-N-benzyl-2-((tetrahydro-2H-pyran-2-yl)oxy)propan-1-amine (d2) (950 mg, 3.81 mmol, 1.0 eq) in dichloromethane (10 mL) was added dropwise to a suspension of benzyl bromide (592 μL, 4.95 mmol, 1.3 eq) and sodium hydride (198 mg, 4.95 mmol, 1.3 eq) in dry THF/DMF (2:1, 60 mL) at -10 °C. The reaction mixture was stirred for 1 hour before warmed to rt. (30 min) and finally heated to 50 °C for 2

hours. The reaction mixture was poured into a mixture of water and pentane (2.5:1.5 (40 mL)). The organic layer was separated, washed with water and brine before dried over sodium sulphate. The crude reaction mixture was purified by silica gel column chromatography.⁵⁶

TLC: (SiO₂, pentane/TBME (60:1)): R_f = 0.25

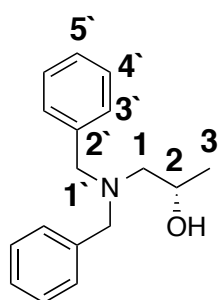
Diastereoisomer 1: ¹H-NMR (600MHz, CDCl₃, 298 K, δ in ppm): 7.34-7.32 (m, 4H, H4'); 7.29-7.32 (m, 4H, H3'); 7.21-7.24 (m, 2H, H5'); 3.95 ("sextett", ³J_{H,H} = 6.2 Hz, 1H, H2); 3.87-3.92 (m, 1H, H5''); 3.61 (d, ²J_{H,H} = 13.7 Hz, 1H, H1''); 3.58 (d, ²J_{H,H} = 13.7 Hz, 1H, H1'); 3.45-3.49 (m, 1H, H5''); 2.57 (dd, ²J_{H,H} = 13.2 Hz, ³J_{H,H} = 6.2 Hz, 1H, H1); 2.39 (dd, ²J_{H,H} = 13.2 Hz, ³J_{H,H} = 5.9 Hz, 1H, H1); 1.76-1.83 (m, 1H, H3''); 1.65-1.71 (m, 1H, H2''); 1.49-1.55 (m, 1H, H2''); 1.47-1.60 (m, 2H, H4''); 1.47-1.54 (m, 1H, H4'); 1.19 (d, ³J_{H,H} = 6.3 Hz, 3H, H3).

Diastereoisomer 2: ¹H-NMR (600MHz, CDCl₃, 298 K, δ in ppm): 7.34-7.32 (m, 4H, H4'); 7.29-7.32 (m, 4H, H3'); 7.21-7.24 (m, 2H, H5'); 3.97-4.03 (m, 1H, H2); 3.92-3.98 (m, 1H, H5''); 3.72 (d, ²J_{H,H} = 13.7 Hz, 1H, H1''); 3.53 (d, ²J_{H,H} = 13.7 Hz, 1H, H1'); 3.45-3.49 (m, 1H, H5''); 2.63 (dd, ²J_{H,H} = 12.9 Hz, ³J_{H,H} = 5.3 Hz, 1H, H1); 2.47 (dd, ²J_{H,H} = 12.9 Hz, ³J_{H,H} = 7.3 Hz, 1H, H1); 1.76-1.83 (m, 1H, H3''); 1.65-1.71 (m, 1H, H2''); 1.49-1.55 (m, 1H, H2''); 1.47-1.60 (m, 2H, H4''); 1.47-1.54 (m, 1H, H4'); 1.11 (d, ³J_{H,H} = 6.1 Hz, 3H, H3).

Diastereoisomer 1: $^{13}\text{C-NMR}$ (151 MHz, CDCl_3 , 298 K, δ in ppm): 20.5 (1C, C3); 20.1 (1C, C3''); 25.7 (1C, C4''); 31.2 (1C, C2''); 59.40 (2C, C1'); 59.73 (1C, C1); 62.84 (1C, 5''); 72.0 (1C, C2); 98.9 (1C, C1''); 126.97 (2C, C5'); 128.3 (4C, C3'); 129.0 (4C, C4'); 139.74 (2C, C2').

Diastereoisomer 2: $^{13}\text{C-NMR}$ (151 MHz, CDCl_3 , 298 K, δ in ppm): 17.91 (1C, C3); 19.71 (1C, C3''); 27.13 (1C, C4''); 31.19 (1C, C2''); 59.33 (1C, C1'); 59.58 (2C, C1); 62.47 (1C, 5''); 70.0 (1C, C2); 96.0 (1C, C1''); 126.89 (2C, C5'); 128.28 (4C, C3'); 129.05 (4C, C4'); 139.86 (2C, C2').

Synthesis of (S)-1-(dibenzylamino)propan-2-ol (d4)



(2S)-N,N-dibenzyl-2-((tetrahydro-2H-pyran-2-yl)oxy)propan-1-amine (d3) (1.1 g, 3.24 mmol, 1.0 eq) was dissolved in acetic acid/THF/water (4:2:1, 55 mL) and heated to 45 °C for 4 hours. Water (10 mL) was added and extracted with DCM. The crude mixture was purified by silica gel column chromatography pentane/TBME 4:1 followed by a second column using DCM/EtOAc

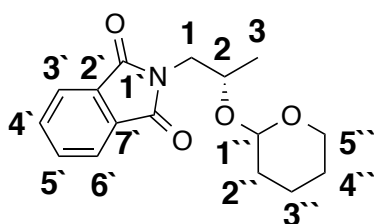
(9:1) as eluent.

Rf.: dichloromethane/ethyl acetate (9:1) = 0.2.⁵²

$^1\text{H-NMR}$ (250 MHz, CDCl_3 , 298 K, δ in ppm): 7.18-7.40 (m, 10H, H3'-H5'); 4.29 (d, $^3J_{\text{H,H}} = 4.2$ Hz, 1H, OH); 3.74-3.86 (m, 1H, H2); 3.61 (d, $^2J_{\text{H,H}} = 13.8$ Hz, 2H, H1'); 3.48 (d, $^2J_{\text{H,H}} = 13.8$ Hz, 2H, H1''); 2.36 (dd, $^2J_{\text{H,H}} = 12.6$ Hz, $^3J_{\text{H,H}} = 6.1$ Hz, 1H, H1); 2.24, (dd, $^2J_{\text{H,H}} = 12.6$ Hz, $^3J_{\text{H,H}} = 6.4$ Hz, 1H, H1); 0.99 (d, $^3J_{\text{H,H}} = 6.1$ Hz, 3H, H3).

$^{13}\text{C-NMR}$ (63 MHz, CDCl_3 , 298 K, δ in ppm): 20.1 (1C, C3); 58.6 (2C, C1'); 61.6 (1C, C1); 63.3 (1C, C2); 127.4 (2C, C5'); 128.6 (4C, C3'); 129.2 (4C, C4'); 138.7 (2C, C2').

Synthesis of 2-((2S)-2-((tetrahydro-2H-pyran-2-yl)oxy)propyl)isoindoline-1,3-dione (d6)



To a solution of triphenylphosphine (3.3 g, 12.5 mmol, 2.0 eq) in tetrahydrofuran (50 mL, degassed) was added diethylazodicarboxylate (2.29 mL, 12.5 mmol, 2.0 eq, 40% in toluene). The resulting solution was stirred for 30 min, before (2S)-2-((tetrahydro-2H-pyran-2-yl)oxy)propan-1-ol (1000 mg, 6.24 mmol, 1.0 eq) and phthalimide (1.86 g, 12.5 mmol,

2.0 eq) in THF (20 mL, degassed) were added simultaneously and the reaction was stirred for another 10 min at 0 °C, overnight at rt. and concentrated under reduced pressure before purified by silica gel column chromatography using pentane/tert-butylmethylether (4:1) as eluent to yield the title compound (900 mg, 3.11 mmol, 50%) as white crystals in mixture with phthalimide. No further purification was performed, directly deprotected as the purification of the alcohol has shown to be easier.⁶⁶ Assignment of the carbon frequencies for the minor isomer was not possible.

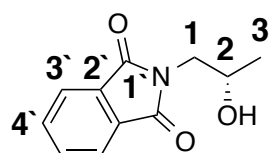
Rf: pentane/TBME (4:1) = 0.28.

Diastereoisomer 1: **¹H-NMR** (500 MHz, CDCl₃, 298 K, δ in ppm): 7.83-7.90 (m, 2H, H4', H5'); 7.71-7.78 (m, 2H, H3', H6'); 4.72 (t, ³J_{H,H} = 3.9 Hz, 1H, H1''); 4.08-4.14 (m, 1H, H2); 3.81-3.92 (m, 1H, H5''); 3.75 (d, ³J_{H,H} = 5.5 Hz, 2H, H1); 3.48 (dt, ²J_{H,H} = 10.7 Hz, ³J_{H,H} = 4.9 Hz, 1H, H5''); 1.76-1.80 (m, 1H, H3''); 1.61-1.67 (m, 1H, H2''); 1.41-1.56 (m, 4H, H2'', H3'', H4''); 1.28 (d, ³J_{H,H} = 6.4 Hz, 3H, H3).

Diastereoisomer 2: **¹H-NMR** (500 MHz, CDCl₃, 298 K, δ in ppm): 7.83-7.90 (m, 2H, H4', H5'); 7.71-7.78 (m, 2H, H3', H6'); 4.60 (dd, ³J_{H,H} = 4.7 Hz, ³J_{H,H} = 2.5 Hz, 1H, H1''); 4.14-4.19 (m, 1H, H2); 3.81-3.92 (m, 1H, H5''); 3.64 (dd, ²J_{H,H} = 13.8 Hz, ³J_{H,H} = 4.5 Hz, 2H, H1); 3.37 (ddd, ²J_{H,H} = 11.2 Hz, ³J_{H,H} = 7.8 Hz, ³J_{H,H} = 3.5 Hz, 1H, H5''); 3.18-3.28 (m, 1, H1); 1.76-1.80 (m, 1H, H3''); 1.61-1.67 (m, 1H, H2''); 1.41-1.56 (m, 4H, H2'', H3'', H4''); 1.20 (d, ³J_{H,H} = 6.3 Hz, 3H, H3).

Diastereoisomer 1: **¹³C-NMR** (126 MHz, CDCl₃, 298 K, δ in ppm): 19.7 (1C, C3); 19.8 (1C, C3''); 25.4 (1C, C4''); 30.5 (1C, C2''); 42.3 (1C, C1); 62.5 (1C, C5''); 71.0 (1C, C2); 98.6 (1C, C1''); 123.5 (2C, C3', C6'); 132.6 (2C, C2', C7'); 134.3 (2C, C4', C5'); 168.5 (2C, C1').

Synthesis of (S)-2-(2-hydroxypropyl)isoindoline-1,3-dione (d7)



2-((2S)-2-((tetrahydro-2H-pyran-2-yl)oxy)propyl)isoindoline-1,3-dione (**d6**) (0.9 g, 3.1 mmol, 1.0 eq) was dissolved in acetic acid/THF/water (4:2:1, 35 mL) and heated to 45 °C for 6 hours.

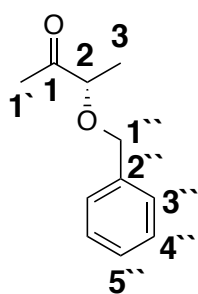
The solvent was removed under reduced pressure (30 °C) and purified by silica gel column chromatography using cyclohexane/ethyl acetate (4:1 -> 0:1) as eluent.⁵²

Rf.: cyclohexane/ethyl acetate (4:1) = 0.02.

$^1\text{H-NMR}$ (250 MHz, CDCl_3 , 298 K, δ in ppm): 7.82-7.90 (m, 2H, H4); 7.69-7.77 (m, 2H, H3'); 4.04-4.19 (m, 1H, H2); 3.65-3.83 (m, 2H, H1); 2.36 (b"s", 1H, OH); 1.26 (d, $^3J_{\text{H,H}} = 6.3$ Hz, 3H, H3).

$^{13}\text{C-NMR}$ (63 MHz, CDCl_3 , 298 K, δ in ppm): 21.2 (1C, C3); 45.7 (1C, C1); 67.0 (1C, C2); 123.6 (2C, C3'); 132.1 (2C, C2'); 134.3 (2C, C4'); 169.1 (2C, C1').

Synthesis of (S)-3-(benzyloxy)butan-2-one (d9)



(S)-2-(benzyloxy)propan-1-ol (**b3**) (5.0 g, 24.0 mmol, 1.0 eq) was dissolved in THF and cooled to -110 °C (internal temp) (ethanol/liquid nitrogen mixture) and methyllithium (16.5 mL, 1.6 M in diethylether, 26.4 mmol, 1.1 eq) was added dropwise over 30 min and the temperature kept below -98 °C. The reaction mixture was stirred for additional 25 min before TMSCl was added dropwise. The

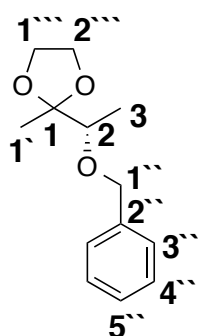
resulting mixture was stirred for 2 min before warmed to rt. and stirred for another 25 min. The reaction was quenched with HCl (1 M, aq, 70 mL) and stirred for 60 min. The reaction mixture was neutralized with solid sodium carbonate. The resulting reaction mixture was extracted with dichloromethane, the organic phase was dried over sodium sulphate and the solvent removed under reduced pressure. The title compound (90%) was obtained in 90% purity and used without further purification.⁶⁷

Rf.: pentane/TBME (1:1) = 0.83.

$^1\text{H-NMR}$ (400 MHz, CDCl_3 , 298 K, δ in ppm): 7.27-7.42 (m, 5H, H3''-H5''); 4.57 (d, $^2J_{\text{H,H}} = 11.7$ Hz, 1H, H1''); 4.50 (d, $^2J_{\text{H,H}} = 11.7$ Hz, 1H, H1''); 3.91 (q, $^3J_{\text{H,H}} = 6.9$ Hz, 1H, H2); 2.20 (s, 3H, H1'); 1.35 (d, $^3J_{\text{H,H}} = 6.9$ Hz, 3H, H3).

$^{13}\text{C-NMR}$ (101 MHz, CDCl_3 , 298 K, δ in ppm): 17.5 (1C, C3); 25.2 (1C, C1'); 72.0 (1C, C1''); 81.0 (1C, C2); 127.9 (2C, C3''); 128.1 (1C, C5''); 128.7 (2C, C4''); 137.7 (1C, C2'').

Synthesis of (S)-2-(1-(benzyloxy)ethyl)-2-methyl-1,3-dioxolane (d10)



To (S)-3-(benzyloxy)butan-2-one (**d9**) (1.0g, 5.61 mmol, 1.0eq) in toluene (20 mL) was added ethylene glycol (3.1 mL, 56.1 mmol, 10.0 eq) and p-TsOH (107 mg, 0.561 mmol, 0.1 eq) and heated to reflux in a dean stark apparatus for 30 hours. The reaction mixture was cooled to rt. and quenched with sodium carbonate (aq. sat, 10 mL) and extracted with ethyl acetate. The combined organic layer was

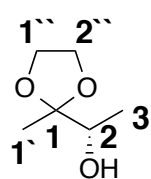
dried over sodium sulphate and the solvent removed under reduced pressure, before purified by silica gel column chromatography using pentane/*tert*butyl methyl ether (2:1) as eluent to yield the title compound (520 mg, 2.34 mmol, 42%) as colourless oil.⁵²

TLC: (SiO₂, pentane/TBME 2:1): **R_f** = 0.91

¹H-NMR (400 MHz, CDCl₃, 298 K, δ in ppm): 7.23-7.39 (m, 5H, H3''-H5''); 4.68 d, ²J_{H,H} = 12.1 Hz, 1H, H1''); 4.64 (d, ²J_{H,H} = 12.1 Hz, 1H, H1''); 3.92-4.03 (m, 4H, H1'', H2''); 3.48 (q, ³J_{H,H} = 6.4 Hz, 1H, H2); 1.34 (s, 3H, H1'); 1.19 (d, ³J_{H,H} = 6.4 Hz, 3H, H3).

¹³C-NMR (101 MHz, CDCl₃, 298 K, δ in ppm): 15.6 (1C, C3); 20.2 (1C, C1'); 65.1 (1C, C1); 65.3 (1C, C2''); 72.2 (1C, C1''); 78.2 (1C, C2); 111.2 (1C, C3); 127.5 (1C, C5''); 127.8 (2C, C3''); 128.4 (2C, C4''); 139.1 (1C2'').

Synthesis of (S)-1-(2-methyl-1,3-dioxolan-2-yl)ethan-1-ol (d11)



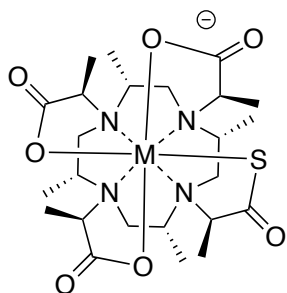
(S)-2-(1-(benzyloxy)ethyl)-2-methyl-1,3-dioxolane (**d10**) (862 mg, 3.88 mmol, 1.0 eq) was dissolved in methanol (5 mL) and palladium on activated charcoal (41.3 mg, 0.388 mmol, 0.1 eq, 10%) add. A hydrogen pressure of 10 bar was applied and the resulting suspension was stirred

for 3 hours, filtered over celite and the solvent removed under reduced pressure. The crude mixture was purified by silica gel column chromatography using pentane/*tert*-butylmethylether (2:1 → 0:1) as eluent to yield the title compound (90 mg, 0.68 mmol, 18 %) as colourless oil. 500 mg of the starting material could be recovered.⁵²

R_f: pentane/*tert*-butyl methyl ether (1:1) = 0.27.

¹H-NMR (400 MHz, CDCl₃, 298 K, δ in ppm): 3.99-4.03 (m, 4H, H1'', H2''); 3.73 (q, ³J_{HH} = 6.5 Hz, 1H, H2); 1.63 (bs, 1H, OH); 1.31 (s, 3H, H1'); 1.21 (d, ³J_{HH} = 6.5 Hz, 3H, H3).

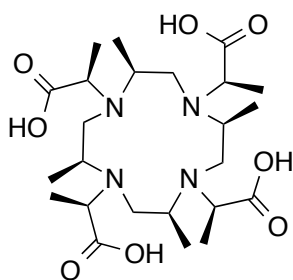
¹³C-NMR (101 MHz, CDCl₃, 298 K, δ in ppm): 16.8 (1C, C3); 19.1 (1C, C1'); 65.3 (2C, C1'', C2''); 71.1 (1C, C2); 110.7 (1C, C3).

Synthesis of DOTA-M7-3R,4S-thiol-Metal (Lutetium + Samarium)

DOTA-M7-(3R,4S)-thiol (10 mg, 0.02 mmol, 1.0 eq) was dissolved in ammonium acetate (100 mM, aq., 5 mL) and metal chloride hexa hydrate (3.0 eq) added. The pH was adjusted to 5.5 and the resulting solution heated to 75 °C for 18 hours. A full conversion was obtained by ESI-MS and the excess metal removed by a single use SepPak C18 column on an peristaltic pump using water to water/methanol (2:8) as eluent.²⁵

ESI-MS: Lutetium complex calc. 676.2 (M+1); measured 698.2 (M+Na).

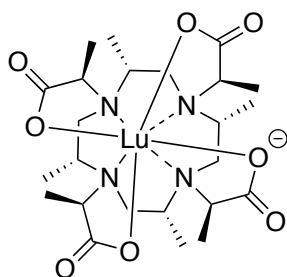
ESI-MS: Samarium complex calc. 100% peaks 653.2 (M+1); measured 653.2 (M+1) the characteristic samarium pattern was detected.

Synthesis of (2R,2'R,2''R,2'''R)-2,2',2'',2'''-((2S,5S,8S,11S)-2,5,8,11-tetramethyl-1,4,7,10-tetraazacyclododecane-1,4,7,10-tetrayl)tetrapropionic acid

(DOTA-M8-(4R,4S)-tertbutyl) (100 mg, 0.07 mmol, 1.0 eq) was dissolved in hydrochloric acid (1M, 20 mL) and heated to reflux for 60 minutes. The pH was adjusted to 7.0 using potassium hydroxide. The volume was reduced to 10 mL and the crude mixture purified by preparative HPLC under the standard conditions. The product was obtained as colourless

waxy solid in 80% yield.⁵²

ESI-MS: calc. 517.3 (M+1); measured 517.4 (M+1); 539.3 (M + Na); 555.3 (M+K).

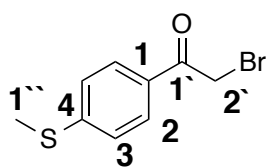
Synthesis of DOTA-M8-4R,4S-Lutetium

DOTA-M8-(4R,4S) (25 mg, 0.05 mmol, 1.0 eq) was dissolved in ammonium acetate (100 mM, aq., 5 mL) and Lutetium chloride hexa hydrate (56 mg, 0.15 mmol, 3.0 eq) the pH was adjusted to 5.5 and the resulting solution heated to 75 °C for 18 hours. A full conversion was obtained by ESI-MS and the excess metal removed by a single use SepPak C18 column on

an peristaltic pump using water to water/methanol (2:8) as eluent.²⁵

ESI-MS (negative mode): calc. 687.2 (M-1); measured 687.2 (M-1).

Synthesis of 2-bromo-1-(4-(methylthio)phenyl)ethan-1-one



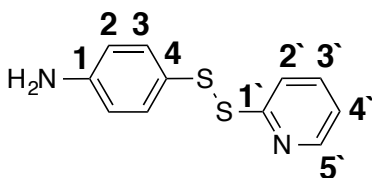
4-(Methylthio)acetophenone (320 g, 1.92 mmol, 1.0 eq) was added to diethylether (20 mL) and a suspension was formed. NBS (356 mg, 2.0 mmol, 1.014 mmol) was added followed by catalytic amounts of ammonium acetate (30.8 mg, 0.4 mmol, 0.2 eq), which rapidly induced the bromine formation. The reaction mixture was stirred at rt. overnight. The reaction mixture was filtered and the resulting precipitate was washed with ethyl acetate (about 20 mL). The resulting organic phase was extracted with water (3 times 10 mL), dried over sodium sulphate and the solvent removed under reduced pressure. The crude mixture was purified by silica gel column chromatography using cyclohexane/ethyl acetate (4:1) as eluent. The desired product (220 mg, 46.7 %) was obtained as white crystals.⁴⁹

TLC: (SiO₂, cyclohexane/ethyl acetate (4:1)): **R_f** = 0.45.

¹H-NMR (400 MHz, 298 K, CDCl₃, δ in ppm): 7.89-7.91 (m, 2H, H₂); 7.28-7.30 (m, 2H, H₃); 4.40 (s, 2H, H_{2'}); 2.54 (s, 3H, H_{1''}).

¹³C-NMR (101 MHz, 298 K, CDCl₃, δ in ppm): 14.7 (1C, C_{1''}); 30.6 (1C, C_{2'}); 125.0 (2C, C₃); 129.3 (2C, C₂); 130.1 (1C, C₁); 147.4 (1C, C₄); 190.4 (1C, C₁).

Synthesis of 4-(pyridin-2-yl)disulfanyl)aniline

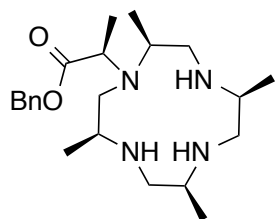


To a solution of 2,2'-dipyridyl disulphide (1.75 g, 7.99 mmol, 1.0 eq) in ethanol/acetic acid (20:1, 53 mL) was added 4-aminothiophenol and stirred for 1 hour at rt.. The solvent was removed under reduced pressure and the remaining solid was redissolved in dichloromethane (70 mL). The mixture was extracted with sodium carbonate (aq. sat., 5 times), dried over sodium sulphate and the solvent removed under reduced pressure. The crude mixture was purified by silica gel column chromatography using chloroform/acetic acid/tetrahydrofuran (95:3:2) as eluent followed by a second column using cyclohexane/acetone 4:1 as eluent. Pure product (40 %) was obtained after recrystallization from hexane.²⁵

¹H NMR (400 MHz, 298 K, CDCl₃, δ in ppm): 8.46 (ddd, ³J_{HH} = 4.8, ⁴J_{HH} = 1.8, ⁵J_{HH} = 1 Hz, 1H, H_{5'}), 7.76 (dt, ³J_{HH} = 8.1, ⁴J_{HH} = 1.1 Hz, 1H, H_{2'}), 7.63 (ddd, ³J_{HH} = 8.1, ³J_{HH} = 7.4, ⁴J_{HH} = 1.8 Hz, 1H, H_{3'}), 7.38 (m, 2H, H₃), 7.07 (ddd, ³J_{HH} = 7.4, ³J_{HH} 4.8, ⁴J_{HH} 1.1 Hz, 1H, H_{4'}), 6.62 – 6.56 (m, 2H, H₂), 3.76 (s, 2H, NH₂).

Synthesis of benzyl (*R*)-2-((2*S*,5*S*,8*S*,11*S*)-2,5,8,11-tetramethyl-1,4,7,10-tetraazacyclododecan-1-yl)propanoate

(M5-cyclen-(*R*)-Bn-lactate)



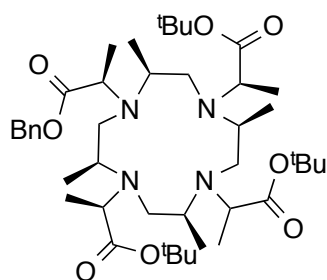
M4-cyclen (416 mg, 1.28 mmol, 1.0 eq) was dissolved in dichloromethane (30 mL) and (*S*)-Bn-lactic acid-OTf (398 mg, 1.28 mmol, 0.7 eq) in dichloromethane (5 mL) was added over 60 min via a dropping funnel. The reaction mixture was stirred for 3 hours before it was quenched with triethylamine (1 mL).

(ESI-MS indicated a high conversion.) The solvent was removed under reduced pressure and the crude mixture purified by silica gel column chromatography chloroform/ethanol/triethylamine 12:4:0.05 to yield 270 mg (54 %) of the title compound as white waxy solid. M4-cyclen and 2 times alkylated by products were isolated.²⁵

ESI-MS: calc. 391.3 (M+1); measured 391.3 (M+1).

Synthesis of di-*tert*-butyl 2,2'-((2*S*,5*S*,8*S*,11*S*)-4-((*R*)-1-(benzyloxy)-1-oxopropan-2-yl)-10-(1-(*tert*-butoxy)-1-oxopropan-2-yl)-2,5,8,11-tetramethyl-1,4,7,10-tetraazacyclododecane-1,7-diyl)(2*R*,2'*R*)-dipropionate

(M8-benzyl-tri-*tert*butyl)

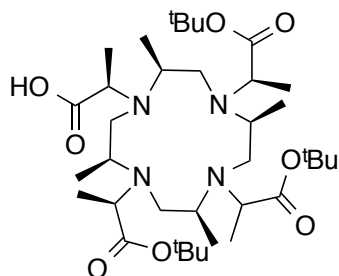


M4-cyclen-(*R*)-Bn-lactate (270mg, 0.691 mmol, 1.0 eq.) was dissolved in acetonitrile (20 mL), (*S*)-*t*Bu-lactic acid-OTf (**24**) (827 mg, 2.83 mmol, 4.1 eq.) in acetonitrile (6 mL) and freshly powdered potassium carbonate (459 mg, 3.32 mmol, 4.8 eq.) was added and the resulting mixture was stirred for 15 hours, until completion of the reaction was indicated by

ESI-MS. After the reaction was finished triethylamine (400 μ L) was added to quench excess reagent. Stirring was continued for additional 10 min before filtered over celite. Removal of volatile materials under reduced pressure yielded a waxy solid that was purified by silica gel column chromatography (chloroform/ethanol, 9:1) and yielded the title compound (300 mg, 56%) as yellowish waxy solid.²⁵

ESI-MS: calc. 775.6 (M+1); measured 775.6 (M+1); 797.6 (M+Na).

Synthesis of (2R)-2-((2S,5S,8S,11S)-4,10-bis((R)-1-(tert-butoxy)-1-oxopropan-2-yl)-7-(1-(tert-butoxy)-1-oxopropan-2-yl)-2,5,8,11-tetramethyl-1,4,7,10-tetraazacyclododecan-1-yl)propanoic acid

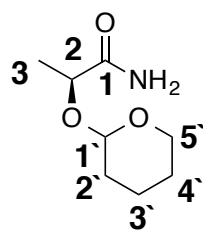


(M8-benzyl-tri-*tert*butyl) (100 mg, 0.129 mmol, 1.0 eq) was dissolved in methanol (5mL) and Pd/C (18 mg) as hydrogenation catalyst was added. The reaction mixture was stirred under 8 bars H₂-pressure in an autoclave for 2 hours. The mixture was filtered over celite and volatile material was removed under reduced pressure. The title

compound was obtained as waxy yellow solid in 80 % yield.²⁵

ESI-MS: calc. 685.5 (M+1); measured 685.5 (M+1).

Synthesis of (2S)-2-((tetrahydro-2H-pyran-2-yl)oxy)propanamide g2



Lactamide (1.0 g, 11.2 mmol, 1.0 eq) was dissolved in dichloromethane (20 mL). pyridinium para toluene sulfonate (PPTS, 282mg 1.12 mmol, 0.1 eq) and 3,4-dihydro-2H-pyran (1.13 mL, 12.3 mmol, 1.1 eq) were added and stirred for 5 hours at rt. The solvent was removed under reduced pressure and the crude mixture purified

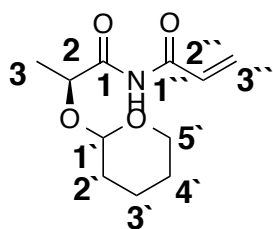
by silica gel column chromatography using cyclohexane/ethyl acetate (2:10 → 0:1). The title compound was obtained as colourless oil in 74% (1.45 g) yield as mixture of the two diastereoisomers. After a few days' parts of the oil crystallized. After isolation the NMR of one single isomer could be recorded.⁶⁸

TLC: (SiO₂, cyclohexane/ethyl acetate (1:5)): R_f = 0.21 and 0.14 for the two diastereoisomers.

NMR data of the crystallized diastereoisomer:

¹H NMR (400 MHz, 298 K, CDCl₃, δ in ppm): 6.74 ("b"s, 1H, NH); 5.40 ("b"s, 1H, NH, 4.62-4.70 (m, 1H, H1'); 4.23 (q, ³J_{HH} = 6.9 Hz, 1H, H2); 3.82-3.91 (m, 1H, H5'); 3.45-3.58 (m, 1H, H5'); 1.77-1.87 (m, 2H, H2'); 1.51-1.62 (m, 4H, H3',H4'); 1.41 (d, ³J_{HH} = 6.9 Hz, 3H, H3).

¹³C NMR (101 MHz, 298 K, CDCl₃, δ in ppm): 17.7 (1C, C3); 20.4 (1C, C3'); 25.3 (1C, C4'); 31.1 (1C, C2'); 64.0 (1C, C5'); 73.1 (1C, C2); 98.3 (1C, C3); 176.2 (1C, C1).

Synthesis of *N*-((2*S*)-2-((tetrahydro-2*H*-pyran-2-yl)oxy)propanoyl)acrylamide **g3**

To a stirring suspension of NaH (98 mg, 2.44 mmol, 1.3 eq, 60% in mineral oil) in THF (25 mL) at rt. was added (2*S*)-2-((tetrahydro-2*H*-pyran-2-yl)oxy)propanamide (325 mg, 1.88 mmol, 1.0 eq) in THF (5 mL). Vigorous bubbling began near the end of the addition, and the reaction mixture became thick and opaque. After stirring for 1 h, a solution of acryloyl chloride (175 μ L, 2.06 mmol, 1.1 eq) and THF (5 mL) was added over 2 min. The reaction mixture was stirred at rt. for 3.5 h, then H₂O (50 mL) was added and the layers were separated. The aqueous layer was extracted with EtOAc (3 x 20 mL). The organic layers were combined, washed with brine (25 mL), dried over Na₂SO₄, filtered and concentrated under reduced pressure. Purification was performed by silica gel column chromatography using cyclohexane/ethyl acetate (4:1) as eluent to yield a yellowish oil (50mg, 12%). (The desired product was used for a tagging test using HCAII as protein. The desired linker could be attached to the protein overnight in about 90%.)

TLC: (SiO₂, cyclohexane/ethyl acetate (4:1)): **R_f** = 0.35; 0.17.

ESI-MS: calc. 228.1 (M+1); measured 250.1 (M+Na)

Diastereomer 1: **¹H NMR** (600 MHz, 298 K, DMSO-d₆, δ in ppm): 10.75 ("b"s, 1H, NH); 6.67 (dd, ²J_{HH} = 17.0 Hz, ³J_{HH} = 10.3 Hz, 1H, H3''); 6.33 (dd, ²J_{HH} = 17.0, ³J_{HH} = 1.5 Hz, 1H, H3''); 5.89 (dd, ³J_{HH} = 10.3 Hz, ³J_{HH} = 1.5 Hz, 1H, H2''); 4.62 (q, ³J_{HH} = 6.9 Hz, 1H, H2); 4.45-4.56 (m, 1H, H1'); 3.71-3.76 (m, 1H, H5'); 3.43-3.47 (m, 1H, H5'); 1.68-1.75 (m, 1H, H3'); 1.61-1.68 (m, 1H, H2'); 1.46-1.55 (m, 1H, H2'); 1.43-1.52 (m, 1H, H3'); 1.40-1.50 (m, 2H, H4'); 1.31 (d, ³J_{HH} = 6.9 Hz, 3H, H3).

Diastereomer 2: **¹H NMR** (600 MHz, 298 K, DMSO-d₆, δ in ppm): 10.51 ("b"s, 1H, NH); 6.25 (dd, ²J_{HH} = 17.2 Hz, ³J_{HH} = 1.7 Hz, 1H, H3''); 6.08 (dd, ³J_{HH} = 10.6, ³J_{HH} = 1.7 Hz, 1H, H2''); 5.87 (dd, ²J_{HH} = 17.2 Hz, ³J_{HH} = 10.6 Hz, 1H, H3''); 4.65-4.69 (m, 1H, H1'); 4.42 (q, ³J_{HH} = 6.5 Hz, 1H, H2); 3.72-3.78 (m, 1H, H5'); 3.33-3.37 (m, 1H, H5'); 1.68-1.75 (m, 1H, H3'); 1.61-1.68 (m, 1H, H2'); 1.46-1.55 (m, 1H, H2'); 1.43-1.52 (m, 1H, H3'); 1.40-1.50 (m, 2H, H4'); 1.28 (d, ³J_{HH} = 6.5 Hz, 3H, H3).

Diastereomer 1: **¹³C NMR** (151 MHz, 298 K, DMSO-d₆, δ in ppm): 18.25 (1C, C3); 18.77 (1C, C3'); 24.8 (1C, C4'); 30.1 (1C, C2'); 61.5 (1C, C5'); 71.1 (1C, C2); 130.3 (2C, C2'', C3''); 164.4 (1C, C1''); 173.7 (1C, C1).

Diastereomer 2: ^{13}C NMR (151 MHz, 298 K, DMSO- d_6 , δ in ppm): 17.85 (1C, C3); 18.77 (1C, C3'); 24.8 (1C, C4'); 30.1 (1C, C2''); 62.0 (1C, C5''); 73.7 (1C, C2); 129.3 (1C, C2''); 130.4 (1C, C3''); 166.7 (1C, C1''); 173.44 (1C, C1).

A.9 References

1. Kendrew, J. C. *et al.* A Three-Dimensional Model of the Myoglobin Molecule Obtained by X-Ray Analysis. *Nature* **181**, 662–666 (1958).
2. Wüthrich, K. The way to NMR structures of proteins. *Nat. Struct. Mol. Biol.* **8**, 923–925 (2001).
3. Freedberg, D. I. & Selenko, P. Live Cell NMR. *Annu. Rev. Biophys.* **43**, 171–192 (2014).
4. Razzaghi, S. *et al.* EPR Relaxation-Enhancement-Based Distance Measurements on Orthogonally Spin-Labeled T4-Lysozyme. *ChemBioChem* **14**, 1883–1890 (2013).
5. Lueders, P. *et al.* Distance determination from dysprosium induced relaxation enhancement: a case study on membrane-inserted WALP23 polypeptides. *Mol. Phys.* **111**, 2824–2833 (2013).
6. Joseph, B., Korkhov, V. M., Yulikov, M., Jeschke, G. & Bordignon, E. Conformational Cycle of the Vitamin B12 ABC Importer in Liposomes Detected by Double Electron-Electron Resonance (DEER). *J. Biol. Chem.* **289**, 3176–3185 (2014).
7. Sun, Y., Hays, N. M., Periasamy, A., Davidson, M. W. & Day, R. N. in *Methods in Enzymology* (ed. P. Michael conn) **Volume 504**, 371–391 (Academic Press, 2012).
8. Bertini, I., Luchinat, C. & Parigi, G. Magnetic susceptibility in paramagnetic NMR. *Prog. Nucl. Magn. Reson. Spectrosc.* **40**, 249–273 (2002).
9. Mar, G. N. L. Pseudocontact Shifts in Paramagnetic Complexes. *J. Chem. Phys.* **43**, 1085–1085 (1965).
10. McConnell, H. M. & Robertson, R. E. Isotropic Nuclear Resonance Shifts. *J. Chem. Phys.* **29**, 1361–1365 (1958).
11. Kurland, R. J. & McGarvey, B. R. Isotropic NMR shifts in transition metal complexes: The calculation of the fermi contact and pseudocontact terms. *J. Magn. Reson.* **1969** **2**, 286–301 (1970).

12. Mayo, B. C. Lanthanide shift reagents in nuclear magnetic resonance spectroscopy. *Chem. Soc. Rev.* **2**, 49–74 (1973).
13. Hinckley, C. C. Paramagnetic shifts in solutions of cholesterol and the dipyridine adduct of trisdipivalomethanatoeuropium(III). A shift reagent. *J. Am. Chem. Soc.* **91**, 5160–5162 (1969).
14. Sanders, J. K. M. & Williams, D. H. A shift reagent for use in nuclear magnetic resonance spectroscopy. A first-order spectrum of n-hexanol. *J. Chem. Soc. Chem. Commun.* 422–423 (1970). doi:10.1039/C29700000422
15. Barry, C. D., North, A. C. T., Glasel, J. A., Williams, R. J. P. & Xavier, A. V. Quantitative Determination of Mononucleotide Conformations in Solution using Lanthanide Ion Shift and Broadening NMR Probes. *Nature* **232**, 236–245 (1971).
16. Bertini, I. & Luchinat, C. New applications of paramagnetic NMR in chemical biology. *Curr. Opin. Chem. Biol.* **3**, 145–151 (1999).
17. Tolman, J. R., Flanagan, J. M., Kennedy, M. A. & Prestegard, J. H. Nuclear magnetic dipole interactions in field-oriented proteins: information for structure determination in solution. *Proc. Natl. Acad. Sci.* **92**, 9279–9283 (1995).
18. Tjandra, N. & Bax, A. Direct Measurement of Distances and Angles in Biomolecules by NMR in a Dilute Liquid Crystalline Medium. *Science* **278**, 1111–1114 (1997).
19. Gaponenko, V., Dvoretzky, A., Walsby, C., Hoffman, B. M. & Rosevear, P. R. Calculation of z-Coordinates and Orientational Restraints Using a Metal Binding Tag†. *Biochemistry (Mosc.)* **39**, 15217–15224 (2000).
20. Ma, C. & Opella, S. J. Lanthanide Ions Bind Specifically to an Added ‘EF-Hand’ and Orient a Membrane Protein in Micelles for Solution NMR Spectroscopy. *J. Magn. Reson.* **146**, 381–384 (2000).
21. Wöhnert, J., Franz, K. J., Nitz, M., Imperiali, B. & Schwalbe, H. Protein Alignment by a Coexpressed Lanthanide-Binding Tag for the Measurement of Residual Dipolar Couplings. *J. Am. Chem. Soc.* **125**, 13338–13339 (2003).
22. Martin, L. J. *et al.* Double-Lanthanide-Binding Tags: Design, Photophysical Properties, and NMR Applications. *J. Am. Chem. Soc.* **129**, 7106–7113 (2007).
23. Su, X.-C., Huber, T., Dixon, N. E. & Otting, G. Site-Specific Labelling of Proteins with a Rigid Lanthanide-Binding Tag. *ChemBioChem* **7**, 1599–1604 (2006).
24. Su, X.-C., McAndrew, K., Huber, T. & Otting, G. Lanthanide-Binding Peptides for NMR Measurements of Residual Dipolar Couplings and Paramagnetic Effects

- from Multiple Angles. *J. Am. Chem. Soc.* **130**, 1681–1687 (2008).
25. Häussinger, D., Huang, J. & Grzesiek, S. DOTA-M8: An Extremely Rigid, High-Affinity Lanthanide Chelating Tag for PCS NMR Spectroscopy. *J. Am. Chem. Soc.* **131**, 14761–14767 (2009).
26. Gaponenko, V. *et al.* Improving the Accuracy of NMR Structures of Large Proteins Using Pseudocontact Shifts as Long-Range Restraints. *J. Biomol. NMR* **28**, 205–212 (2004).
27. Gaponenko, V., Altieri, A. S., Li, J. & Byrd, R. A. Breaking symmetry in the structure determination of (large) symmetric protein dimers. *J. Biomol. NMR* **24**, 143–148 (2002).
28. Ikegami, T. *et al.* Novel Techniques for Weak Alignment of Proteins in Solution Using Chemical Tags Coordinating Lanthanide Ions. *J. Biomol. NMR* **29**, 339–349 (2004).
29. Rodriguez-Castañeda, F., Haberz, P., Leonov, A. & Griesinger, C. Paramagnetic tagging of diamagnetic proteins for solution NMR. *Magn. Reson. Chem.* **44**, S10–S16 (2006).
30. Prudêncio, M. *et al.* A Caged Lanthanide Complex as a Paramagnetic Shift Agent for Protein NMR. *Chem. – Eur. J.* **10**, 3252–3260 (2004).
31. Vlasie, M. D. *et al.* Long-Range-Distance NMR Effects in a Protein Labeled with a Lanthanide–DOTA Chelate. *Chem. – Eur. J.* **13**, 1715–1723 (2007).
32. Keizers, P. H. J., Desreux, J. F., Overhand, M. & Ubbink, M. Increased Paramagnetic Effect of a Lanthanide Protein Probe by Two-Point Attachment. *J. Am. Chem. Soc.* **129**, 9292–9293 (2007).
33. Housecroft, C. E. & Sharpe, A. G. *Inorganic Chemistry*. (Prentice Hall, 2007).
34. Bleaney, B. Nuclear magnetic resonance shifts in solution due to lanthanide ions. *J. Magn. Reson.* 1969 **8**, 91–100 (1972).
35. Bertini, I., Janik, M. B. L., Lee, Y.-M., Luchinat, C. & Rosato, A. Magnetic Susceptibility Tensor Anisotropies for a Lanthanide Ion Series in a Fixed Protein Matrix. *J. Am. Chem. Soc.* **123**, 4181–4188 (2001).
36. Otting, G. Prospects for lanthanides in structural biology by NMR. *J. Biomol. NMR* **42**, 1–9 (2008).
37. G. Otting ANU. at <<http://rsc.anu.edu.au/~go/>>
38. Current Projects. at <<http://rsc.anu.edu.au/~go/projects.html>>
39. Feeney, J., Birdsall, B., Bradbury, A. F., Biekofsky, R. R. & Bayley, P. M.

Calmodulin tagging provides a general method of using lanthanide induced magnetic field orientation to observe residual dipolar couplings in proteins in solution. *J. Biomol. NMR* **21**, 41–48 (2001).

40. Franklin, S. J. & Raymond, K. N. Solution Structure and Dynamics of Lanthanide Complexes of the Macrocyclic Polyamino Carboxylate DTPA-dien. NMR Study and Crystal Structures of the Lanthanum(III) and Europium(III) Complexes. *Inorg. Chem.* **33**, 5794–5804 (1994).

41. Leonov, A., Voigt, B., Rodriguez-Castañeda, F., Sakhaii, P. & Griesinger, C. Convenient Synthesis of Multifunctional EDTA-Based Chiral Metal Chelates Substituted with an S-Mesylcysteine. *Chem. – Eur. J.* **11**, 3342–3348 (2005).

42. Port, M. *et al.* Efficiency, thermodynamic and kinetic stability of marketed gadolinium chelates and their possible clinical consequences: a critical review. *BioMetals* **21**, 469–490 (2008).

43. Otting, G. Protein NMR Using Paramagnetic Ions. *Annu. Rev. Biophys.* **39**, 387–405 (2010).

44. Anet, F. A. L. & Bourn, A. J. R. Nuclear Magnetic Resonance Spectral Assignments from Nuclear Overhauser Effects¹. *J. Am. Chem. Soc.* **87**, 5250–5251 (1965).

45. Jeener, J., Meier, B. H., Bachmann, P. & Ernst, R. R. Investigation of exchange processes by two-dimensional NMR spectroscopy. *J. Chem. Phys.* **71**, 4546–4553 (1979).

46. Loh, C. T. *et al.* Lanthanide Tags for Site-Specific Ligation to an Unnatural Amino Acid and Generation of Pseudocontact Shifts in Proteins. *Bioconjug. Chem.* **24**, 260–268 (2013).

47. Schmidt, T. & Kirschning, A. Total Synthesis of Carolacton, a Highly Potent Biofilm Inhibitor. *Angew. Chem. Int. Ed.* **51**, 1063–1066 (2012).

48. Decicco, C. P., Nelson, D. J., Corbett, R. L. & Dreabitt, J. C. Asymmetric Synthesis of 2,3-Disubstituted Succinates via Chiral Oxazolidinone Controlled Displacement of α -Trifluoromethanesulfonate Substituted Esters. *J. Org. Chem.* **60**, 4782–4785 (1995).

49. Tanemura, K., Suzuki, T., Nishida, Y., Satsumabayashi, K. & Horaguchi, T. A mild and efficient procedure for α -bromination of ketones using N-bromosuccinimide catalysed by ammonium acetate. *Chem. Commun.* 470–471 (2004).

doi:10.1039/B315340A

50. Mekonnen, B., Crank, G. & Craig, D. A new and facile synthesis of imidazo[2,1- *b*]oxazoles. *J. Heterocycl. Chem.* **34**, 589–599 (1997).
51. Vasalatiy, O., Gerard, R. D., Zhao, P., Sun, X. & Sherry, A. D. Labeling of Adenovirus Particles with PARACEST Agents. *Bioconjug. Chem.* **19**, 598–606 (2008).
52. Wuts, P. G. M. & Greene, T. W. *Greene's Protective Groups in Organic Synthesis*. (John Wiley & Sons, 2006).
53. Podgoršek, A., Stavber, S., Zupan, M. & Iskra, J. Bromination of ketones with H₂O₂–HBr 'on water'. *Green Chem.* **9**, 1212–1218 (2007).
54. Utsukihara, T., Nakamura, H., Watanabe, M. & Akira Horiuchi, C. Microwave-assisted synthesis of α -hydroxy ketone and α -diketone and pyrazine derivatives from α -halo and α,α' -dibromo ketone. *Tetrahedron Lett.* **47**, 9359–9364 (2006).
55. Reaxys Literature Service. at <<http://sc.elsevier.com/xflink?aulast=Srinivasan&title=Journal%20of%20the%20Chemical%20Society%2C%20Perkin%20Transactions%202%3A%20%20Physical%20Organic%20Chemistry%20%281972-1999%29&volume=&issue=&spage=17&date=1985&coden=JCPKBH&doi=&issn=0300-9580>>
56. Huang, Z. & Knaus, E. E. O₂-(N-Hydroxy(methoxy)-2-ethanesulfonamido) Protected Diazen-1-ium-1,2-diolates: Nitric Oxide Release via a Base-Induced β -Elimination Cleavage. *Org. Lett.* **13**, 1178–1181 (2011).
57. Allen, C., Allen, C. F. H. & Humphlett, W. J. THE THERMAL REVERSIBILITY OF THE MICHAEL REACTION: V. THE EFFECT OF THE STRUCTURE OF CERTAIN THIOL ADDUCTS ON CLEAVAGE. *Can. J. Chem.* **44**, 2315–2321 (1966).
58. Li, L. *et al.* Vinyl Sulfone Bifunctional Derivatives of DOTA Allow Sulfhydryl- or Amino-Directed Coupling to Antibodies. Conjugates Retain Immunoreactivity and Have Similar Biodistributions. *Bioconjug. Chem.* **13**, 110–115 (2002).
59. Morikawa, T. *et al.* Stereoselective radical additions of γ -oxy- α,β -unsaturated ester derivatives; 1,2-asymmetric induction in acyclic and cyclisation systems. *J. Chem. Soc. [Perkin 1]* 271–281 (1995). doi:10.1039/P19950000271
60. Asakawa, M. *et al.* Constitutionally Asymmetric and Chiral [2]Pseudorotaxanes. *J. Am. Chem. Soc.* **120**, 920–931 (1998).
61. Halimehjani, A. Z., Jalali, A., Khalesi, M., Ashouri, A. & Marjani, K. Catalyst-Free Efficient Regioselective Ring Opening of Oxiranes with Thioacids in Water.

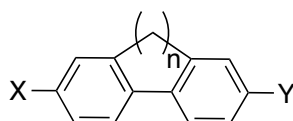
Synth. Commun. **41**, 1638–1643 (2011).

62. Avetisyan, A. A., Alvandzhyan, A. G. & Avetisyan, K. S. New syntheses on the basis of 4-hydroxy-2H-chromen-2-ones. *Russ. J. Org. Chem.* **45**, 1086–1090 (2009).
63. Michaelis, S. & Blechert, S. Total Synthesis of (+)-Phomopsolide C by Ring-Size Selective Ring-Closing Metathesis/Cross-Metathesis. *Org. Lett.* **7**, 5513–5516 (2005).
64. Ushakov, D. B. *et al.* Total Synthesis and Biological Evaluation of (–)-9-Deoxy-englerin A. *Org. Lett.* **13**, 2090–2093 (2011).
65. Baughman, T. W., Sworen, J. C. & Wagener, K. B. The facile preparation of alkenyl metathesis synthons. *Tetrahedron* **60**, 10943–10948 (2004).
66. Carocci, A. *et al.* Design, synthesis, and pharmacological effects of structurally simple ligands for MT1 and MT2 melatonin receptors. *Bioorg. Med. Chem.* **18**, 6496–6511 (2010).
67. Denmark, S. E. & Stavenger, R. A. The Chemistry of Trichlorosilyl Enolates. Aldol Addition Reactions of Methyl Ketones. *J. Am. Chem. Soc.* **122**, 8837–8847 (2000).
68. Miyashita, M., Yoshikoshi, A. & Grieco, P. A. Pyridinium p-toluenesulfonate. A mild and efficient catalyst for the tetrahydropyranylation of alcohols. *J. Org. Chem.* **42**, 3772–3774 (1977).

B) Thermodynamic studies of 4,4' substituted torsion angle restricted 2,2' alkyl-bridged biphenyl cyclophanes

B.1 Research goal

A series of 4 and 4' di substituted 2,2'-alkyl bridged biphenyl cyclophanes was systematically analysed. The atropisomerization of such molecules is of high interest in many different fields of material sciences and more and more also in catalysis.¹⁻³ Applications in OLEDs,⁴ nonlinear optics,⁵ molecular motors⁶ and many more have been presented recently. Therefore, different analytical methods were used to gain insights into the thermodynamics of such biphenyls. Propyl-bridged biphenyls were investigated using dynamic NMR spectroscopy (dNMR) whereas butyl-bridged biphenyls were analysed with dynamic high pressure liquid chromatography (dhplc) on a chiral column. Theoretical calculations for both classes were performed to get information about the transition state of such atropisomerization processes as different mechanisms were published earlier. The results of this work are published^{7,8} and will be discussed in detail in the following section. The main focus will be on the dynamic NMR measurements.



Structure B-1: 4,4'-disubstituted 2,2'-alkyl bridged biphenyls^{7,8} with $n = 2,3,4$.

The above-mentioned tasks of the project were investigated in collaboration of three different research groups. Dr. J. Rotzler and Prof. Dr. M. Mayor initiated the project. Dr. J. Rotzler, M. Gantenbein and Dr. D. Vonlanthen synthesized all molecules in the group of Prof. Dr. M. Mayor. Angela Bihlmeier performed theoretical calculations in

the group of Prof. Dr. W. Klopper at Karlsruhe Institute of Technology (KIT). NMR measurements and line shape analysis were performed in the group of PD. Dr. D. Häußinger by myself.

B.2 Introduction

B.2.1 Dynamic NMR Spectroscopy (dNMR)

Most processes in biology and chemistry take place in solution state. Many of these molecules have a specific functionality. The origin of the functionality is in many cases a dynamic process. To understand the function of such molecules, special spectroscopic methods that can deal with dynamics are necessary. Spectroscopic methods like X-ray crystallography or mass spectrometry miss such dynamic processes as they deliver a static picture of the molecules. Investigation of such processes is in most cases challenging. Only a few spectroscopic methods like react IR, UV-Vis^{9,10}, HPLC¹¹⁻¹⁴, Polarimetry¹⁵⁻¹⁷ and NMR^{18,18-29} are suitable for this investigation. Each method is limited to a different range of rate constants. For NMR spectroscopy the range of rate constants is dependent on the chemical shift difference of the interchanging spins and the temperature range. A standard equipped system has a temperature range of -80 °C to +150 °C, with special equipment even lower or higher temperatures can be reached (in this cases often the solvent is the limiting factor). This permits the investigation of a wide variety of exchange processes in different solvents. The chemical shift difference ($\Delta\nu$ in Hz) delivers in general the life time (τ) (according to Equation B-1) of the two different spin states²⁰ directly.

$$\tau = \frac{\sqrt{2}}{2\pi\Delta\nu} [\text{s}]$$

Equation B-1: Calculation of the life time. τ = life time, $\Delta\nu$ = chemical shift difference.

The chemical shift difference is a result of different chemical environments and/or different magnetic shielding. The lifetime is directly correlated to the rate constant $r = \frac{1}{\tau}$ [Hz]. From these two equations it becomes obvious that, if the exchange is much faster than the chemical shift difference, then a averaged signal is measured on the other hand if the exchange is much slower two individual signals are obtained. Between this two extreme the line shape of the signal becomes broad. At the point

where the signal shows a plateau, the coalescence is reached (Figure B-1). It is important to mention that, if the two states are populated equally, the resulting chemical shift in the fast exchange is centred in the middle of the two original peaks, and if the two states are populated differently, the resulting chemical shift in the fast exchange is a weighted average.

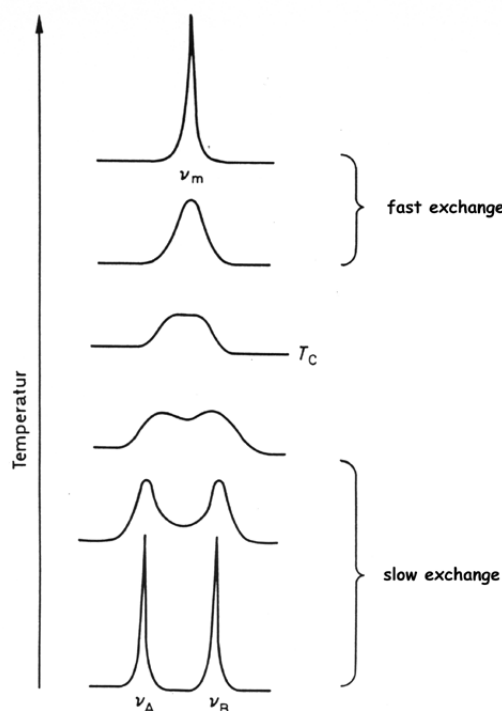


Figure B-1: Temperature dependent NMR spectra of equally populated uncoupled interchanging spins.³⁰

The activation energy (ΔG^\ddagger) can be estimated from the coalescence temperature T_c and the chemical shift difference in the slow exchange using Equation B-2.

$$\Delta G^\ddagger = RT_c \ln \frac{RT_c \sqrt[2]{2}}{\pi N_A h |\nu_A - \nu_B|}$$

$$\Delta G^\ddagger = 0.0191 * T_c (9.97 + \log \left(\frac{T_c}{\Delta \nu} \right))$$

Equation B-2: Calculation of the free activation energy from $^1\text{H-NMR}$ spectra. ΔG^\ddagger = Gibbs free activation energy, T_c = coalescence temperature, $\Delta \nu$ = chemical shift difference of the two spins in slow exchange.
7,8,19,31,32

The calculation of the Gibbs free activation energy from T_c and $\Delta \nu$ delivers only thermodynamic activation data. Besides the thermodynamic data also kinetic data are required in order to study dynamic processes in detail. To gain further insights, line shape analysis is necessary. For equally populated and uncoupled systems the Equation B-3 can estimate the rate constant at the coalescence temperature.³³

$$k_c = \frac{\pi}{\sqrt{2}} \Delta\nu_c$$

Equation B-3: Approximation of the rate constant for equally populated and uncoupled systems. k_c = rate constant at the coalescence point, $\Delta\nu_c$ = half width of the signal at the coalescence temperature.

For calculation of equally populated and coupled systems the approximation is given by Equation B-4.

$$k_c = \frac{\pi}{\sqrt{2}} (\Delta\nu^2 + 6J^2)^{1/2}$$

Equation B-4: Approximation of the rate constant for equally populated but coupled systems. k_c = rate constant at the coalescence point, $\Delta\nu$ = chemical shift difference in the slow exchange and J = coupling constant in the slow exchange.^{26,33–35}

A general approximation for the calculation of rate constants is given by the following expression in Equation B-5.^{26,34,35}

$$k = \frac{\pi\Delta\nu^2}{2(\omega - \omega_0)}$$

Equation B-5: General approximation for the rate constant determined by NMR. k = rate constant at a given temperature, $\Delta\nu$ = chemical shift difference at this specific temperature, ω = line width at this temperature, ω_0 = linewidth in the fast exchange ($k = \infty$).

More precise rate constants are available when computer based programs can be used to determine rate constants. An example for such a program is dNMR from Bruker[®], where the spin systems can be fitted to the original spectra and coupling constants can be included. Eyring plots can then convert the rate constants in combination with the measured temperatures to deliver the thermodynamic data for activation enthalpy ΔH^\ddagger and the activation entropy ΔS^\ddagger using Equation B-6.

$$\Delta H^\ddagger = -m R$$

$$y(x = 0) = \ln\left(\frac{k_B}{h}\right) + \left(\frac{\Delta S}{R}\right)$$

Equation B-6: ΔH^\ddagger = activation enthalpy, m = slope of the Eyring plot, R = universal Gas constant = 8.3144 [kJ/(mol K)], $y(x = 0)$ = intercept of the Eyring plot, k_B = Boltzmann constant = 1.38×10^{-23} [J/K], h = Plank constant = 6.626×10^{-23} [J s].

B.2.2 Historical development of dNMR

First investigations were performed on dimethylformamide^{22–25,36,37} (DMF) where the two methyl groups are diastereotopic at ambient temperature due to the partial double bond.

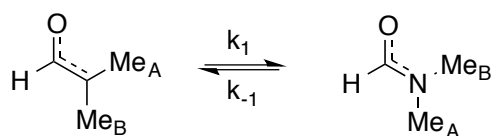
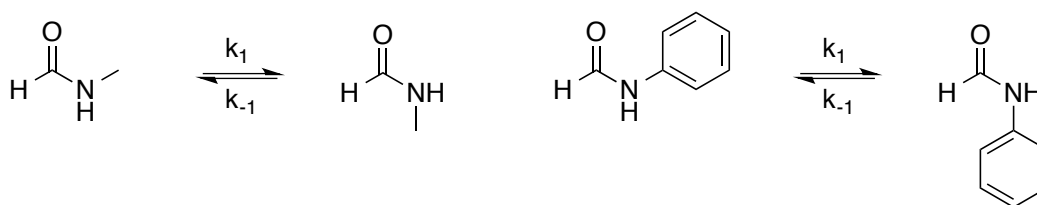


Figure B-2: Isomerization of *N,N*-dimethylformamide.

The advantage of this system compared to others is the fact that a 1:1 ratio of the two states was obtained. Heating the sample led to a signal broadening and finally one averaged signal was obtained at higher temperatures. With the development of new mathematical methods the investigation of unequally populated amides became possible and systems like *N*-Methylformamide or *N*-Phenylformamide (Structure B-2) could be investigated.³⁸

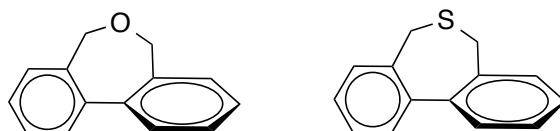


Structure B-2: Isomerization of *N*-methylformamide and *N*-phenylformamide

The limit of the method is reached when the chemical shift difference of the two states is too small to be resolved or the exchange rates of the system are too fast to reach the coalescence. On the other hand systems with high activation energy reach the upper limit when no further heating of the NMR-system is possible. To overcome the low temperature limit, lanthanide shift reagents (LSR) can be used to enlarge the chemical shift difference of the exchanging spins.^{39–43} Titration experiments are required to allow the calculation of the activation parameters at zero concentration. The activation energies ΔG^\ddagger have to be calculated for each concentration of LSR. The resulting pairs of concentrations and activation energies are plotted and a regression towards zero concentration performed. It is worth to mention that a fast exchange in the substrate/LSR complex is necessary. A slow exchange would lead to two independent species. The resulting LSR-substrate complex will deliver one set of activation parameters, independent of the concentration. To increase the high temperature range high pressures can be applied, to lower the coalescence temperature. Also in this case titration experiments with different pressures are required to allow back calculation. High-pressure experiments are limited to substances with a negative volume of activation. High pressure favours in this case the transition state leading to decreased activation energies.

B.2.3 Biphenyls in dynamic NMR

The atropisomerization process of different biphenyl systems has been studied by dNMR during the past 50 years. Atropisomerization is a special case of isomerization of axial chiral molecules. Hindered rotation around a single bond leads to two stable isomers. In 1964 Kurland et al.²⁰ investigated 2,7-dihydrodibenz[*c,e*]oxepin **L1a** and 2,7-dihydrodibenz[*c,e*]thiepin **L2c**. They showed that the activation energy for the atropisomerization of oxepins is much lower than for thiepins (Table B-1, Table B-2).



Structure B-3: The first bridged biphenyls investigated by dNMR, Oxepin 1a (left structure) and Thiepin 2c (right structure).²⁰

Oki²¹ studied a series of oxepins and ethyl bridged biphenyls to investigate the steric effect of *ortho* substituents of biphenyl molecules in detail. Measurements of the unfunctionalized oxepin were in good agreement with data presented by Kurland²⁰ earlier. They demonstrated that methyl substituents have more or less the same effect on the rotation barrier, as a second methyl-O-methyl bridge. Whereas an ethyl bridge only slightly increases the activation energy compared to the unfunctionalized oxepin. An *ortho*-nitro substituent also increased the activation barrier. It was suggested that the steric effect was affected by hydrogen bonding (Figure B-3) which was investigated for other molecules in more detail.^{34,35}

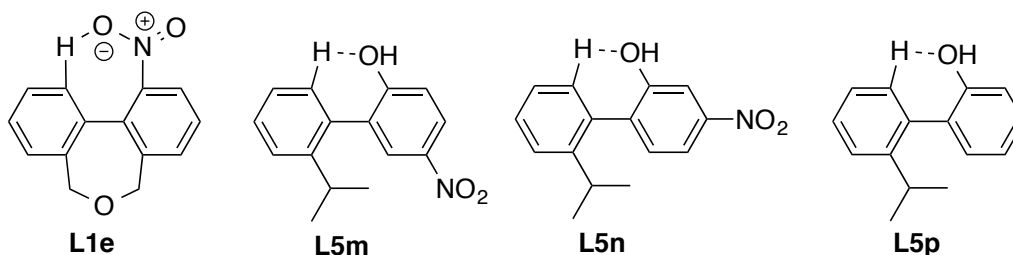


Figure B-3: Hydrogen bonding obtained in different biphenyl systems.

The chemical shift difference of the resulting two atropisomers of ethyl-bridged biphenyls was rather small as long as no other *ortho* substituent was introduced. The activation barrier of this class of biphenyls was therefore not suitable for dNMR experiments. Surprisingly the ethyl-bridged-6,6'-Me,Me substituted molecules showed an even higher activation barrier than their oxepin analogues. Sutherland et al.²³ published a series of CH₂XCH₂ bridged molecules where X = SO₂, S, C=NOH, C(CO₂Et)₂, NMe₂Br, CO, NH and CH₂ (**L2c**, **L2e**, **L3a**, **L3b**, **L3c**, **L3d**). The results

for the thiepin was comparable to earlier published data. For the CO and NH bridged biphenyls no coalescence was reached. The activation energy calculated for SO₂ bridged biphenyl was higher than for thiepins whereas the sterically demanding molecules **L3c** and **L3d** showed decreased activation energies. They showed that fine-tuning of the activation parameters was possible by the variation of the heteroatom in the middle of the bridge. The sterically demanding structure **L1d** showed an increased activation barrier whereas for the ester **L1j** no coalescence could be determined. For **L3e** and **L3f** the activation energy was higher due to the enlarged conjugation, leading to a more hindered rotation. In 1968 Oki et al.³⁴ demonstrated that hydrogen bonding could stabilize oxepin biphenyls by about 4 kJ/mol (**L1f**). To confirm this finding also the methoxy compound (**L1g**) was measured in chloroform and DMSO and the activation parameters calculated. In this case a much smaller effect was obtained. The same effect was also measured for *ortho* substituted biphenyls **L5l-L5p**.³⁵ It became obvious that electron-withdrawing groups (EWG) can increase the stability of the hydrogen bonding when resonance stabilization is present. Nevertheless, the effect was quite small and close to the experimental error but a systematic shift for all compounds is obtained. Oki³³ et al. extended the series of thiepins to 4,4'-di-substituted ones. The di-fluorine **L2d** showed similar properties as the di-hydrogen **L2c**, which is in good agreement with the small electronic effect suggested for fluorine. The push-pull system **L2a** and the push-push system **L2b** showed decreased activation energy compared to the di-hydrogen **L2c**. This effect can be easily understood for the push-pull system where a planar transition state seems to be favoured due to conjugation. For the push-push system resonance seems to be possible but also an out of plane bending was suggested. Oki²⁶ et al. were able to show that 4,4' di-substitution can be used to fine-tune the activation parameters of a variety of biphenyls **L5a-L5k**.

Table B-1: Series of Oxepin molecules investigated by dynamic NMR spectroscopy showing the influence of substituents on the activation barrier.

Compound	Structure	T_c/K	ΔG^\ddagger (kJ/mol)	Solvent
L1a ^{20,21}		189	38.5 ± 4.2	Carbon disulfide
			40.2 ± 2.9	
L1d ²³		282	55.7	pyridine
L1e ²¹		---	69.1 ± 2.9	
L1f ³⁴		321	70.8 ± 4.2	chloroform
		293	66.6 ± 5.0	dimethylsulfoxide
L1g ³⁴		319	70.8 ± 4.2	chloroform
		321	72.0 ± 5.9	dimethylsulfoxide
L1h ²¹		---	83.7	
L1i ²¹		---	84.6	
L1j ²³		---	---	too fast

Table B-2: Series of thiepin molecules showing the influence of *para* substituents on the activation barrier of rotation about the c-c single bond.

Compound	Structure	T_c/K	ΔG^\ddagger (kJ/mol)	Solvent
L2a ³³		293 ± 5	61.1 ± 1.3	
L2b ³³		297 ± 2	63.6 ± 1.3	
L2c ^{20,23,34}		315	67.4 ± 1.3	chloroform pyridine
			67	
L2d		311 ± 2	67.4 ± 1.3	

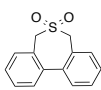
Compound	Structure	T_c/K	ΔG^\ddagger (kJ/mol)	solvent
L2e ²³		360.5	76.2	

Table B-3: Series of propyl bridged molecules showing the influence of hybridisation on the activation barrier.

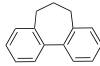
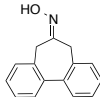
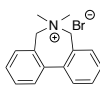
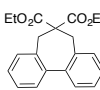
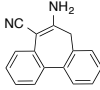
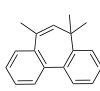
Compound	Structure	T_c/K	ΔG^\ddagger (kJ/mol)	solvent
L3a ²³		---	54.4	
L3b ²³		syn 283.5 anti 264.5	57.4 55.3	
L3c ²³		272	56.1	
L3d ²³		282	58.6	
L3e ²³		351.5	74.9	Pyridine
L3f ²³		375	78.8	Pentachloroethane

Table B-4: Series of ethyl bridged biphenyls showing the low limits of dynamic NMR as the coalescence for 4a and 4b were not reachable as either the chemical shift difference was too small or the coalescence temperature was too low.

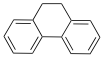
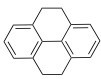
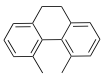
Compound	Structure	T_c/K	ΔG^\ddagger (kJ/mol)	solvent
L4a ²¹		---	<37.7	
L4b ²¹		---	<37.7	
L4c ²¹		---	96.7	

Table B-5: The series of unbridged biphenyls shows clearly that the activation energy of these systems was higher due to larger torsion angles resulting from steric repulsion.

Compound	Structure	T ₀ /K	ΔG [‡] (kJ/mol)	solvent
L5a ²⁶		331	73.7	
L5c ²⁶		338	75.4	
L5d ²⁶		343	76.6	
L5e ³⁵		342	77	tetrachloroethane
L5f ^{26,35}		347	77.5	
L5g ³⁵		343	78.3	tetrachloroethane
L5h ^{26,35}		352	78.7	tetrachloroethane
L5i ²⁶		355	79.5	
L5j ^{26,35}		359	80.4	tetrachloroethane
L5k ²⁶		359	80.4	tetrachloroethane
L5l ³⁵		315	69.9	dimethylsulfoxide
		328	73.7	tetrachloroethane
L5m ³⁵		322	73.7	dimethylsulfoxide
		338	78.3	tetrachloroethane
L5n ³⁵		331	73.7	dimethylsulfoxide
		349	80.0	tetrachloroethane
L5o ³⁵		333	74.5	dimethylsulfoxide
		330	74.1	tetrachloroethane
L5p ³⁵		331 ± 2	75.5 ± 0.8	dimethylsulfoxide
		350	80.8	tetrachloroethane

B.2.4 Dynamic High Pressure Liquid Chromatography (DHPLC)

Dynamic chromatography can be used as extension for dynamic NMR spectroscopy for molecules with an activation energy above 80 kJ/mol.^{11–13} The only requirement is that the two enantiomers can be at least partial separated during a HPLC run. As enantiomers show the same properties in achiral environment the two enantiomers cannot be separated in achiral media. However, if the achiral solid phase is doped with a chiral dopant, the two enantiomers will form different diastereoisomers in complex with the solid phase. Diastereoisomers can be separated from each other, as their physical properties are different. If the two enantiomers isomerize during the HPLC run then a plateau between the two peaks can be observed. This plateau formation is required to study the dynamic processes. Calculations of activation parameters are complicated but nowadays with the help of specific computer software, they are easier to handle. The calculations include the different rate constants k_m (rate constant in the mobile phase) and k_s (rate constant in the stationary phase) and the equilibrium constants K_m and K_s .

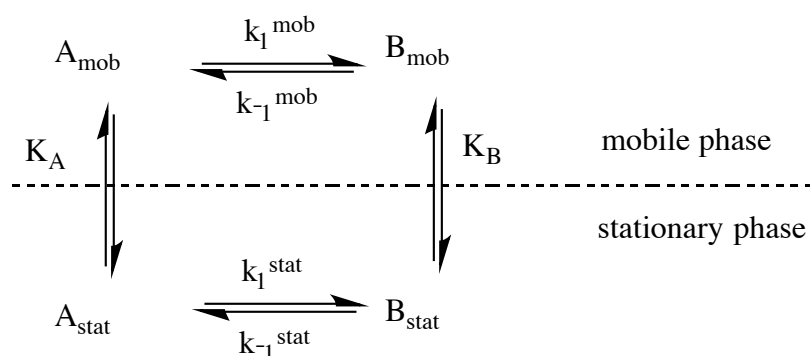


Figure B-4: Equilibrium in a chromatographic theoretical plate model. A is the first eluted compound and B the second eluted one. The values k_1 for the forward reaction and k_{-1} for the back reaction represent the rate constants in the mobile and stationary phase. K describes the distribution constant. The figure is reprinted from Trapp.⁴⁴

To calculate the activation parameters, the same molecule has to be measured at different temperatures on the same column under the same elution method (typical temperature ranges for HPLC runs are in the range of -80 to $+120^\circ\text{C}$).¹² To solve these equations also pressure variations can be performed. This is usually done when temperature variations are not possible.¹³ A reason could be the instability of the investigated molecule at high temperatures. For a deeper understanding of the different k values the separation has to be performed on different chiral column to keep the k_m constant while k_s is changed. Usually molecules with activation energy in a range of 80–120 kJ/mol can form such a plateau. The reason for this small range is

the fact that molecules with lower activation energy are racemizing too fast to allow separation and compounds with higher activation energies are racemizing so slow that an extreme long column would be required to detect a plateau formation. The second case can be useful anyway as the properties of the two enantiomers could be analysed or the racemization monitored by polarimetry. The main advantage of dHPLC over dNMR is the low substrate loadings required for a single run. The same procedure can be performed by Gas chromatography (GC) using a chiral column for separation¹⁴.

B.2.5 Applications of biphenyls

Biphenyls are one of the most investigated molecular building blocks. The hindered rotation around a single C-C bond leads to unique chemical and physical properties as the degree of π -conjugation can be varied.^{5,20,26,33,34,45-50} Many different systems have been studied to develop molecules with fixed or flexible torsion angles to induce a defined range of π -conjugation. This intensive research afforded a wide range of applications for substituted biphenyls. Applications are found in a variety of materials such as organic light emitting device (OLEDs),⁴ Non linear optics (NLO)⁵ or molecular electronics^{47,49} to name just a few of them.

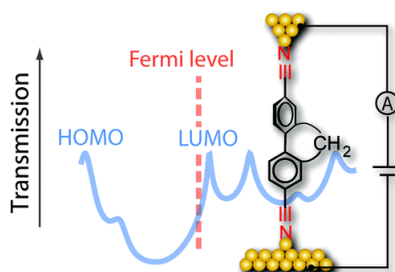


Figure B-5: Representation of molecular electronic device created from bridged biphenyls.⁵¹

A fixed torsion angle in combination with separation of the two enantiomers allowed also applications in catalytic processes providing products in high enantiomeric excess. Biphenyls also found there application in medicinal chemistry as flexible building block in inhibitors for example as inhibitor for angiotensin II AT1 receptor.⁵² In most cases the fine-tuning of the torsion angle is performed using different 2,2'-sterically demanding substituents or 2,2'-bridges with different chain length.⁵⁰ A quite important feature of biphenyls is the fact that *ortho*-substituents mainly influence the torsion angle without elongation of the carbon backbone. Therefore, a variety of 2,2'-ethyl, -propyl, and -butyl bridged biphenyls with variable substituents in 4 and 4'

position were systematically investigated by dNMR, dHPLC and theoretical calculations.

B.3 Methods and Materials

The studies of Oki²¹ showed that the rotation of ethyl bridged biphenyl is too fast to be investigated by dNMR, this result was also observed in our work for 4,4'-disubstituted-2,2'-ethylbridged biphenyls.⁸ Trials using Eu(fod)₃, Eu(hfc)₃ and Pr(hfc)₃ as lanthanide shift reagents (LSR) did not allow investigations of the thermodynamic data by NMR. The 4,4'-disubstituted-2,2'-propylbridged biphenyls showed a fast exchange at rt. but cooling of the system sufficient, delivering molecules in the slow exchange regime. Therefore, thermodynamic studies could be performed for this class of molecules by dNMR. The activation energy of 4,4'-disubstituted-2,2'-pentylbridged biphenyls is about 40 - 50 *kJ/mol*⁷ higher and therefore above the limit of dNMR. This means that even at 150 °C slow exchange was observed and the coalescence temperature of about 170 - 210 °C was suggested from the results obtained by dynamic HPLC measurements.

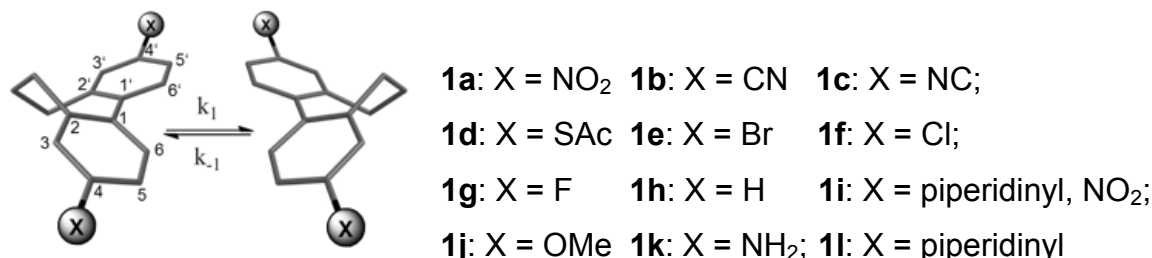


Figure B-6: Biphenyls investigated by dynamic NMR and theoretical calculations.

B.3.1 Dynamic NMR measurements and analysis

All samples were prepared in deuterated solvents (<99.8% D, Cambridge Isotope Laboratories, Burgdorf, CH). The NMR experiments were performed on a Bruker Ultra Shield Avance III – 600 MHz NMR spectrometer, equipped with a self shielded z-axis pulsed field gradient dual channel broadband inverse probe head (BBI)⁷. Referencing was done on residual solvent peaks and the temperature unit of the spectrometer was calibrated using a 4% methanol in 96% methanol-d₄ sample⁵³. The temperature calibration was performed in the range between 200 and 265 K using Equation B-7

$$T = \frac{3.92 - \Delta\delta}{0.008}$$

Equation B-7: Temperature calibration, T = corrected temperature $\Delta\delta$ = chemical shift difference between CH_3 and OH resonance in MeOH.

and for higher temperatures in the range of 265 to 300 K by Equation B-8.

$$T = \frac{4.109 - \Delta\delta}{0.008708}$$

Equation B-8: Temperature calibration, T = corrected temperature $\Delta\delta$ = chemical shift difference between CH_3 and OH resonance in MeOH.

A detailed description of the temperature calibration is shown in the experimental section. The graphical representation is seen in Figure B-7.

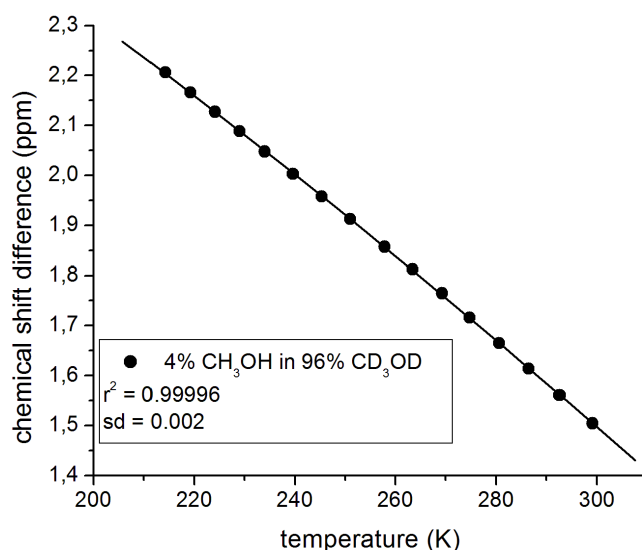


Figure B-7: Temperature calibration curve 4% MeOH in 96% MeOD-d4

The thermal equilibrium was ensured by at least 15 min equilibration time for each temperature step. Experimental activation energies ($\Delta G_{\text{exp}}^\ddagger$) were calculated using Equation B-2. Theoretical activation energies were calculated from the data obtained by line shape analysis using Equation B-9.

$$\Delta G_{\text{theo}}^\ddagger = \Delta H - T \Delta S \left[\frac{\text{kJ}}{\text{mol}} \right]$$

Equation B-9: Calculation of the Gibbs free activation energy ΔG^\ddagger from line shape analysis.

The computer software dNMR (Bruker Bio Spin AG[®]) was used to perform the line shape analysis. To perform the line shape analysis successfully, several experimental parameters had to be added to the software. The chemical shift of the two different spins in the slow exchange regime in ppm, the coupling constant of the

spins in the slow exchange. Additionally the range for the simulation has to be set as not the whole molecule was fitted. For analysis of the biphenyl systems only the propyl bridge spin system was investigated. Experimental impurities were not fitted and decreased in some cases the accuracy of the fitted spectra. The confidence interval was set to 95 % as the impurities were not fitted but in most cases values of 98 - 99% accuracy were calculated. The resulting rate constants were further analysed using Eyring plots and the rate constants at the coalescence temperature were compared to values calculated by the approximation method. The experimental coalescence temperature were estimated between two measured spectra and have an accuracy of about ± 1 °K, the theoretical coalescence temperature was calculated from the line width of the signals followed by lorentzian fitting as shown for the di-cyano-biphenyl **1b** in Figure B-8. For all other compounds the results are shown in the experimental section.

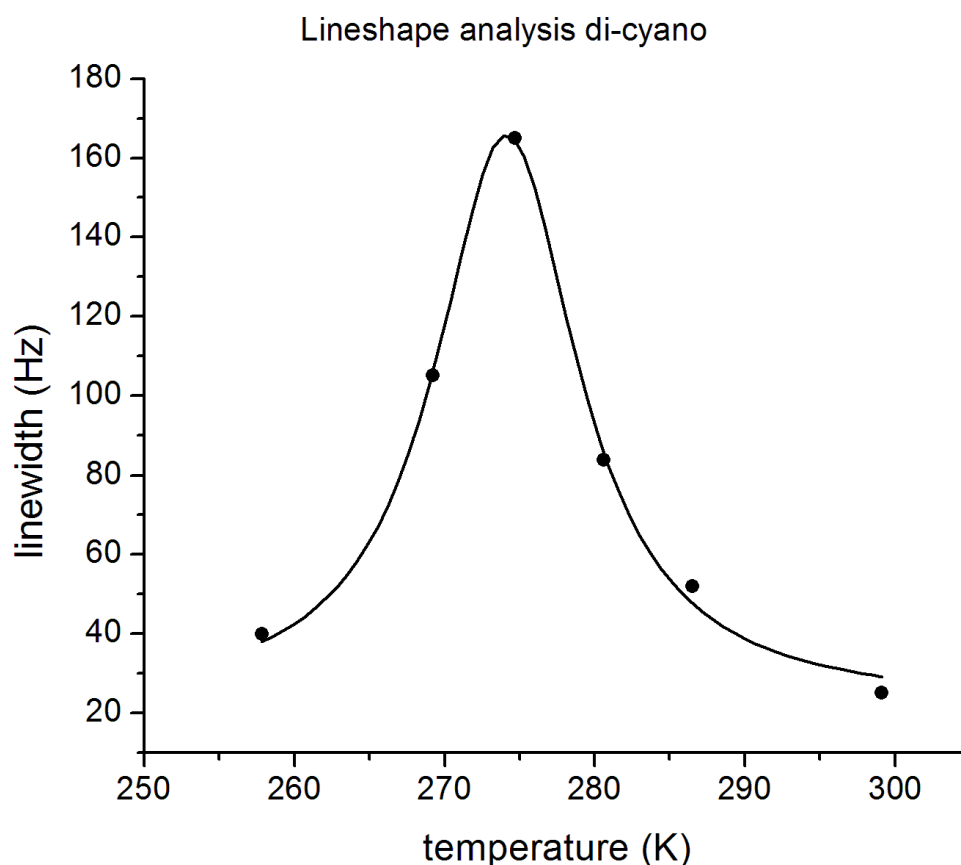


Figure B-8: Calculation of the coalescence temperature from the line width of the peak at different temperature.

All compounds were fully assigned using ^1H , ^{13}C , HMQC, HMBC and NOESY NMR-experiments.

B.3.2 Dynamic HPLC measurements and fitting

All samples were prepared in a concentration of about 1 mg/mL in *i*PrOH. For the separation of the resulting atropisomers a chiralpak AD-H column (0.46 x 25 cm; Daicel Chemical Industries Ltd.[®]) was used and the temperature was adjusted with an oven (CTO-10AS VP oven from Shimadzu[®]). A sample volume of 3 μ L and a mixture of *n*-hexane/*i*PrOH (97:3) were used for all compounds except for the di-SAc-substituted molecule, which was eluted with *n*-hexane/*i*PrOH (95:5). An SCL-10A VP HPLC from Shimadzu[®] with a flow rate of 0.5 mL/min was used for the experiments. The solvents were prepared as a 94:6 or 90:10 mixture of *n*-hexane and *n*-hexane/*i*PrOH (1:1) to allow perfect mixing of the solvents. The HPLC run were detected with SPD-M10A VP UV/Vis detector from Shimadzu[®]. A fixed wavelength of $\lambda = 254$ nm was used corresponding the absorption maximum of the compounds. The column was equilibrated for 2 hours before the experiments were performed and conditioned for 30 min after each run. Experiments were performed in a temperature range between 15 and 35 $^{\circ}$ C in 5 $^{\circ}$ C steps. All compounds were measured twice over the whole temperature cycle. The rate constants were determined with the unified equation,⁴⁴ allowing the calculation of first order rate constants by direct integration of the elution profile with the program DCXplorer. The thermodynamic parameters were determined in a similar way as for the dNMR case using Eyring plots for the analysis of the rate constants.

B.3.3 Theoretical calculations

The computational work was performed with the TURBOMOLE program package.⁵⁴ Density functional theory (DFT) was used to optimize the framework for equilibrium and transition state structures of symmetrically di-substituted biphenyls, which are involved in the atropisomerization process.

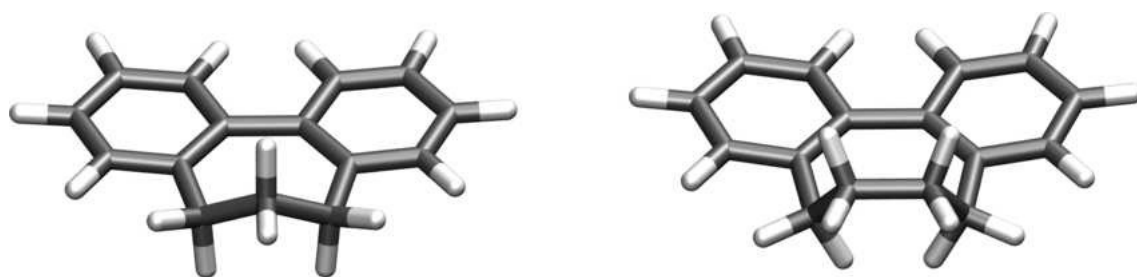


Figure B-9: C_s -symmetric first order transition state for the propyl-bridged biphenyl (di-H) and the C_s -symmetric second order transition state of butyl-bridged biphenyl (di-H).

In order to assess the performance of different types of density functionals, the generalized gradient approximation (GGA) functional BP86,^{55,56} the meta-GGA functional TPSS⁵⁷ and the hybrid functional B3LYP⁵⁸ were chosen. Each functional was used in combination with a def2-TZVP basis set,⁵⁹ tight convergence criteria (SCF energy: 10^{-8} E_h, energy gradient: 10^{-4} E_h/a₀ or less, inclusion of derivatives of quadrature weight), and fine grids (m5),⁶⁰ For non-hybrid functional, the effect of resolution of the identity (RI) approximation for two electron Coulomb integrals was employed. The nature of the obtained stationary points (minimum or first order saddle point) was confirmed through analysis of the force constants and vibrational frequencies.

The coalescence temperatures T_c obtained by dNMR were used as temperatures for the calculation of the Gibbs free activation energy (ΔG^\ddagger) at a pressure of 0.1 MPa. For calculations of the partition functions, the vibrational frequencies were scaled by a factor of 0.9914 (BP86 and TSS) and 0.9614 (B3LYP).⁶¹

For biphenyls with substituents that allowed rotations within the substituent like NH₂, OMe, SAc and piperidinyl several isomers (not only the rotation about the c-c axis) were obtained. In this case all structures with an energetically low-lying equilibrium structure with C₂-symmetry in combination with their transition states were taken into account. The reported values for these substituents were obtained from the Boltzmann average of the respective conformers.

B.3.4 Synthesis

Most compounds were previously used for single molecular conductance measurements. The synthesis of all compounds was therefore reported previously in different publications^{5,7,8,47,49,50}.

B.4 Results

The di-CN ethyl bridged biphenyl (Structure B-4) was investigated by variable temperature NMR measurements. A fast exchange was observed even at 233 K as shown in Figure B-10.

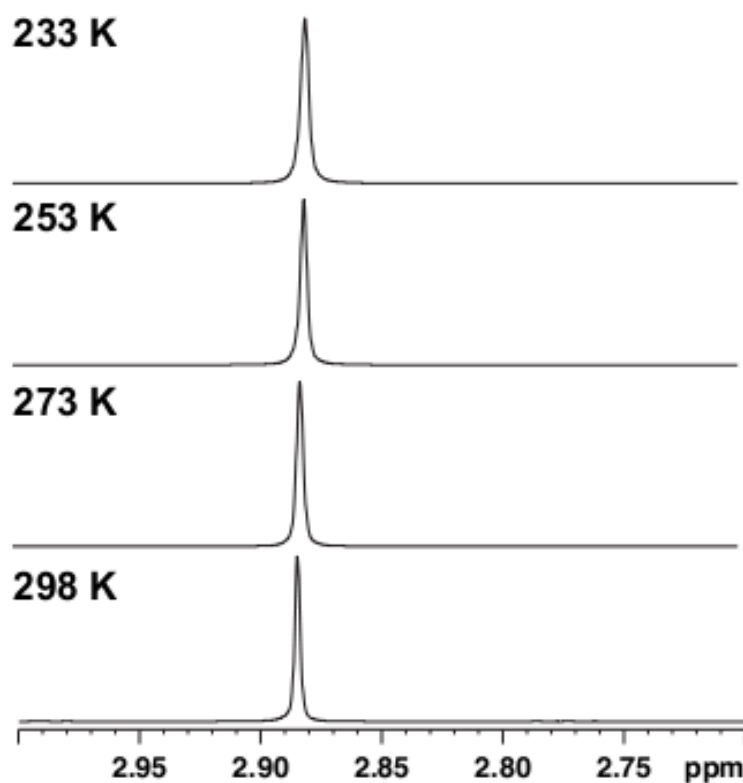
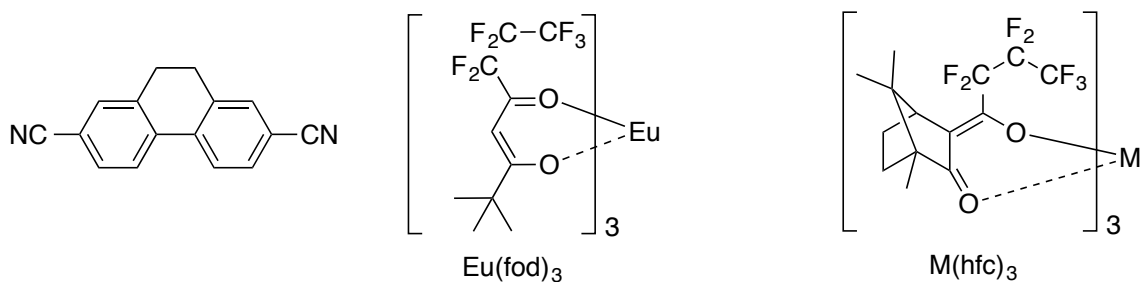


Figure B-10: Variable temperature NMR spectra of the ethyl protons of 4,4'-dicyano-2,2'-ethylbridged biphenyl. Showing a small increase of the line width from 298 K to 233 K.

This result was predicted from measurements performed by Oki²¹ for ethyl-bridged biphenyls. Therefore variable temperature NMR titration experiments using $\text{Eu}(\text{fod})_3$ (Structure B-4) as paramagnetic achiral lanthanide shift reagent were done. The induced pseudo contact shift was too small to reach the coalescence temperature even when high concentrations of the LSR were used. The resulting NMR spectra are shown in the experimental section. From these data it can be concluded that the effect of the LSR is small on the bridging ethyl group. Therefore, chiral lanthanide shift reagents were used for the variable temperature titration experiments. A chiral shift reagent should deliver stronger geometrical differences on the two different sites of the molecule.



Structure B-4: 4,4'-dicyano-2,2'-ethylbridged biphenyl investigated by variable temperature NMR, europium(III)-tris(1,1,1,2,2,3,3-heptafluoro-7,7-dimethyl-4,6-octanedionate) ($\text{Eu}(\text{fod})_3$) used as achiral paramagnetic shift reagent, tris[3-(heptafluoropropylhydroxymethylene)-*d*-camphorato]metal(III) (with $\text{M} = \text{Eu}, \text{Pr}, \text{Tm}$) used as chiral shift reagent.

Thus, a bigger shift difference of the two protons in a slow exchange regime was predicted. This is an important fact, as an increased chemical shift difference would also increase the coalescence temperatures.

A series of tris[3-(heptafluoropropylhydroxymethylene)-*d*-camphorato]metal(III) complexes namely $\text{Eu}(\text{hfc})_3$, $\text{Pr}(\text{hfc})_3$, and $\text{Tm}(\text{hfc})_3$ (Structure B-4) were used for these investigations. In this series we gradually increased the anisotropy of the magnetic susceptibility tensor to induce stronger pseudo contact shifts in a stepwise manner.

Nevertheless, the coalescence temperature was not accessible with any of these metal complexes. This means that the chemical environment of the two sides could not be changed in a way that the chemical shift difference of the two protons in the slow exchange became huge to make the coalescence temperature accessible for variable temperature NMR measurements. For the strongest paramagnetic metal Thulium (Tm) measurements in toluene were performed to allow temperature measurements down to 188.5 K. Only weak broadening, which has its main origin in the reduced shim quality at low temperatures was detected. The experimental spectra of the paramagnetic samples measured at different concentrations of LSR are shown in the experimental section for all different complexes. For the Tm samples strong paramagnetic relaxation enhancement (PRE) at low temperatures and higher Tm concentrations was visible. The high viscosity of toluene at low temperatures in combination with the PRE effects led to signal broadening. These effects limited therefore the investigation of the rotation process.

For all propyl-bridged biphenyls **1a-1l** (Figure B-6) NMR coalescence measurements were successfully performed. For all molecules, the three necessary states were reached by variable temperature (VT) NMR experiments to allowing thermodynamic investigations of the molecules.

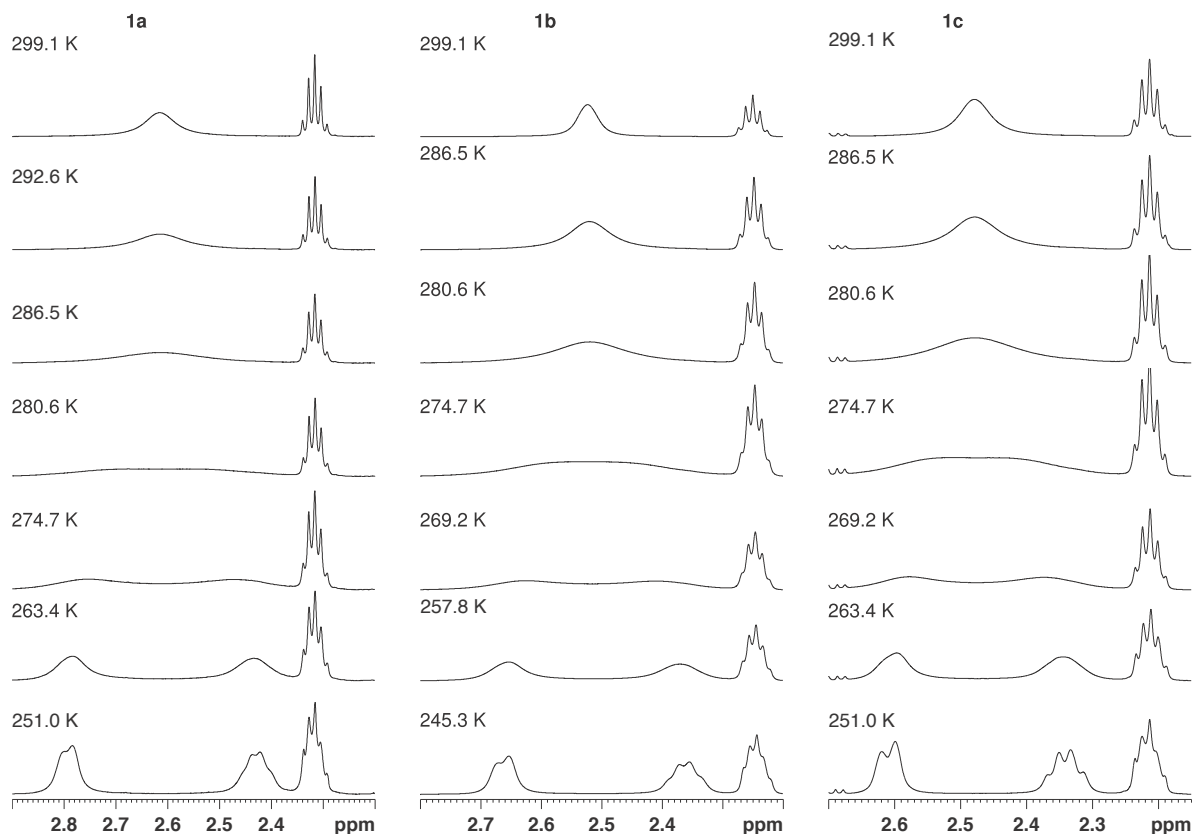


Figure B-11: Variable temperature NMR experiments of compounds 1a-1c in CDCl₃, showing the three different states fast exchange, coalescence and the slow exchange.

The slow exchange regime corresponds to a spectrum where the resulting NMR signals are obtained as well defined separated resonances. The coalescence is the point where the signal reaches a plateau and finally the fast exchange regime where an averaged signal is obtained. A representation of such spectra is shown in Figure B-11 for compounds **1a-1c**, all other spectra can be found in the experimental section. For the determination of the experimental Gibbs free activation energy (ΔG^\ddagger), the coalescence temperature T_c and the chemical shift difference $\Delta\nu$ (in Hz) were determined from the spectra and used for the modified form of the Eyring equation (Equation B-2). Coalescence temperatures were estimated with an accuracy of about 1 K. In Table B-6 the results of the calculation are shown. The activation energies are in a range of 44 to 55 kJ/mol for all propyl-bridged compounds **1a-1l**.

Table B-6: Experimentally determined Gibbs free activation energies $\Delta G_{\text{exp}}^{\ddagger}$ for compounds 1a-1l determined by dynamic NMR measurements

Compound	T_c / K	$\Delta\nu / \text{Hz}$	$\Delta G_{\text{exp}}^{\ddagger} / \text{kJ/mol}$
1a	281.4 ± 1	218.0	54.2 ± 0.5
1b	275.1 ± 1	181.0	53.3 ± 0.5
1c	270.1 ± 1	161.0	52.6 ± 0.5
1d	259.6 ± 1	111.0	51.3 ± 0.5
1e	260.2 ± 1	113.0	51.3 ± 0.5
1f	260.7 ± 1	118.0	51.4 ± 0.5
1g	265.0 ± 1	109.0	52.4 ± 0.5
1h	263.3 ± 1	95.0	52.4 ± 0.5
1i	245.0 ± 1	132.0	47.9 ± 0.5
1j	242.1 ± 1	79.0	48.4 ± 0.5
1k	224.2 ± 1	31.0	46.4 ± 0.5
1l	218.9 ± 1	44.0	44.6 ± 0.5

For compound **1b**, **1e**, **1i** and **1j** the influence of different solvents (Table B-7) was studied. Thereby, it was shown that the influence of the solvents with different polarities on $\Delta G_{\text{exp}}^{\ddagger}$ was in a range of 1 to 2 kJ/mol. For compound **1i** it was found that the acidic solvent TFA led to an increase of the activation barrier by about 4 kJ/mol. This fact can be easily understood as a protonation of the push-pull system led to a push-push system. Compound **1i** was measured in several solvents to get detailed information about the influence of the solvent to the activation barrier. Viscosity and polarity of the solvent could not explain the obtained trend.

Table B-7: Solvent effect of compounds 1b, 1e, 1l and 1j on the free Gibbs activation energy $\Delta G_{\text{exp}}^{\ddagger}$. (* Chemical shift difference of the central CH₂-group)

Compound	Solvent	T_c / K	$\Delta\nu / \text{Hz}$	$\Delta G_{\text{exp}}^{\ddagger} / \text{kJ/mol}$
1b	CDCl ₃ -d1	275.1 ± 1	181	53.3 ± 0.5
1b	toluene-d8	257 ± 1	61	52.0 ± 0.5
1b	MeOH-d4	274 ± 1	247	52.4 ± 0.5

Compound	Solvent	T_c / K	$\Delta\nu / \text{Hz}$	$\Delta G^\ddagger_{\text{exp}} / \text{kJ/mol}$
1e	CDCl ₃ -d1	260.2 ± 1	113	51.3 ± 0.5
1e	toluene-d8	263.4 ± 1	181	51.0 ± 0.5
1e	MeOH-d4	242.0 ± 1	49	49.3 ± 0.5
1i	CDCl ₃ -d1	245.0 ± 1	132	47.9 ± 0.5
1i	MeOH-d4	249.9 ± 1	174	48.3 ± 0.5
1i	toluene-d8	239.6 ± 1	102	47.3 ± 0.5
		233.3	60*	47.1 ± 0.5
1i	DMF-d7	240.8 ± 1	144	46.9 ± 0.5
1i	TFA-d1	274.7 ± 1	180	53.3 ± 0.5
1i	C ₂ D ₂ Cl ₄ -d2	242 ± 1	108	47.7 ± 0.5
1j	CDCl ₃ -d1	242.1 ± 1	79.0	48.4 ± 0.5
1j	toluene-d8	250 ± 1	132	48.9 ± 0.5
1j	MeOH-d4	247.3 ± 1	125	48.5 ± 0.5

For all compounds a line shape analysis was performed to gain insights into the kinetics of the rotation around the C1-C1' bond.^{31,62,63} The rate constants were determined with dNMR Bruker® for all compounds **1a-1l** in all measured solvents and the rate constants were further analysed with Eyring plots, establishing the connection between kinetics and thermodynamics. Equation B-6 was used for the calculation of the activation enthalpy and entropy. To calculate the Gibbs free activation energy of this data, the coalescence temperature T_c had to be calculated as well. The line width of the experimental spectra was therefore plotted against the temperature and a lorentzian fitting was performed to determine the maximum linewidth corresponding to T_c . The coalescence temperatures are in high agreement to the experimental ones except for those with a low T_c close to the freezing point of the solvent. Only a few spectra below T_c limit the accuracy of the fit tremendously. The resulting thermodynamic values are summarized in Table B-8.

Table B-8: Overview of the thermodynamic data calculated from line shape analysis. The coalescence temperatures T_c were determined from the line width of the signals followed by a Lorentzian fitting. Activation entropy ΔH^\ddagger and activation Entropy ΔS^\ddagger were calculated from Eyring plots using equation 6. The Gibbs free activation energy ΔG^\ddagger was calculated using equation 9.

Compound	$T_{c\text{-line shape}} / \text{K}$	$\Delta G_{\text{Eyring}}^\ddagger / \text{kJ/mol}$	$\Delta H_{\text{Eyring}}^\ddagger / \text{kJ/mol}$	$S_{\text{Eyring}}^\ddagger / \text{J}/(\text{mol K})$
1a	280.4 ± 1.1	54.2 ± 0.1	50.7 ± 1.6	-12.6 ± 5.6
1b	274.1 ± 1.3	53.3 ± 0.1	52.7 ± 2.0	-1.9 ± 7.3
1c	269.1 ± 1.1	52.6 ± 0.1	49.9 ± 1.3	-10.0 ± 4.6
1d	261.6 ± 1.7	52.0 ± 0.1	45.9 ± 1.0	-21.8 ± 3.6
1e	263.2 ± 1.3	51.7 ± 0.1	50.0 ± 2.7	-6.4 ± 10.4
1f	259.7 ± 1.3	51.5 ± 0.1	46.0 ± 1.0	-21.0 ± 3.7
1g	263.0 ± 1.6	52.6 ± 0.1	47.8 ± 1.3	-18.5 ± 4.7
1h	262.3 ± 1.4	52.4 ± 0.1	47.4 ± 1.2	-19.1 ± 4.6
1i	244.0 ± 1.2	47.8 ± 0.1	37.4 ± 0.8	-42.6 ± 3.0
1j	241.1 ± 1.3	48.8 ± 0.1	43.4 ± 1.5	-22.5 ± 6.2
1k	221.6 ± 2.1	46.8 ± 0.1	39.3 ± 1.5	-33.8 ± 6.6
1l	217.9 ± 1.4	45.4 ± 0.2	28.3 ± 1.7	-78.4 ± 7.3

The calculation of the coalescence temperature of the di-CN-substituted biphenyl is shown in Figure B-8. The determined rate constants for this molecule are shown in Table B-9 and the corresponding Eyring plot is shown in Figure B-12. A comparison of the experimental and the fitted NMR spectra are shown in the experimental section for all molecules. For all other compounds the detailed results of our calculations is shown in the experimental section.

Table B-9: Rate constant determined by line shape analysis of compound 1b with dNMR Bruker®.

Temperature in K	Rate constant k in Hz
299.1	3050
286.5	1200
280.6	720
274.7	410
269.2	260
257.8	90

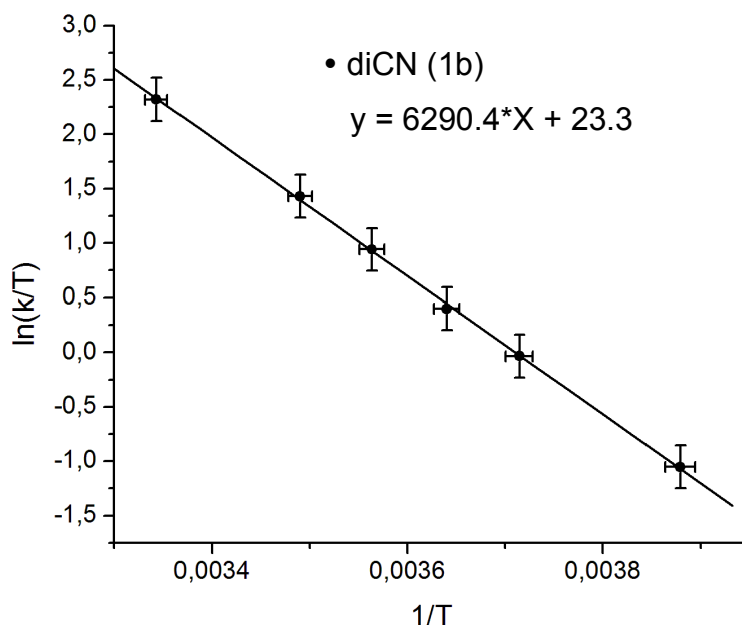


Figure B-12: Eyring plot for the di-CN-compound 1b.

The comparison of the Gibbs free activation energies obtained by line shape analysis and experimental spectra are necessary to validate the two-side model. It was shown that the differences between the experimental approximation (Equation B-2) and the line shape analysis (Equation B-9) are below 1 kJ/mol, which is for almost all compounds within the experimental error (Table B-10) (except for I). This result validates the two state model for each molecule. For other models with more states the fit and experiment should show stronger deviations, as then more than one coalescence phenomena should be detectable. Therefore differences in $\Delta G^\ddagger(T)$, which are larger than 1 kJ/mol are statistically significant. The main distinction between approximation and line shape analysis results from differences in T_c . For molecules like **1k** and **1i** the coalescence temperature was close to the freezing point of the solvent. For Lorentzian fitting to generate calculated coalescence temperatures it is necessary to have enough data points in the slow and fast exchange regime. Therefore the temperature accuracy for compounds with low T_c is less precise.

Table B-10: Comparison of experimental and calculated Gibbs free activation energies ($\Delta G_{\text{exp}}^\ddagger$ vs. $\Delta G_{\text{Eyr}}^\ddagger$).

Compound	$\Delta G_{\text{exp}}^\ddagger$ / kJ/mol	$\Delta G_{\text{Eyring}}^\ddagger$ / kJ/mol	$\Delta\Delta G$ /kJ/mol
1a	54.2 ± 0.5	54.2 ± 0.1	0
1b	53.3 ± 0.5	53.3 ± 0.1	0
1c	52.6 ± 0.5	52.6 ± 0.1	0
1d	51.3 ± 0.5	52.0 ± 0.1	0.7

Compound	$\Delta G_{\text{exp}}^{\ddagger} / \text{kJ/mol}$	$\Delta G_{\text{Eyring}}^{\ddagger} / \text{kJ/mol}$	$\Delta\Delta G / \text{kJ/mol}$
1e	51.3 ± 0.5	51.7 ± 0.1	0.4
1f	51.4 ± 0.5	51.5 ± 0.1	0.1
1g	52.4 ± 0.5	52.6 ± 0.1	0.2
1h	52.4 ± 0.5	52.4 ± 0.1	0
1i	47.9 ± 0.5	47.8 ± 0.1	0.2
1j	48.4 ± 0.5	48.8 ± 0.1	0.4
1k	46.4 ± 0.5	46.8 ± 0.1	0.4
1l	44.6 ± 0.5	45.4 ± 0.2	0.8

Simulations of compound **1j** and **1l** were inaccurate because of their low coalescence temperature. The increased viscosity of the samples led to a loss of shim quality, which enlarged the rate constants as a result of line broadening. To overcome this problem the error of the k values for our calculations were increased and a simulation of the solvent signal was performed to get an idea of the error of the k values induced from the loss of shim quality. Therefore the rate constants were recalculated at low temperatures as shim correction. Temperature errors ($T = \pm 1$ K) and rate constant errors ($k \pm 5$ % and for **1l** ($k = \pm 20$ %)) were used to calculate the errors stated in the different tables. For the data calculated from Eyring plots the regression coefficients were additionally included.

A variety of mechanisms were suggested for the atropisomerization process of bridged biphenyls. A detailed investigation was therefore necessary to get a more detailed idea of the mechanism present in our system. Theoretical calculations are a valid tool for such investigations. The comparison between experimentally determined and calculated activation energies can be used to validate the predicted mechanism. Theoretical calculations were successfully performed for all symmetrically substituted biphenyls. The calculation of the push-pull system **1i** failed and is therefore not further mentioned. The symmetrically substituted biphenyls showed a C_2 -symmetry after optimization and a quite similar torsion angle of about 47° was calculated. This is in good agreement with literature values for propyl-bridged biphenyls. The different ground state structures are shown in Figure B-13.

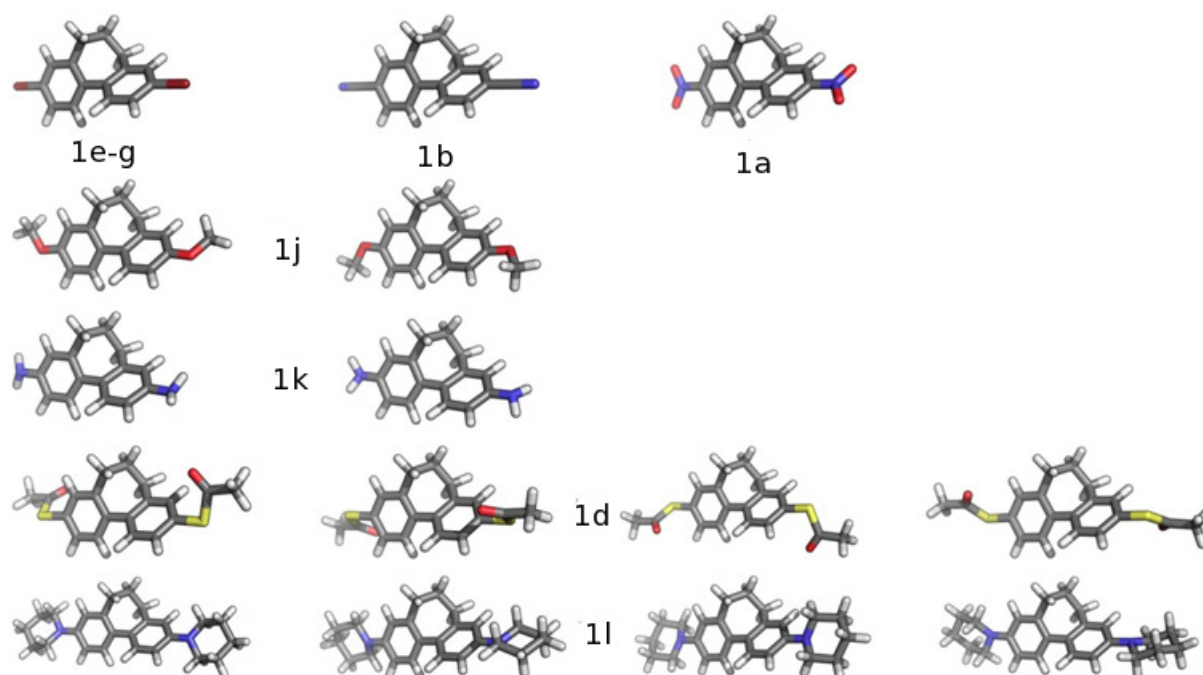


Figure B-13: Different ground state conformations of the investigated propyl-bridged biphenyls.

An example of the transition pathway is shown for the di-hydrogen substituted compound **1h** in Figure B-14.

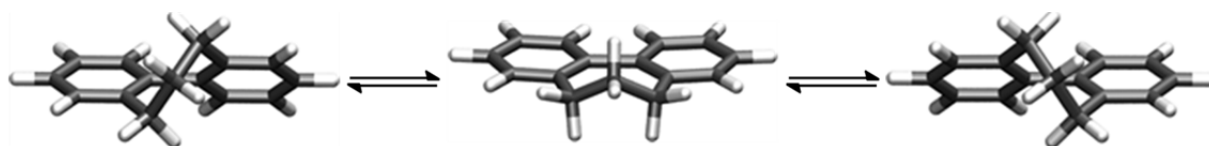


Figure B-14: Calculated reaction mechanism for propyl-bridged biphenyls.

This presented transition state shows nicely the two coplanar biphenyls with a torsion angle of about 0° , which is reached after rotation of the *ortho* methylene group. The central methylene group is still out of plane and a slight bent of the C-C bond between C1 and C1' is obtained leading to a non perfect linear structure. This model was used to calculate the Gibbs free activation energy for all compounds (Table B-11) with three different density functionals (BP86, TPSS, B3LYP). For all different functionals a similar trend in the activation energy was determined. But the absolute values show an offset for the different functionals in all cases. The obtained trend of the activation energies was similar to the experimental measured values.

The high agreement of the Gibbs free activation energy between DFT calculations and experimentally measured values gave strong evidence, that the calculated transition state is the correct one.

Table B-11: Gibbs free activation energy (ΔG^\ddagger in kJ/mol) of the series of propyl-bridged biphenyls obtained by three different density functionals and the experimental values as reference.

Compound	$\Delta G_{\text{BP86}}^\ddagger$	$\Delta G_{\text{TPSS}}^\ddagger$	$\Delta G_{\text{B3LYP}}^\ddagger$	$\Delta G_{\text{exp}}^\ddagger$
1a	48.4	49.7	52.0	54.2 ± 0.5
1b	47.6	48.7	51.2	53.3 ± 0.5
1c	47.2	48.2	50.6	52.6 ± 0.5
1d	48.0	48.9	52.4	51.3 ± 0.5
1e	47.0	48.0	50.4	51.3 ± 0.5
1f	47.0	48.0	50.3	51.4 ± 0.5
1g	48.4	49.4	51.6	52.4 ± 0.5
1h	48.4	49.3	51.7	52.4 ± 0.5
1j	45.7	46.5	48.9	48.4 ± 0.5
1k	44.0	44.8	47.3	46.4 ± 0.5
1l	42.5	43.3	46.2	44.6 ± 0.5

Table B-12: Calculated activation enthalpy (ΔH^\ddagger in kJ/mol) and the activation entropy (ΔS^\ddagger in J/(mol*K)) for the three different density functionals

Compound	$\Delta H_{\text{BP86}}^\ddagger$	$\Delta S_{\text{BP86}}^\ddagger$	$\Delta H_{\text{TPSS}}^\ddagger$	$\Delta S_{\text{TPSS}}^\ddagger$	$\Delta H_{\text{B3LYP}}^\ddagger$	$\Delta S_{\text{B3LYP}}^\ddagger$	$\Delta H_{\text{Eyring}}^\ddagger$	$\Delta S_{\text{Eyring}}^\ddagger$
1a	49.1	2.5	50.1	1.4	52.5	1.8	50.7	-12.6
1b	48.1	1.9	48.8	0.6	51.7	1.6	52.7	-1.9
1c	47.6	1.5	48.3	0.5	50.9	1.2	49.9	-10.0
1d	47.8	-0.9	48.5	-1.5	51.5	-3.7	45.9	-21.8
1e	47.3	0.9	48.0	-0.1	50.6	0.8	50.0	-6.4
1f	47.2	0.8	47.9	-0.2	50.5	0.7	46.0	-21.0
1g	48.6	0.6	49.3	-0.3	51.8	0.5	47.8	-18.5
1h	48.8	1.2	49.4	0.3	52.0	1.2	47.4	-19.1
1j	45.9	0.9	46.5	0.0	49.0	0.8	43.4	-22.5
1k	44.2	0.7	44.8	-0.1	47.5	0.5	39.3	-33.8
1l	43.1	2.8	43.7	1.9	46.7	2.3	28.3	-78.4

The activation enthalpy ΔH^\ddagger and the activation entropy ΔS^\ddagger were calculated for all compounds and density functionals (Table B-12). The activation entropy was small for all functionals and close to the experimental error. A strong deviation between experimental and DFT calculated values was therefore obtained. DFT calculations are performed for isolated molecules (vacuum conditions) this means there are no interactions either with similar or solvent molecules. NMR-measurements in different solvent were performed and the activation parameters calculated. It was shown before that the solvent effect on the Gibbs free activation energy is rather small but line shape analysis was not performed in this case. The Gibbs free activation energy is in general way independent, which should deliver similar activation energies as obtained, but the origin can vary strongly. The influence of the solvent on ΔH^\ddagger and ΔS^\ddagger was therefore investigated in more detail for the electron withdrawing di-cyano compound **1b**, for the neutral di-bromo compound **1e** and the electron donating compound **1j**. Polar protic methanol and π -donating toluene were chosen as solvent and compared to the previously measured polar chloroform. It can be seen that the di-cyano and the di-bromo compound showed the same trend in this three solvents. For the di-methoxy compound the inverse trend (Table B-13) was observed.

Table B-13: Activation entropy ΔS^\ddagger , activation enthalpy ΔH^\ddagger and the Gibbs free activation energy ΔG^\ddagger of selected molecules in three different solvents.

Compound	Solvent	$\Delta S_{\text{Eyring}}^\ddagger / \text{J}/(\text{molK})$	$\Delta H_{\text{Eyring}}^\ddagger / \text{kJ}/\text{mol}$	$\Delta G_{\text{Eyring}}^\ddagger / \text{kJ}/\text{mol}$
1b	CDCl ₃ -d1	-1.9 ± 7.3	52.7 ± 2.0	53.2 ± 0.1
1b	MeOD-d4	-8.3 ± 4.2	50.1 ± 1.2	52.3 ± 0.1
1b	Toluene-d8	-39.9 ± 3.5	41.7 ± 0.9	51.9 ± 0.1
1e	CDCl ₃ -d1	-6.4 ± 10.4	50.0 ± 2.7	51.7 ± 0.1
1e	MeOD-d4	-8.0 ± 4.2	49.0 ± 1.3	51.1 ± 0.1
1e	Toluene-d8	-18.0 ± 5.5	45.9 ± 1.4	50.4 ± 0.1
1j	CDCl ₃ -d1	-22.5 ± 6.2	43.4 ± 1.5	48.8 ± 0.1
1j	MeOD-d4	-12.8 ± 4.0	45.6 ± 1.0	48.7 ± 0.1
1j	Toluene-d8	-5.0 ± 4.9	47.9 ± 1.3	49.1 ± 0.1

The strong variations obtained in this limited series of solvents show clearly that a solvent effect is present. It is therefore clear that changing from solution to vacuum conditions would have an influence on activation parameters. This means that the

number of molecules that can interact with each other play an role in the atropisomerization process as the solvent can interact with the biphenyl in a specific way.

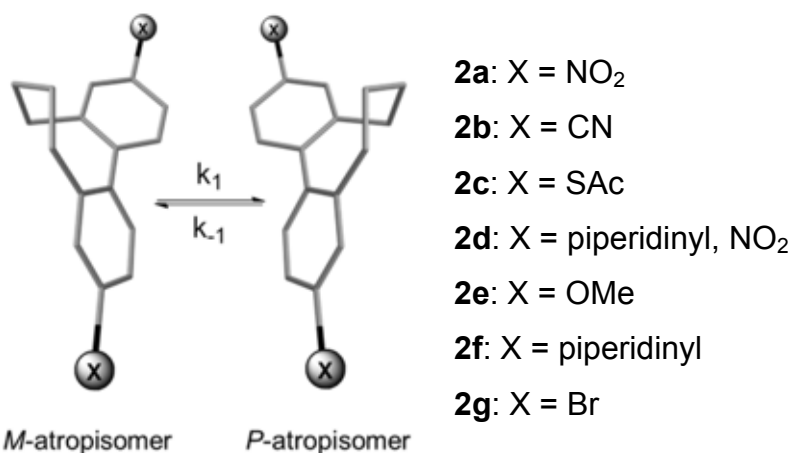


Figure B-15: Investigated butyl-bridged biphenyls 2a-2f.

The influence of an additional CH₂ group in the bridge of the biphenyl was investigated leading to butyl-bridged compounds. ¹H-NMR experiments were performed at rt. to determine the exchange regime. Two distinct signals for each proton were observed, leading to the conclusion that a slow exchange is present at rt.. The chemical shift differences at rt. were quite large as summarized in Table B-14 therefore high temperature experiments were performed.

Table B-14: Chemical shift difference of the butyl bridged biphenyls at 298K.

Compound	Solvent	$\Delta\nu$ at slow exchange
2g	CDCl ₃	362 Hz
2b	CDCl ₃	418 Hz
2c	CDCl ₃	356 Hz
2e	CDCl ₃	321 Hz
2e	C ₂ D ₂ Cl ₄	328 Hz

The high boiling solvent 1,1,2,2-tetrachloroethane-d₂ was used and experiments up to 410 K measured. Nevertheless, no significant changes in the line shape of the signals were observed as shown in Figure B-16. Only little temperature shifts of the bridging protons were obtained.

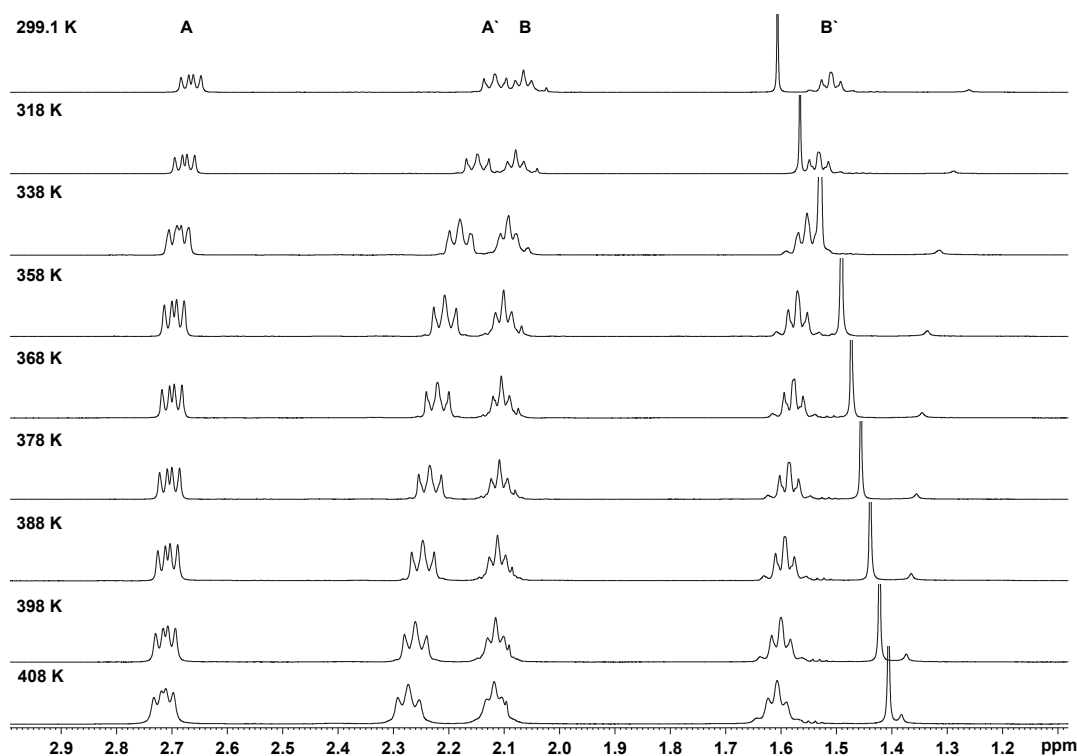
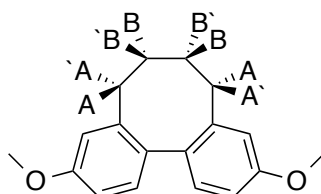


Figure B-16: High temperature NMR of 4,4'-dimethoxy-2,2'-butyl bridged biphenyl (Structure B-5) in tetrachloroethane-d₂ showing the signals of the butyl bridge.



Structure B-5: 4,4'-dimethoxy-2,2'-butyl bridged biphenyl

Due to the high activation barrier observed, a separation of the two atropisomers should be possible, as described in literature¹¹. To be able to separate such isomers a rotation barrier in a range of 80 – 120 kJ/mol at 300 K is required.^{11–13} For this system dynamic HPLC turned out to be the method of choice. A plateau was obtained for all compounds during the dynamic HPLC experiments using a Chiralpak AD-H column (Figure B-17). The temperature dependent experiments were performed in a range of 283 - 308 K in 5 K steps using *i*PrOH/*n*-hexane mixtures of 97:3 for **2a**, **2b**, **2d-2f** and 95:5 for **2c**. The different elution profiles are shown in Figure B-17.

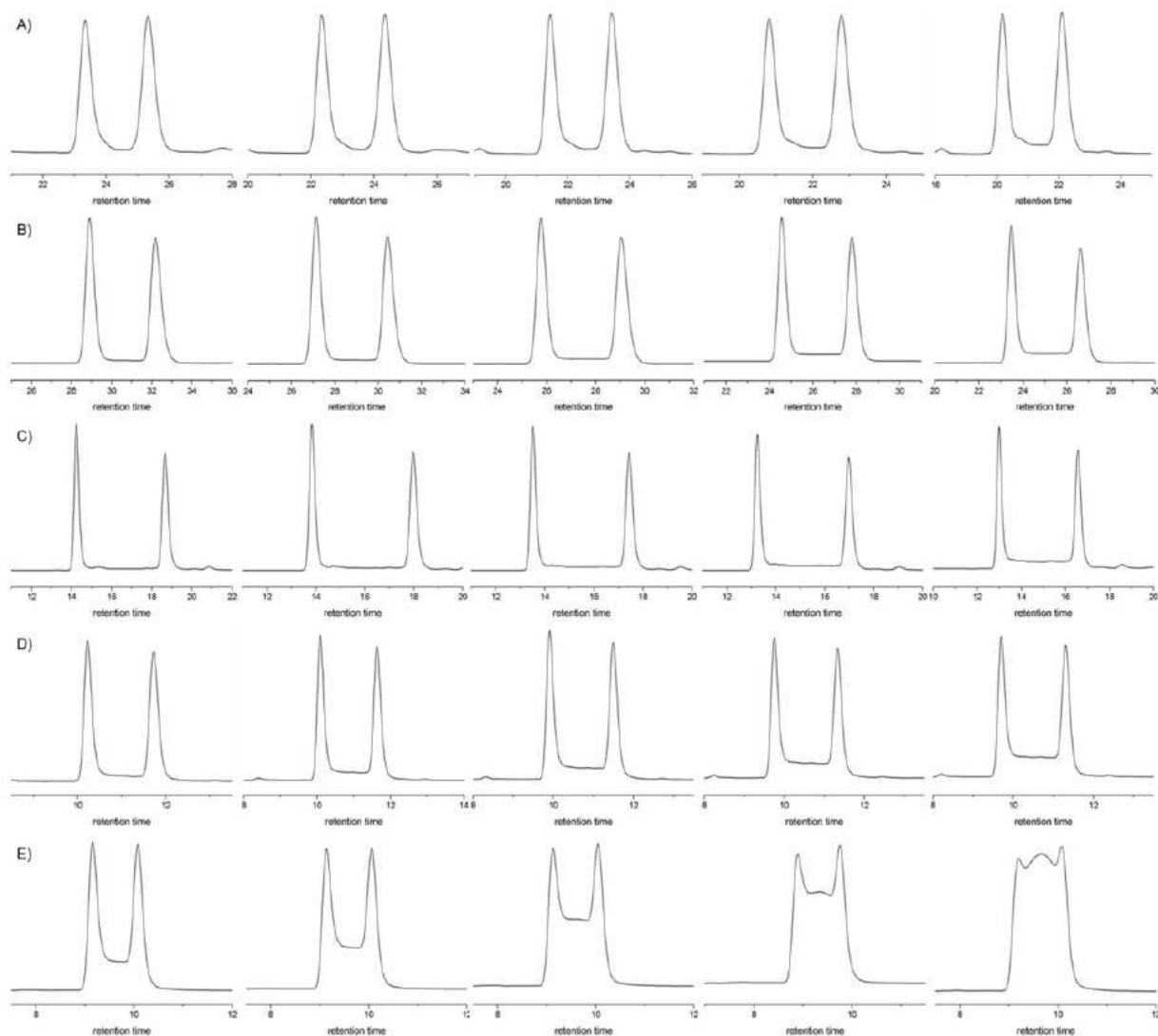


Figure B-17: Dynamic HPLC elution profiles of the A = 2a, B = 2b, C = 2c, D = 2e, E = 2f, on an amylose coated Chiralpak-ADH column at different temperature starting at 288 K (left) ending at 308 K (right) in 5 K steps.

For determination of the thermodynamic data the software DCXplorer was used and the rate constants calculated. Three different processes are taking place during the separation 1.) Equilibrium between of the two atropisomers between the mobile and stationary phases in the presence of a chiral column, 2.) Reversible first order enantiomerization on the chiral surface, 3.) Shifting of the mobile phase to the next plate. These three processes allow the direct relation between rate constants and the peak heights. The experimental details are described in the thesis of Jürgen Rotzler.⁵⁰ The thermodynamic data obtained by dHPLC are summarized in Table B-15.

Table B-15: Thermodynamic data obtained from dynamic HPLC measurements. All experiments were performed four times and the averaged value are presented.

Compound	ΔG^\ddagger / kJ/mol	ΔH^\ddagger / kJ/mol	ΔS^\ddagger / J/(molK)
2a	96.75 ± 0.12	47.11 ± 6.2	-166 ± 21
2b	96.29 ± 0.04	51.42 ± 0.8	-150 ± 3
2c	94.31 ± 0.05	49.30 ± 1.2	-151 ± 4
2d	90.30 ± 0.20	54.50 ± 4.0	-120 ± 14
2e	92.22 ± 0.04	45.50 ± 0.4	-157 ± 2
2f	89.52 ± 0.03	42.48 ± 0.4	-158 ± 2

Theoretical calculations were performed in the same way as described before for the propyl-bridged biphenyls to gain deeper insights into the mechanism of the isomerization. Valid data for all measured compounds except for the push pull system **2d** could be generated. The calculated thermodynamic data are shown in Table B-16.

Table B-16: Computationally calculated Gibbs free activation energy $\Delta G^\ddagger_{\text{theo}}$ (kJ/mol), $\Delta H^\ddagger_{\text{theo}}$ (kJ/mol), and $\Delta S^\ddagger_{\text{theo}}$ (J/(mol*K)) for the series of experimentally measured butyl bridged biphenyls except the push-pull system.

Compound	$\Delta G^\ddagger_{\text{TPSS}}$	$\Delta H^\ddagger_{\text{TPSS}}$	$\Delta S^\ddagger_{\text{TPSS}}$	$\Delta G^\ddagger_{\text{B3LYP}}$	$\Delta H^\ddagger_{\text{B3LYP}}$	$\Delta S^\ddagger_{\text{B3LYP}}$
2a	92.8	90.4	-7.9	101.9	99.9	-6.7
2b	91.0	88.7	-7.6	100.5	98.7	-6.1
2c	93.1	90.4	-9.0	101.7	100.4	-4.0
2e	88.6	86.2	-7.7	97.8	95.9	-6.3
2f	84.0	82.5	-5.3	94.5	93.2	-4.4

The DFT calculated Gibbs free activation energies were again close to the experimental values (same trend, little offsets), which validates the transition states and the reaction mechanism. On the other hand the differences in the activation enthalpy and activation entropy are even stronger than for the propyl bridged biphenyls.

These discrepancies could be explained by the different experimental set ups. Indeed, DFT calculations are performed for molecules in the gas phase, NMR experiments are performed in solution whereas dHPLC experiments were performed

in a mixture of mobile and stationary phase. To get an idea of the effect of the different media it would be great to investigate at least one sample with all three methods. As mentioned before it is not possible to perform dHPLC for molecules with an activation barrier below 80 kJ/mol. The only way to compare the theoretical calculations with two experimental methods on the same molecule would be high temperature NMR. To get an idea of the temperatures required, the coalescence temperatures were recalculated from the thermodynamic data obtained by dHPLC and the chemical shift difference at rt. of the corresponding NMR spectra (Table B-17).

Table B-17: Calculation of the Coalescence Temperatures for the molecules measured by dynamic HPLC.

Compound	$\Delta G^{\ddagger}_{\text{dHPLC}} / \text{kJ/mol}$	Δv_{exp}	$T_{\text{c-predicted}}$
2a	96.75 ± 0.12	431 Hz	505 K
2b	96.29 ± 0.04	418 Hz	502 K
2c	94.31 ± 0.05	356 Hz	489 K
2d	90.30 ± 0.20	---	---
2e	92.22 ± 0.04	328 Hz	477 K
2f	89.52 ± 0.03	297 Hz	462 K

From Table B-17 it is obvious that the coalescence temperatures for donor and acceptor substituted molecules are extremely high and special high-temperature NMR equipment would be required. For compound **2e**, high temperature NMR experiments up to 410 K were performed without destroying the molecule. Special equipment for high temperature experiments up to 500 K was not available. For detailed NMR analysis at least 500 K would be necessary for line shape analysis with high accuracy, as also the fast exchange regime has to be covered.

Therefore we focused on 3,9-dimethoxy-5,5,7,7-tetramethyl-5,7-dihydrodibenzo-(c,e)oxepine as candidate for both analytical methods as an Gibbs free activation energy between the propyl- and butyl-bridged biphenyls was predicted.

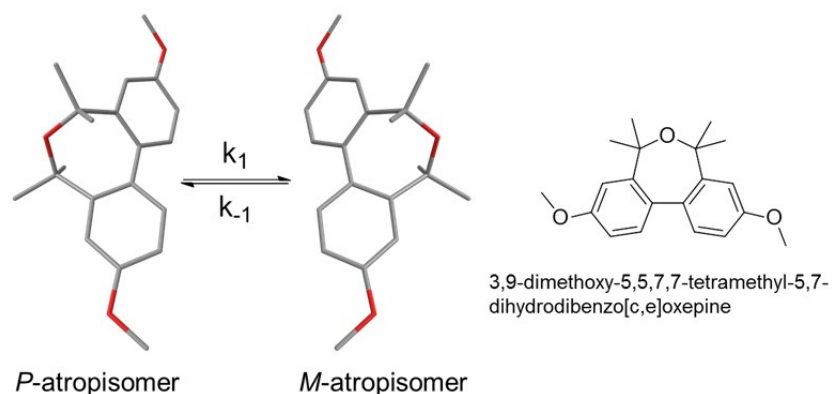


Figure B-18: Schematic representation of the two atropisomers of dihydrodibenzo(c,e)oxepine.

High temperature NMR experiments were performed and a coalescence temperature of 314 K determined. The resulting Gibbs free activation energy $\Delta G^\ddagger = 59.5$ kJ/mol was higher than for the propyl bridged compounds but unfortunately far too small to allow separation on a HPLC column.

B.5 Discussion

In the presented work three different types of 2,2'-bridged-4,4'-substituted biphenyls were investigated by dNMR spectroscopy, dHPLC chromatography and DFT calculations. The two experimental methods were used to validate the output of the DFT calculations.

Oki et al.²¹ demonstrated that the rotation of ethyl bridged biphenyls is quite fast and only 5- or 5,5'-substituted ones showed an increased activation barrier suitable for NMR measurements. We tried to extend this series to 2,2'-ethyl-4,4'-substituted biphenyls by the usage of lanthanide shift reagents. We could show that an increasing amount of shift reagent leads to stronger pseudo contact shifts but unfortunately the coalescence could not be reached for any of the measured concentrations. The main problem is most likely the distance and the geometry between the coordination group and the ethyl bridge. The influence on all protons of the ethyl bridge is quite similar as the distances from the lanthanide to the two protons are similar. Additionally, coordination from both sides of the molecule is possible leading to average and similar PCS on both sides. Variable temperature experiments in toluene demonstrated, that at lower temperatures a strong shift of up to 180 Hz for all four protons was induced. On the other hand it remarkable that increasing concentrations at constant temperature led to weak shift differences. This

means that the influence of the lanthanide shift reagent to the chemical shift difference on the two sides is rather small and only the increased paramagnetic strength at lower temperatures leads to stronger shifts. A successful study of 2,2'-ethyl-bridged-4,4'-disubstituted biphenyls was therefore not possible with dNMR spectroscopy.

In contrast to the ethyl-bridged biphenyls, the atropisomerization process of 2,2'-propyl-bridged-4,4'-disubstituted biphenyls was successfully monitored by dynamic NMR spectroscopy and theoretical calculations. The results obtained for the unfunctionalized compound **1h** fit quite nicely to results obtained by Sutherland et al.²³ **L3a** and the difference is within the experimental error. For the series of oxepins (Table B-1) it was shown as the activation energy is lower (**L1a**) and reaches comparable values to the propyl bridged molecules if steric demand on the bridge is introduced (**L1d**). The introduction of an additional substituent in the 5 position led to a tremendously increased activation energy of about 70-85 kJ/mol. In the series of measured thiopins the activation energy is in a range of 70-77 kJ/mol and therefore higher than for propyl bridged biphenyls. The di-H compound (**L2c**) and the di-F compound (**L2d**) showed more or less the same activation energies, this is also true for our analogues **1g** and **1h**. The series of sterically demanding molecules **L5a-p** showed activation energies between 70 and 80 kJ/mol. In this case they found that the push-push substituted molecules show much lower activation energy than the pull-pull substituted. The same effect was observed for propyl- and butyl-bridged biphenyls. It was demonstrated that substituents in 4 and 4'-position can be used for fine-tuning of the activation barrier whereas the change of the substituents in 2,2'-position led to changes of the activation energy in the order of 20-40 kJ/mol. We further showed by dHPLC that the butyl-bridged biphenyl **2a-e** have larger activation energies than 2,2'-di substituted biphenyls **L5a-p**.

The main objective of this project was to investigate the influence of substituents with different strength on the activation energy of the atropisomerization of bridged biphenyls with different chain length. Therefore, the resulting Gibbs free activation energies were plotted against the Hammett-parameter σ_p (Figure B-19). The Hammett σ -parameter represents the resonance and inductive effect in such a system and is therefore a good measure of the total electronic effects. This means that the σ -

parameter shows the ability of the substituents to donate or to accept electrons to the C1-C1'-bond of the biphenyl. To gain accurate parameters for 4,4'-di substituted biphenyls, the σ -parameters of each of the two substituents were summed up as demonstrated earlier by Hart⁶⁴ and Wirz⁶⁵. Influences of the different bridges were not investigated, as they are constant all over the series. It was possible to directly correlate the Hammett parameters to the Gibbs free activation energy ΔG^\ddagger as the ΔG^\ddagger is correlated with its logarithm to the rate constant. The Hammett diagram delivers insights into the effect of the substituents on the transition state. A linear relationship allows the assumption that all molecules isomerize with the same mechanism. The di-H compound **1h** was used as internal reference and therefore no normalization required. A Hammett diagram for the propyl bridged biphenyl **1a-l** is shown in Figure B-19.

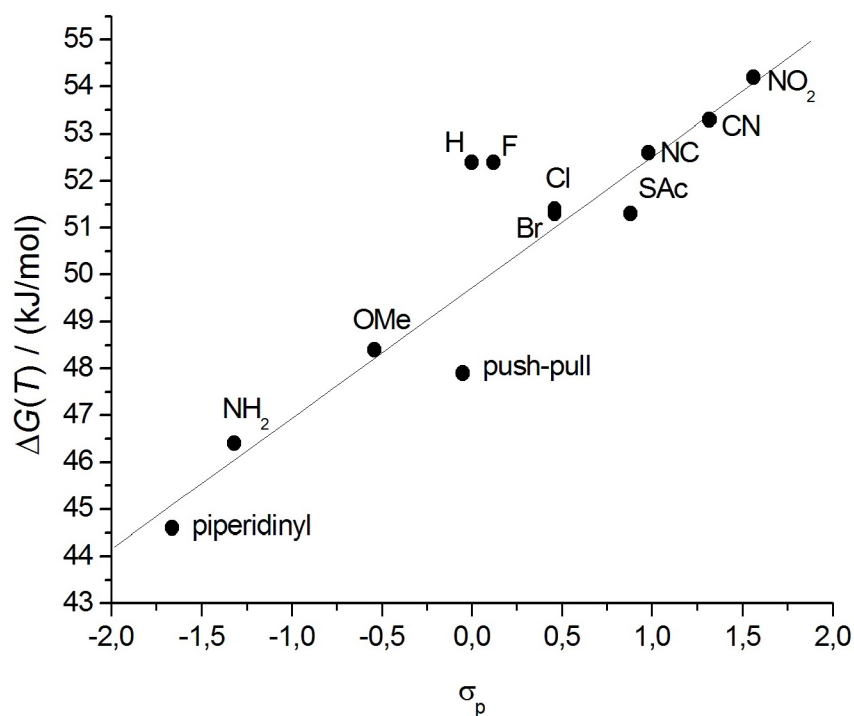


Figure B-19: Hammett diagram (Correlation of the σ -parameter vs. Gibbs free activation enthalpy ΔG^\ddagger) of the propyl-bridged biphenyls **1a-l**.

The Hammett correlation diagram shows clearly a linear dependence between the Gibbs free activation energy and the σ -parameter. This result indicates that the atropisomerization process is depending on the electron density at the central C1-C1'-bond. This linear relationship allows now the prediction of the rotation barrier of other substituents as a high electron density leads to lower activation energies and reduction of the electron density leads to an increase of the activation energy. The slope of the Hammett diagram is a measure for the sensitivity of the system to the

electronic effects. In our case the slope ($\rho = 2.99$) is quite steep, that means that the rotation process is strongly influenced by the electronic configuration. The almost linear relationship between all compounds gives strong evidence that all compounds follow the same rotation mechanism. A deeper insight into the origin of the electronic effects can be gained by splitting the σ -parameter into two separate effects, namely the field/inductive effect (F) and the resonance effect (R) as it was shown by Swain and Lupton.⁶⁶ The inductive effect gives information about the polarisation of the σ -bond in the substituent and is strongly distance dependent whereas the resonance effect gives a description of the π -interactions.

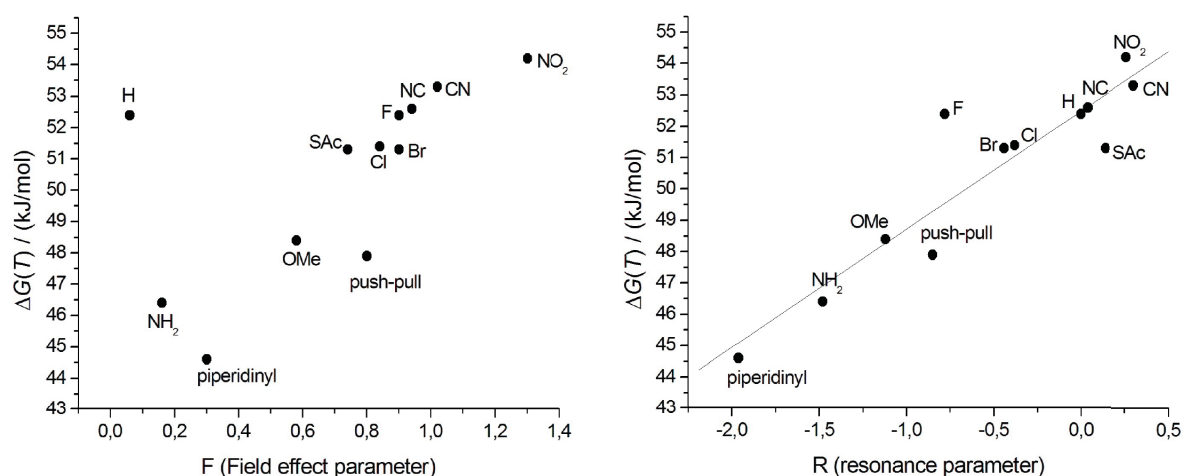


Figure B-20: Representation of the Hammett-plot of propyl-bridged biphenyl separated in their field effect (F) (left diagram) and their resonance effect (R) (right diagram).

The field parameters and the resonance parameters can be correlated to the Gibbs free activation energy in a similar way. The result of these correlations are presented in Figure B-20. It is obvious that the data fit much better to the resonance parameter than to field parameter. This correlation demonstrates that the substituents mainly influence the π -system. This finding is in contrast to the mechanisms published earlier where a partial rehybridization of the central C1-C1'-bond was postulated, which should deliver a high agreement with the field parameter (F).²⁶

Line shape analysis delivered insights into the thermodynamics of the system. Therefore the calculated rate constants were correlated in Eyring plots to the temperatures delivering directly the enthalpy and entropy of this process (Table B-8). Table B-8 indicates that the enthalpy mainly influences the rotation process. It was observed that the influence of the enthalpy is decreased as stronger the electron donating ability of the substituents in 4,4'-position are (push-push-system). The enthalpy is the energy required to reach the transition state. The generated enthalpy

values can be correlated in a same way as the Gibbs free activation energies to the Hammett-parameter.

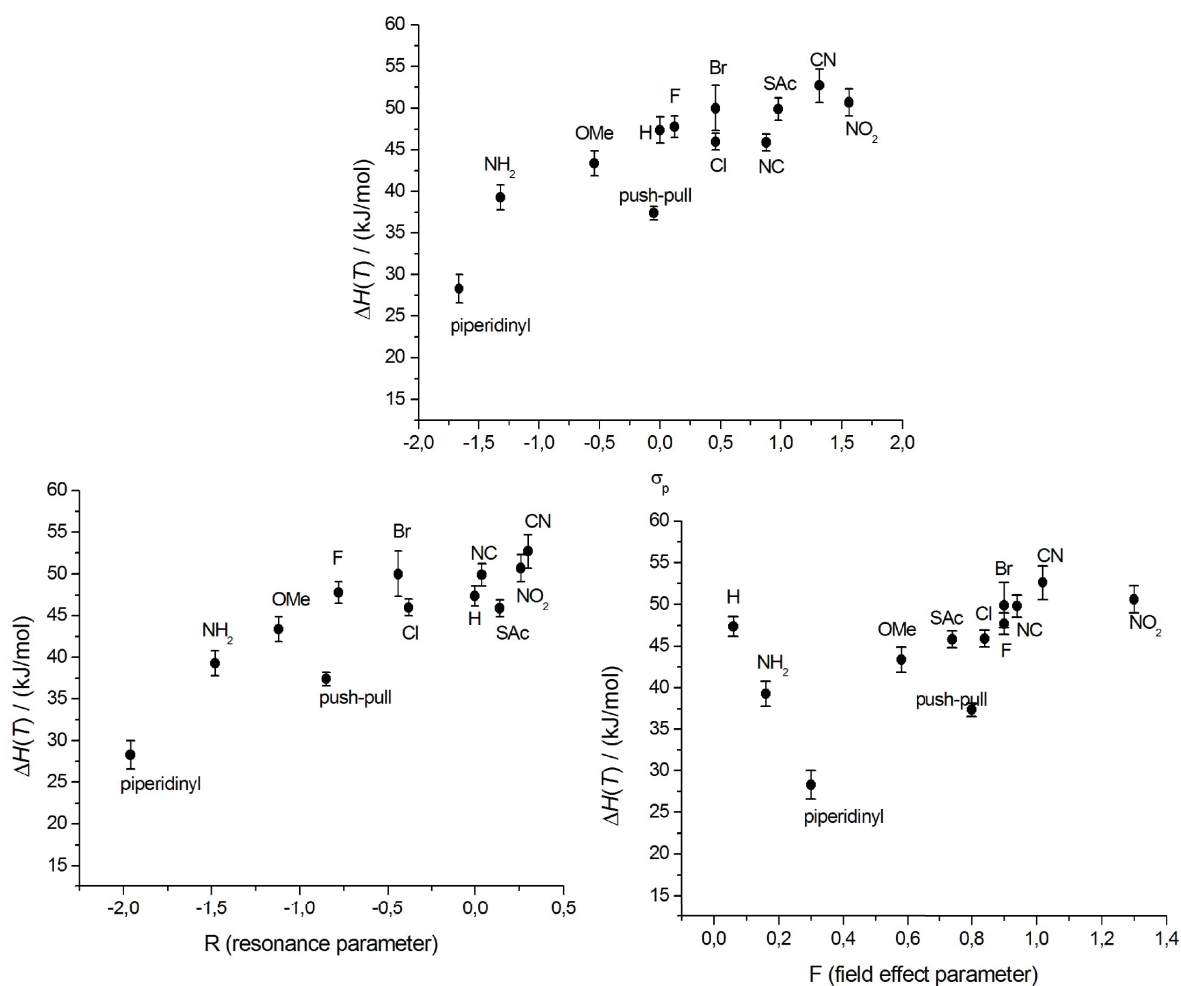


Figure B-21: Hammett-diagrams, correlation of the enthalpy ΔH^\ddagger vs Hammett-parameter σ (top), the resonance parameter R (bottom left) and the field effect parameter F (bottom left).

A similar trend is observed for the σ -parameter and the R-parameter for the activation enthalpy (Figure B-21) but the deviations from linearity are stronger compared to the results obtained the Gibbs free activation energy. Exactly the same situation is present for the activation entropy ΔS^\ddagger as shown in Figure B-22. The results of the shown Hammett correlations deliver some insights on the inversion mechanism. The linear relationship between the Gibbs free activation energy and the resonance parameter R indicates that the main influence on the activation energy of 4,4'-di substituted biphenyls for the rotation around the C1-C1'-bond is dominated by the π -distortion of the system. This gives strong evidence of a planar transition state. This means on the other hand that the activation energy of the system is mainly influenced from the electron density around the C1-C1'-bond. As conclusion from the

trend observed for substituents, a partial negative charge at C1 seems to be most likely for strong donors, whereas a positive charge is possible for strong acceptors.

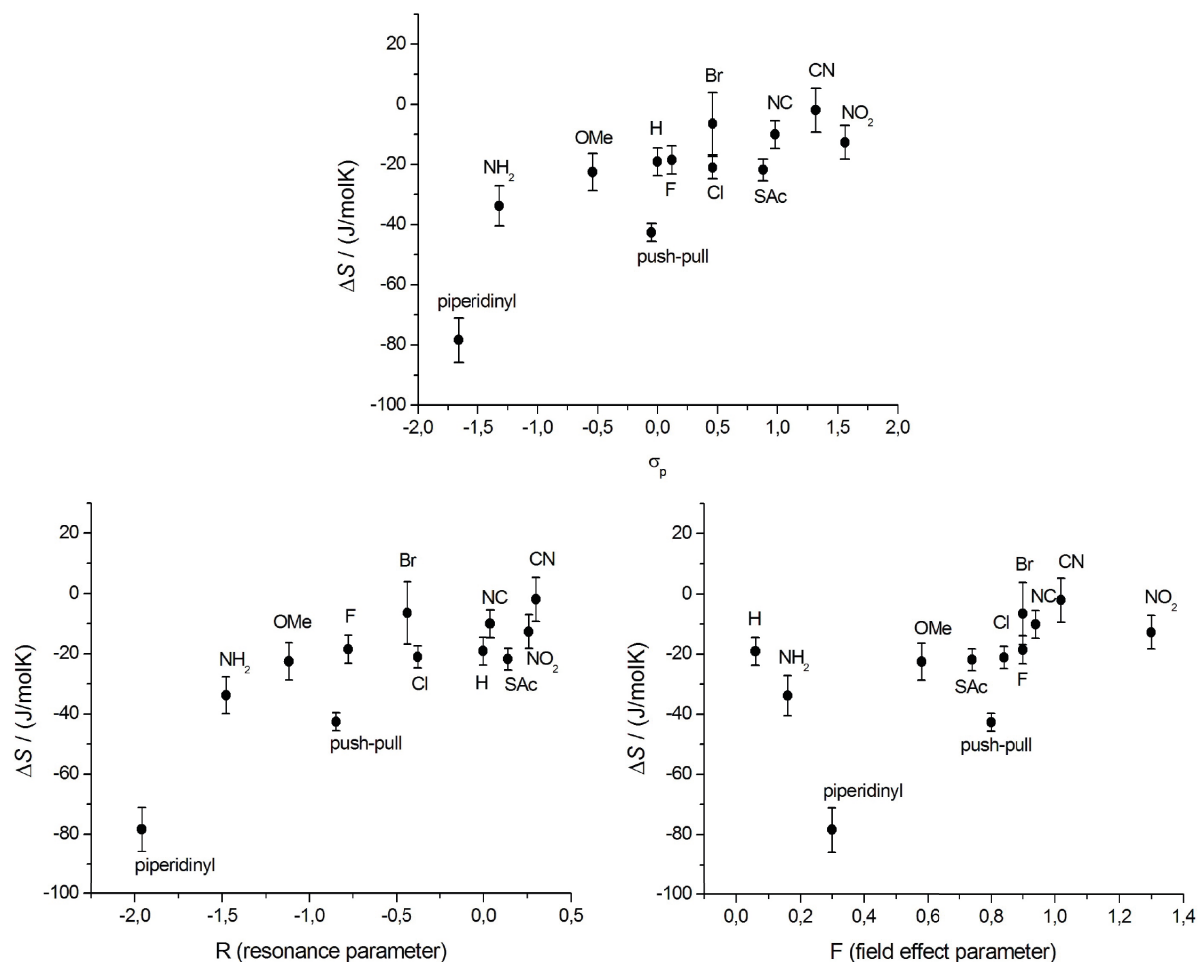


Figure B-22: Hammett-diagramms, correlation of the entropy ΔS^\ddagger vs Hammett-parameter σ (top), the resonance parameter R (bottom left) and the field effect parameter F (bottom left).

As shown before, the experimentally determined Gibbs free activation energies are in good agreement with the theoretically determined ones (Table B-11). A graphical representation is shown in Figure B-23. A linear relationship was obtained for all, but for the different density functions an offset can be observed. The calculated energies for the donor substituted fit best for the TPSS functional whereas the best fit for the acceptors is obtained by the B3LYP functional. The BP86 functional delivers overall energies lying slightly below the experimental ones. The high agreement between experiment and calculation validates the calculated rotation mechanism. The calculated mechanism shows only one transition state (Figure B-24) where the two phenyl rings are planar, the CH₂-group in the middle of the bridge is out of plane but the molecule is no longer linear. The equilibrium state of the molecules shows C₂ symmetry. Therefore, the two *ortho* CH₂-groups of the bridge have to pass by each

other to overcome the transition state, this seems to be the crucial factor dictating the inversion energy.

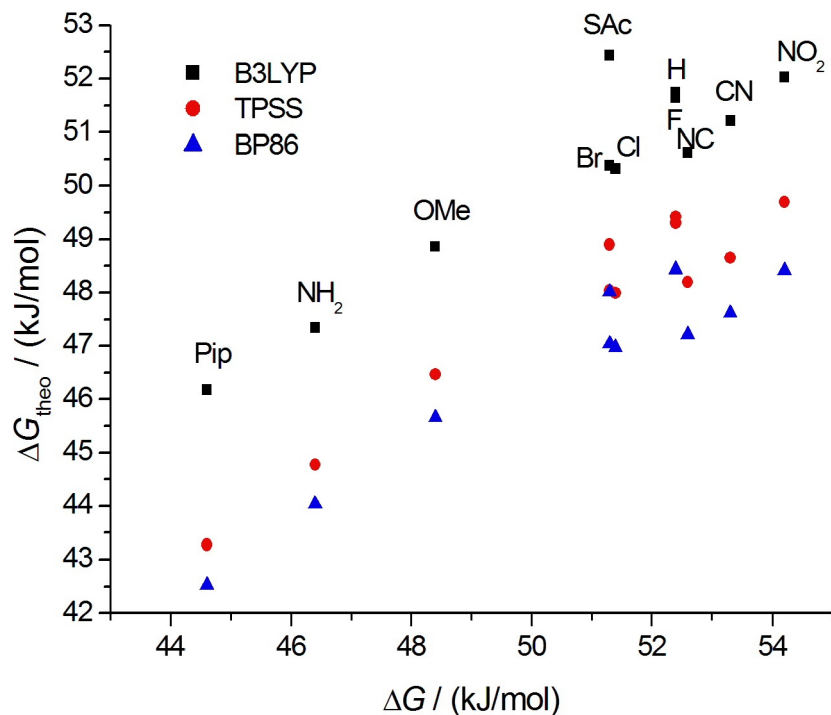


Figure B-23: Comparison of the Gibbs free activation energies ΔG^{\ddagger} for the propyl-bridged biphenyls obtained by dynamic NMR spectroscopy and DFT calculations.

The bond between the C1-C1' is elongated in the transition state (151-152 pm) compared to the ground state (148 pm), whereas the distance between H6-H6' is decreased as a bending of the two phenyl rings occurs. The elongation in the transition state is depending on the Gibbs free activation energy calculated for the different molecules. Therefore, the distance is dependent on the substituents.

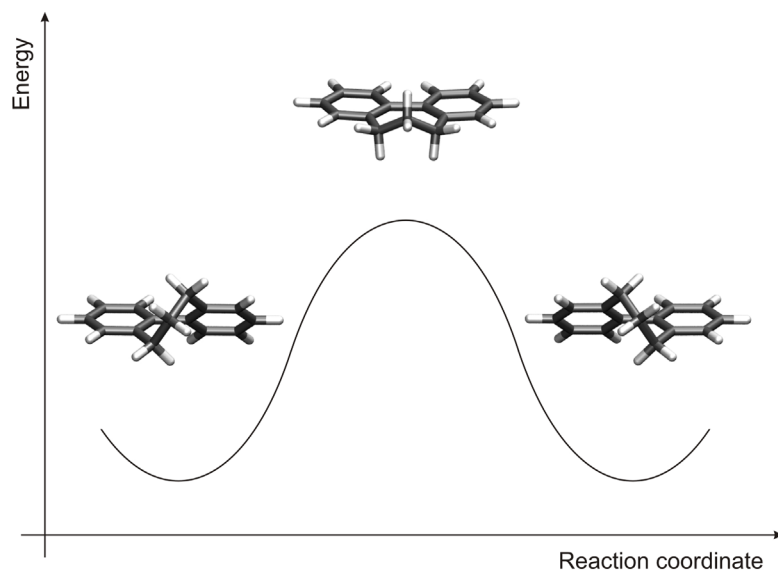


Figure B-24: Calculated atropisomerization mechanism of propyl-bridged biphenyls.

The changes of the bond distance are small for electron donors and stronger for electron acceptors (Figure B-25). This means that lower activation energies also correspond to shorter distances of the two phenyl rings in the transition state. The length of a chemical bond is strongly related to the electron density of this bond. The elongations are represented in the Gibbs free activation energy, which are in good agreement with the measured experimental data.

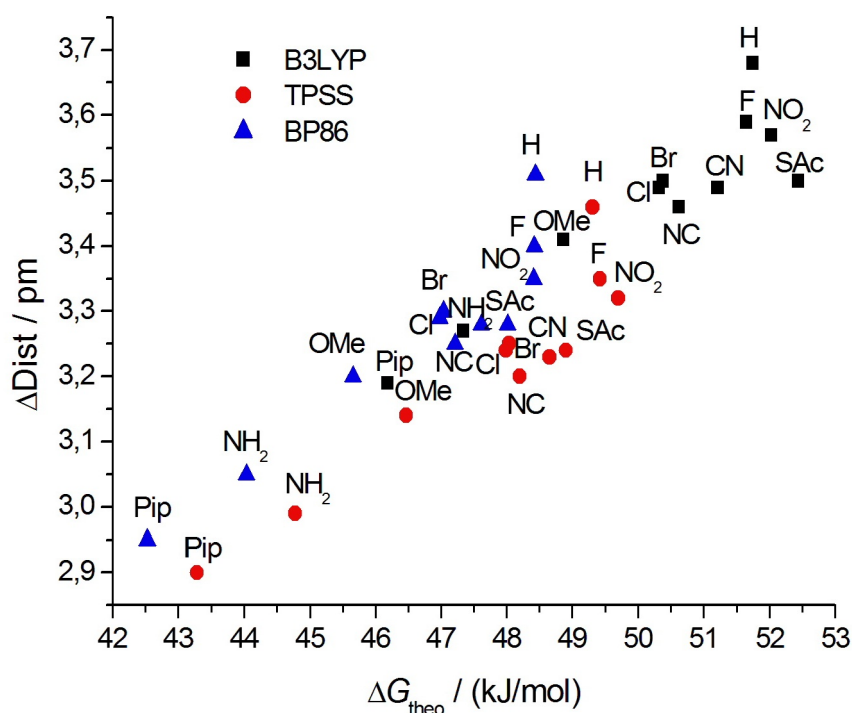


Figure B-25: Calculated Gibbs free activation energies ΔG^{\ddagger} correlated to the transition state distances of the different propyl-bridged biphenyls.

This elongation of the central C1-C1'-bond gives further evidence for the postulated mechanism and forces the conclusion that the dominating factor for the rotation is the electron density at this bond. The elongation facilitates the rotation of the two phenyl rings as it additionally enlarges the space for the two sterically demanding CH₂-groups to pass by each other as it leads to stronger bending of the molecules. The push-pull system **1i** showed experimentally an extreme low activation energy. It can be postulated that partial positive and negative charges are located on each side of the bond. This would lead to a partial double bond with shorter distance between the two phenyl rings explaining the low activation energy.

The consistency of the experimental and theoretical values for the activation Enthalpy ΔH^{\ddagger} and Entropy ΔS^{\ddagger} are low compared to the Gibbs free activation energy ΔG^{\ddagger} . Especially for electron donating substituents a large deviation is obtained.

The main difference between the calculation and the experiment is the different surrounding of the molecules, whereas the calculations are single molecule calculations, the NMR measurements were performed as an ensemble in solution. On the other hand interactions with other biphenyls are also possible in the NMR experiment, which is excluded in the calculation of single molecules by DFT calculations. The interaction of different biphenyls was proven by NMR titration experiments of different concentrations and showed that no interactions are present. Therefore, the solvent effect was investigated for three different biphenyls in three different solvents. From Table B-13 it can be seen that changes in the Gibbs free activation energy are small whereas strong deviations for the activation enthalpy and entropy are present.

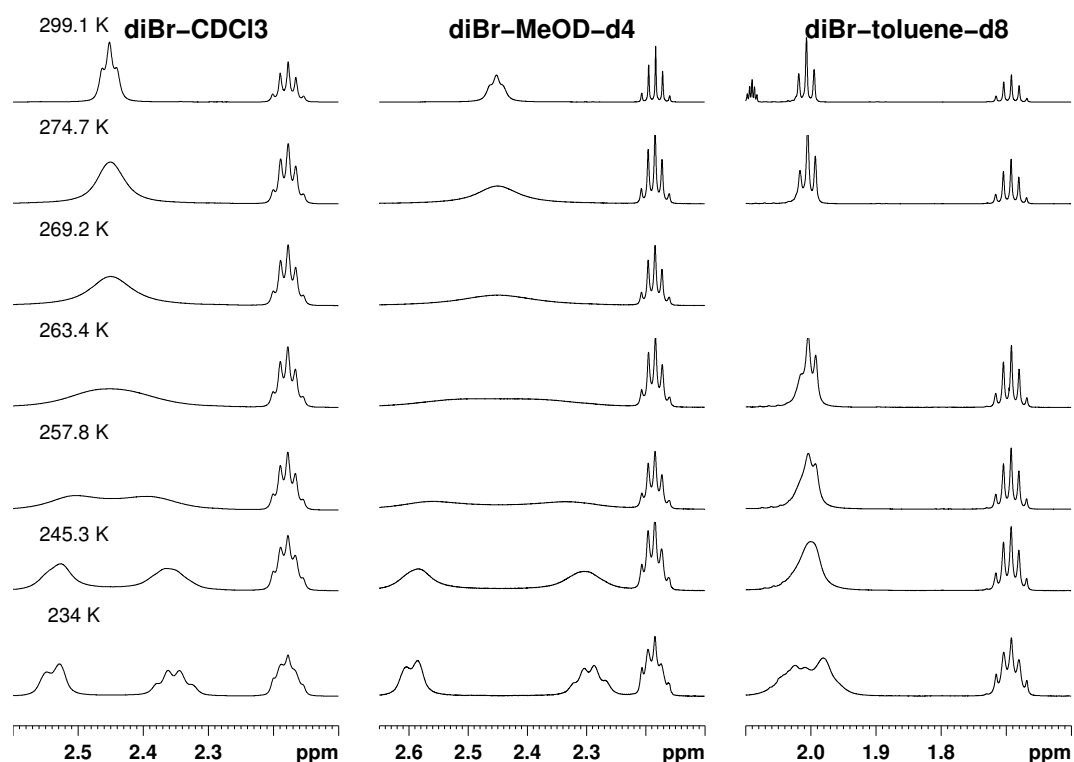


Figure B-26: Variable Temperature NMR of the neutral biphenyl **1e** in different solvents.

For electron accepting molecules, electron rich solvents like toluene show the strongest negative activation entropy values whereas for electron-donating molecules chloroform delivered the strongest negative activation entropy showing an opposite trend. This can be explained by the different electronic properties of the transition states. The electron donating molecules have an electron rich transition state with a partial negative charge on the C1-C1'-bond, which is stabilized by a protic solvent

leading to lowered activation enthalpy. For electron accepting molecules the situation is reversed, the transition state is partially positively charged. Electron rich solvents like toluene can stabilize this transition state more efficiently leading to a lowered activation enthalpy. This effect is changed in both cases for the activation entropy, as the Gibbs free activation energy remains constant. The resulting spectra of the variable temperature NMR are presented in Figure B-26, the coalescence temperatures vary tremendously but also the chemical shift difference in the slow exchange regime. The different combinations of chemical shift difference and coalescence temperature led to the same Gibbs free activation energy as shown for several molecules. This means that also a change of the solvent can help to make molecules accessible for dynamic NMR measurements.

The results of the butyl-bridged biphenyls **2a-f** are quite similar to those of the propyl-bridged ones. The introduction of one more CH₂-group in the bridge has a stronger effect on the activation barrier than the substituents in 4,4'-position. Indeed, the measured Gibbs free activation energies are in a range of 89 to 97 kJ/mol for the butyl-bridged ones whereas the energy for the propyl-bridged ones were in a range of 45 to 55 kJ/mol. The rotation barrier follows the same trend within the series of propyl-bridged so that the donor-substituted biphenyls show lower activation energy than the acceptors.

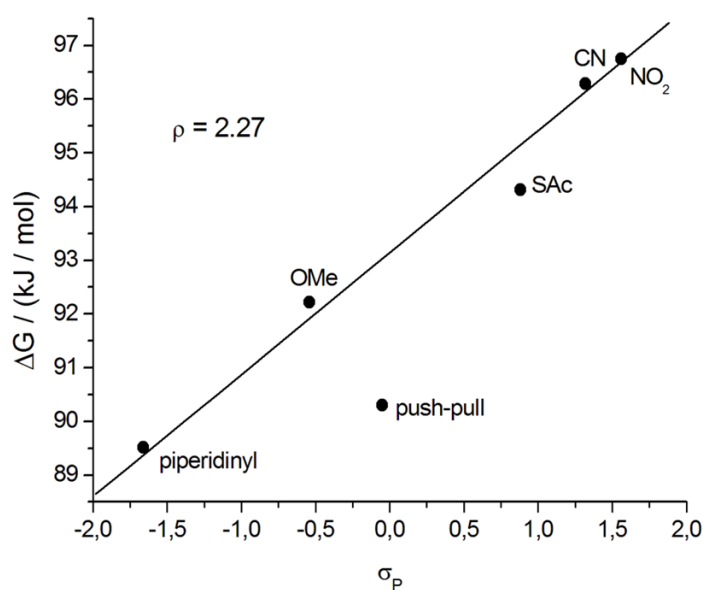


Figure B-27: Hammett-correlation of the atropisomerization energies of butyl-bridged biphenyls **2a-f**

The high degree of linearity obtained for acceptors and donors (Figure B-27) gives again strong evidence for a similar transition state throughout the series. Only the push-pull system **2d** shows a stronger deviation from linearity in the butyl case. The reasons for this are so far unknown, but a slightly different transition state seems to be possible for this molecule. If again a partial double bond can be assumed for this transition, then a more linear transition state could to be favoured explaining the difference to the other molecules. For the butyl-bridged system the slope of the resulting linear curve fitting is less steep ($\rho = 2.27$) compared to the propyl bridged molecules. This indicates that the electronic effect of *para*-substituents is less pronounced for butyl-bridged biphenyls but still significant. Again the σ -parameter was separated into the resonance parameter (R) and the Field effect (F) according to Lupton and Swain⁶⁶ to deliver insights on the origins of the electronic effects.

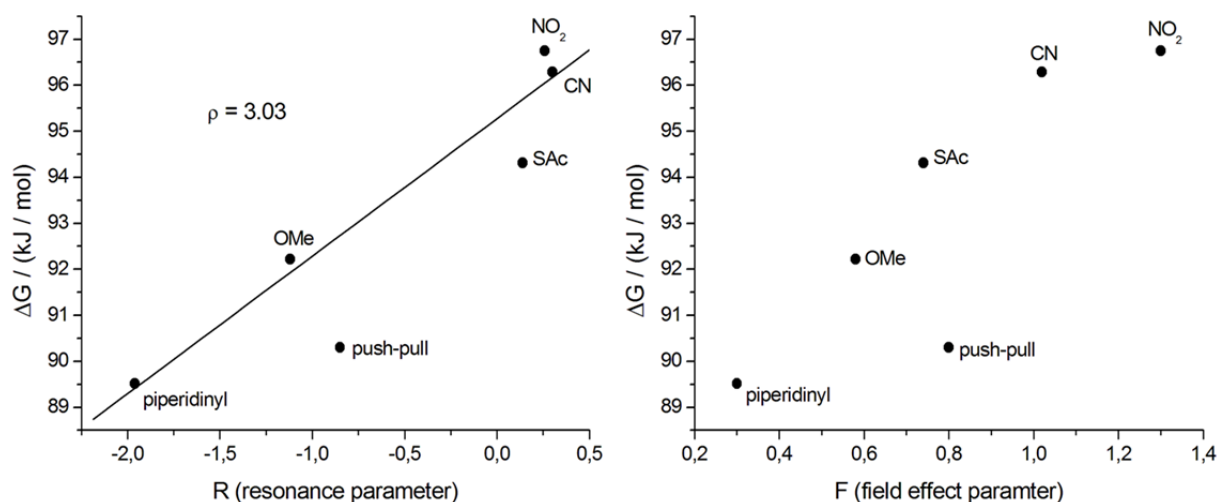


Figure B-28: Correlation of the Gibbs free activation energy ΔG^\ddagger of butyl-bridged biphenyls to the resonance parameter (left) and the field effect (right). The push-pull system was excluded for linear regression, as the reason for the strong deviation is not clear.

For the linear regression the push-pull system was excluded as from the σ -parameter a different transition state seems to be possible. For all others an almost linear correlation to the resonance parameter was obtained ($R^2 = 0.96$) and therefore again a strong influence from the π -skeleton suggested. This means that electronic effects again dominate the inversion process. In this limited series also a quite strong correlation to the field effect ($R^2 = 0.84$) was obtained. This suggests that in this case also the σ -skeleton is distorted in the transition state.

Comparison of the relationship between Gibbs free activation energy and its origin activation enthalpy and entropy indicated that for the butyl-bridged case the influence of the activation enthalpy (Figure B-29) is less pronounced than for the propyl-

bridged case. There are two possible reasons for the strong influence of the activation entropy to the transition state. Either the molecular structure has to be reorganized to reach the transition state or the separation technique itself is the reason. A strong interaction between the stationary phase of the column used and the eluted molecule can induce an orientation of the system leading to a strong entropy effect when the atropisomerization process takes place. The σ -parameter was again correlated to the activation enthalpy ΔH^\ddagger and the activation entropy ΔS^\ddagger .

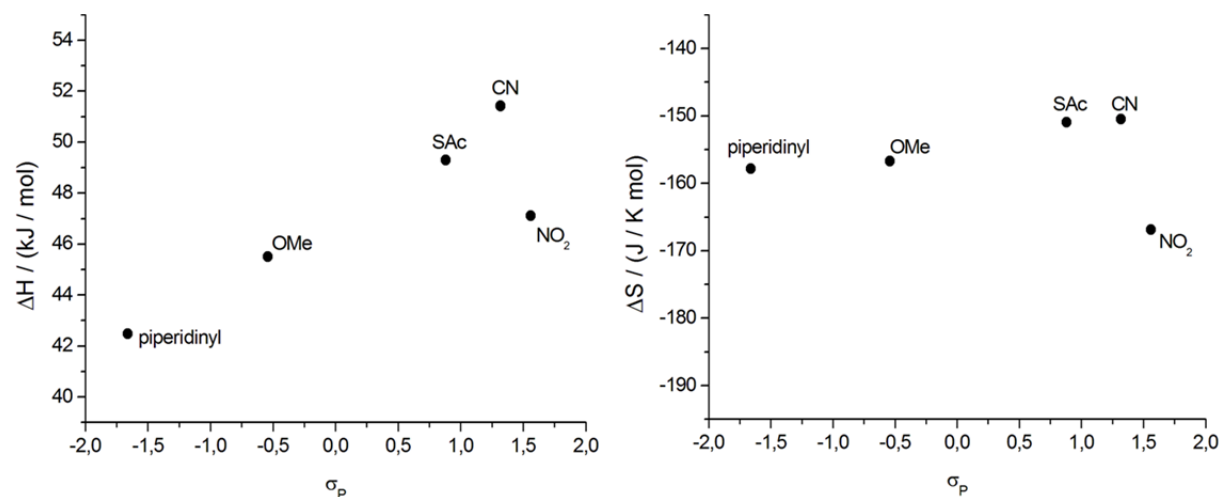


Figure B-29: Hammett diagram for the activation enthalpy ΔH^\ddagger and entropy ΔS^\ddagger for the series butyl-bridged biphenyls.

The Hammett correlation (Figure B-29) indicates that the activation enthalpy is dependent on the nature of the substituent in 4,4'-position, whereas the activation entropy remains mostly constant. This indicates that the electronic effect seems to be small for the entropy, and further supports the hypothesis that the high entropy values have their origin in the separation technique and not in the reorganization of the molecule for the transition state. Comparison of the experimentally obtained Gibbs free activation energies of the two different sets of biphenyls show the same trend for the different substituents (Figure B-30).

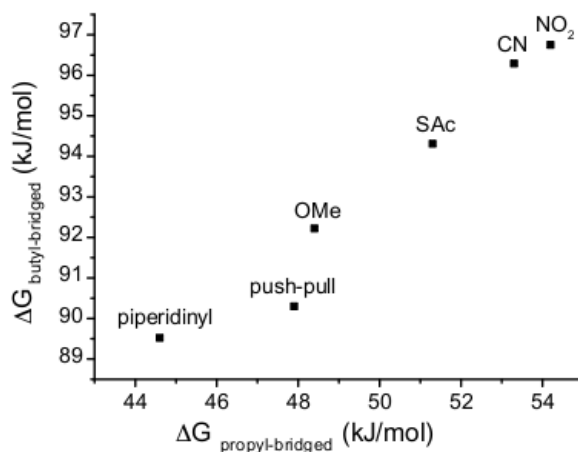


Figure B-30: Comparison of the Gibbs activation energies ΔG^\ddagger for the propyl- and butyl-bridged biphenyls.

To gain further insights into the atropisomerization process theoretical calculations were performed. The trends of the calculated Gibbs free activation energies are in good agreement to the experimental ones (Figure B-31). Nevertheless, they have a slight offset of the absolute values. The situation is slightly different when moving to the activation enthalpy and activation entropy. Whereas the activation enthalpy is the dominating factor in the calculations, it is only a minor factor in the experiments, which leads to strong deviations. Also the trend is different for the electron acceptors. As both methods deliver the same Gibbs free activation energies the differences in the activation entropy has to be strong as well.

The differences in the activation enthalpy and entropy between experiments and DFT calculation are most likely due to the different environments. The calculations are performed in vacuum where no interactions are taken into account. In the case of dHPLC the separation of the peaks and therefore the parameters for the evaluation of the thermodynamic data is due to interactions between the molecules, the stationary and the mobile phase. Some differences had already been observed between the NMR experiments and the DFT calculations for the propyl-bridged molecules. In that case the presence of interactions was confirmed by a study of the solvent dependence of the values. High temperature NMR experiments were not successful and therefore no data available for comparison. The similar results for the Gibbs free activation energies for donor and acceptor substituted molecules give strong evidence that the calculated transition state (Figure B-32) is valid for the whole series of butyl-bridged biphenyls.

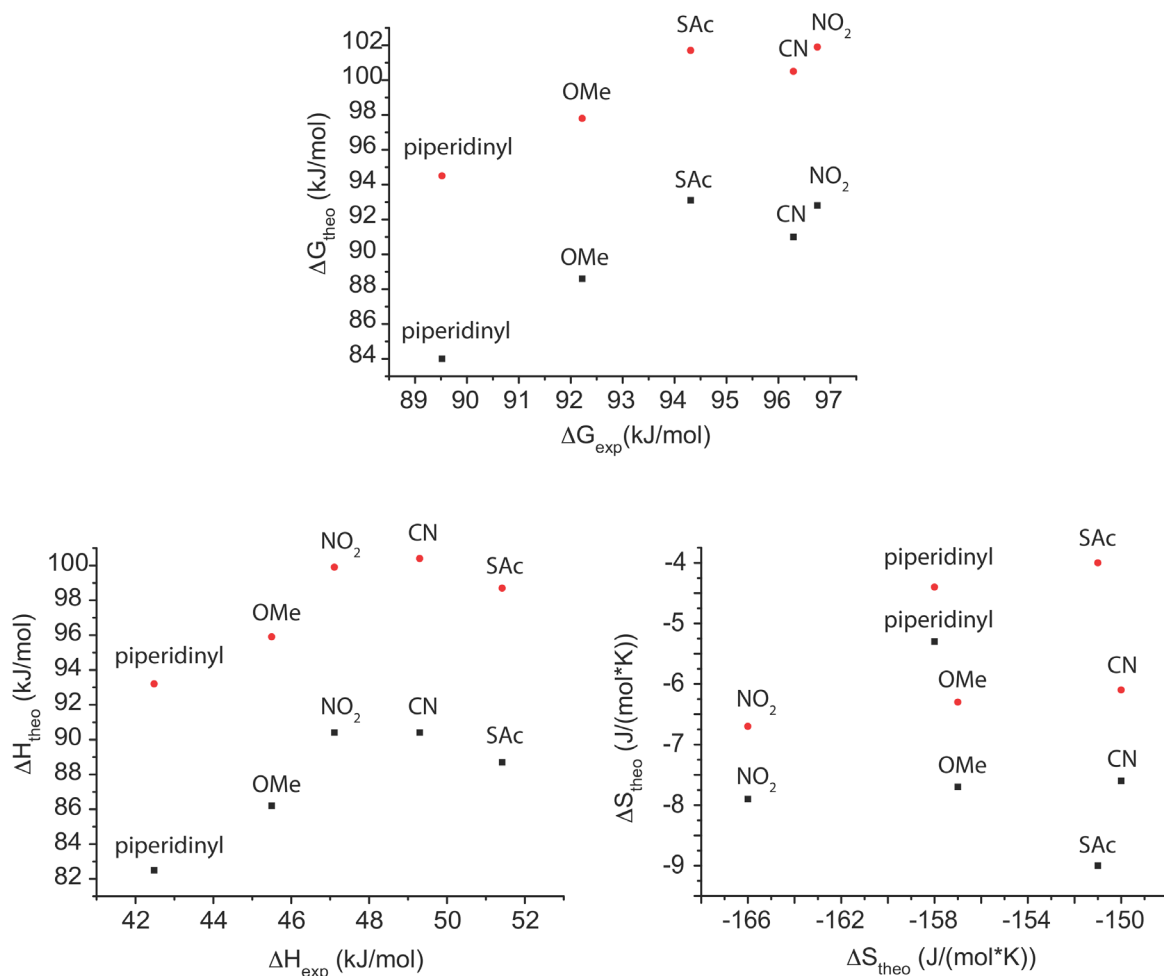


Figure B-31: Comparison of the experimental and calculated thermodynamic data for butyl-bridged biphenyls. The red coloured dots are for the TPSS and the black one for the B3LYP functionals. The comparison of the Gibbs free activation energy ΔG^{\ddagger} is shown on top, the comparison of the activation enthalpy ΔH^{\ddagger} is shown on the left hand side whereas the activation entropy ΔS^{\ddagger} is shown on the right hand side.

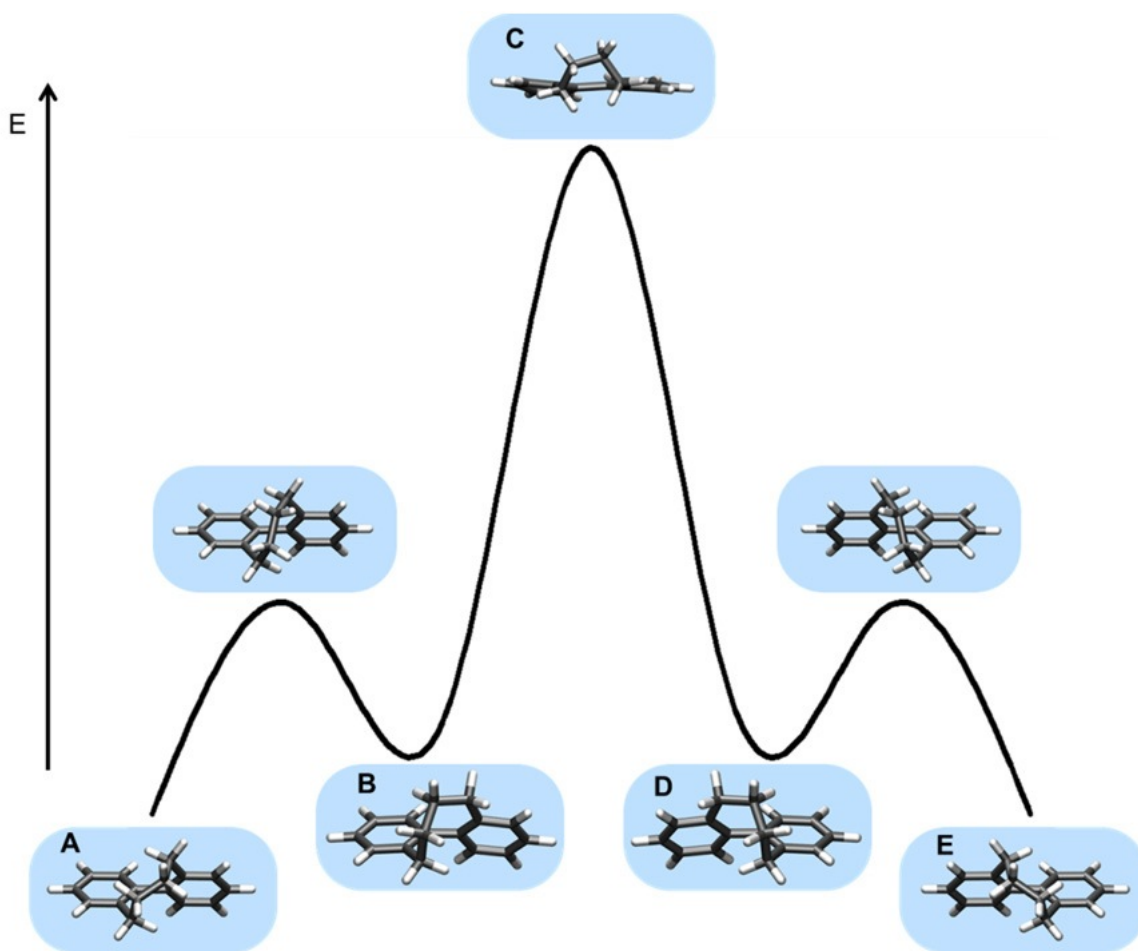


Figure B-32: Energy profile of the isomerization process of butyl-bridged biphenyls. The enantiomer **A** is converted to the intermediate **B** in a preequilibrium. Intermediate **B** is then able to reach the transition state **C** to undergo the inversion to intermediate **D**. **D** is then converted to the second isomer **E**.

The mechanism shows two transition states. Starting from the isomer **A/E** a first transition state is reached where the butyl bridge is distorted and intermediate **B** is formed. This preorganized state **B/D** is then able to undergo atropisomerization when the transition state **C** is reached. The transition state **C** is quite similar to the one obtained for the propyl bridged molecules. The two phenyl rings are in a plane and two CH_2 -groups are pointing out of this plane. The energies required for the interconversion of **A/E** to **B/D** are comparable for all molecules of the investigated series of butyl-bridged biphenyls whereas a strong deviation from **B/D** to **C** is observed. This means that the substituents are influencing mainly the second transition state **C** where the two phenyl rings are in one plane. This is again in high agreement with the Hammett correlations.

B.6 Conclusions

It was possible to study two different sets of 4,4'-disubstituted-2,2'-bridged biphenyls by different methods. The investigation of ethyl-bridged biphenyls by dynamic NMR measurements was not possible due to the small chemical shift differences and the low activation energies and therefore the predicted rotation barriers from Oki could not be confirmed.

In contrast to the ethyl-bridged biphenyls, the propyl bridged biphenyls **1a-1l** were investigated by dynamic NMR experiments at variable temperatures. Hammett correlations of the Gibbs free activation energy ΔG^\ddagger to the σ -parameter showed that the rotation process is strongly dependent on the electron density on the C-C bond. Separating the σ -parameter into its Resonance Parameter R and field effect F gave more insight. This allowed the conclusion that the π -electron density mainly influences the rotation barrier. The linear dependence of the whole series of propyl-bridged biphenyls indicated that the rotation processes have the same reaction mechanism. Density functional theory calculations delivered a planar and almost linear transition state. The resulting Gibbs free activation energies are in excellent agreement with the experiment supporting the reaction mechanism strongly. It was further shown that an elongation of the C1-C1'-bond is obtained in the transition state varying strongly with the nature of the para-substituents. Solvent dependent NMR experiments showed that a partial-negative charged transition state could be stabilized with protic solvents whereas electron rich solvents stabilized the partial-positive transition state.

The butyl-bridged biphenyls **2a-2f** were investigated by dynamic HPLC measurements. Hammett correlations of the Gibbs free activation energy ΔG^\ddagger to the σ -parameter showed that the rotation process is less dependent on the electron density on the C-C bond than the propyl-bridged ones. Separating the σ -parameter into its resonance parameter R and the field effect F showed that rotation barrier is influenced by the π -electron density as well as distortion of the σ -skeleton. For acceptors and donors the same reaction mechanism is predicted whereas a slightly different one for the push-pull system seems to be possible. DFT calculations delivered a reaction mechanism with two transition states. The second transition state shows higher activation energy and is therefore the rate limiting one. In this transition state the phenyl rings are in one plane and the two middle CH₂-groups are

pointing out of the plane. Large differences of the activation enthalpy and entropy are most likely explained by the different methods used for the calculation.

Comparison of the propyl-bridged and butyl-bridged biphenyls indicates that the para-substituents deliver energy changes in a range of 10 kJ/mol whereas the additional CH₂-group contributes about 45 kJ/mol. The para-substituents are therefore a valid tool for fine-tuning the activation energy.

B.7 Outlook

The influence of lanthanide shift reagents LSR will be investigated for the propyl-bridged biphenyls to get an idea how much the rotation barrier could be influenced. To access the rotation barrier of butyl-bridged biphenyls high-temperature experiments on specially equipped NMR spectrometers and high-pressure NMR experiments should be performed. These measurements are of special interest as the differences of activation enthalpy and entropy are extremely different for all three methods used in this investigation.

B.8 Experimental

B.8.1 Temperature Calibration

The temperature calibration was performed in a range from 298 to 223 K using a 4% MeOH in 96 % MeOD sample. Each temperature was measured three times and the average value was used as the new temperature. The experimental measured samples are shown in Figure B-33. The chemical shift differences of all measurements and the new temperature are shown in Table B-18. The corrected temperatures were calculated using Equation B-7 and Equation B-8.

Table B-18: Temperature calibration for temperatures between 298 and 223 K in 5 K steps.

$T_{\text{spectrometer}}$	$\Delta\nu$ in ppm	$T_{\text{corrected}}$	T_{average}
298	1.5046	299.08	
298	1.05045	299.09	
298	1.5052	299.01	299.1
293	1.5603	292.68	
293	1.5606	292.65	
293	1.5610	292.60	292.6
288	1.6138	286.54	
288	1.6140	286.52	
288	1.6144	286.47	286.5
283	1.6651	280.65	
283	1.6653	280.63	
283	1.6657	280.58	280.6
278	1.7162	274.78	
278	1.7165	274.74	
278	1.7168	274.71	274.7
273	1.7645	269.24	
273	1.7650	269.18	
273	1.7652	269.15	269.2

$T_{\text{spectrometer}}$	$\Delta\nu$ in ppm	$T_{\text{corrected}}$	T_{average}
268	1.8123	263.46	
268	1.8127	263.41	
268	1.8131	263.36	263.4
263	1.8571	257.86	
263	1.8574	257.83	
263	1.8578	257.78	257.8
258	1.9123	250.96	
258	1.9123	250.96	
258	1.9123	250.96	251.0
253	1.9581	245.24	
253	1.9574	245.33	
253	1.9572	245.35	245.3
248	2.0033	239.59	
248	2.0031	239.61	
248	2.0027	239.66	239.6
243	2.0480	234.00	
243	2.0477	234.04	
243	2.0473	234.09	234.0
238	2.0888	228.90	
238	2.0884	228.95	
238	2.0880	229.00	229.0
233	2.1265	224.19	
233	2.1301	223.74	
233	2.1256	224.30	224.1
228	2.1665	219.19	
228	2.1662	219.23	
228	2.1659	219.26	219.2
223	2.2073	214.09	
223	2.2059	214.26	
223	2.2057	214.29	214.2

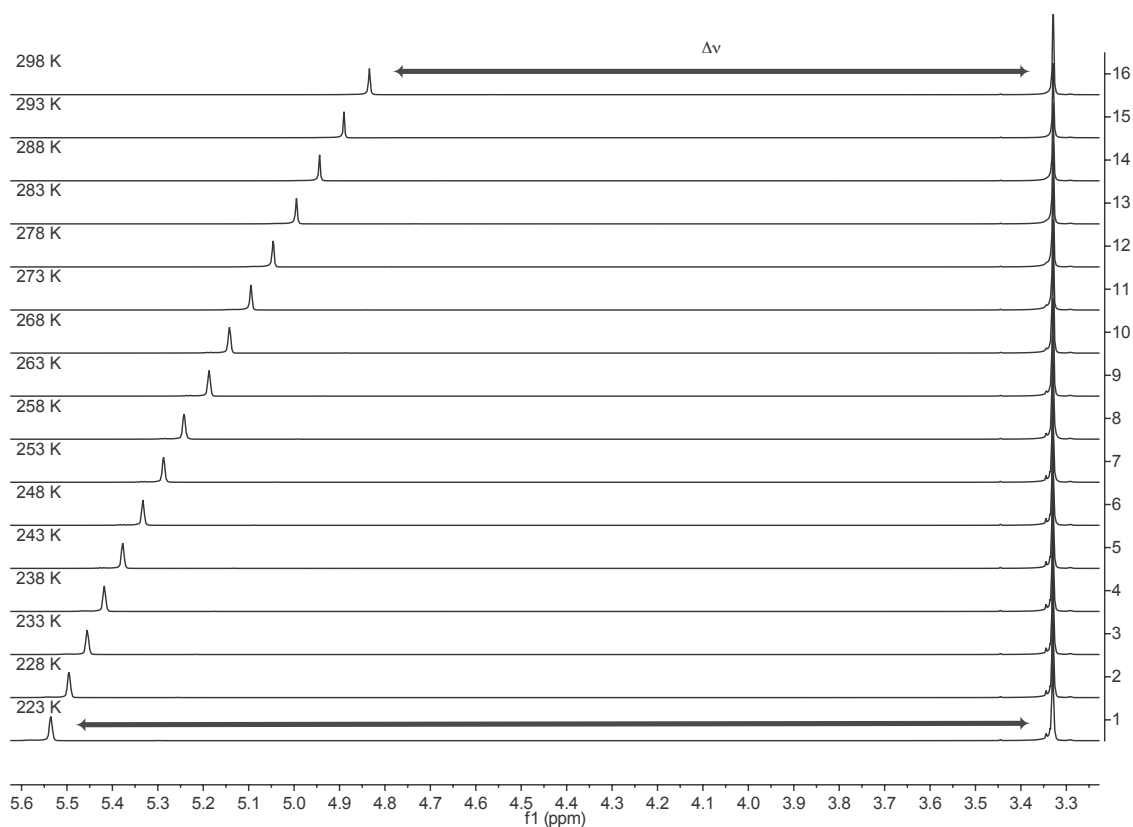


Figure B-33: Variable temperature NMR spectra of 4% MeOH in 96 % MeOD-d4 for calibration of the internal temperature.

B.8.2 Lanthanide shift reagents

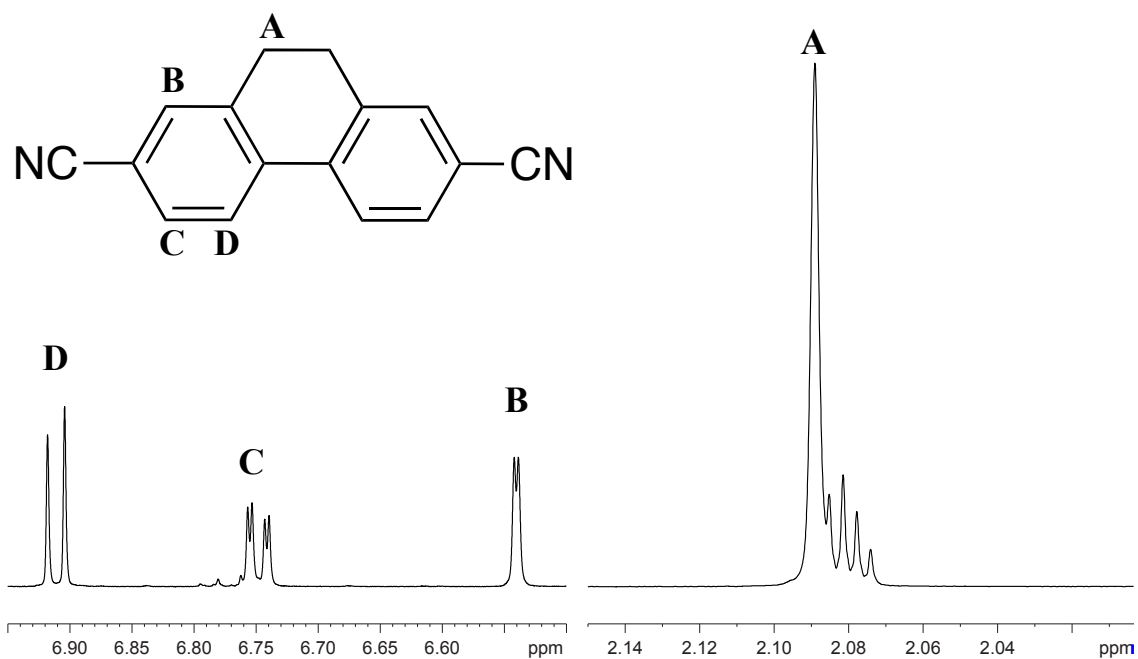


Figure B-34: NMR assignment of 4,4'-dicyano-2,2'-ethylbridged biphenyl in toluene-d8 at 298 K.

The LSR $\text{Eu}(\text{fod})_3$, $\text{Eu}(\text{hfc})_3$ and $\text{Pr}(\text{hfc})_3$ were purchased from Fluka and used without further purification. All samples were measured in CDCl_3 (99.9% D) purchased from Cambridge Isotopes. All samples were referenced to the residual solvent peak. The shim quality at temperatures below 250 K decreased due to paramagnetic relaxation enhancement.

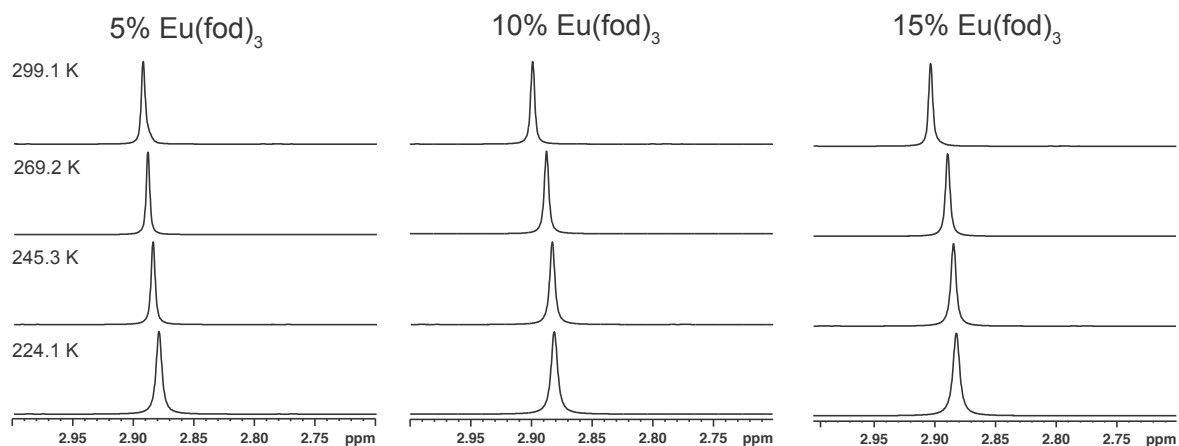


Figure B-35: Variable temperature NMR titration experiments of 4,4'-dicyano-2,2'-ethylbridged biphenyl with $\text{Eu}(\text{fod})_3$ as achiral lanthanide shift reagent

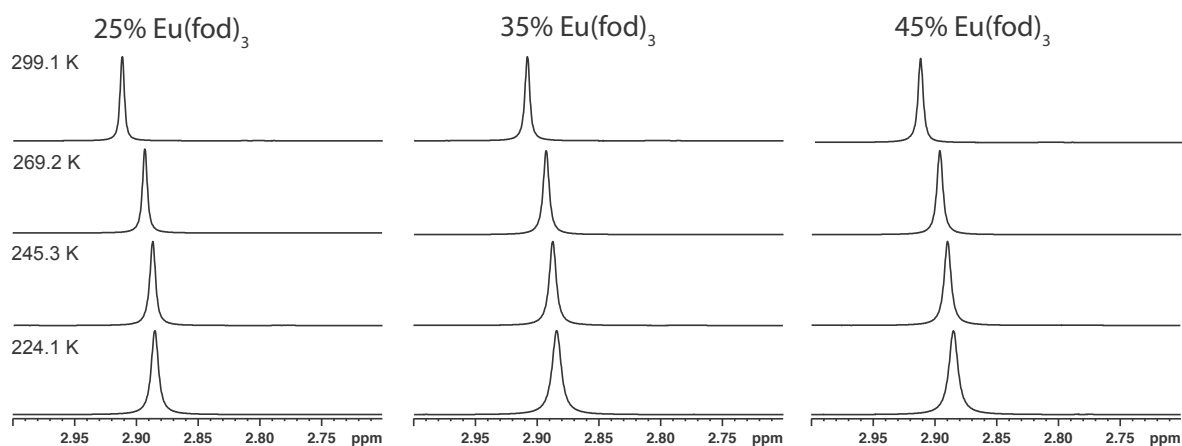


Figure B-36: Variable temperature NMR titration experiments of 4,4'-dicyano-2,2'-ethylbridged biphenyl with $\text{Eu}(\text{fod})_3$ as achiral lanthanide shift reagent.

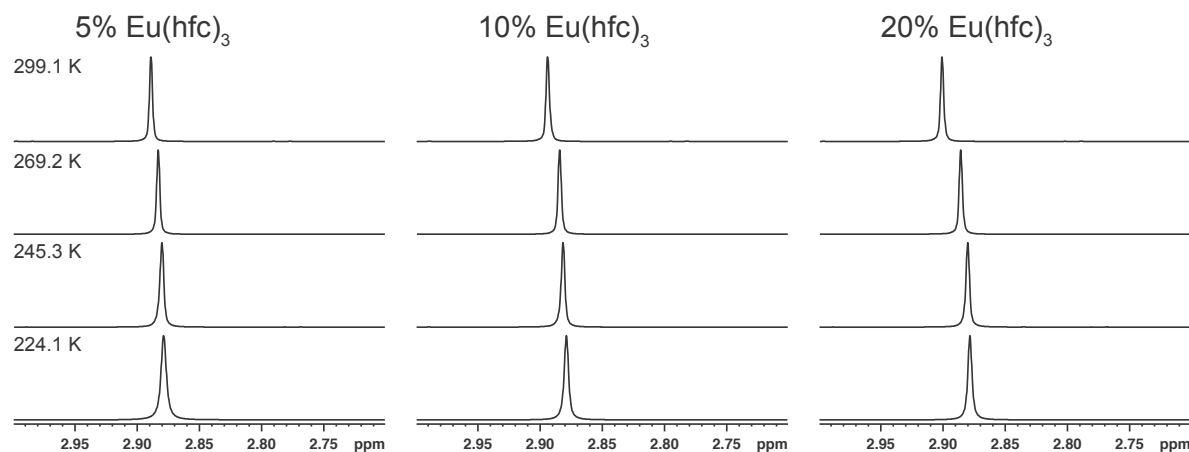


Figure B-37: Variable temperature NMR titration experiments of 4,4'-dicyano-2,2'-ethylbridged biphenyl with $\text{Eu}(\text{hfc})_3$ as chiral lanthanide shift reagent.

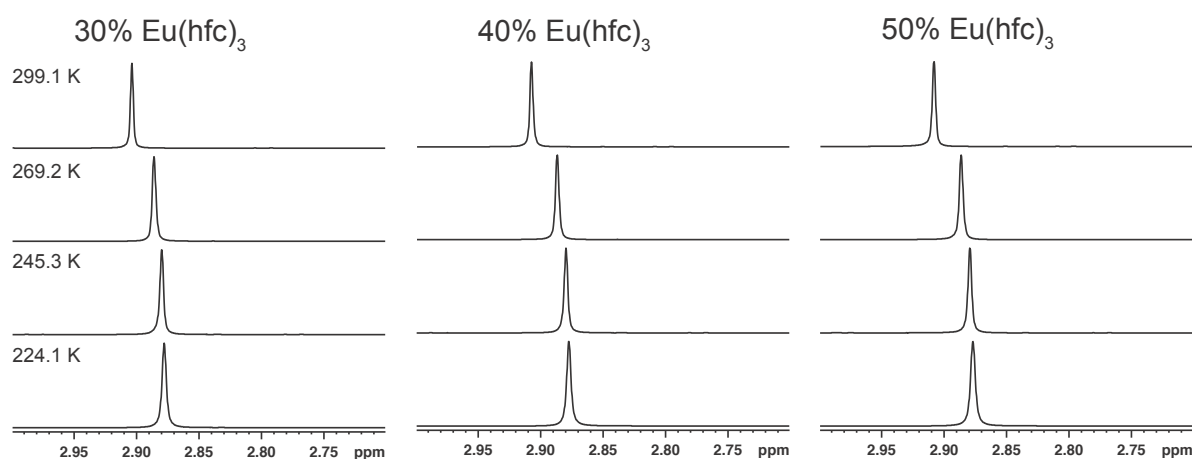


Figure B-38: Variable temperature NMR titration experiments of 4,4'-dicyano-2,2'-ethylbridged biphenyl with $\text{Eu}(\text{hfc})_3$ as chiral lanthanide shift reagent.

The effect of both Europium samples was low even at concentrations of 50%. Therefore, no further experiments at higher concentrations were performed, as a recalculation of the activation energy is impossible even if the coalescence could be reached at higher concentrations.

The NMR spectra of 4,4'-dicyano-2,2'-ethylbridged biphenyl containing 10% $\text{Pr}(\text{hfc})_3$ show clearly that the pseudo contact shift increases at lower temperatures and that the main influence of the LSR is on the phenyl rings, what indicates that probably the distance between the LSR and ethyl-bridge is too long for Praseodym. As Praseodym induces stronger pseudocontact shifts than Europium higher concentrations were measured to see if one can influence the shift of the ethyl

protons in a stronger way. Nevertheless, also at concentrations of 200 % (1.0 eq per coordination group) no strong effects were obtained.

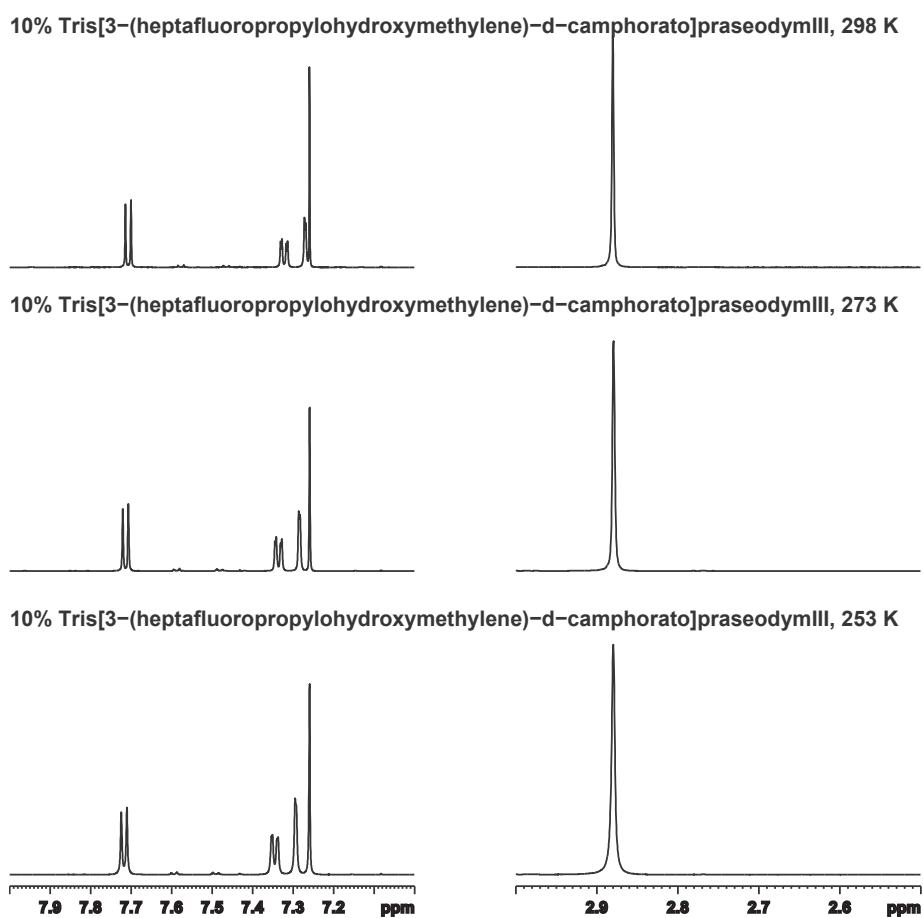


Figure B-39: Variable temperature NMR titration experiments of 4,4'-dicyano-2,2'-ethylbridged biphenyl with Pr(hfc)₃ as chiral lanthanide shift reagent.

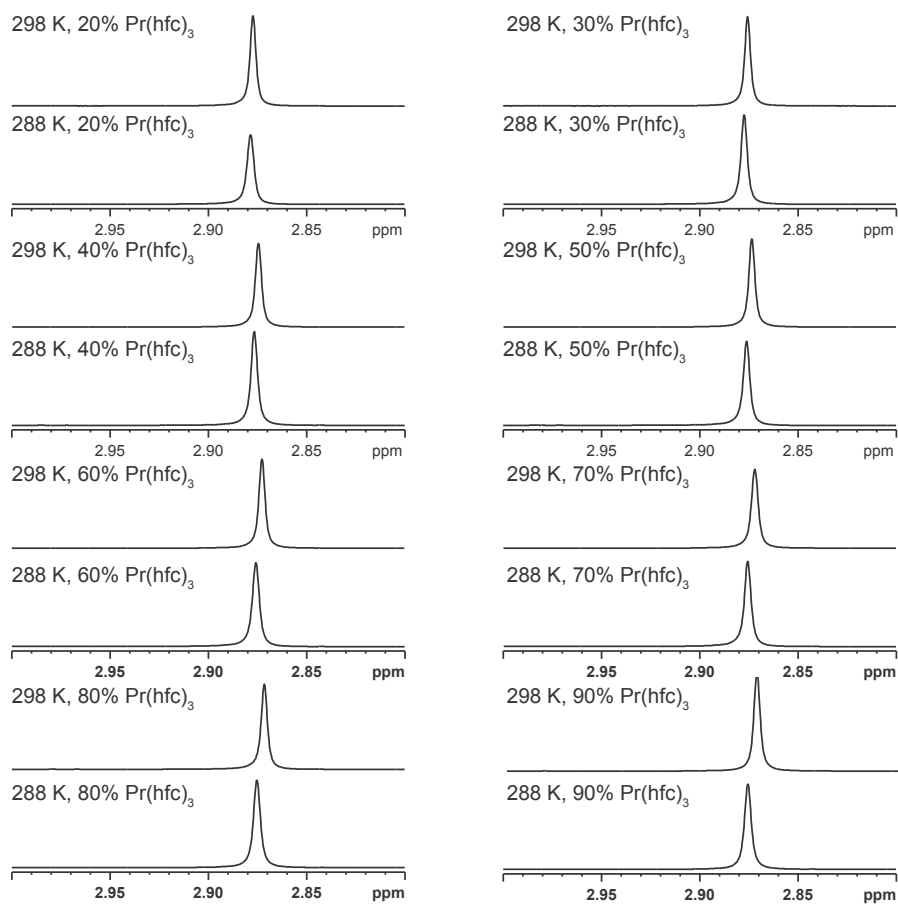


Figure B-40: Variable temperature NMR titration experiments of 4,4'-dicyano-2,2'-ethylbridged biphenyl with $\text{Pr}(\text{hfc})_3$ as chiral lanthanide shift reagent.

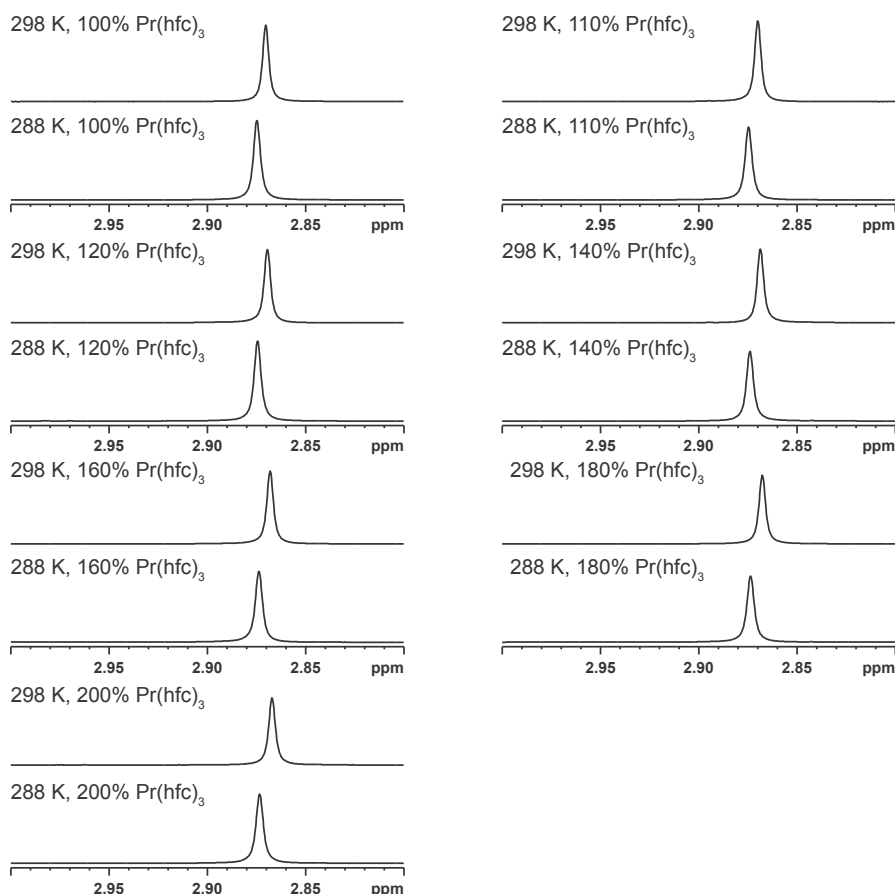
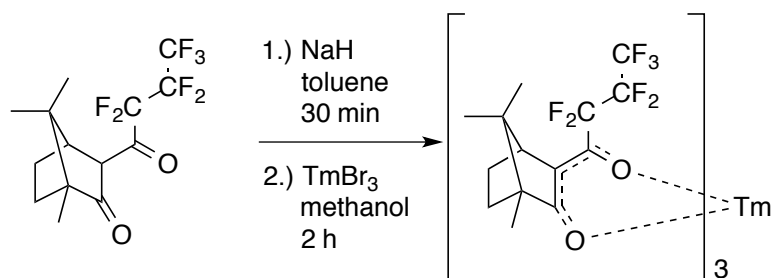


Figure B-41: Variable temperature NMR titration experiments of 4,4'-dicyano-2,2'-ethylbridged biphenyl with PrEu(hfc)₃ as chiral lanthanide shift reagent.

Synthesis of Tris[3-(heptafluoropropylhydroxymethylene)-d-campherato]Tm(III)



Structure B-6: Synthesis scheme of Tm(hfc)₃.

To a suspension of NaH (14.6 mg 60% in mineral oil, 0.34 mmol, 1.2 eq) in toluene (2 ml) hfc (82 μ l, 0.29 mmol, 1.0 eq) was added slowly. The mixture was stirred for 30 min. The solution was filtered and the solvent was removed under reduced pressure to yield the sodium salt of hfc. The resulting salt was re dissolved in methanol (2 ml) and a solution of TmBr₃ (53.7 mg, 0.12 mmol, 0.4 eq) in methanol (2 ml) was added. The mixture was stirred for 2 h at room

temperature and additional 30 min at 64 °C. The solvent was removed and the product was redissolved in n-hexane (4 ml), filtered over celite, washed with water (3 x 10 ml) and dried over Na₂SO₄ to yield Tris[3-(heptafluoropropylhydroxymethylene)-d-camphorato]Tm(III) 3 as pail orange crystals.

Thullium is known as one of the metals that can induce the strongest pseudo contact shifts, therefore titration experiments were performed up to 70 % in 10 % steps. The effect was again small at high temperatures but increased at lower temperatures. The coalescence could again not be reached as the PRE effect at low temperatures became dominant leading to signal broadening. At NMR measurements at 188.5 K the melting point of toluene was almost reached so that these two problems stopped the experiments.

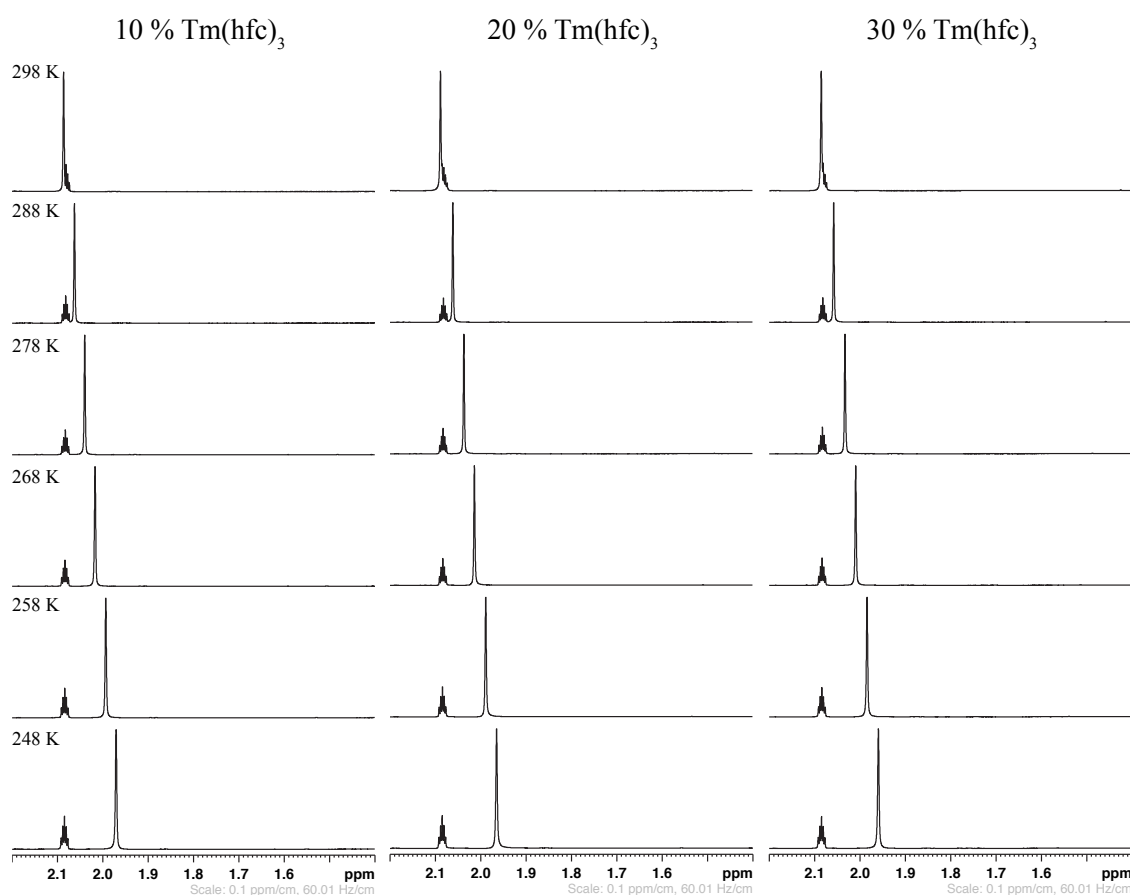


Figure B-42: Variable temperature NMR titration experiments of 4,4'-dicyano-2,2'-ethylbridged biphenyl with Tm(hfc)₃ as chiral lanthanide shift reagent in toluene-d₈.

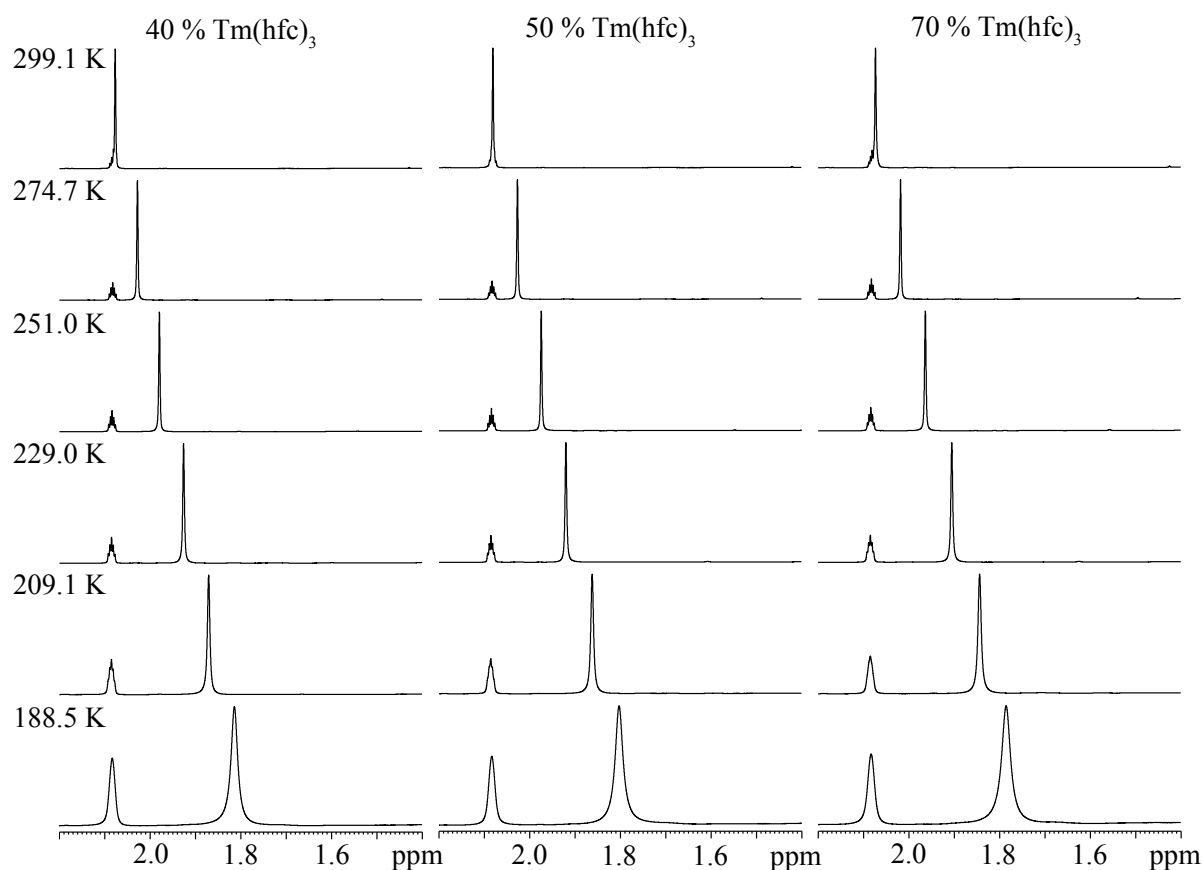


Figure B-43: Variable temperature NMR titration experiments of 4,4'-dicyano-2,2'-ethylbridged biphenyl with $\text{Tm}(\text{hfc})_3$ as chiral lanthanide shift reagent in toluene- d_8 .

B.8.3 Line shape analysis

All experimental spectra were fitted with dNMR Bruker® to determine the rate constants at different temperatures. The procedure for all spectra was the following. The spin system containing 6 different protons was generated. The coupling constants at slow exchange regime were determined and added to the corresponding spin. Afterwards the position of the spins in the slow exchange was added. The rate constant was then varied to generate a fit with accuracy above 95%, which was set as confidence interval. The position of the nucleus was kept constant and only varied if a temperature dependent shift in the experimental spectra was obtained. These definitions were used to fit the spectra from the slow exchange regime to the coalescence temperature. From the coalescence to the fast exchange regime the coupling constants were exchanged to the ones obtained in the fast exchange regime to allow more precise calculations. The determined spectra with their corresponding accuracy values are shown in the following section. Problems were

obtained if the coalescence temperature was close to the melting point of the solvent or the separation of the two signals was small. Additional problems were detected for non-pure samples, solvent peaks close to the reaction centre or overlaps of the bridging CH₂. For samples with a low coalescence temperatures the rate constants at higher temperatures are too small as the resolution of the signals was not good enough.

The coalescence temperatures were determined from line width analysis of the experimental spectra. The line width was measured at each temperature. The line width was then correlated to the temperature and a lorentzian fitting performed. This calculation allowed a quite precise calculation of the coalescence temperature. For compounds with a low coalescence point this method is less suitable as not many data points below the coalescence could be determined. The graphical representation for each compound is shown below the measured NMR spectra.

The obtained rate constants were further analysed using Eyring plots. Therefore, the logarithm of the rate constant over the temperature was correlated to inverse temperature. The data points are then fitted in a linear regression. Figure B-80 shows the graphical outcome of the calculations. The resulting linear equation is then used to calculate the activation enthalpy, the activation entropy and finally the Gibbs free activation energy.

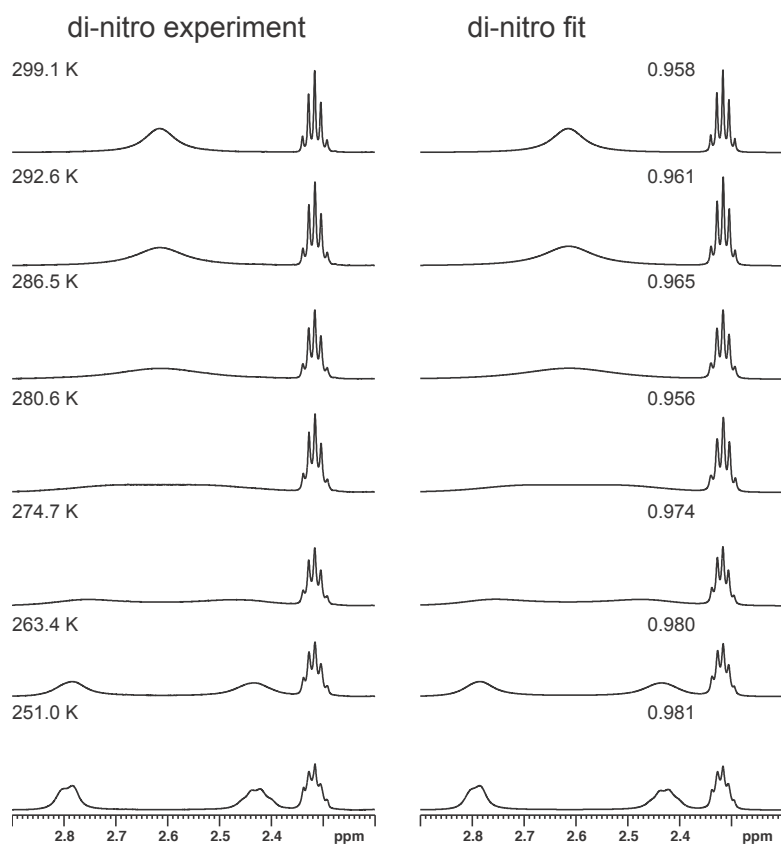


Figure B-44: Comparison of experimental and dNMR fitted spectra of compound 1a in CDCl₃.

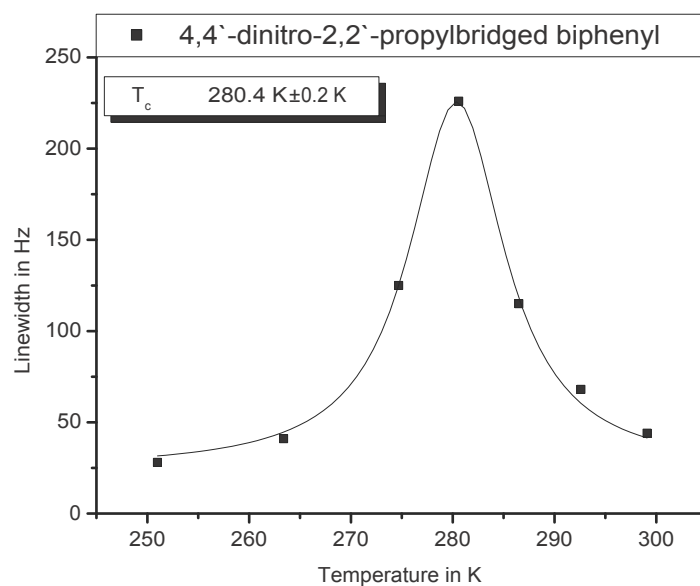


Figure B-45: Calculation of the theoretical coalescence temperature of compound 1a from the experimental line width in CDCl₃.

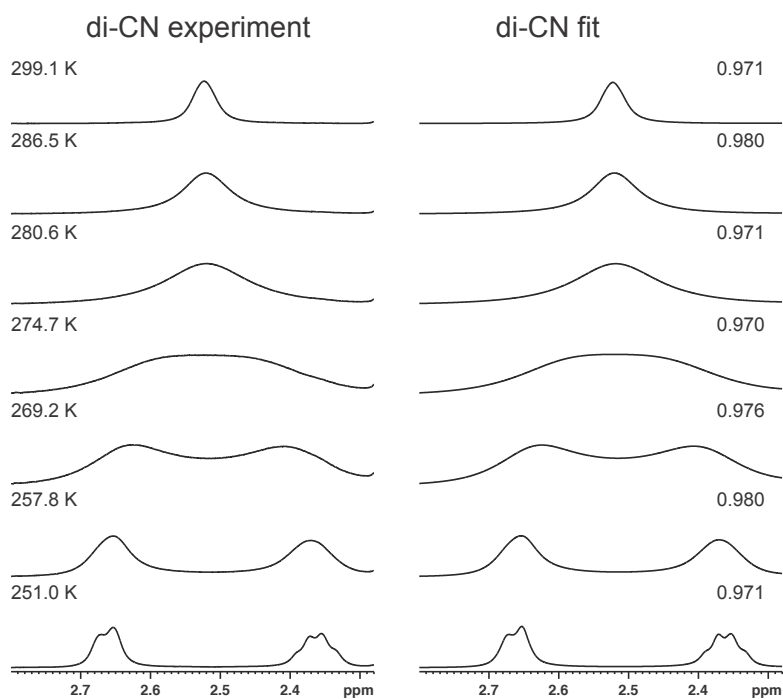


Figure B-46: Comparison of experimental and dNMR fitted spectra of compound 1b in CDCl₃.

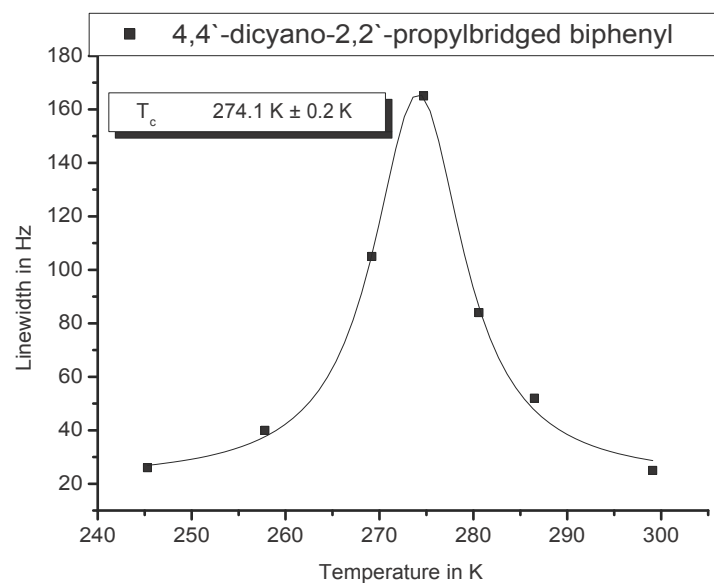


Figure B-47: Calculation of the theoretical coalescence temperature of compound 1b from the experimental line width in CDCl₃.

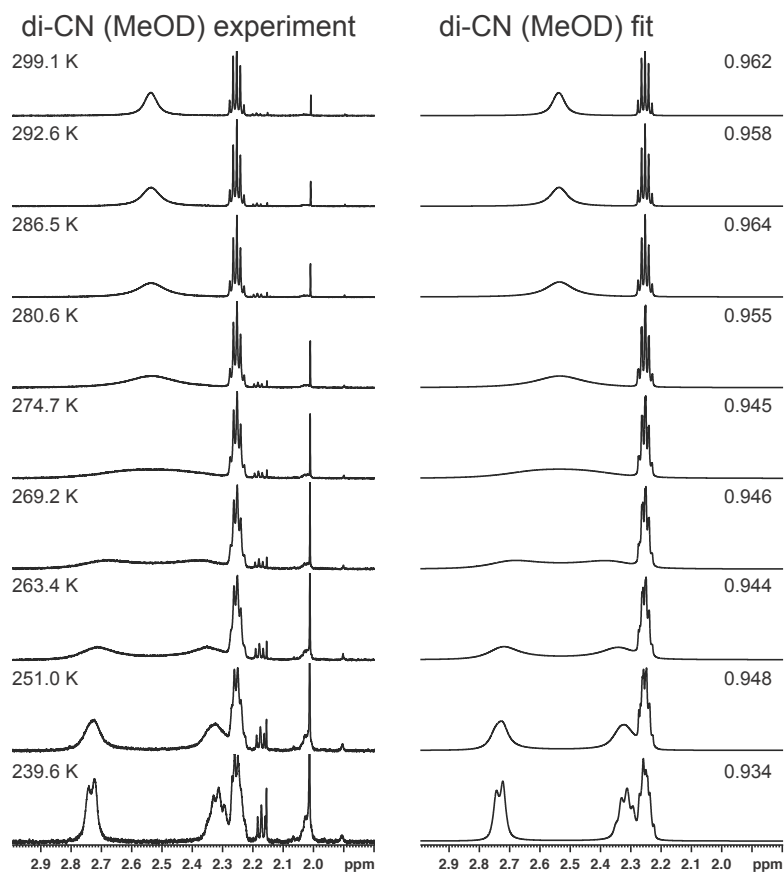


Figure B-48: Comparison of experimental and dNMR fitted spectra of compound 1b in MeOD-d₄. The lowered accuracy of the spectra below 280 K is due to signal overlaps.

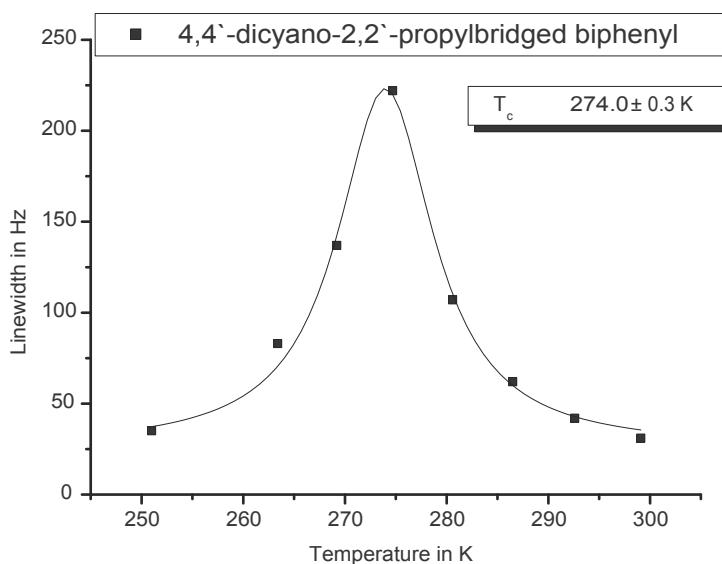


Figure B-49: Calculation of the theoretical coalescence temperature of compound 1b from the experimental line width in MeOD-d₄.

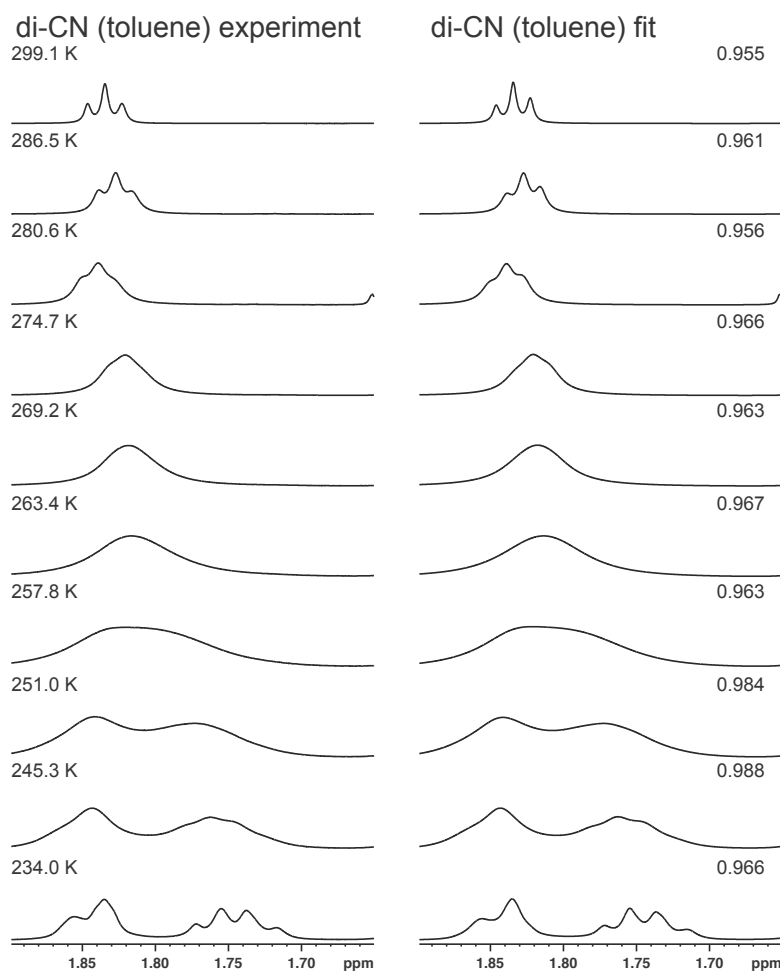


Figure B-50: Comparison of experimental and dNMR fitted spectra of compound 1b in toluene-d8.

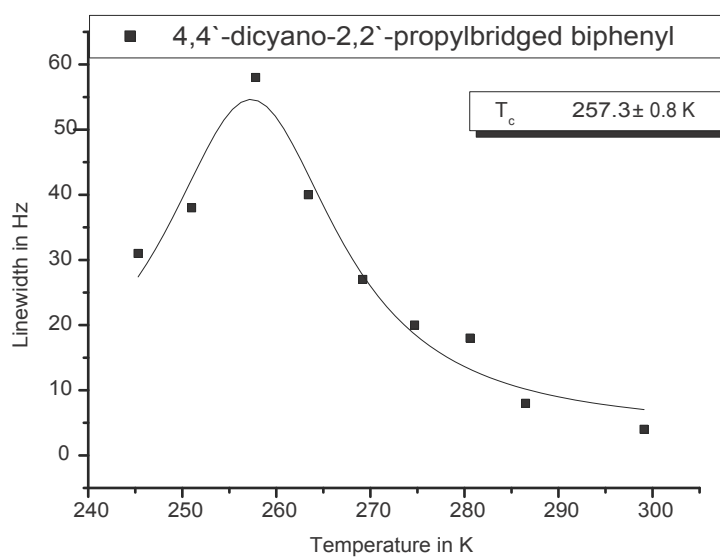


Figure B-51: Calculation of the theoretical coalescence temperature of compound 1b from the experimental line width in toluene-d8.

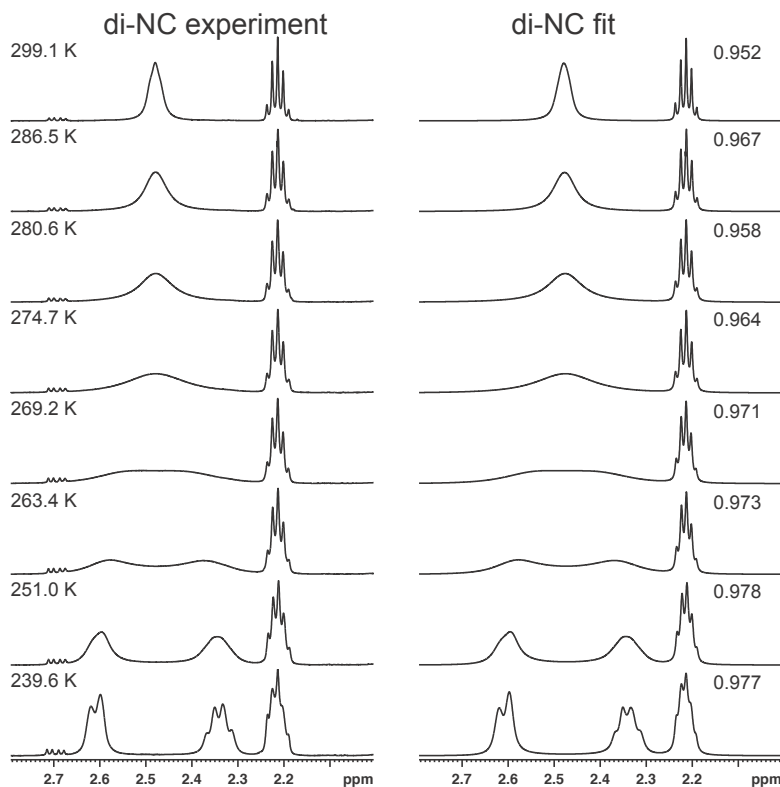


Figure B-52: Comparison of experimental and dNMR fitted spectra of compound 1b in CDCl_3 .

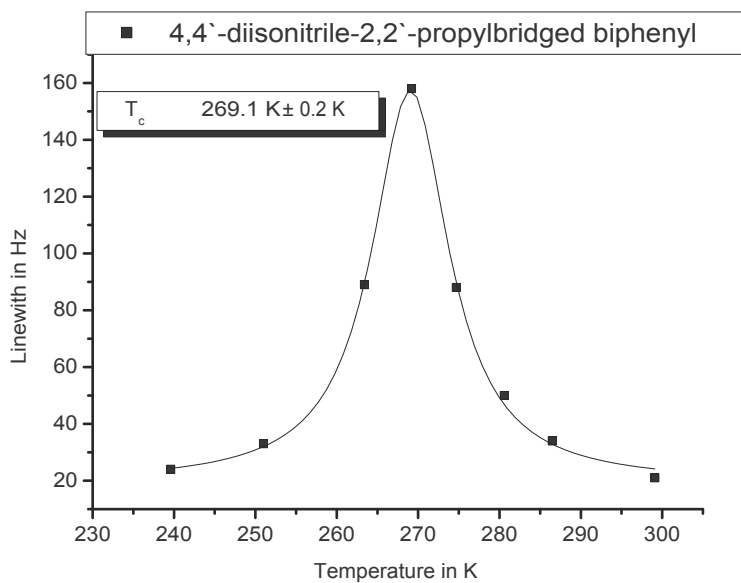


Figure B-53: Calculation of the theoretical coalescence temperature of compound 1c from the experimental line width.

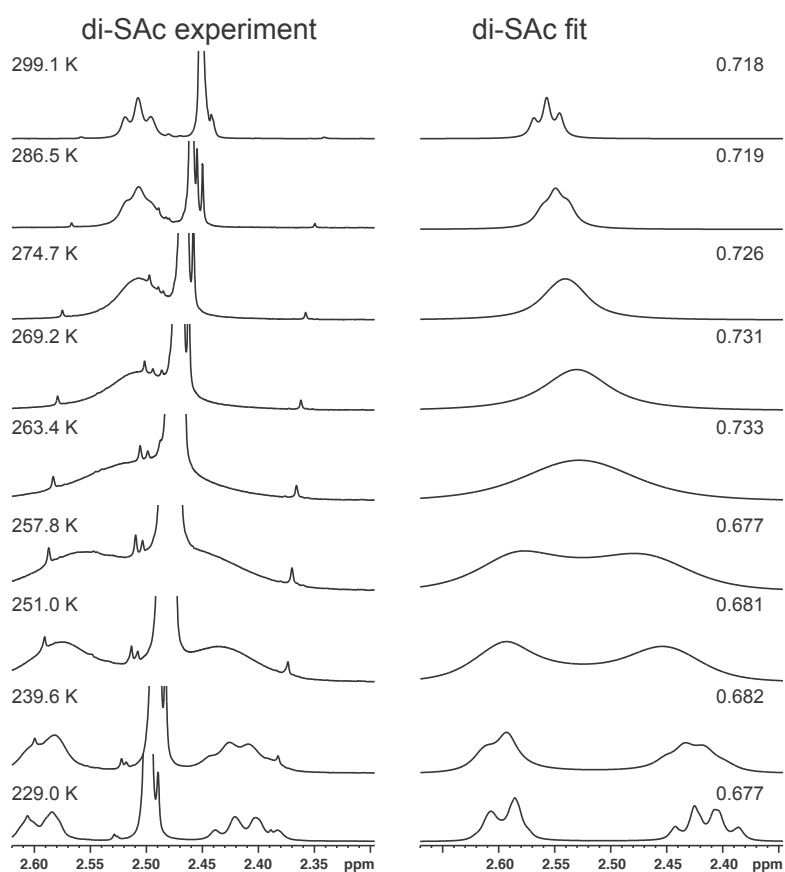


Figure B-54: Comparison of experimental and dNMR fitted spectra of compound 1d in CDCl_3 . The high impurity of the compound lead to low overall accuracy but the accuracy of the isolated signals was above 0.95 for all temperatures.

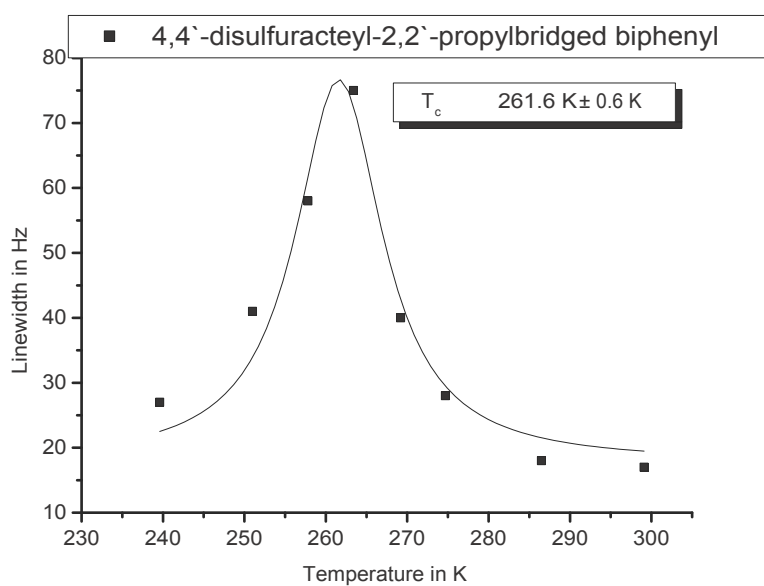


Figure B-55: Calculation of the theoretical coalescence temperature of compound 1d from the experimental line width in CDCl_3 .

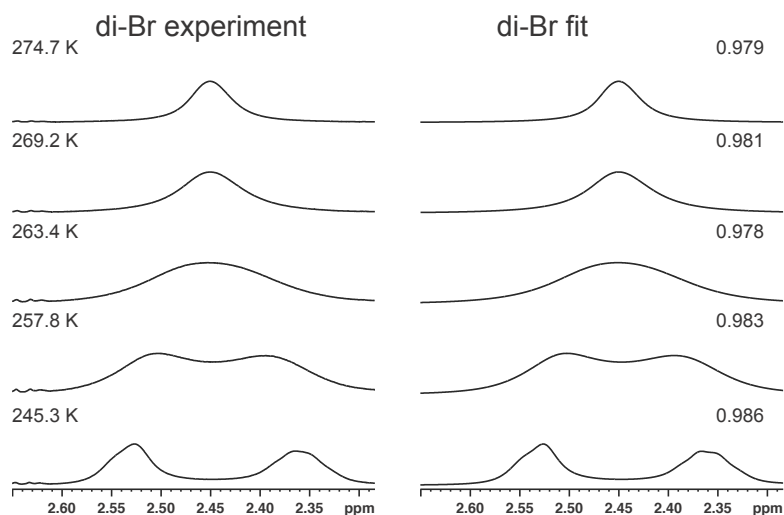


Figure B-56: Comparison of experimental and dNMR fitted spectra of compound 1e in CDCl₃.

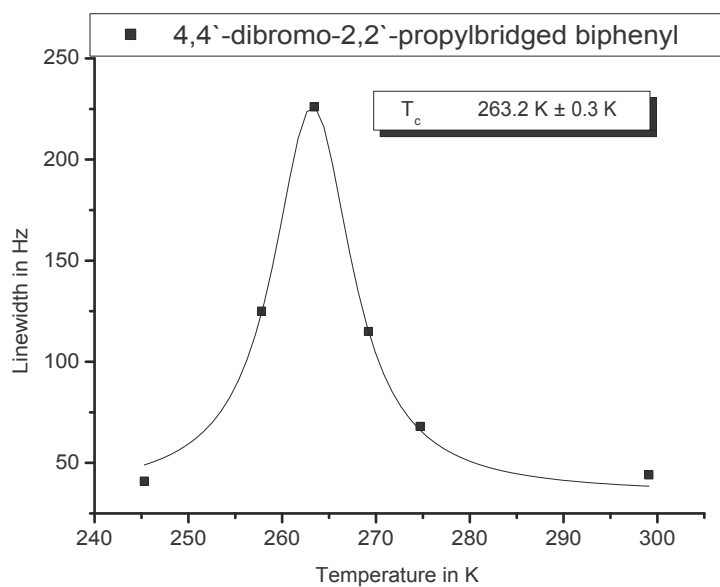


Figure B-57: Calculation of the theoretical coalescence temperature of compound 1e from the experimental line width in CDCl₃.

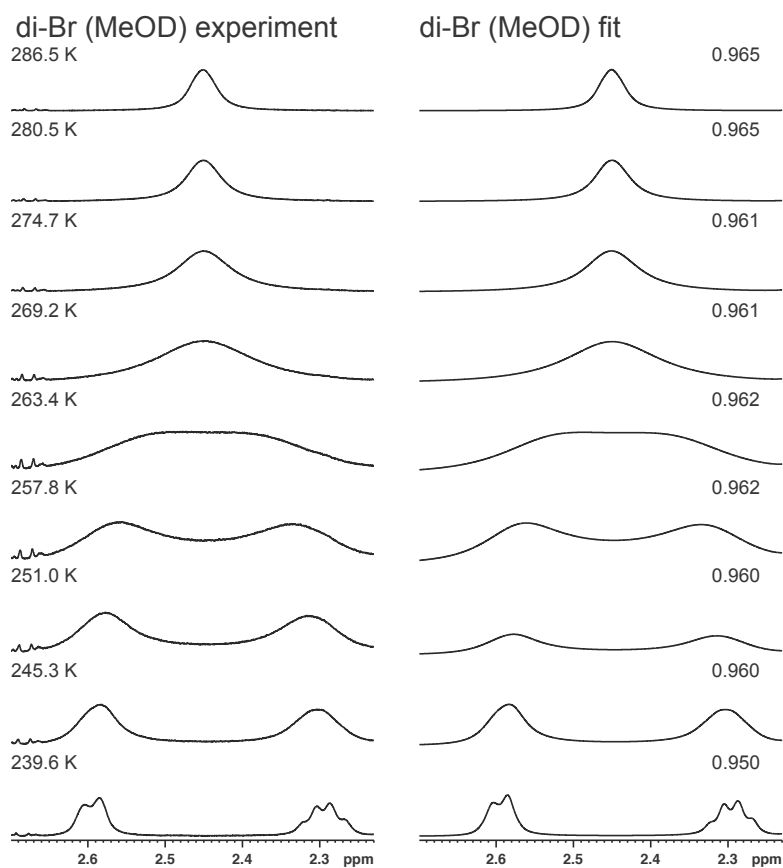


Figure B-58: Comparison of experimental and dNMR fitted spectra of compound 1e in MeOD-d4.

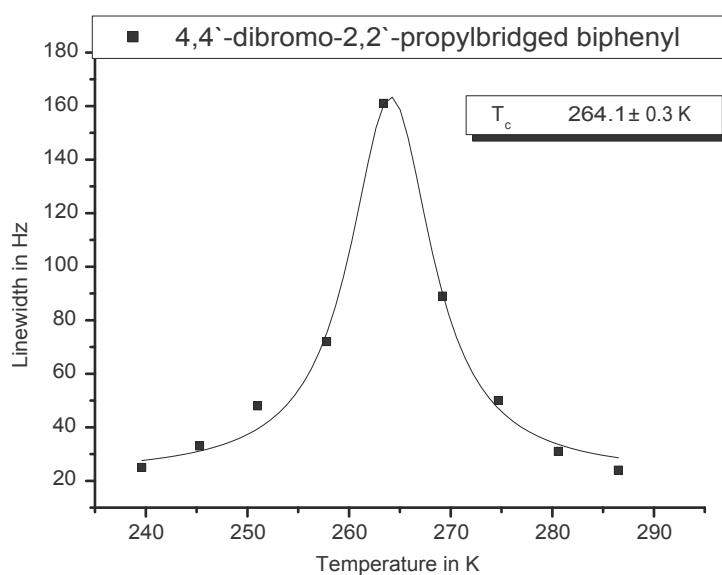


Figure B-59: Calculation of the theoretical coalescence temperature of compound 1e from the experimental line width in MeOD-d4.

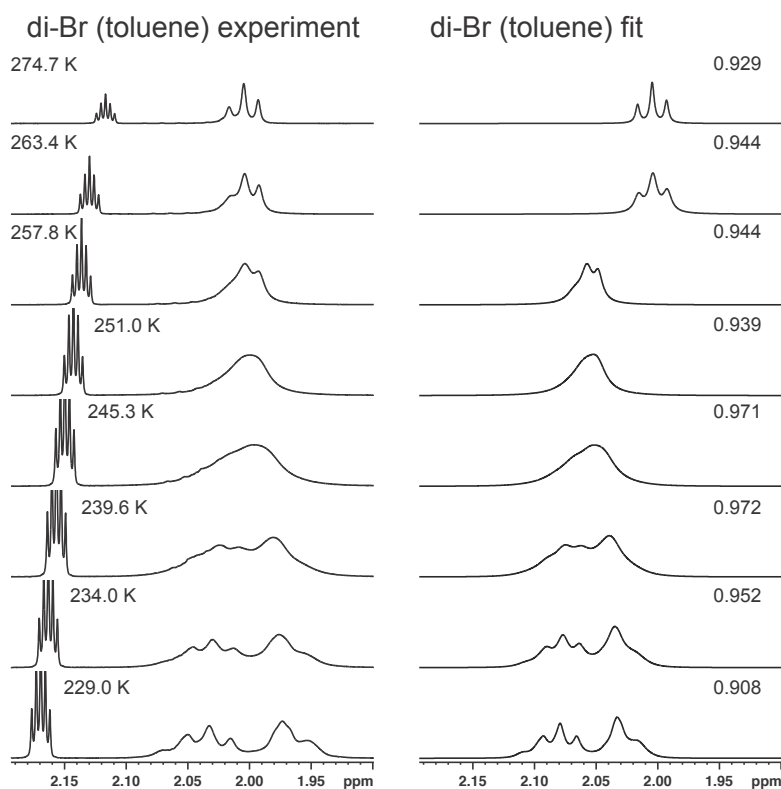


Figure B-60: Comparison of experimental and dNMR fitted spectra of compound 1e in toluene-d8. The low accuracy of all spectra is due to second species lying on the left hand side of the signal resulting in a strong tailing on the left side of the signal.

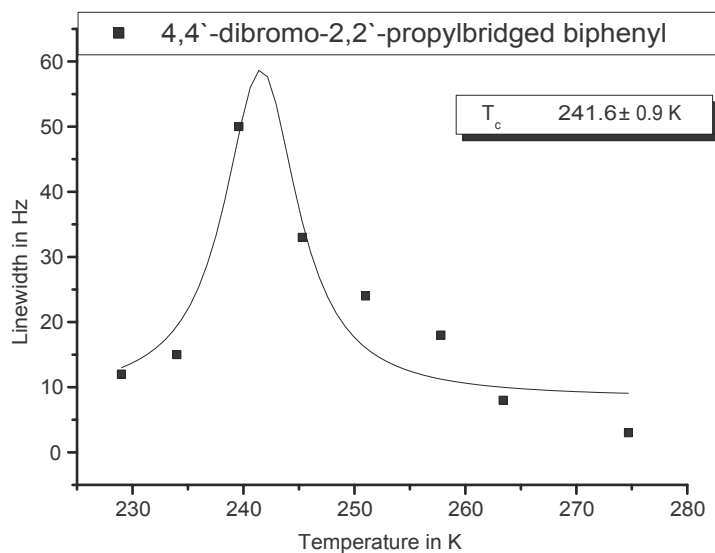


Figure B-61: Calculation of the theoretical coalescence temperature of compound 1e from the experimental line width in toluene-d8.

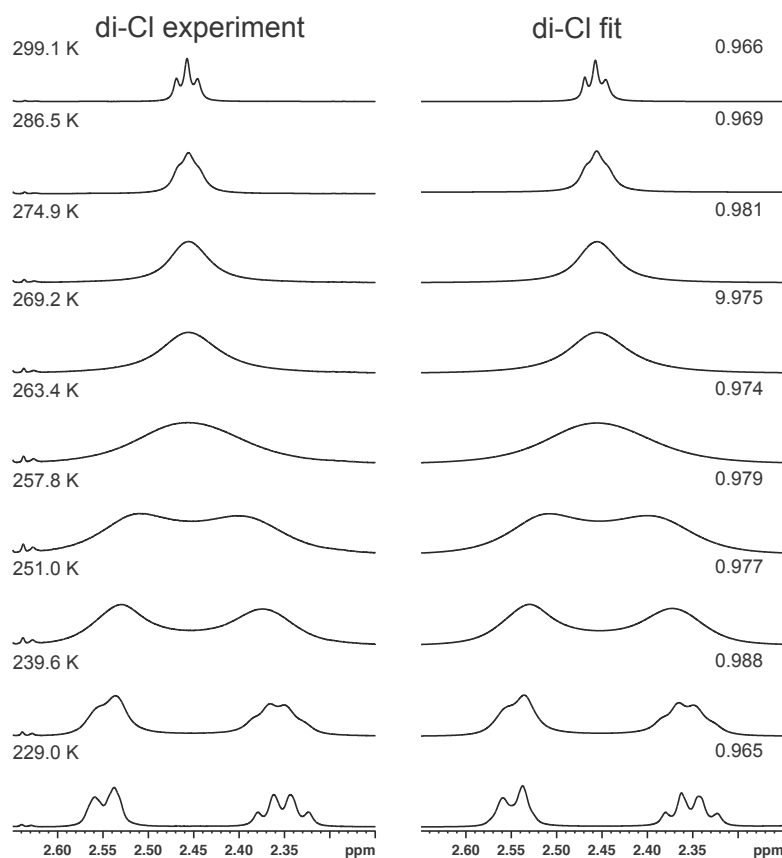


Figure B-62: Comparison of experimental and dNMR fitted spectra of compound 1f in CDCl₃.

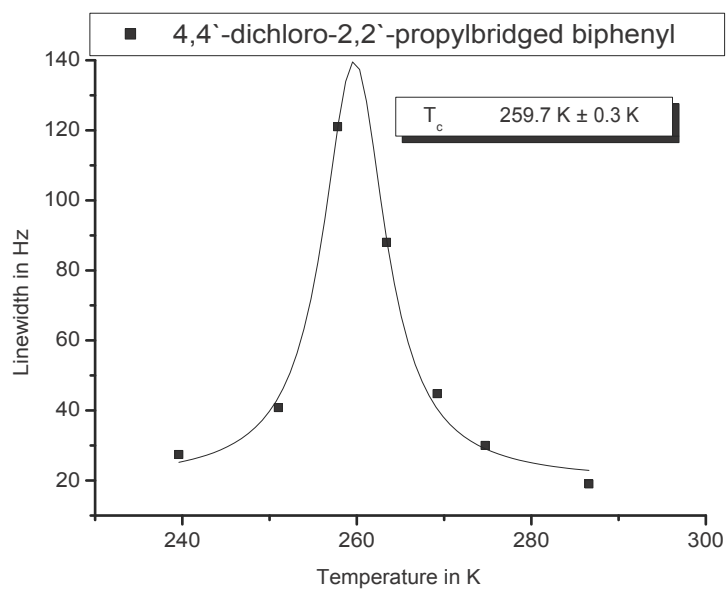


Figure B-63: Calculation of the theoretical coalescence temperature of compound 1f from the experimental line width in CDCl₃.

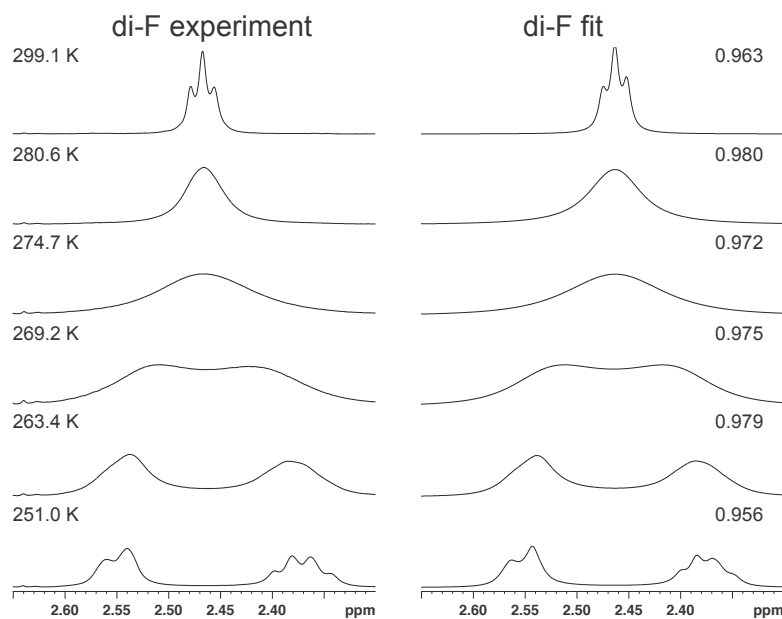


Figure B-64: Comparison of experimental and dNMR fitted spectra of compound 1g in CDCl₃.

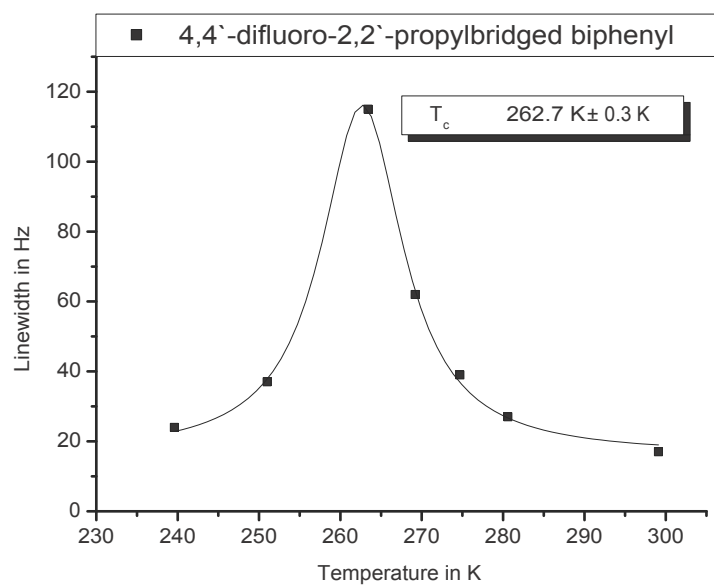


Figure B-65: Calculation of the theoretical coalescence temperature of compound 1g from the experimental line width in CDCl₃.

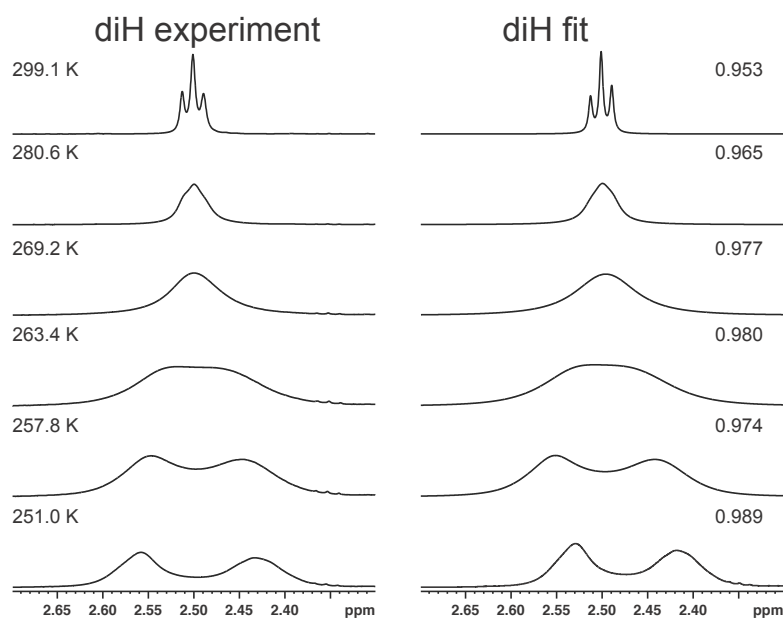


Figure B-66: Comparison of experimental and dNMR fitted spectra of compound 1h in CDCl₃.

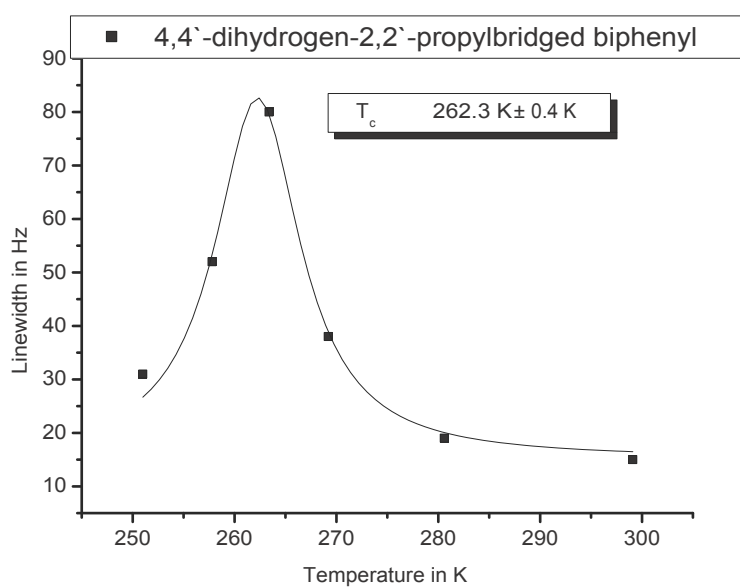


Figure B-67: Calculation of the theoretical coalescence temperature of compound 1h from the experimental line width in CDCl₃.

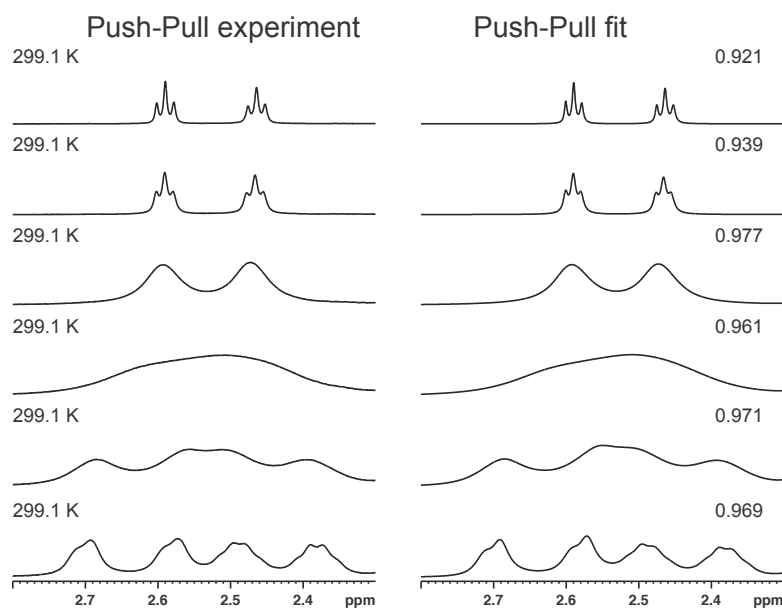


Figure B-68: Comparison of experimental and dNMR fitted spectra of compound 1i in CDCl_3 .

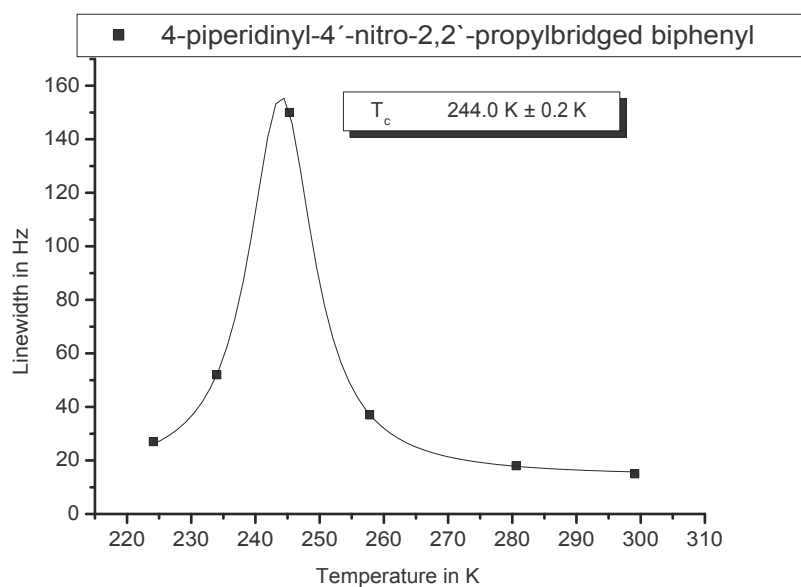


Figure B-69: Calculation of the theoretical coalescence temperature of compound 1i from the experimental line width in CDCl_3 .

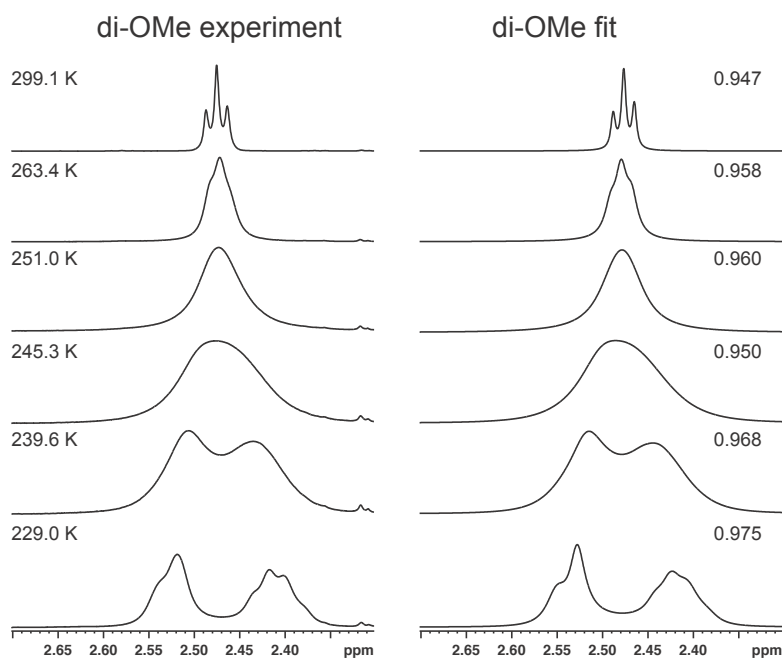


Figure B-70: Comparison of experimental and dNMR fitted spectra of compound 1j in CDCl₃.

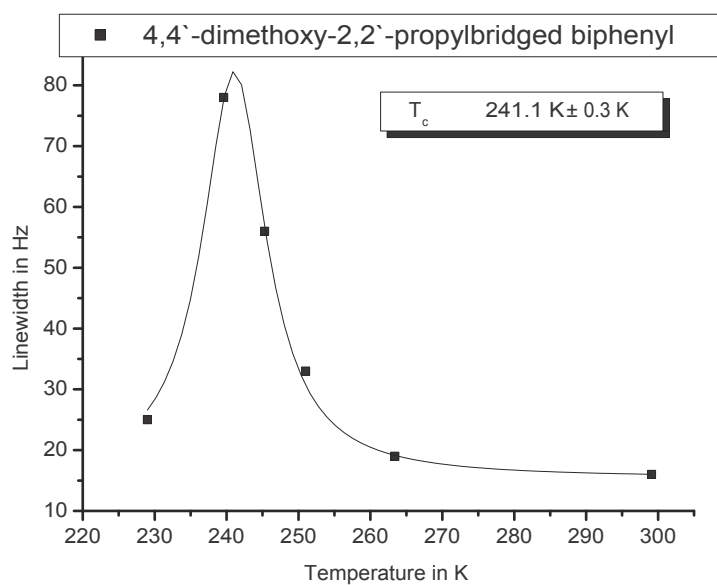


Figure B-71: Calculation of the theoretical coalescence temperature of compound 1k from the experimental line width in CDCl₃.

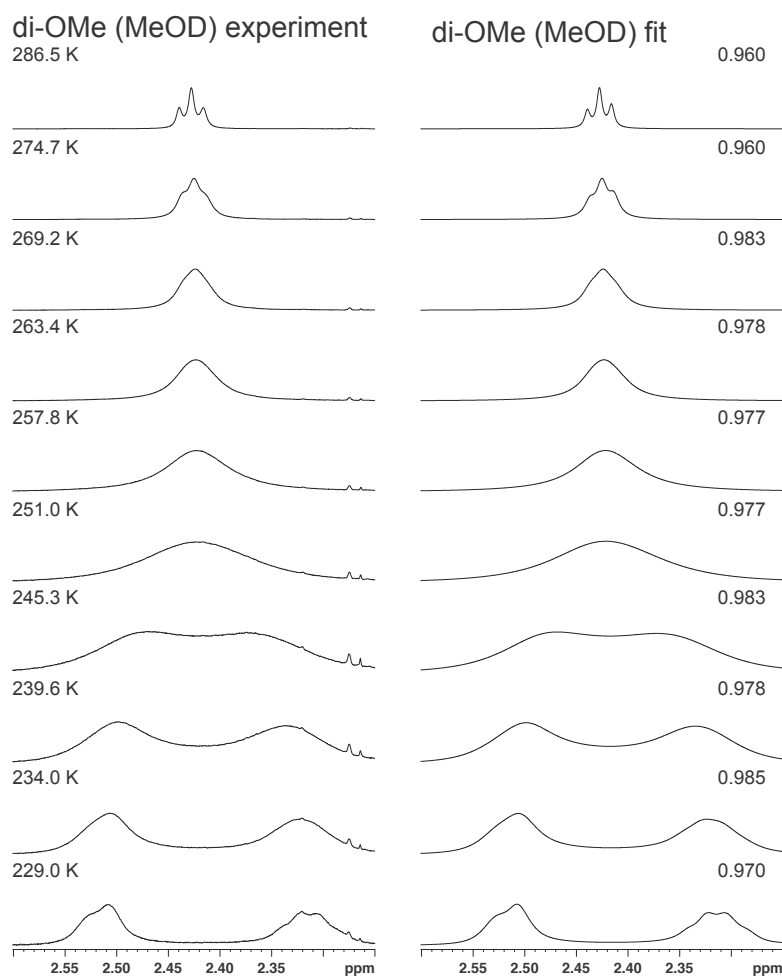


Figure B-72: Comparison of experimental and dNMR fitted spectra of compound 1j in MeOD-d4.

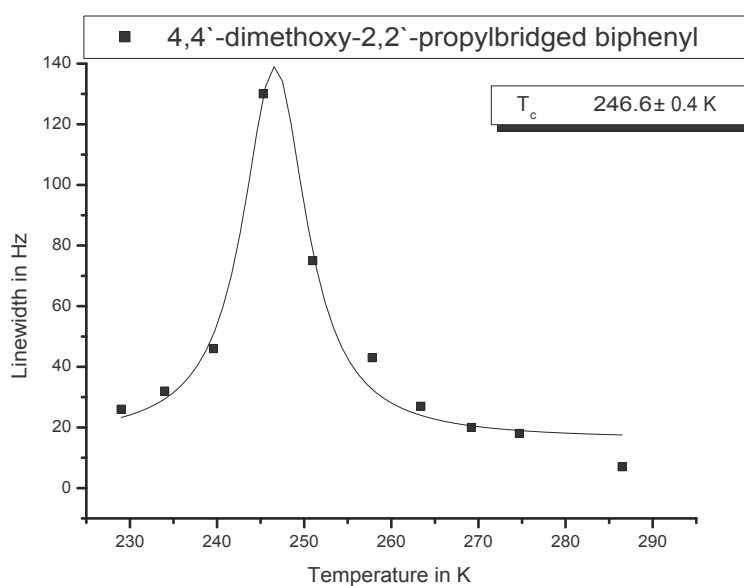


Figure B-73: Comparison of experimental and dNMR fitted spectra of compound 1j in MeOD-d4.

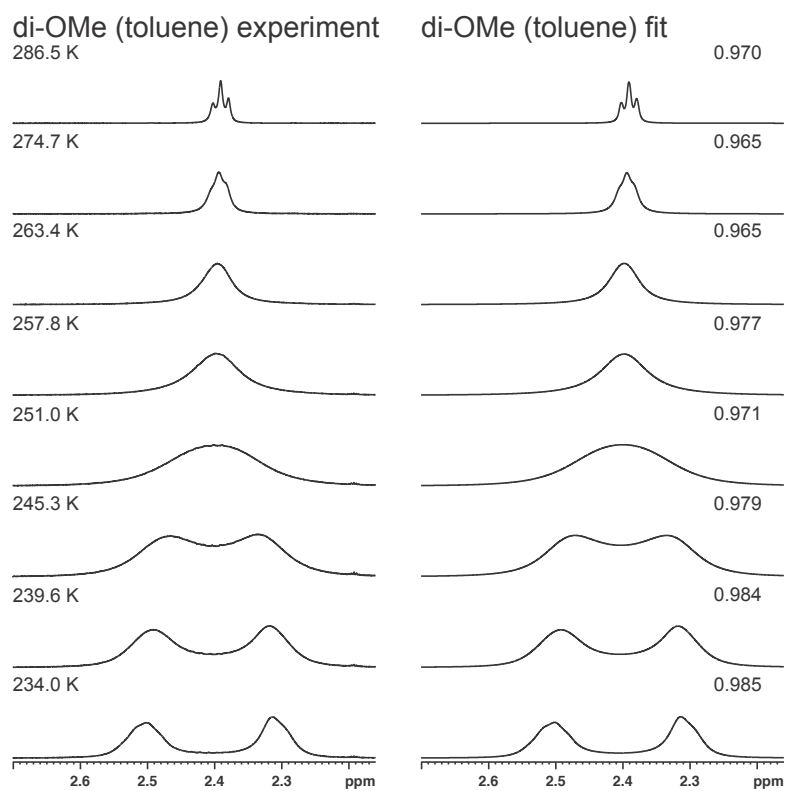


Figure B-74: Comparison of experimental and dNMR fitted spectra of compound 1j in toluene-d8.

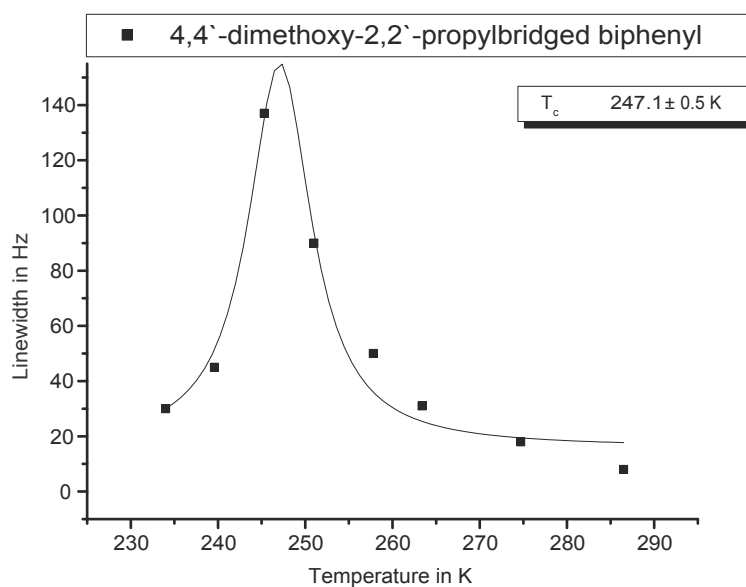


Figure B-75: Comparison of experimental and dNMR fitted spectra of compound 1j in toluene-d8.

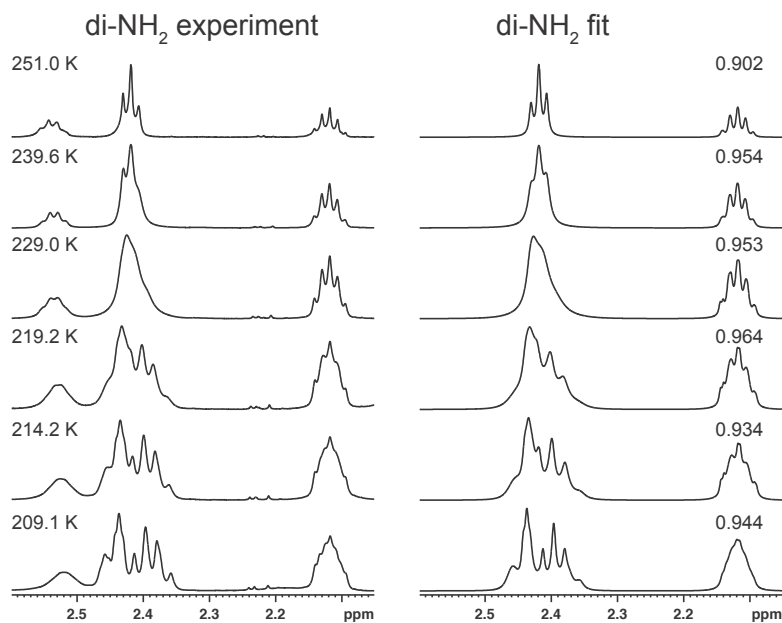


Figure B-76: Comparison of experimental and dNMR fitted spectra of compound 1k in CDCl₃. The low accuracy of the spectra is mainly due to the low coalescence temperature and the low shim quality of the spectra at lower temperatures. The simulation of roof effects as it is obtained in the first spectra is also difficult for the simulation.

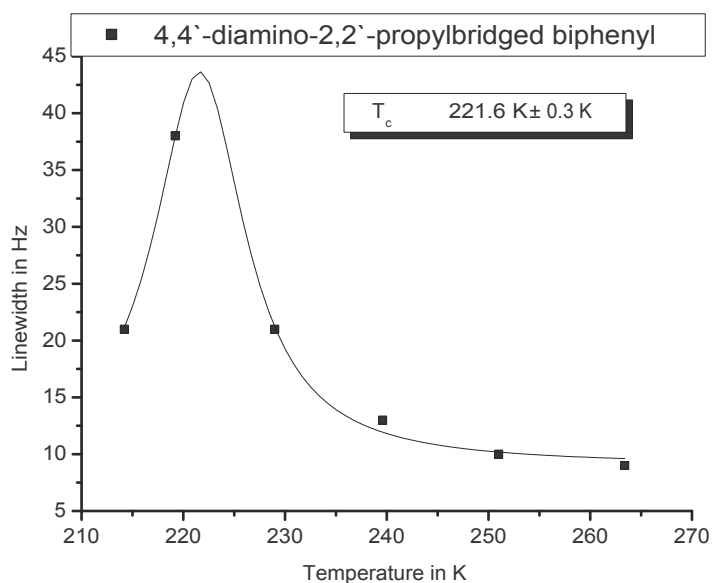


Figure B-77: Calculation of the theoretical coalescence temperature of compound 1k from the experimental line width in CDCl₃.

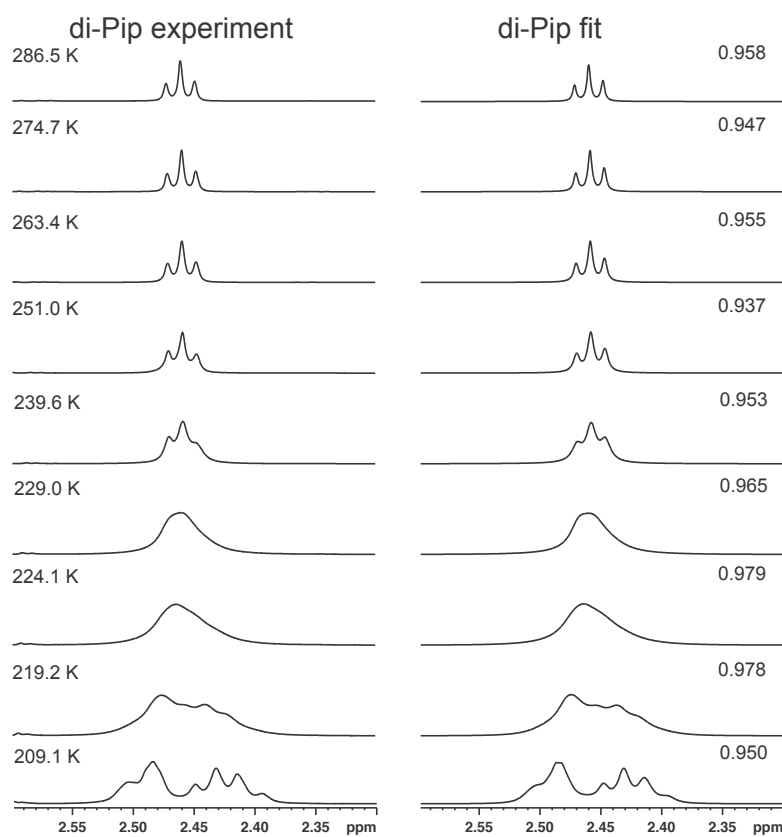


Figure B-78: Comparison of experimental and dNMR fitted spectra of compound 1l in CDCl₃.

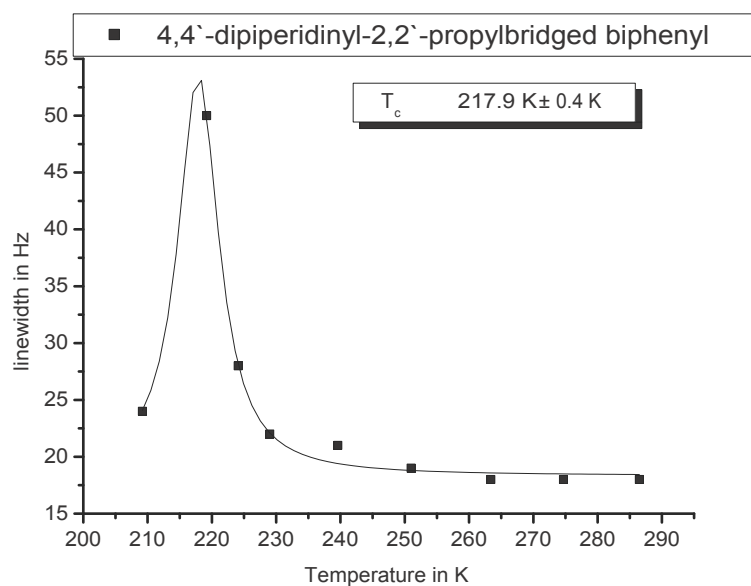


Figure B-79: Calculation of the theoretical coalescence temperature of compound 1l from the experimental line width in CDCl₃.

Table B-19: Rate constants determined by dNMR for propyl bridged biphenyls.

1a	<i>fitted</i>	1b	<i>fitted</i>	1c	<i>fitted</i>
<i>T</i>	<i>k</i>	<i>T</i>	<i>k</i>	<i>T</i>	<i>k</i>
299.1	2000	299.1	3050	299.1	3800
292.6	1200	286.5	1200	286.5	1450
286.5	760	280.6	705	280.6	900
280.6	450	274.7	415	274.7	560
274.7	290	269.2	260	269.2	340
263.4	97	257.8	90	263.4	200
251.0	35			251.0	65
				239.6	21

Table B-20: Rate constants determined by dNMR for propyl bridged biphenyls.

1d	<i>fitted</i>	1e	<i>fitted</i>	1f	<i>fitted</i>
<i>T</i>	<i>k</i>	<i>T</i>	<i>k</i>	<i>T</i>	<i>k</i>
299.1	4200	274.7	850	299.1	4800
286.5	1900	269.2	515	286.6	2050
274.7	820	263.4	295	274.7	810
269.2	500	257.8	172	269.2	500
263.4	320	245.3	55	263.4	325
257.8	180			257.8	185
251.0	105			251.0	105
239.6	35			239.6	38
				229.0	13

Table B-21: Rate constants determined by dNMR for propyl bridged biphenyls.

1g	<i>fitted</i>	1h	<i>fitted</i>	1i	<i>fitted</i>
<i>T</i>	<i>k</i>	<i>T</i>	<i>k</i>	<i>T</i>	<i>k</i>
299.1	3100	299.1	3200	299.1	10200
280.6	840	280.6	1000	281.6	4200
274.7	530	269.2	395	257.8	820
269.2	315	263.4	195	245.3	345
263.4	186	257.8	128	234.0	130
251.0	63	251.0	72	224.1	50
239.6	22	239.6	25		

Table B-22: Rate constants determined by dNMR for propyl bridged biphenyls.

1j	<i>fitted</i>	1k	<i>fitted</i>	1l	<i>fitted</i>
<i>T</i>	<i>k</i>	<i>T</i>	<i>k</i>	<i>T</i>	<i>k</i>
274.7	1500	251.0	550	274.7	1500
263.4	950	239.6	230	263.4	900
251.0	380	234.0	160	251.0	600
245.3	180	229.0	100	239.6	400
239.6	104	224.0	50	229.0	175
229.0	37	219.2	32	224.1	120
219.2	16	214.2	20	219.2	54
				209.2	21

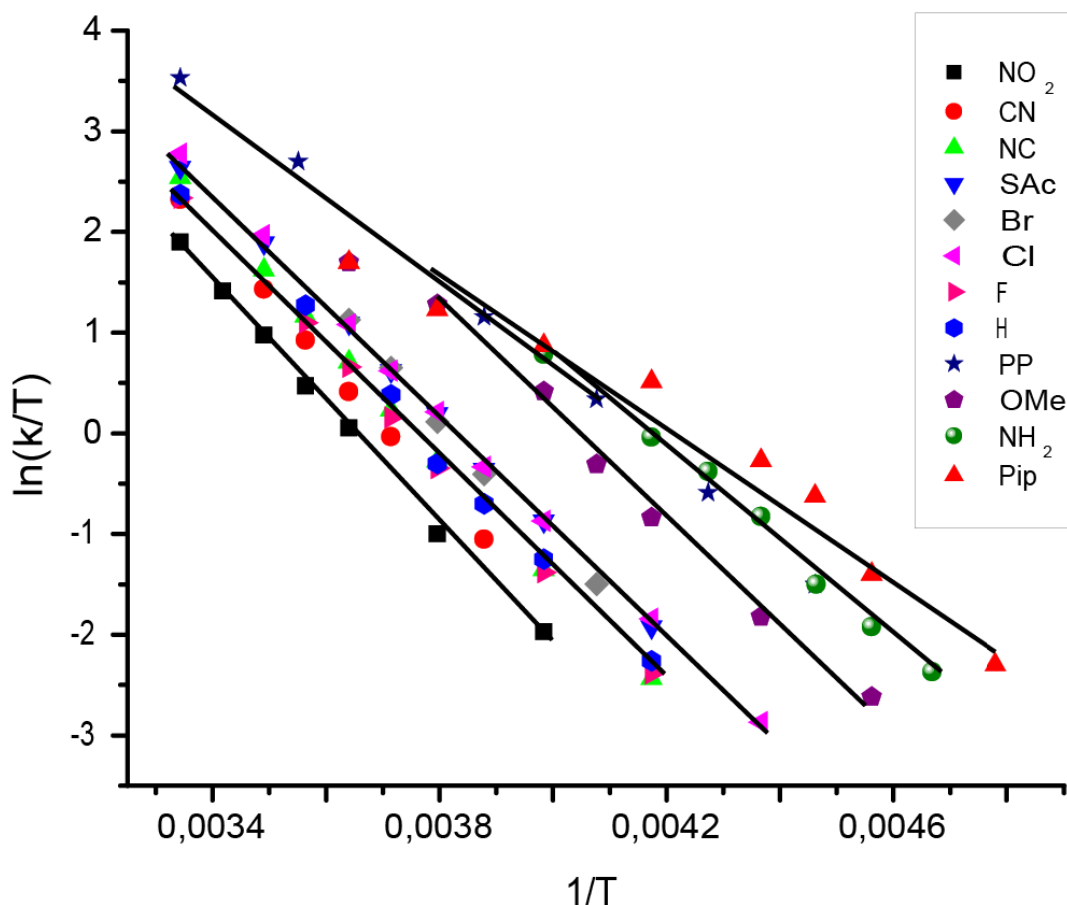


Figure B-80: Overview of Eyring plots from popyl-bridged biphenyls 1a – 1l determined from dNMR data

B.8.4 Determination of the Standard Deviation for $\Delta H_{\text{Eyring}}^{\ddagger}$, $\Delta S_{\text{Eyring}}^{\ddagger}$, $\Delta G_{\text{Eyring}}^{\ddagger}$

The standard deviations σ for the enthalpy, entropy, and Gibbs free energy values given in Table B-8 of the main paper were obtained from the following procedure: firstly, the experimental reaction rate constants $\ln(k/T)$ were plotted against $1/T$ in a single Eyring plot and fitted by linear regression. From this fit, the values $\Delta H_{\text{Eyring}}^{\ddagger}$, $\Delta S_{\text{Eyring}}^{\ddagger}$, and $\Delta G_{\text{Eyring}}^{\ddagger}$ given in Table B-8 of the main paper were obtained. Secondly, at the experimental temperatures T_i , $i = 1, \dots, n$, the corresponding reaction rate constants k_i were computed from the equation

$$k_i = k_B T_i \exp\{-(\Delta H_{\text{Eyring}}^{\ddagger} - T_i \Delta S_{\text{Eyring}}^{\ddagger}) / (RT_i)\} / h, \quad i = 1, \dots, n.$$

Obviously, these computed points lie on a perfect straight line. Thirdly, a total number of $j = 1, \dots, 2500$ individual simulations were performed. In each of these simulations, n data points $(T_i + \delta_T, k_i + \delta_k)$ were generated using a random number generator, taking random numbers δ_T and δ_k from a Gaussian distribution about the temperature T_i and about the reaction rate constant k_i . The Gaussian distributions were chosen according to the standard deviations of $\sigma_T = 1$ K and $\sigma_k = 5\%$, respectively. An Eyring plot for these n data points yielded $\Delta H_{\text{Eyring}}^\ddagger(j)$, $\Delta S_{\text{Eyring}}^\ddagger(j)$, and $\Delta G_{\text{Eyring}}^\ddagger(j)$. Finally, the standard deviations σ for the enthalpy, entropy, and Gibbs free energy values given in Table B-8 were obtained from the distribution of the 2500 values obtained in the simulations. As an illustration, Figure B-81 shows all of the 2500 data points used in the above procedure for **1b**, which involved $2 \times 6 \times 2500 = 30000$ random numbers in total.

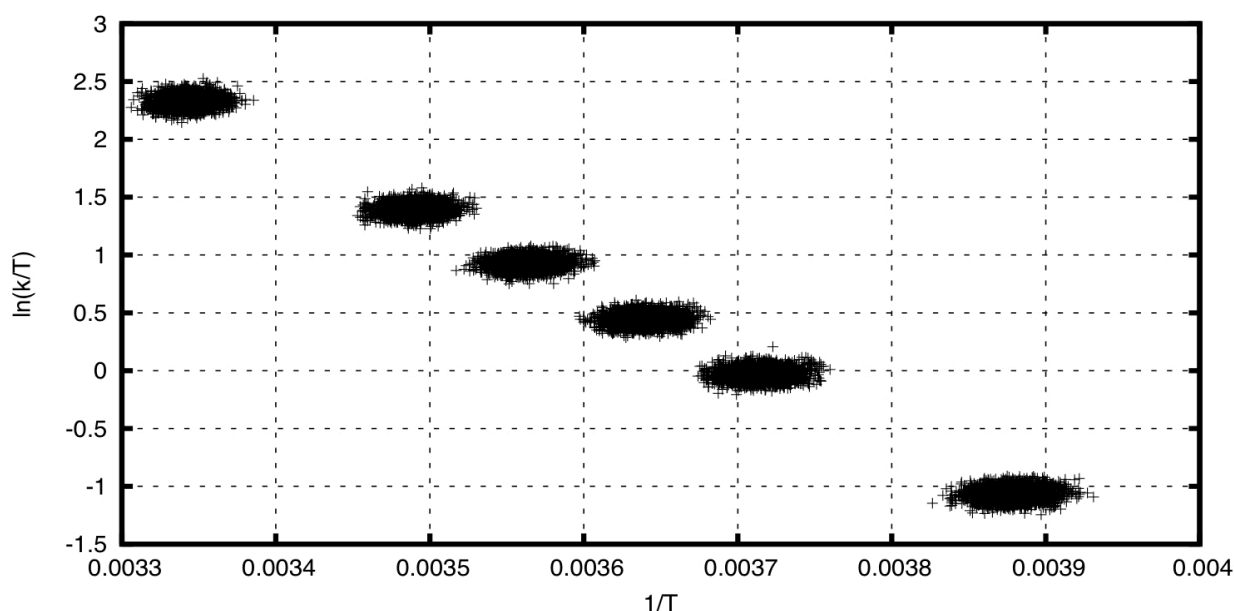


Figure B-81: Data points for **1b** from 2500 simulations ($n = 6$).

B.9 References

1. Strieter, E. R., Blackmond, D. G. & Buchwald, S. L. Insights into the Origin of High Activity and Stability of Catalysts Derived from Bulky, Electron-Rich Monophosphinobiaryl Ligands in the Pd-Catalyzed C–N Bond Formation. *J. Am. Chem. Soc.* **125**, 13978–13980 (2003).
2. Lee, S., Jørgensen, M. & Hartwig, J. F. Palladium-Catalyzed Synthesis of Arylamines from Aryl Halides and Lithium Bis(trimethylsilyl)amide as an Ammonia Equivalent. *Org. Lett.* **3**, 2729–2732 (2001).
3. Mikami, K. *et al.* Conformationally Flexible Biphenyl-phosphane Ligands for Ru-Catalyzed Enantioselective Hydrogenation. *Angew. Chem. Int. Ed.* **38**, 495–497 (1999).
4. Wong, W.-Y. & Ho, C.-L. Functional metallophosphors for effective charge carrier injection/transport: new robust OLED materials with emerging applications. *J. Mater. Chem.* **19**, 4457–4482 (2009).
5. Rotzler, J. *et al.* Variation of the Backbone Conjugation in NLO Model Compounds: Torsion-Angle-Restricted, Biphenyl-Based Push-Pull-Systems. *Eur. J. Org. Chem.* **2010**, 1096–1110 (2010).
6. Tepper, C. & Haberhauer, G. Unidirectional Redox-Stimulated Movement around a C–C Single Bond. *Chem. – Eur. J.* **17**, 8060–8065 (2011).
7. Rotzler, J. *et al.* Atropisomerization of di-para-substituted propyl-bridged biphenyl cyclophanes. *Org. Biomol. Chem.* **11**, 110 (2013).
8. Rotzler, J. *et al.* Racemisation dynamics of torsion angle restricted biphenyl push-pull cyclophanes. *Org. Biomol. Chem.* **9**, 86 (2011).
9. Trznadel, M. *et al.* UV-VIS-NIR and Raman spectroelectrochemistry of regioregular poly(3-octylthiophene): comparison with its non-regioregular analogue. *J. Chem. Soc. Faraday Trans.* **92**, 1387 (1996).
10. Chung, C.-Y., Wen, T.-C. & Gopalan, A. In situ UV-Vis spectroelectrochemical studies to identify electrochromic sites in poly(1-naphthylamine) modified by diphenylamine. *Spectrochim. Acta. A. Mol. Biomol. Spectrosc.* **60**, 585–593 (2004).
11. Trapp, O., Schoetz, G. & Schurig, V. Determination of enantiomerization barriers by dynamic and stopped-flow chromatographic methods. *Chirality* **13**, 403–414 (2001).
12. Gasparri, F., Lunazzi, L., Misiti, D. & Villani, C. Organic Stereochemistry and

- Conformational Analysis from Enantioselective Chromatography and Dynamic Nuclear Magnetic Resonance Measurements. *Acc. Chem. Res.* **28**, 163–170 (1995).
13. Jung, M. & Schurig, V. Determination of enantiomerization barriers by computer simulation of interconversion profiles: enantiomerization of diaziridines during chiral inclusion gas chromatography. *J. Am. Chem. Soc.* **114**, 529–534 (1992).
 14. Bürkle, W., Karfunkel, H. & Schurig, V. Dynamic phenomena during enantiomer resolution by complexation gas chromatography. *J. Chromatogr. A* **288**, 1–14 (1984).
 15. Christie, G. H., Holderness, A. & Kenner, J. XCIII. The molecular configurations of polynuclear aromatic compounds. Part VI. 2,4-Dinitro-diphenic acid; its constitution and resolution into optically active components. *J. Chem. Soc. Resumed* **129**, 671 (1926).
 16. Yuan, H. C. & Adams, R. stereochemistry of diphenyl. XXIII. ¹ optically active 2,5-dimethoxy-2'-nitro-6'-carboxydiphenyl and the mutarotations of its salts. *J. Am. Chem. Soc.* **54**, 2966–2973 (1932).
 17. Yuan, H. C. & Adams, R. stereochemistry of diphenyl. ¹ XXVI. the effect of substitution on the rate of racemization of certain optically active diphenyls. *J. Am. Chem. Soc.* **54**, 4434–4443 (1932).
 18. Kistiakowsky, G. B. & Smith, W. R. Kinetics of Thermal Cis-Trans Isomerization. III. *J. Am. Chem. Soc.* **56**, 638–642 (1934).
 19. Gutowsky, H. S. & Holm, C. H. Rate Processes and Nuclear Magnetic Resonance Spectra. II. Hindered Internal Rotation of Amides. *J. Chem. Phys.* **25**, 1228 (1956).
 20. Kurland, R. J., Rubin, M. B. & Wise, W. B. Inversion Barrier in Singly Bridged Biphenyls. *J. Chem. Phys.* **40**, 2426 (1964).
 21. Oki, M., Iwamura, H. & Hayakawa, N. NMR Studies of the Rates of Inversion of o,o'-Bridged Biphenyls. *Bull. Chem. Soc. Jpn.* **37**, 1865–1870 (1964).
 22. Allerhand, A., Chen, F. & Gutowsky, H. S. Spin-Echo NMR Studies of Chemical Exchange. III. Conformational Isomerization of Cyclohexane and d11-Cyclohexane. *J. Chem. Phys.* **42**, 3040 (1965).
 23. Sutherland, I. O. & Ramsay, M. V. J. The conformational mobility of bridged biphenyls. *Tetrahedron* **21**, 3401–3408 (1965).
 24. Allerhand, A., Gutowsky, H. S., Jonas, J. & Meinzer, R. A. Nuclear Magnetic Resonance Methods for Determining Chemical-Exchange Rates ¹. *J. Am. Chem.*

- Soc. **88**, 3185–3194 (1966).
25. Nakagawa, T. The NMR Signal Shape of Identical Nuclei Exchanging between Two Different Environments. *Bull. Chem. Soc. Jpn.* **39**, 1006–1008 (1966).
26. Oki, M. & Yamamoto, G. Effects of para-Substituents on the Rates of Inversion of Biphenyl Derivatives. II. 2-Isopropyl-2'-methoxybiphenyls. *Bull. Chem. Soc. Jpn.* **44**, 266–270 (1971).
27. Verma, S. & Singh, N. A study of conformation about the aryl C-N bonds in N-aryl imides by dynamic N.M.R. spectroscopy. *Aust. J. Chem.* **29**, 295–300 (1976).
28. Ogawa, S., Sato, S., Erata, T. & Furukawa, N. Dynamic NMR studies on the solution-state structure and the pseudorotation of bis(2,2'-biphenylene)selenurane and tellurane. *Tetrahedron Lett.* **33**, 1915–1918 (1992).
29. Braverman, S., Zafrani, Y. & Gottlieb, H. E. Dynamic NMR Study of the Rotation around 'Biphenyl-Type' Bonds in Polycyclic Sulfoxides. *J. Org. Chem.* **67**, 3277–3283 (2002).
30. Denk, M. Structure and Spectroscopy. at http://131.104.156.23/Lectures/CHEM_207/CHM_207_NMR.htm
31. Oki, M. *Applications of Dynamic Nmr Spectroscopy to Organic Chemistry*. (Vch Pub, 1985).
32. Bienz, S. *et al. Spektroskopische Methoden in der organischen Chemie, 8. überarb. Auflage 2011*. (Thieme, 2011).
33. Oki, M., Iwamura, H. & Yamamoto, G. Effects of para-Substituents on the Rates of Inversion of Biphenyl Derivatives. I. 5,7-Dihydrodibenzo[c,e]thiepins. *Bull. Chem. Soc. Jpn.* **44**, 262–265 (1971).
34. Oki, M., Iwamura, H. & Nishida, T. The Effect of Hydrogen Bonding on the Rates of Inversion of 1-Hydroxy-5, 7-dihydrodibenz[c,e]oxepin. *Bull. Chem. Soc. Jpn.* **41**, 656–660 (1968).
35. Oki, M., Akashi, K., Yamamoto, G. & Iwamura, H. Nuclear Magnetic Resonance Study of the Effect of the Hydrogen Bond on the Internal Rotation of Biphenyls. *Bull. Chem. Soc. Jpn.* **44**, 1683–1686 (1971).
36. Kessler, H. Detection of Hindered Rotation and Inversion by NMR Spectroscopy. *Angew. Chem. Int. Ed. Engl.* **9**, 219–235 (1970).
37. Stewart, W. E. & Siddall, T. H. Nuclear magnetic resonance studies of amides. *Chem. Rev.* **70**, 517–551 (1970).
38. Jaeschke, A., Muensch, H., Schmid, H. G., Friebolin, H. & Mannschreck, A.

The conformers of a nitrosamine and a carboxamide: Comparison of NMR line shape and equilibration methods. *J. Mol. Spectrosc.* **31**, 14–31 (1969).

39. Cheng, H. *Use of shift reagents in NMR studies of chemical exchange.* (1972).

40. Cheng, H. N. & Gutowsky, H. S. Use of shift reagents in nuclear magnetic resonance studies of chemical exchange. *J. Am. Chem. Soc.* **94**, 5505–5507 (1972).

41. Tanny, S. R., Pickering, M. & Springer, C. S. Increasing the time resolution of dynamic nuclear magnetic resonance spectroscopy through the use of lanthanide shift reagents. *J. Am. Chem. Soc.* **95**, 6227–6232 (1973).

42. Cheng, H. N. & Gutowsky, H. S. Temperature dependence of lanthanide induced chemical shifts. *J. Phys. Chem.* **82**, 914–921 (1978).

43. Cheng, H. N. & Gutowsky, H. S. Lanthanide shift reagents and their use in dynamic NMR studies. *J. Phys. Chem.* **84**, 1039–1043 (1980).

44. Trapp, O. Unified Equation for Access to Rate Constants of First-Order Reactions in Dynamic and On-Column Reaction Chromatography. *Anal. Chem.* **78**, 189–198 (2006).

45. Wang, J., Cooper, G., Tulumello, D. & Hitchcock, A. P. Inner Shell Excitation Spectroscopy of Biphenyl and Substituted Biphenyls: Probing Ring–Ring Delocalization. *J. Phys. Chem. A* **109**, 10886–10896 (2005).

46. Venkataraman, L., Klare, J. E., Nuckolls, C., Hybertsen, M. S. & Steigerwald, M. L. Dependence of single-molecule junction conductance on molecular conformation. *Nature* **442**, 904–907 (2006).

47. Vonlanthen, D. *et al.* Chemically Controlled Conductivity: Torsion-Angle Dependence in a Single-Molecule Biphenyldithiol Junction. *Angew. Chem. Int. Ed.* **48**, 8886–8890 (2009).

48. Vonlanthen, D., Rotzler, J., Neuburger, M. & Mayor, M. Synthesis of Rotationally Restricted and Modular Biphenyl Building Blocks. *Eur. J. Org. Chem.* **2010**, 120–133 (2010).

49. Vonlanthen, D. *et al.* Conformationally Controlled Electron Delocalization in n-Type Rods: Synthesis, Structure, and Optical, Electrochemical, and Spectroelectrochemical Properties of Dicyanocyclophanes. *Chem. – Eur. J.* **17**, 7236–7250 (2011).

50. Rotzler, J. *Tailoring Intra- and Intermolecular Properties: From Cyclophanes to Daisy Chains.* **1**, (Dr. Hut, 2012).

51. Mishchenko, A. *et al.* Single-Molecule Junctions Based on Nitrile-Terminated

Biphenyls: A Promising New Anchoring Group. *J. Am. Chem. Soc.* **133**, 184–187 (2011).

52. Li, Z., Wang, J., Zhang, J. & Zhou, Z. [(4-methyl-2-propyl-N-methoxyl-substituted benzene alkyl-1H-benzimidazole-6-formamide)-1-yl] methylidiphenyl compound and preparation method thereof. (2010). at http://worldwide.espacenet.com/publicationDetails/biblio;jsessionid=F5A106F105FD102525703FEC67AFC2D5.espacenet_levelx_prod_2?FT=D&date=20100811&DB=EPODOC&locale=en_EP&CC=CN&NR=101798287A&KC=A&ND=4
53. Berger, S. & Braun, S. *200 and More NMR Experiments: A Practical Course*. (Wiley-VCH Verlag GmbH & Co. KGaA, 2004).
54. *Program Package for ab initio Electronic Structure calculations. TURBOMOLE, Version 6.3, a development of University of Karlsruhe and Forschungszentrum Karlsruhe GmbH 1989-2007, Turbomole GmbH since 2007.*
55. Vosko, S. H., Wilk, L. & Nusair, M. Accurate spin-dependent electron liquid correlation energies for local spin density calculations: a critical analysis. *Can. J. Phys.* **58**, 1200–1211 (1980).
56. Becke, A. Density-functional exchange-energy approximation with correct asymptotic behavior. *Phys. Rev. Gen. Phys.* **38**, 3098 (1988).
57. Jianmin *et al.* Climbing the Density Functional Ladder: Nonempirical Meta-Generalized Gradient Approximation Designed for Molecules and Solids. *Phys. Rev. Lett.* **91**, (2003).
58. Becke, A. D. Density-functional thermochemistry. III. The role of exact exchange. *J. Chem. Phys.* **98**, 5648–5652 (1993).
59. Weigend, F. & Ahlrichs, R. Balanced basis sets of split valence, triple zeta valence and quadruple zeta valence quality for H to Rn: Design and assessment of accuracy. *Phys. Chem. Chem. Phys.* **7**, 3297 (2005).
60. Treutler, O. & Ahlrichs, R. Efficient molecular numerical integration schemes. *J. Chem. Phys.* **102**, 346 (1995).
61. Scott, A. P. & Radom, L. Harmonic Vibrational Frequencies: An Evaluation of Hartree-Fock, Møller-Plesset, Quadratic Configuration Interaction, Density Functional Theory, and Semiempirical Scale Factors. *J. Phys. Chem.* **100**, 16502–16513 (1996).
62. Marjani, K., Mousavi, M., Nahzomi, H. T., Arazi, O. & Jafari, R. Dynamic NMR and computational study of 5,5-dimethyl-3,4-di-p-tolyl-2-cyclopenten-1-one.

Spectrochim. Acta. A. Mol. Biomol. Spectrosc. **79**, 1798–1802 (2011).

63. Shinji *et al.* Rotational Isomerism Involving an Acetylenic Carbon II. Effect of 1-Halogen Substituents on Rotamer Population and Rotational Barrier around C(sp)-C(sp³) Bonds in Bis(9-triptycyl)ethynes. *Bull. Chem. Soc. Jpn.* **73**, 2591–2597 (2000).
64. Hart, H. & Sedor, E. A. Mechanism of cyclodehydration of 2-phenyltriarylcarbinols. *J. Am. Chem. Soc.* **89**, 2342–2347 (1967).
65. Kita, F., Adam, W., Jordan, P., Nau, W. M. & Wirz, J. 1,3-Cyclopentanediyli Diradicals: Substituent and Temperature Dependence of Triplet–Singlet Intersystem Crossing. *J. Am. Chem. Soc.* **121**, 9265–9275 (1999).
66. Swain, C. G. & Lupton, E. C. Field and resonance components of substituent effects. *J. Am. Chem. Soc.* **90**, 4328–4337 (1968).

C) Structure elucidation and Synthesis of a novel leukaemia-associated T cell lipid antigen

C.1 Research Goal

The discovery and the characterization of tumour-associated antigens recognized by specific T cells opened novel and promising therapeutic opportunities for treatment of cancer. The tumour-associated antigens identified so far consist of peptides derived from proteins accumulated in cancer cells and presented to T cells by major histocompatibility complex I (MHC-I) antigen-presenting molecules.¹ Research from the group of Prof. Dr. Gennaro De Libero revealed that T cells can also recognize lipid antigens expressed in tumour cells, particularly in leukaemia cells,^{2,3} and suggested that these T cells may be involved in anti-leukaemia immune response. Aim of the present study, developed in collaboration with the group of Prof. Dr. De Libero, has been the structural elucidation of a novel leukaemia-associated T cell lipid antigen and the synthesis of the natural occurring molecules.

C.2 Introduction

CD1 proteins are antigen-presenting molecules specialized in presenting lipids to specific T cells. In humans, they are present in five different isoforms identified as CD1a, CD1b, CD1c, CD1d and CD1e. CD1 molecules form stable T cell stimulatory complexes with a large variety of structurally different lipids antigens derived from microbes or synthesized inside the antigen presenting cells (APC). T lymphocytes, able to recognize lipid antigens bound to CD1 molecules, are known as CD1-restricted T cells and are involved in anti-microbial immunity⁴ as well as in anti-tumor immune response.^{5,6}

In a recent study,³ the group of Prof. Gennaro De Libero identified from healthy individuals particular T cells capable of specifically recognizing and killing leukaemia

cells in CD1c-dependent manner and without addition of exogenous antigens. These data suggested that the lipid molecule(s) recognized by T cells were synthesized inside the leukaemic cells. As tumour cells display a marked alteration in different metabolic pathways,⁷ including those related to the biosynthesis and degradation of lipids, it was hypothesized that the observed CD1c-restricted and lipid-specific T cell reactivity against leukaemia cells could be due to accumulation of unique lipids.

To investigate this issue, biochemical fractionation of lipids extracted from leukaemic cells was coupled with functional *in vitro* T cell activation assays and structural analysis of active lipid fractions, in order to identify and characterize the stimulatory lipids³.

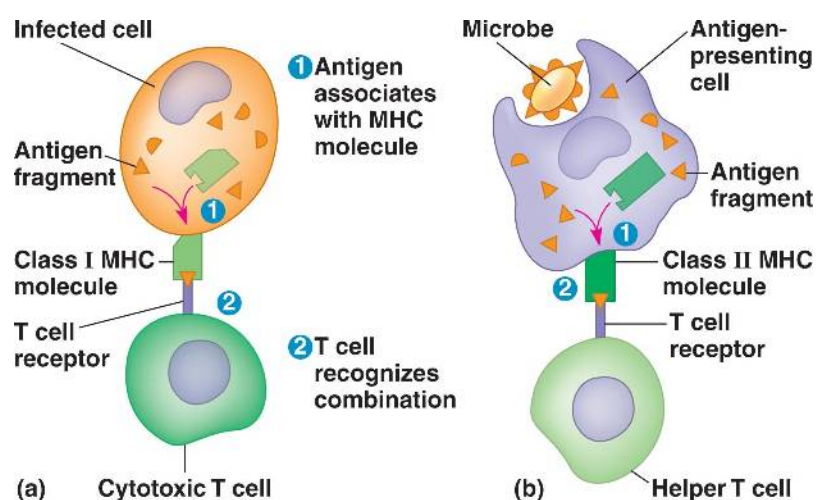


Figure C-1: Schematic representation of a T-cell receptor interaction.⁸

The big limitation of these types of studies, aimed to identify a bioactive molecule out of a complex mixture of different molecules extracted from cells, is the small recovery of active compounds. The multiple steps required for their purification and the need of testing their biological activity *in vitro* significantly impact on the amounts of material remaining for further structural analyses. In our study, lipids were extracted from very high number of leukaemia cells and fractionated according to their polarity. Several protocols were exploited in order to set up a method suitable to obtain acceptable yield and satisfying purity. The purified lipids were then tested for their T cell stimulatory potential. The fractions that showed activity were purified by HPLC chromatography and the resulting sub-fractions were again tested in T cell activation assays. The active sub-fractions were further analysed by spectroscopic methods to gain knowledge about their identity.

Mass spectrometry (MS) can detect small quantities of a compound, in the range of nanograms and provides information about the purity of a sample and the identity of

a molecule. MS is therefore widely used for the identification of compounds accessible only in small quantities. In particular LC-MS, where a HPLC system is coupled to a mass spectrometer, is the most efficient system for such studies. The combination of LC and MS allows precise analysis of complex mixtures and provides important information about single molecules, namely the retention time and the mass. Furthermore, special MS techniques allow fragmentation of a molecule to give insights about its functional groups. Therefore, LC-MS analysis provides a variety of important indications for the assignment of the final structure. Nevertheless, in many cases the structure elucidation remains incomplete, as the substitution pattern might be unclear. In these situations, a further structural proof is needed. The proof is usually achieved by X-ray crystallography or NMR spectroscopy. Both methods have advantages and disadvantages. X-ray analysis delivers an accurate structure of the investigated molecule. However, for X-ray measurements a single crystal is required, which is not easy to grow when only small quantities of a purified molecule are available (crystal growth out of complex mixtures is in most cases impossible). NMR spectroscopy is a good complement to MS spectrometry for structure elucidation. NMR has a mass limitation in the range of milligrams for standard (5 mm probe heads) equipped spectrometers. Nevertheless, the availability of special NMR-tubes like shigemi-tubes, decreased the required mass by a factor of about two and the following development of 1.0 and 1.7 mm micro-probeheads, allowed also investigation of submilligram quantities. The new generation of cryogenic micro-probeheads further increased the sensitivity and allows investigation of samples with quantities in the nanogram region. NMR analysis can therefore be used, on the basis of LC-MS data, to confirm the MS fragmentation patterns and to define the final three-dimensional structure of a molecule also when it is available in small amounts. This identification process requires a series of one and more dimensional experiments. These techniques were applied for the elucidation of the final structure of the leukaemia-associated T cell stimulatory antigen identified in our study.

The identification of such active compounds leads in many cases to the development of a total synthesis. Total synthesis can deliver the active compound in higher quantities. These higher quantities are unambiguously necessary to investigate the active compounds in more detail. Depending on the identified molecule different functions should be investigated. For therapeutic active compounds, the uptake mechanisms and the IC 50 values are quite important. Therefore, a total synthesis of

the identified active compounds was achieved to have larger quantities for investigations in hand.

C.3 Methods and Materials

C.3.1 Cell extraction

The cell extraction protocol used for the presented methyl-lysophosphatidic acid (mLPA) is presented elsewhere.³

C.3.2 LC-MS purification

“Pre purification of the lipid using HPLC was performed on a reverse phase C18 polar endcapped column (3 μ m particle size, 3 mm ID, 125 mm length, Marcherey Nagel). LC-MS-MS was performed using Rheos Allegro pump (Flux instruments) and HTC PAL injector with a 20 μ L loop (LTC Analytics AG). M_s^n were acquired using an LXQ ion trap mass spectrometer equipped with a heated electrospray ionisation (ESI) source (Thermo Fischer Scientific). Source conditions: spray voltage 5 kV; capillary voltage 12 V; capillary temperature 265 °C. tube lens offset voltage 100 V. CID spectra were acquired on an API 4000 LC-MS-MS system with a triple quadrupole analyser (Applied Biosystems / MDS Scicx). Exact mass measurements were performed on a LTQ-MS (Thermo Fischer Scientific). All lipid standards were purchased from Avanti Polar Lipids, Inc..”³

C.3.3 NMR studies

The mLPA samples obtained from cell extracts were recorded on an Avance III 600 MHz spectrometer (Bruker®) operating at 14.1 Tesla and 298 K. The spectrometer was equipped with a triple resonance (^1H , ^{13}C , ^{31}P), 1.7 mm micro probe head with a self-shielded z-gradient coil. All mLPA experiments were performed in sodium formate buffered deuterated methanol d-4 (99.96 % D; Cambridge Isotope Laboratories, Burgdorf CH). All synthetic samples were prepared in deuterated solvents (>99.8 % D; Cambridge Isotope Laboratories, Burgdorf CH). The NMR experiments performed on synthetic samples were recorded using a DRX-600 MHz / Avance III 600 MHz NMR spectrometer equipped with a self shielded z-axis pulsed

field gradient dual-channel broadband inverse 5 mm probe head (BBI) (Bruker®). Chemical shifts were referenced to residual solvent peaks.

The mLPA was dissolved in 30 μ L, solvent, syringe-transferred to a 1.7 mm diameter NMR sample tube. The two dimensional experiments were recorded with 2048 data points in the direct dimension and increments in the indirect dimension numbering 1024 (COSY and HSQC) or 256 (^{31}P -HMBC), resulting in acquisition times of 285 (F2) and 142 ms (F1) for the COSY, 142 and 20.5 ms for the HSQC, 142 and 10.5 ms for the ^{31}P -HMBC. The COSY was performed with 8 scans per increment, leading to a total experimental time of 3 h 21 min; the HSQC (144 scans, 64 h 17 min) and the ^{31}P -HMBC (8 scans, 59 min). A ^{31}P decoupling 180° pulse was applied during the ^{13}C evolution period of the sensitivity-enhanced Echo-Antiecho HSQC experiment and during ^1H acquisition. The long range delay in the ^{31}P -HMBC was set to 62.5 ms. All other NMR experiments were routine experiments.³

C.3.4 Synthesis

All chemicals used were obtained in reaction grade (> 98 %) and used without further purification. Solvents (technical grade) for column chromatography were redistilled prior to use. The reactions were performed in standard glassware. Chloroform for reactions was stabilized with amylenes (amylenes are hydrocarbons with a molecular formula C_5H_{10} , the double bond makes them to good stabilizers) instead of ethanol to prevent side reactions. Reaction control was performed with thin layer chromatography (Merck) if not stated otherwise.

C.4 Retrosynthetic analysis and synthetic strategy

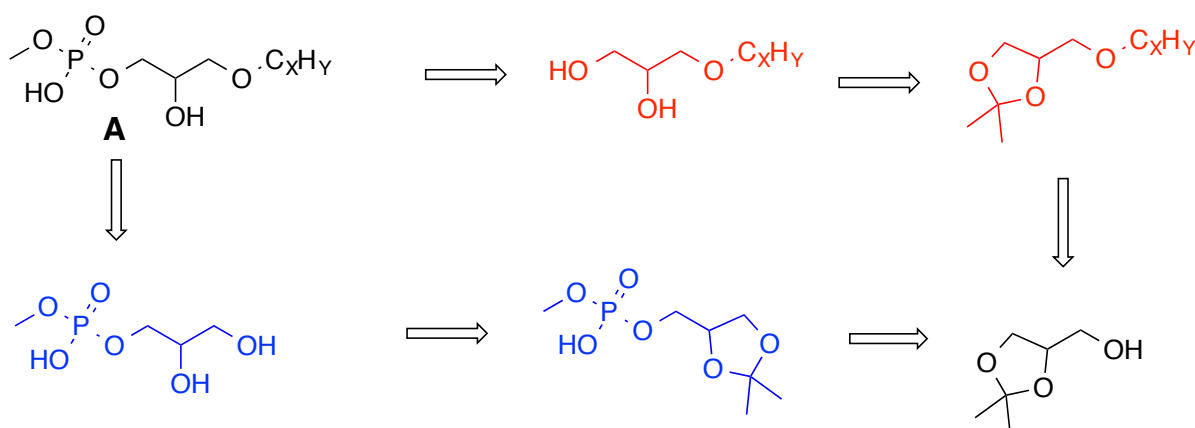


Figure C-2: Retrosynthetic analysis of mLPA (A).

The synthesis of mLPA (**A**) can be performed in different ways. The glycerine backbone is a well known starting point for many lipid syntheses described earlier. For the synthesis of mLPA it is possible to introduce the phosphate in a last step, as shown in the red strategy. In this strategy the alkyl chain is introduced in the first step. After the introduction of the alkyl chain the protection group is removed and a special protection protocol is applied to allow the introduction of a phosphate at the 3'-position in a selective way.

The main advantage of the strategy depicted in red is the higher stability and the easier purification of the synthetic intermediates.

An alternative synthetic route is shown in blue. In this case the phosphate is introduced in the first reaction step and the alkyl chain has to be introduced in a selective way in a later stage of the synthesis.

Both routes allow an enantioselective synthesis by choosing an appropriated protection protocol. The starting material can be purchased enantiopure or as racemic mixture.

C.5 Results

To identify CD1c-presented T cell stimulatory leukaemia antigens, lipids were extracted from THP1 cells, a cell line representative of acute myeloid leukaemia and efficiently recognized by specific CD1c-restricted T cells. The lipids were fractionated by amino cartridge according to their different polarity. One active fraction was identified, which was further sub-fractionated by HPLC. Three resulting sub-fractions with a retention time of 17, 18 and 19.5 min showed high T cell stimulatory capacity. The corresponding chromatogram, mass spectra and T cell activation profile is shown in Figure C-3 and Figure C-4.

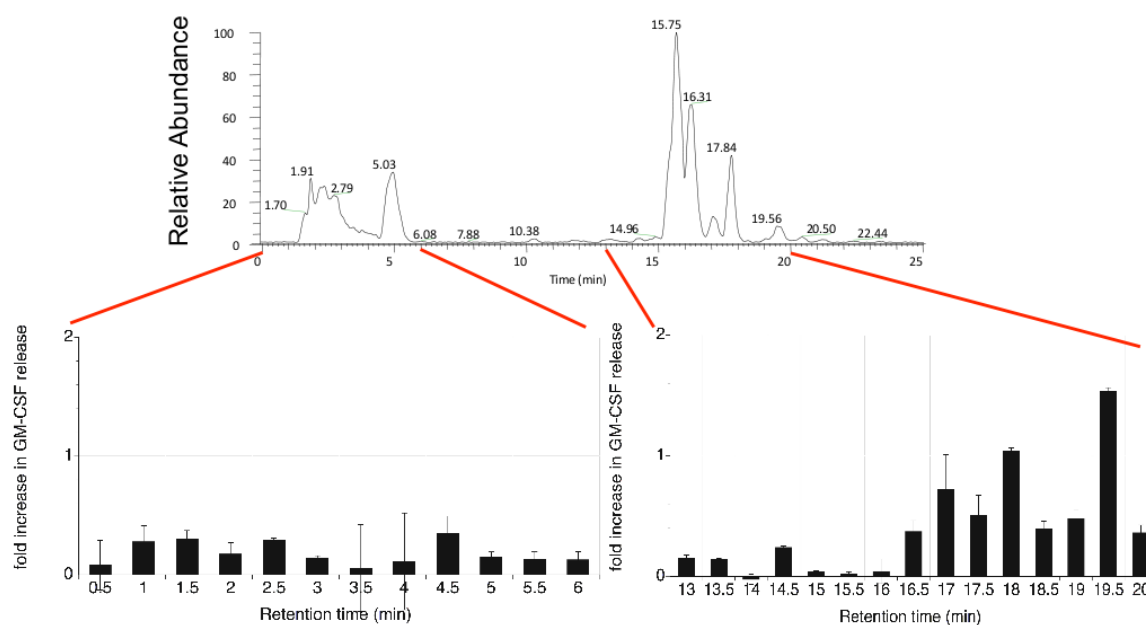


Figure C-3: HPLC profile (on top) and the corresponding T-cell activation tests (bottom).

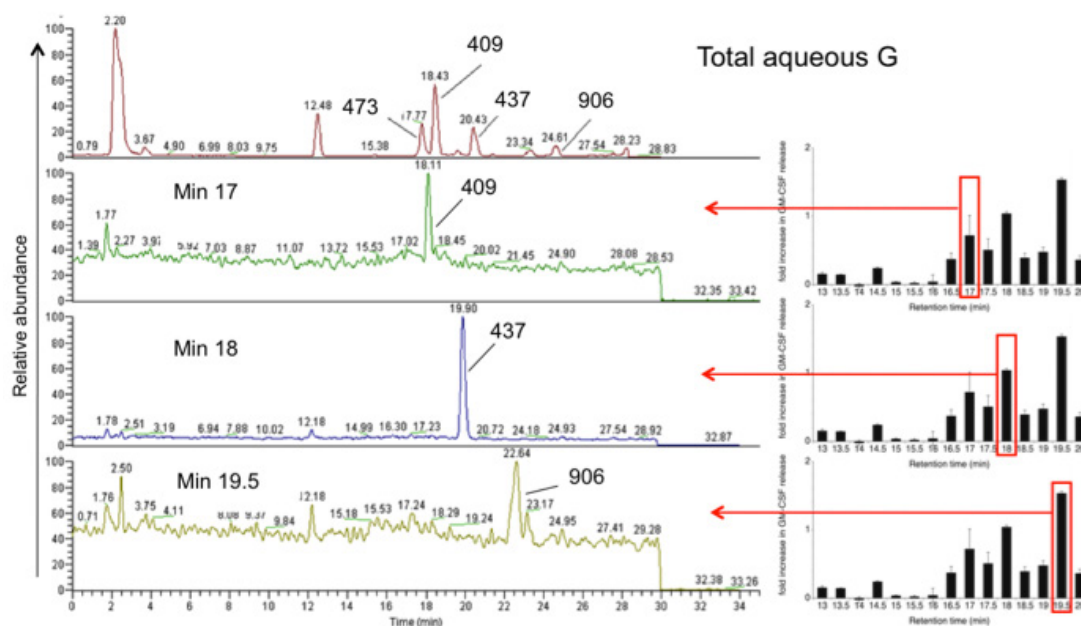


Figure C-4: ESI-MS-spectra (negative measurement mode) of the cell extracts on top the non purified mixture followed by the active fractions resulting from a retention time of 17, 18 and 19.5 min.

To gain structural insights and to identify the functional groups of the molecule with masses 409^- , 437^- and 906^- , eluted at 17, 18 and 19.5 min respectively MS² (MS-MS) fragmentation experiments were performed.

In a study performed by Kertscher,⁹ an ether lipid with a mass of 409^- was described as a synthetic analogue of platelet-activating factor. The corresponding structure **A** is shown in Figure C-5. No NMR and MS fragmentation data for this compound were presented in Kertscher's work, thus no comparison between our identified molecules and those described in this paper could be performed.

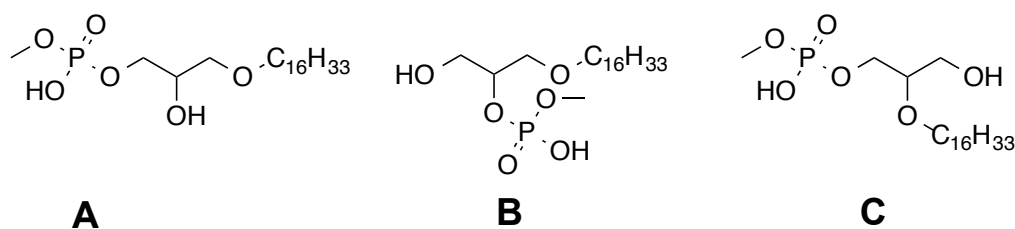


Figure C-5: Suggested isomers of the isolated mLPA with a $m/z = 409^-$ after MS-analysis.

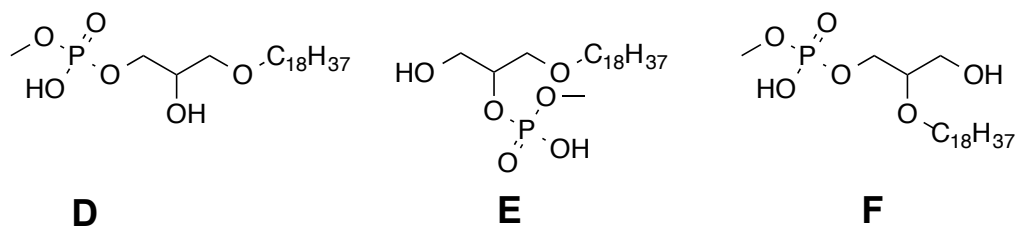


Figure C-6: Suggested isomers of the isolated mLPA with a $m/z = 437^-$ after MS-analysis.

The fragmentation of the compound with a mass of 409^- will be described in detail (Figure C-8, Figure C-9) and a similar fragmentation pattern was obtained for the molecule with a mass of 437^- .³ Fragmentation experiments delivered $m/z = 377^-$ that corresponds to the loss of OCH_3 ($m/z = 32$) group. Triple stage mass spectrometry (MS^3) was performed in negative mode to deliver further insights. In this case the peak with an $m/z = 377^-$ is fragmented a second time delivering a mass of 239^- indicating an $^- \text{OC}_{16}\text{H}_{33}$ group. The fragmentation pathway is shown in Figure C-8. The same experiments were performed in the positive mode to prove the results obtained in the negative mode. Identification of the product mass 411^+ was complicated and only a weak peak could be obtained, as the natural product was unlikely to be protonated. The fragmentation delivered a ion with a $m/z = 299^+$ corresponding to the loss of a $\text{O}=\text{PO}(\text{OH})(\text{OMe})^-$ group. In the positive mode a $m/z = 225^+$ was obtained corresponding to $^+ \text{C}_{16}\text{H}_{33}$ cation (Figure C-9). The glycerine backbone can be assumed from the identification of all other fragments and as standard structural element of lipids. The identified structural elements are therefore: a glycerine backbone, a methylated phosphate and a $\text{OC}_{16}\text{H}_{33}$ side chain. The main differences to lipids identified in this research field so far are an ether bridged side chain and a methylated phosphate moiety. High-resolution mass spectroscopy (HRMS) confirmed the resulting formula ($\text{C}_{20}\text{H}_{43}\text{PO}_6$). Several isomers can be predicted as shown in Figure C-5. Structure **A** shows the most similarities to already known lipids and was assumed as most probable structure after MS-analysis.

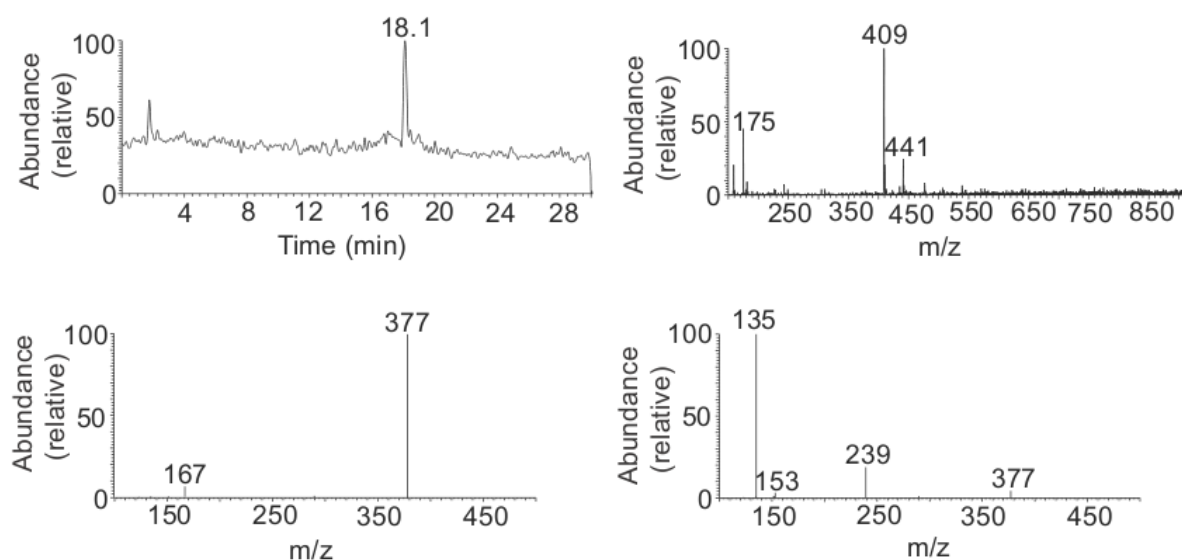


Figure C-7: On top left: HPLC trace of the purified natural mLPA sample. On top right: ESI-MS spectra of the mLPA sample measured in the negative mode. On bottom left: ESI-MS² of the mass 409^- . On bottom right: ESI-MS³ of the mass 377^- .

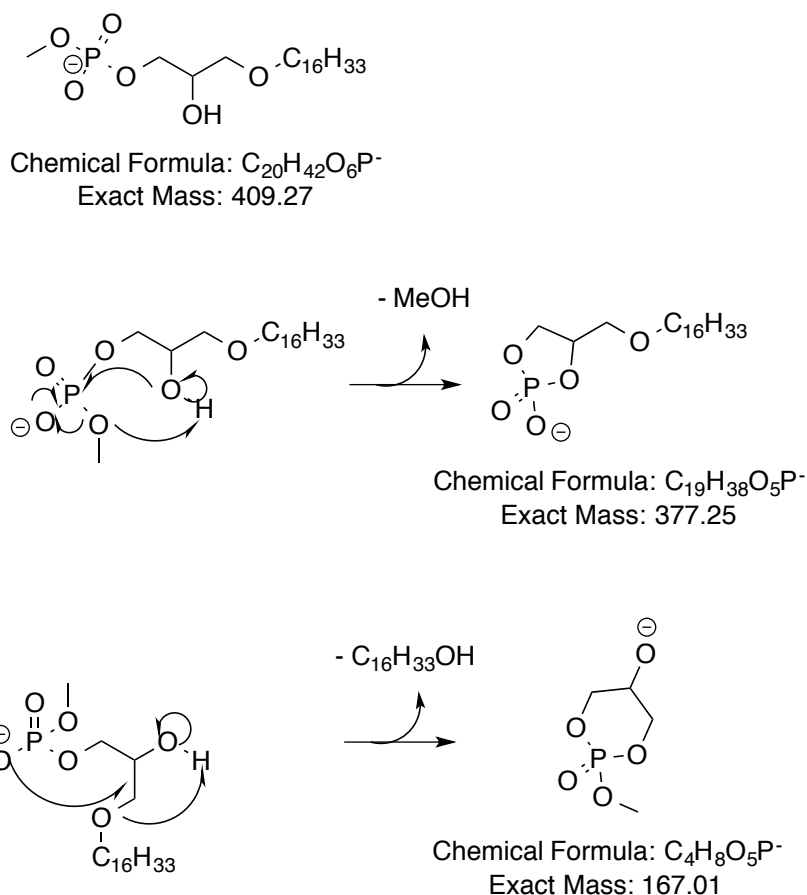
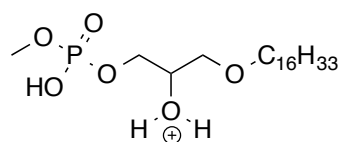


Figure C-8: Fragmentation pathway for structure A in MS-MS experiments recorded in the negative mode.

MS analysis was performed in a similar way for two other highly active compounds. For the mass of 437^- similar fragmentation pattern were detected. The only difference for this molecule was the larger alkyl chain that contains two more CH_2 -groups. Also in this case an ether side chain instead of a ester side chain was predicted. Similar isomers can therefore be expected as shown in Figure C-6 with structure D being the most likely one. Unfortunately no structure could be assigned or proposed yet for the molecule with mass of 906^- eluted at 19.5 min.



Chemical Formula: $C_{20}H_{44}O_6P^+$
Exact Mass: 411.29

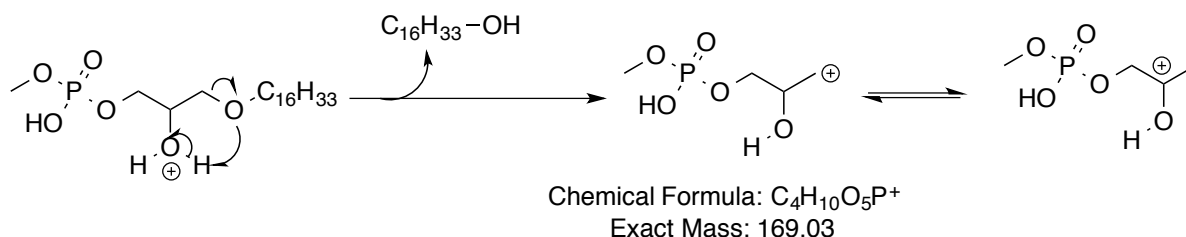
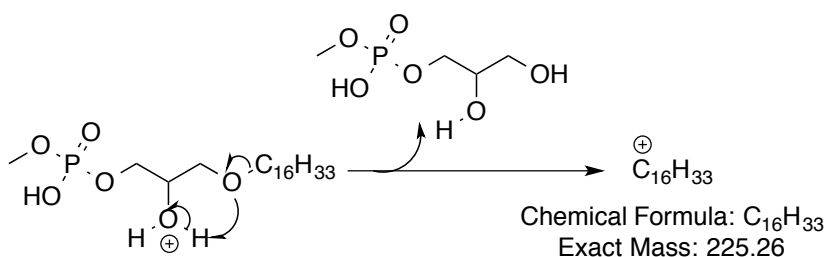
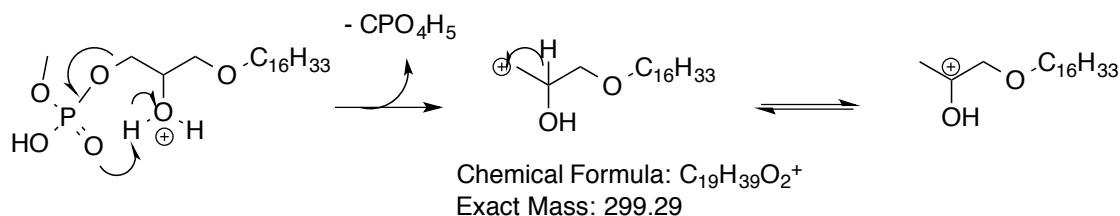


Figure C-9:MS-fragmentation pathway for structure A in MS-MS experiments recorded in the positive mode.

Because of the unusual features of the identified lipids, determined by LC-MS-MS, and considering that such molecules were never described before, further analysis to univocally characterize, define and confirm their structure was required. NMR experiments were indeed performed on the HPLC purified natural product. A lot of impurities (not detected by ESI-MS) were observed, which made structure elucidation with standard equipment impossible as only a few micrograms of the sample contained really the molecule of interest. Overlaps in the proton spectrum were detected, which could be resolved by 2D measurements. The selective ^{31}P decoupled proton ($^1H\{^{31}P\}$) experiment showed that the doublet of the methoxy group collapses to a singlet (Figure C-10) (The complete spectra are shown in the experimental section). Therefore a $^3J_{HP} = 12$ Hz coupling constant could be identified which fits quite nicely to literature values. Two more signals that contained a

phosphorous coupling were identified in a range from 3.8 to 3.9 ppm. This finding indicates strongly structure **A** as a ${}^3J_{\text{HP}}$ is much more likely than a ${}^4J_{\text{HP}}$ as also coupling constants in a range of about 12 Hz could be measured.

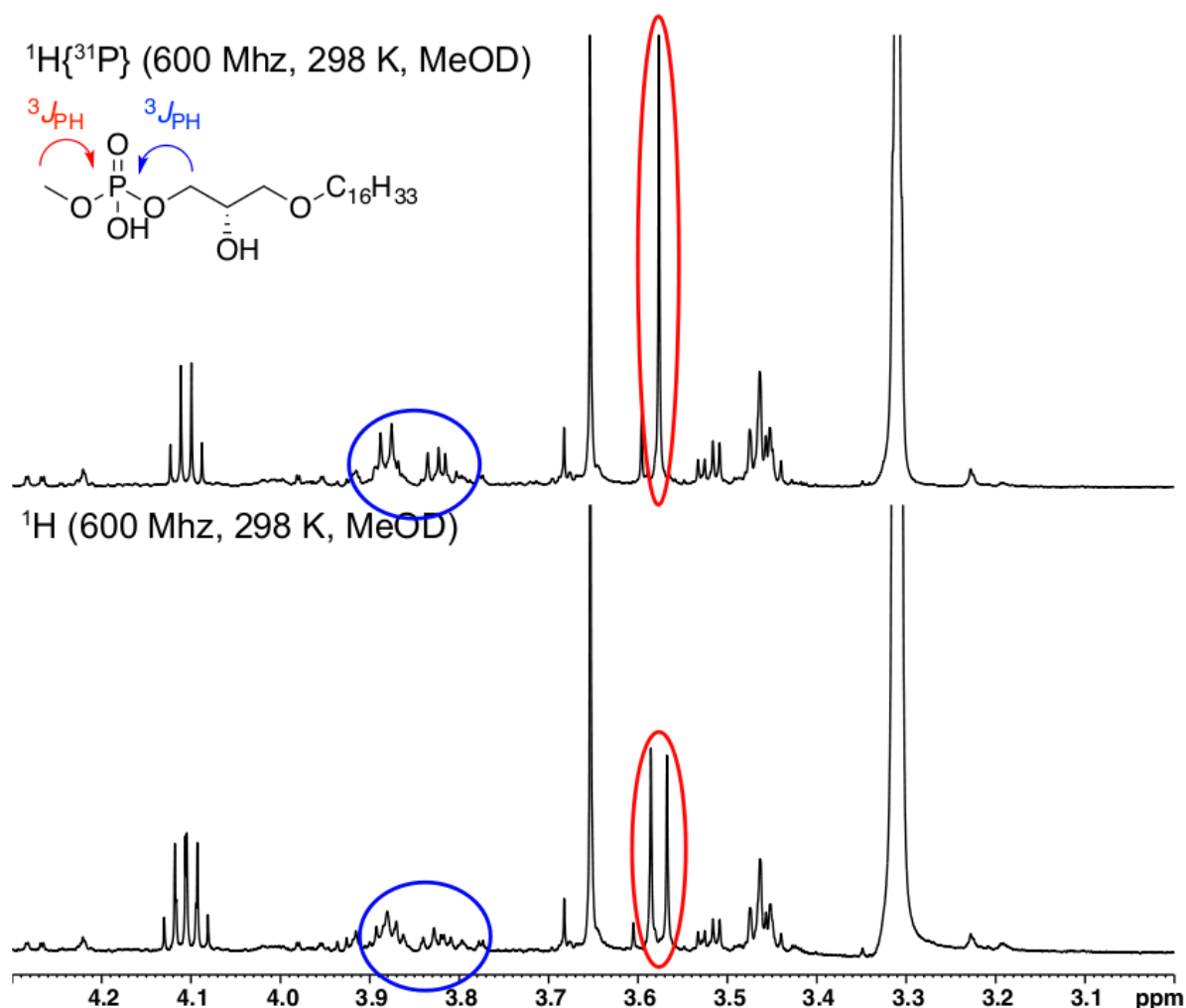


Figure C-10: Comparison of ${}^1\text{H}\{{}^{31}\text{P}\}$ decoupled and ${}^1\text{H}$ NMR spectra. It is nicely shown, that the duplet at 3.58 ppm collapses to a singlet (red label) and the multiplet between 3.8 and 3.9 ppm (blue label) is influenced by the decoupling.

The 2D-heteronuclear experiments with standard equipment could not confirm the suggested structure, as carbons that contained a phosphorous coupling could not be detected. A good explanation for this finding is the carbon-phosphorous coupling (${}^2J_{\text{CP}} = 5\text{-}20$ Hz) that decreases the intensity by a factor of two due to the coupling. The use of a triple resonance 1.7 mm (TXI (${}^1\text{H}$, ${}^{13}\text{C}$, ${}^{31}\text{P}$), 600 MHz) probe allowed the full characterization of the natural sample. With this special probe head 2D-heteronuclear experiments could be performed with additional phosphorous decoupling. This phosphorous decoupling increased the intensity of carbon signals that showed a phosphorous coupling by a factor of two. The usage of 1.7 mm NMR tubes compared to 5.0 mm NMR tubes (Standard NMR equipment) lead to a

reduction from 500 μL to 30 μL solvents. This decreased amount of solvent enlarged the concentration by a factor of 16. The higher concentrations reached with a 1.7 mm NMR tube allowed the measurement of 2D-experiments of only a few micrograms of substance. A HSQC experiment with carbon and phosphorous broadband decoupling (Figure C-11) as well as a HMBC spectrum with phosphorous decoupling could be recorded. The HSQC spectra allowed the identification of the carbon corresponding to the OMe group as well as the CH_2 -group of the glycerine backbone that is coupled to the phosphorous. The combination of COSY, HMBC and HMQC allowed the identification of the alkyl-chain in position 1 and suggested the phosphate moiety in 3 position.

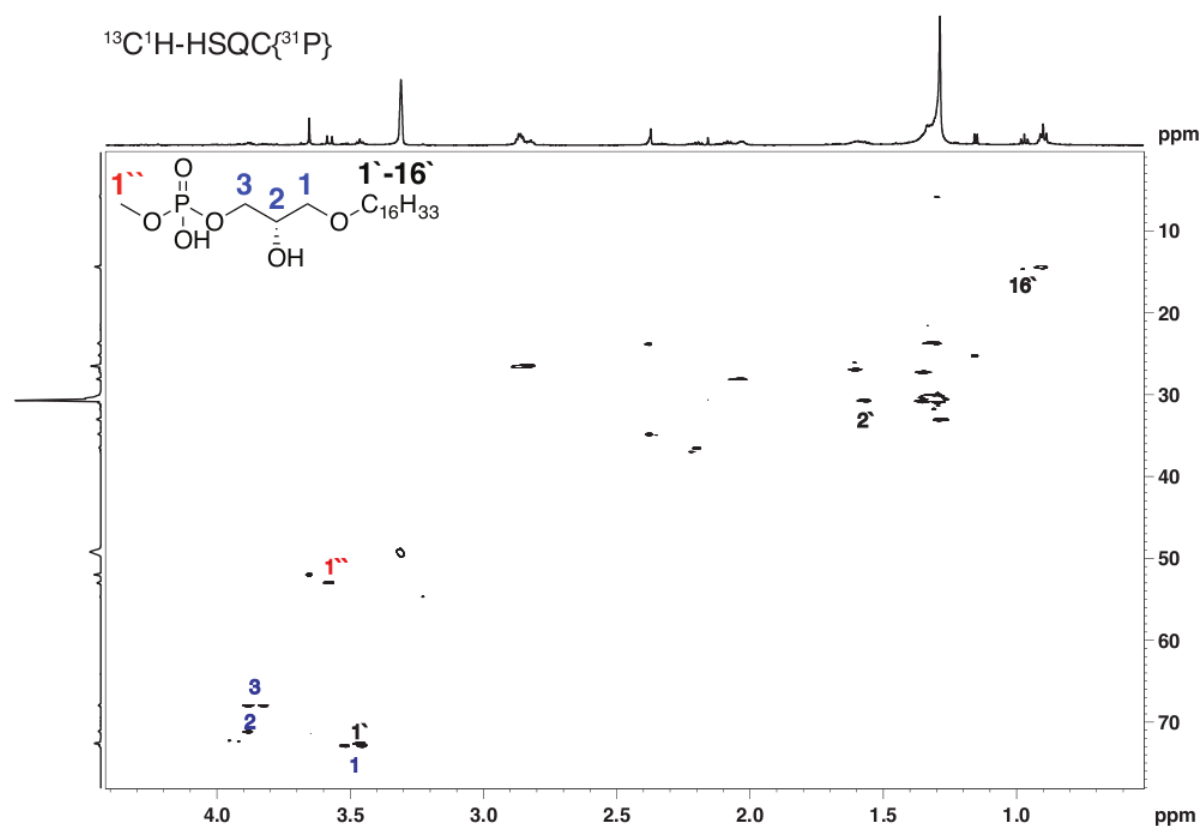


Figure C-11: The presented $^{13}\text{C}\{^1\text{H}\}$ -HSQC $\{^{31}\text{P}\}$ spectrum allowed the identification of 1' and 3, which could not be detected without phosphorous decoupling.

The so far presented spectra could show that the CH_2 -group 3 and OMe-group 1' have a coupling to a ^{31}P , but it remained unclear whether they were located on the same phosphorous or on a different. A one to one mixture of two compounds could also explain the so far presented spectra. It was therefore necessary to measure a ^{31}P -HMBC spectrum. The recorded spectrum could unambiguously confirm that both groups are attached to the same phosphorous as shown in Figure C-12.

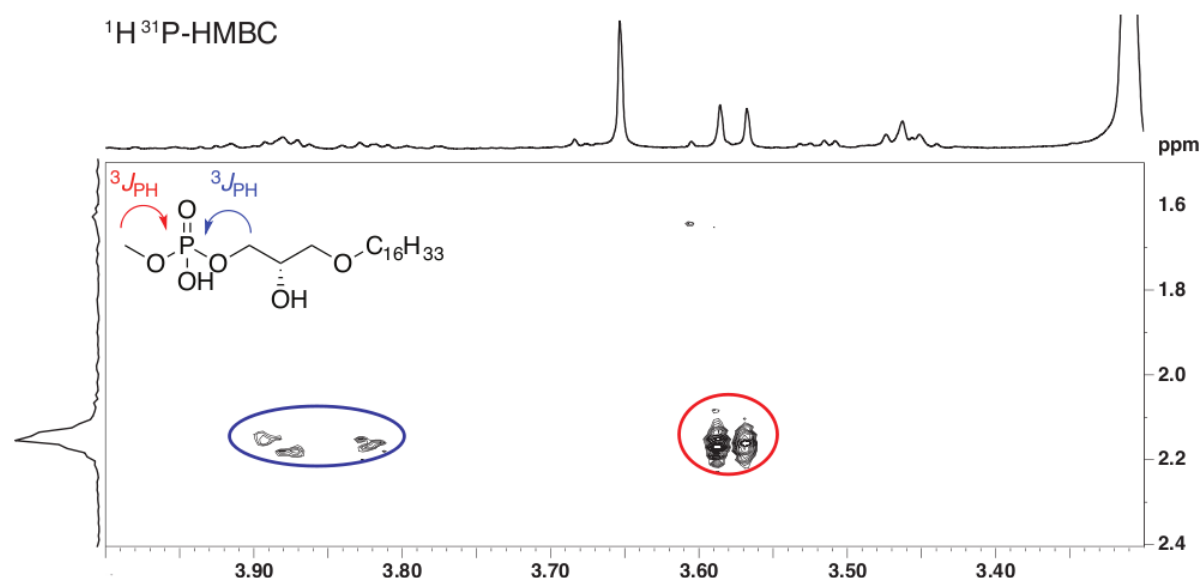
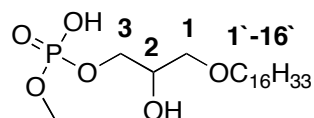


Figure C-12: $^1\text{H } ^{31}\text{P}$ -HMBC spectra confirming that the CH_2 -group from the glycerine backbone and the OMe-group are connected to the same phosphorous.

With these additional experiment the structure of the extracted lipid could be confirmed as being structure **A**. The complete proton, carbon and phosphorous assignment can therefore be shown.



$^1\text{H-NMR}$ (600 MHz, MeOD- d_4 , δ /ppm): 0.88 (t, $^3J_{\text{HH}} = 8$ Hz, 3H, **H16'**); 1.21-1.35 (m, 26H, **H3'-H15'**); 1.57 (q, $^3J_{\text{HH}} = 8$ Hz, 2H, **H2'**); 3.41 (m, 1H, **H1**); 3.46 (m, 2H, **H1'**); 3.47 (m, 1H, **H1**); 3.51 (m, 1H, **H3**); 3.58 (d, $^3J_{\text{HP}} = 12$ Hz, 3H, **OMe**); 3.58 (m, 1H, **H3**); 3.72 (m, 1H, **H2**).

$^{13}\text{C-NMR}$ (151 MHz, MeOD- d_4 , δ /ppm): 14.4 (1C, **C16'**); 26.4 (1C, **C15'**); 27.2 (1C, **C14'**); {29.4 – 30.5, **C3'-C13'**}; 30.6 (1C, **C2'**); 52.8 (1C, **OMe**); 64.9 (1C, **C3**); 72.2 (1C, **C2**); 72.5 (1C, **C1'**); 73.1 (1C, **C1**).

$^{31}\text{P-NMR}$ (243 MHz, MeOD- d_4 , δ /ppm): 2.2 (1P).

Additional NMR spectra are shown in the experimental section.

Total synthesis of the identified lipid was performed. The higher compound quantities were used to confirm unambiguously the identification of lipid **A** as active species. The synthetic strategy is presented in Figure C-13.

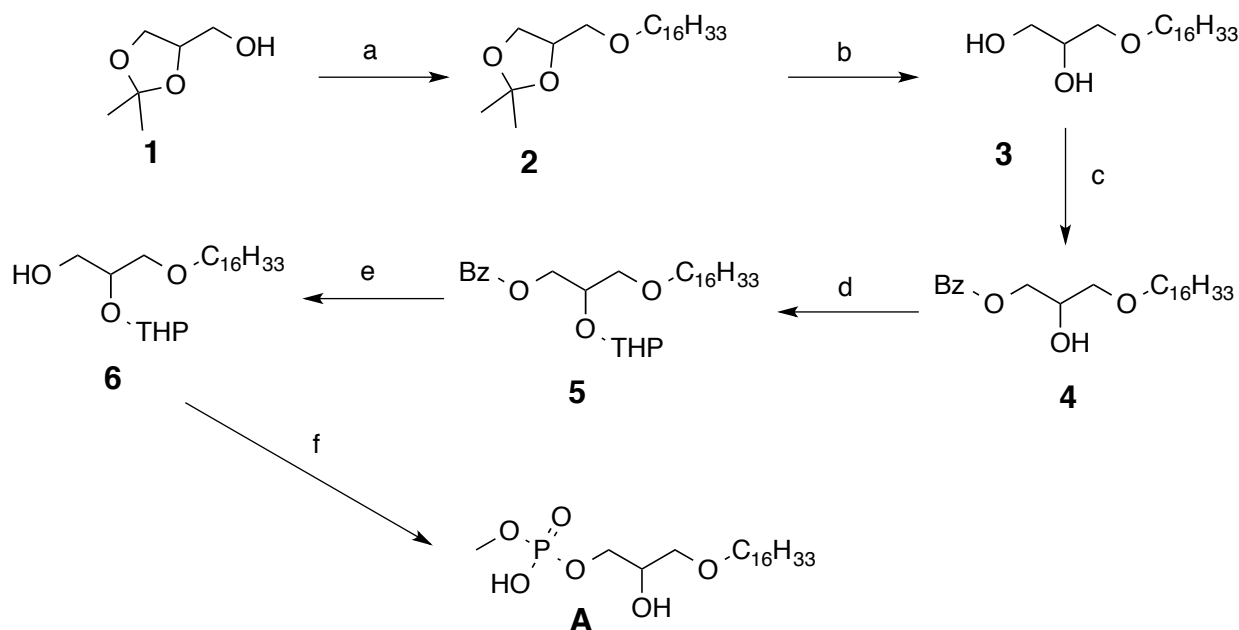


Figure C-13: Synthetic strategy towards mLPA (A): a) sodium, 1-chlorohexadecane, 18h, reflux, 40 %; b) AcOH, rt, overnight, 99%; c) benzoylchloride, triethylamine, DMAP in toluene, rt, 66 %; d) 3,4-dihydro-2-*H*-pyrane, 10 % PPTS in dichloromethane, 4h, rt, 95%; e) NaOMe in MeOH, 0 °C, 15-30 min., 92 %; f) POCl₃, triethylamine, chloroform (stabilized with amylenes), -10 °C, 30 min., rt, 30 min., MeOH, pyridine, rt, 16 h, water, rt, 60 min.

Starting from commercially available racemic-isopropylidene glycerol, the C₁₆ side chain was introduced to yield 40% of intermediate **2** after purification. The acetal-protecting group was removed under acidic conditions in quantitative yield. Selective protection of the primary alcohol using benzoyl chloride delivered compound **4** in moderate yield. Orthogonal protection in 2-position with a THP protecting group worked in excellent yield. The following basic deprotection of the benzoyl group delivered intermediate **6**, which is stable over several months at ambient temperature. The final product could be generated in a one-pot synthesis; the *in situ* generation of HCl cleaved the THP ether. All intermediates were characterized with ESI-MS and 2D NMR experiments. The detailed synthesis and characterization of the compounds is shown in the experimental section. Purification of the final product remained challenging. However, purification with silica column chromatography did not work due to strong interactions with the stationary phase. Changing to alox as stationary phase led to decomposition of the product. Crystallization of the lipid was also not successful. Preparative thin layer chromatography yielded in higher purity but only HPLC purification under the same conditions used for the natural sample delivered a highly pure sample. Due to the purification of only analytical quantities the yield for the last reaction step could not be determined.

The synthesis of the mLPA was performed in six linear steps. The protection protocol was chosen in a way that the stereochemistry of the 2-position of the glycerine backbone was not affected in any step. This allows the preparation of the corresponding enantioselective mLPA molecule.

The synthetic mLPA **A** could be fully characterized by two-dimensional NMR spectroscopy. Buffering of the synthetic sample with sodium formate delivered the identical proton (Figure C-14), carbon and phosphorus NMR spectra.

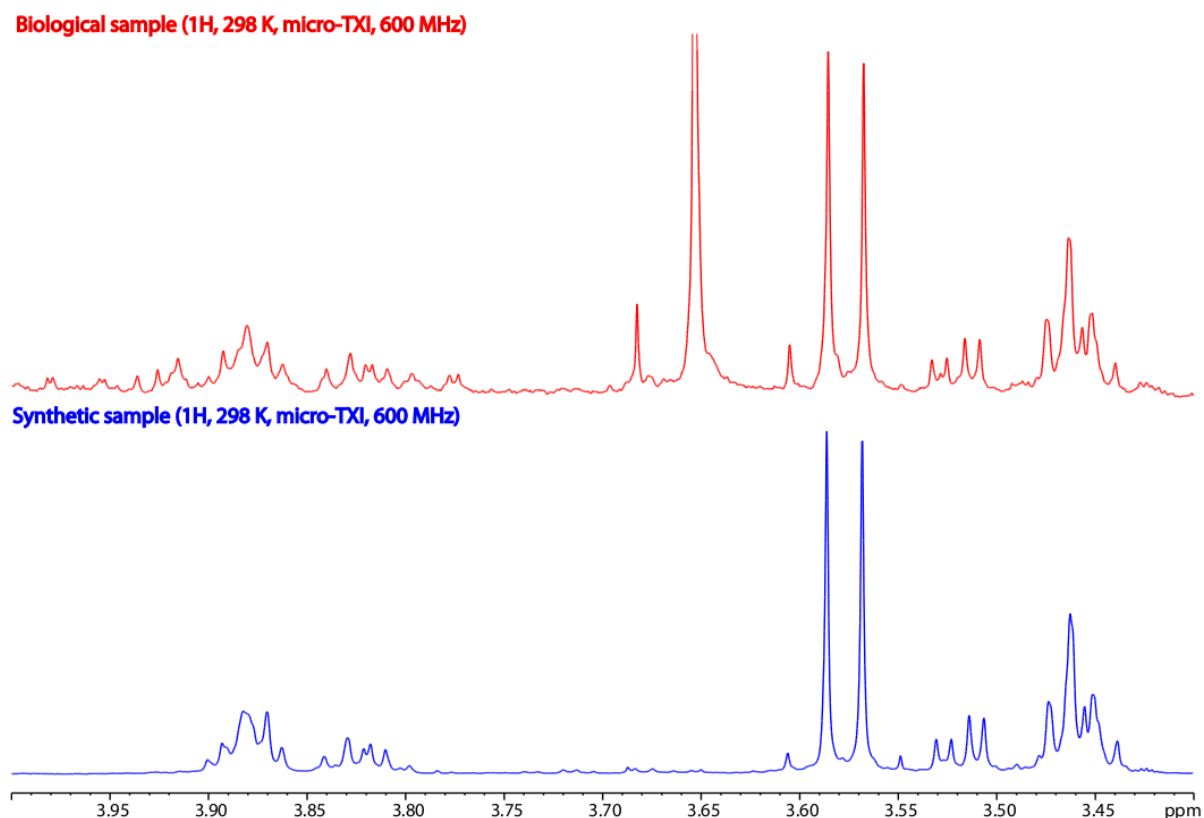


Figure C-14: Comparison of biological and synthetic sample recorded under the same conditions. The synthetic analogue was measured in higher concentrations.

The same ^{31}P - ^1H coupling constants could be measured. All recorded NMR spectra are shown in the experimental section. In both cases the same degradation products where the phosphate was moved to the 2 position were obtained. Under basic conditions this movement was more pronounced than in slightly acidic conditions.

The isomer **A** could be confirmed as the correct structure by comparison of the NMR spectra, ESI-profiles and HPLC retention time of the synthetic and natural compound. The comparison of the two HPLC profiles is presented in Figure C-15. Both samples were eluted at the same day under the same conditions. Both samples show the product **A** (19.4 min) and the side product **B** (17.7 min). The isomerization reaction is favoured under basic conditions.

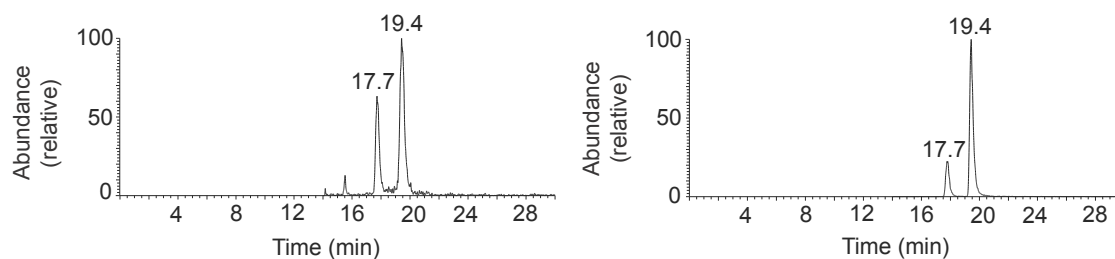


Figure C-15: HPLC profiles of the synthetic sample (left) and the natural sample (right). At 19.4 min the mLPA isomer **A** is eluted. The retention time of 17.7 belongs to isomerized side products (**B**) where the phosphate moiety is bound to the two position.

The presented synthetic route can be used also for the preparation of C18-mLPA, which was synthesized as well and confirmed the structure **D** as the right one. Experimental procedures were similar to the C16-analogue with identical yields. The experimental details of these compounds are therefore not presented.

C.6 Discussion

The MS-analysis gained deep insights into the different functional groups of the target molecule. The identification of a phosphate group, a glycerine backbone, a methoxy group and an alkyl side-chain was possible. A substitution pattern in analogy to known compounds was predicted (structure **A**, structure **D**). The mass limitation of a few micrograms of the natural product made structure elucidation with the insensitive NMR method challenging. Additionally the NMR active phosphorous nucleus with a natural abundance of 100% and strong couplings to protons and carbons lowered the intensity of affected resonances by a factor of two. On the other hand the NMR activity of the spin $\frac{1}{2}$ nucleus ^{31}P allowed the measurements of a variety of NMR experiments that were essential for the assignment. The use of new hardware that can deal with lower concentrations and contained three pulsing channels instead of two was therefore really helpful. The substitution pattern could be solved with special NMR equipment (triple resonance 1.7 mm probe head), that allowed the measurement of a HSQC spectra with phosphorous and carbon decoupling during the acquisition period. 1.7 mm NMR tubes require an amount of 30 μL solvents whereas 5 mm shigemi tube require 250 μL and standard 5 mm NMR tubes need at least 450-500 μL . The sensitivity gain due to the lowered solvent content was great. The additional phosphorous decoupling was the required step to reach a signal to noise level allowing the identification of the carbon chemical shift for

the CH₂-group (3) and the OMe group that showed coupling to the phosphorous. The key step to the structure elucidation was the measurement of the ³¹P-HMBC spectra that confirmed that both carbons are located on the same phosphorous. Additionally we could show the strong pH dependence of the OMe group that showed an increased pH dependent chemical shift compared to the CH₂-group of the glycerine backbone, which is also located on the phosphorous. It was therefore essential to adjust the pH of the synthetic sample using sodium formate to deliver the same proton, carbon and phosphorus NMR-shifts as the natural sample.

The total synthesis of mLPA was achieved in moderate to good yields. The target compound showed enormous T cell activation (Figure C-16) properties and confirmed therefore the activity of the lipid. A direct comparison of the biological activity of the natural sample and the synthetic sample could not be performed. A quantification of the natural sample was not performed due to the small amounts accessible. Concentration dependent experiments could therefore not be done. Nevertheless, one has to mention that the shown activity is from a racemic mixture of *R* and *S* configured glycerines. Phospholipids have in general an *R*-configuration of the glycerine backbone. It remains so far unclear whether the *S*-form can act also as a potential antigen or if it blocks T cells. The obtained good activation profiles obtained by the activation tests are probably changed if the two enantiopure molecules are applied separately to activation assays.

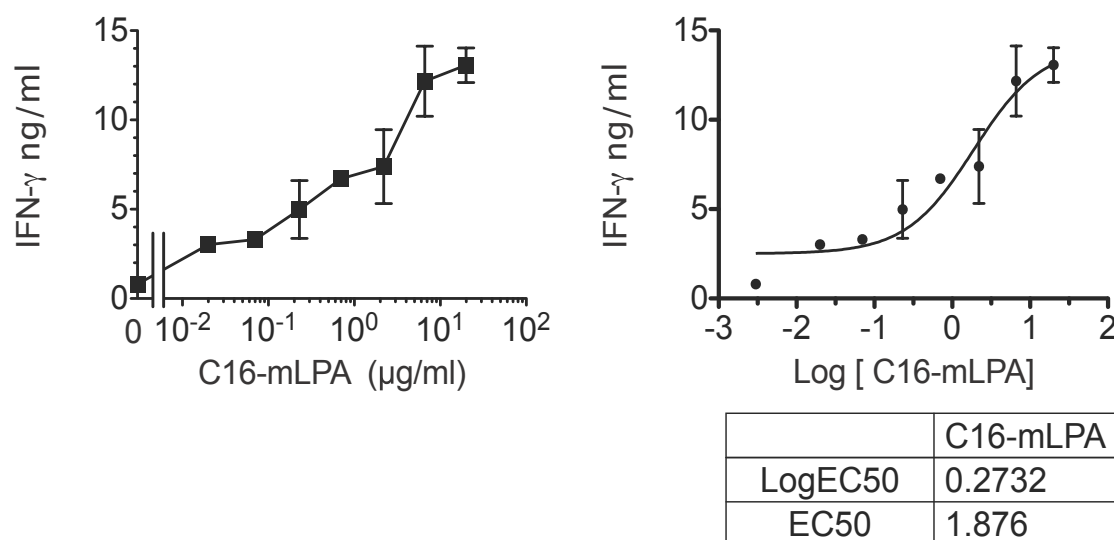


Figure C-16: T cell clones DN 4.99 were stimulated with synthetic C16-mLPA presented by purified primary B-cells.

The synthetic route was therefore developed in a modular way so that it would be easy to adapt to enantiopure starting material without interconversions. The main challenge of the synthesis was the adjustment of the protection protocol for the 2 and 3 position of the glycerine backbone. The two protecting groups had to be orthogonal and the protecting group in 2 position has to be cleaved easily when the phosphate is attached in 3 position. We realized that only an acidic cleavage should be performed in order to avoid movement of the phosphate group to the more stable 2 position. Different protection protocols were tested as shown in Figure C-13 and Figure C-17. An elegant pathway is shown in green, with a selective ring opening of the acetal protecting group, that allowed the direct phosphorylation reaction. Unfortunately, no reaction conditions that deprotected the molecule without destroying the phosphate moiety could be found.

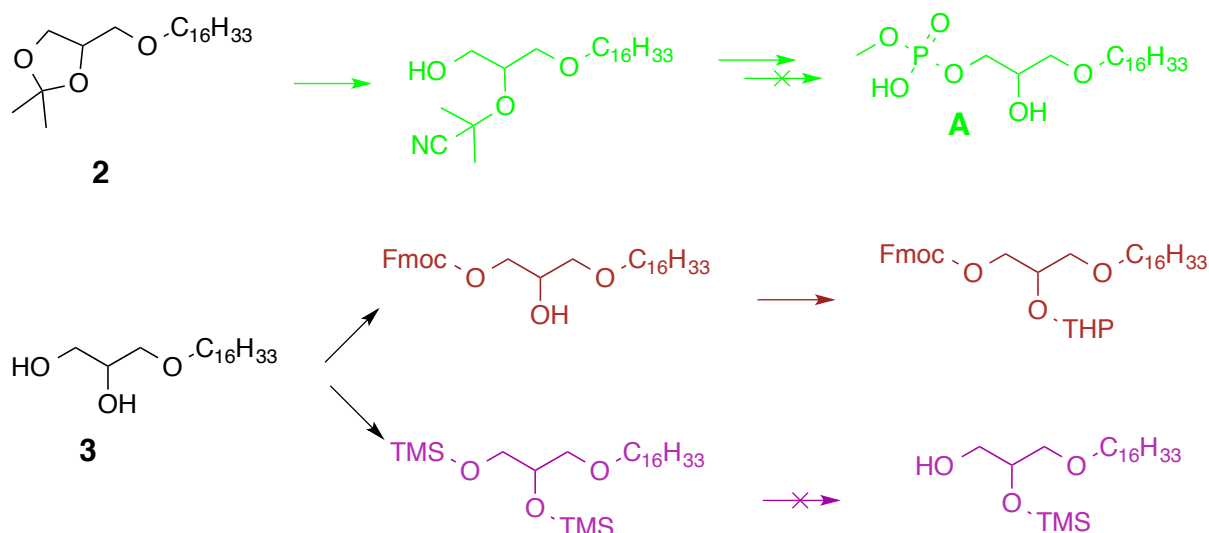


Figure C-17: Different protection protocols tested.

The brown pathway delivered the first synthetic mLPA sample. However the low selectivity of Fmoc to the primary alcohol, with only up to 10% of the mono protected species made this synthetic route unfavourable. The protection protocol shown in pink allowed no selective deprotection of the primary alcohol. The protection protocol shown in Figure C-13, where the acetal protection group is cleaved in high yields by acetic acid, followed by selective protection of the C1 by a benzoyl protection group and orthogonal protection with a THP protection group at C2 delivered high selectivity and good yields. This protocol is therefore the method of choice. Indeed, THP protection and deprotection of the C2 is performed without changing the stereochemistry of the stereogenic centre, which is required for the enantioselective route.

The remaining challenge in the synthetic strategy was the purification of the final product. The stability of the mLPA under basic conditions is quite low and the phosphate end-group tends to move to the C2 position. This is also obtained under neutral conditions after two days in methanol solution. Storage at low temperatures and slightly acidic conditions was therefore essential.

The synthetic mLPA could be used for investigations of the activity of the compound. The positive results confirmed the active compound and excluded that the impurities observed by NMR spectroscopy are the origin for the high T cell activation.

C.7 Conclusion

The characterization and identification of C16- and C18-mLPA was successfully performed using the combination of MS, NMR. In addition a total synthesis of racemic mLPA was successfully developed for the first time. Biological activity, MS and NMR data unambiguously proved the identity of the compound of biological origin and the chemically synthesized sample. The increased sensitivity of the 1.7 mm probe head allowed the full characterization of a few micrograms of the natural sample. The synthesis could be achieved in moderate to good yields and high purity of the products. Optimization of the purification protocol for the final product is required for the synthesis of large quantities. An easy way to the synthesis of enantiomerically pure compounds is presented.

C.8 Experimental

C.8.1 NMR spectra of the biological sample

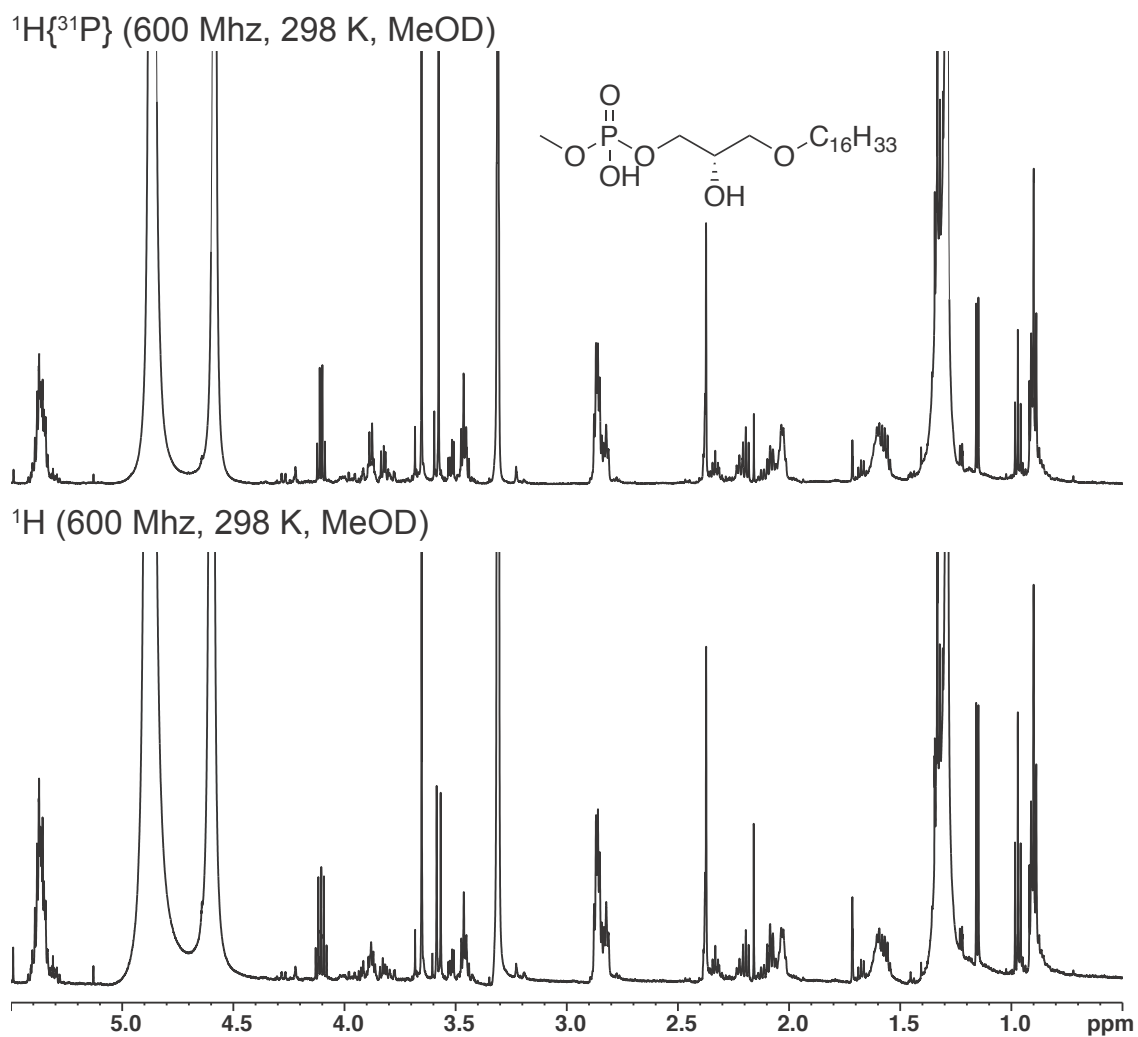


Figure C-18: Comparison of $^1\text{H}\{^{31}\text{P}\}$ decoupled and ^1H NMR spectra in MeOD-d4 at 298 K recorded on a micro-TXI probe head.

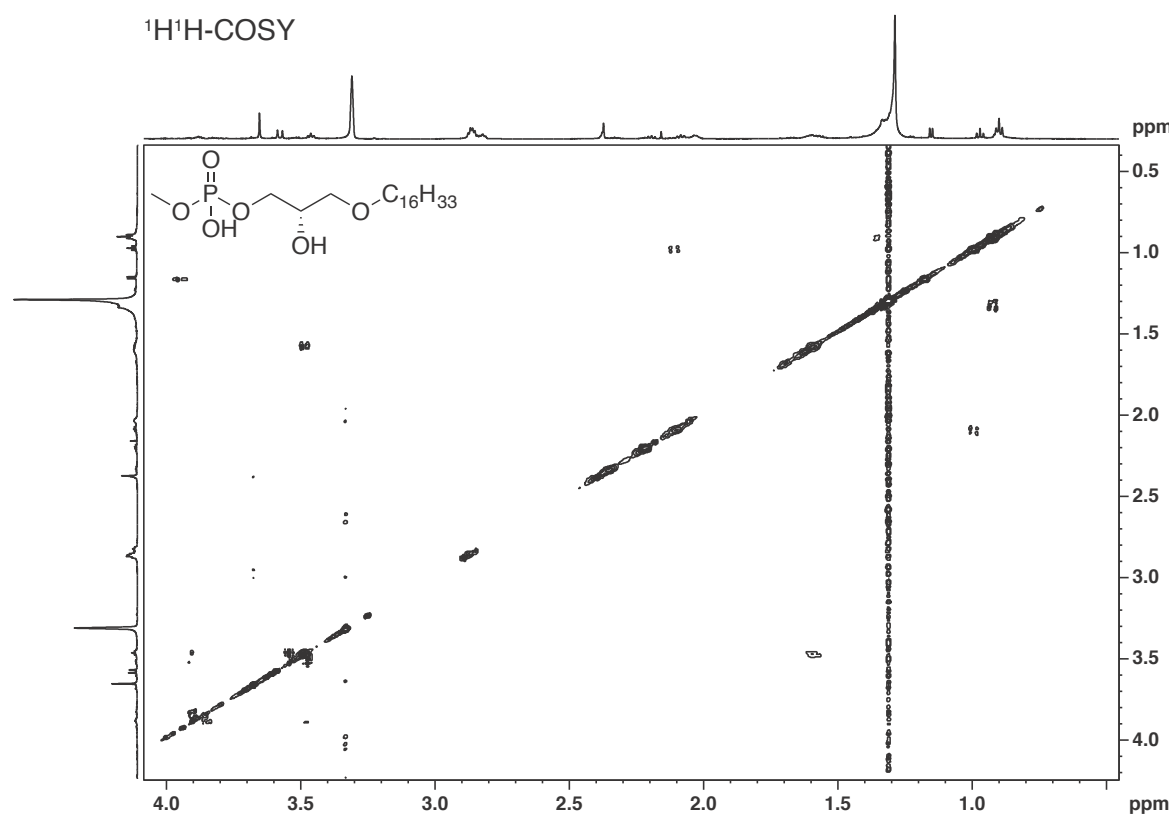
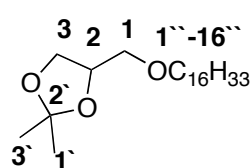


Figure C-19: COSY-experiment for the biological sample in MeOD-d₄ at 298 K recorded on a micro-TXI probe head.

C.8.2 Synthesis

4-((hexadecyloxy)methyl)-2,2-dimethyl-1,3-dioxolane (**2**)



(2,2-dimethyl-1,3-dioxolan-4-yl)methanol (**1**) (4.45 g, 33.7 mmol, 1.2 eq) and sodium (0.161 g, 7.0 mmol, 0.25 eq) were heated to 80 °C and stirred until all sodium had reacted. 1-chlorohexadecane (1.46 g, 5.61 mmol, 0.2 eq) was added and heated to 100°C for 14 hours. The reaction mixture was quenched with water and the combined organic layers were dried over magnesium sulphate and purified by silica gel column chromatography (hexane:diethylether 9:1). 4-((hexadecyloxy)methyl)-2,2-dimethyl-1,3-dioxolane (**2**) (0.687 g, 1.9 mmol, 34.3 %) was obtained as colourless oil.¹⁰

Rf.: Hexane/diethylether (9:1) = 0.68

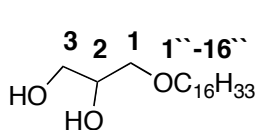
¹H-NMR (600 MHz, CDCl₃, δ/ppm): 0.87 (t, ³J_{HH} = 8 Hz, 3H, **H16''**); 1.21-1.33 (m, 28H, **H15''** - **H3''**); 1.36 (s, 3H, **H3'**); 1.42 (s, 3H, **H1'**); 1.57 (q, ³J_{HH} = 8 Hz, 2H,

H²); 3.39-3.53 (m, 4H, **H¹**, **H¹**); 3.73 (dd, ³J_{HH} = 8 Hz, ³J_{HH} = 12 Hz, 1H, **H³**); 4.05 (dd, ³J_{HH} = 8 Hz, ³J_{HH} = 12 Hz, 1H, **H³**); 4.26 (q, ³J_{HH} = 8 Hz, 1H, **H¹**).

¹³C-NMR (151 MHz, CDCl₃, δ/ppm): 14.3 (1C, **C¹⁶**); 22.9 (1C, **C¹⁵**); 25.6 (1C, **C³**); 26.3 (1C, **C²**); 27.0 (1C, **C¹**); 29.6 - 29.9 (C, **C¹³** - **C³**); 32.1 (1C, **C¹⁴**); 67.2 (1C, **C³**); 72.0 (1C, **C¹**); 72.1 (1C, **C¹**); 75.0 (1C, **C²**); 109.6 (1C, **C²**).

ESI-MS (C₂₂H₄₄O₅: Calc'd 379.3 [M + Na⁺], Found 379.4; Calc'd 735.7 [2M + Na⁺], Found 735.7).

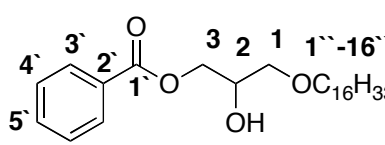
3-(hexadecyloxy)propane-1,2-diol (**3**)

 4-((hexadecyloxy)methyl)-2,2-dimethyl-1,3-dioxolane (**2**) (0.687 g, 1.9 mmol, 1.0eq) was dissolved in AcOH (80 %aq., 10 mL) and stirred overnight at rt. The solvent was removed and analytical pure 3-(hexadecyloxy)propane-1,2-diol (**3**) (0.601 g, 1.89 mmol, 99 %) was obtained as white solid.¹¹

¹H-NMR (600 MHz, CDCl₃, δ/ppm): 0.88 (t, ³J_{HH} = 8 Hz, 3H, **H¹⁶**); 1.20-1.38 (m, 26H, **H³** - **H¹⁶**); 1.58 (q, ³J_{HH} = 8 Hz, 2H, **H²**); 2.24 (s_b, OH), 2.64 (s_b, OH); 3.43-3.55 (m, 4H, **H³**, **H¹**); 3.65 (dd, ³J_{HH} = 8 Hz, ³J_{HH} = 12 Hz, 1H, **H¹**); 3.72 (dd, ³J_{HH} = 8 Hz, ³J_{HH} = 12 Hz, 1H, **H¹**); 3.85 (q, ³J_{HH} = 8 Hz, 1H, **H²**).

¹³C-NMR (151 MHz, CDCl₃, δ/ppm): 14.3 (1C, **C¹⁶**); 22.9 (1C, **C¹⁵**); 26.3 (1C, **C¹⁴**); {29.6 (1C); 29.7 (1C); 29.8 (4C); 29.9 (5C), **C²**, **C⁴** - **C¹³**}; 32.2 (1C, **C³**); 64.4 (1C, **C³**); 70.6 (1C, **C²**); 72.1 (1C, **C¹**); 72.8 (1C, **C¹**).

3-(hexadecyloxy)-2-hydroxypropyl benzoate (**4**)

 3-(hexadecyloxy)propane-1,2-diol (371 mg, 1.2 mmol, 1.0 eq) was dissolved in toluene and benzoyl chloride (165 mg, 0.14 mL, 1.2 mmol, 1.0 eq) was added and stirred at rt for 15 hours. Triethylamine (0.16 mL, 1.2 mmol, 1.0 eq) and DMAP (cat. 5 mol%) were added and stirred for additional 5 hours. The resulting precipitate was filtered and washed with diethyl ether. The combined organic layers were evaporated and purified by silica gel column chromatography (cyclohexane to cyclohexane:ethylacetate 60:40). 3-(hexadecyloxy)-2-hydroxypropyl benzoate was obtained as yellowish oily solid (325 mg, 0.77 mmol, 64 %).¹²

For further reactions NEt₃ and DMAP were added at the beginning.

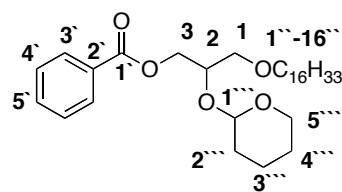
RF.: Cyclohexane/ethylacetate (1:1) = 0.86

¹H-NMR (600 MHz, CDCl₃, δ/ppm): 0.88 (t, ³J_{HH} = 8 Hz, 3H, **H16''**); 1.22-1.34 (m, 26H, **H3''-H15''**); 1.53-1.59 (m, 2H, **H2''**); 2.59 (d, ³J_{HH} = 4 Hz, 1H, **OH**); 3.44-3.60 (m, 4H, **H1''**, **H3'**); 4.12-4.15 (m, 1H, **H2'**); 4.36-4.44 (m, 2H, **H1'**); 7.43-7.46 (m, 2H, **H2**); 7.55-7.59 (m, 1H, **H3**); 8.04-8.06 (m, 2H, **H1**).

¹³C-NMR (151 MHz, CDCl₃, δ/ppm): 14.3 (1C, **C16''**); 18.3 (1C, **C15''**); 21.4 (1C, **C14''**); 22.9 (1C, **C13''**); 29.8 (1C, **C2''**); 28.3-31.8 (8C, **C12''-C4''**); 66.3 (1C, **C3'**); 69.2 (1C, **C2'**); 71.6 (1C, **C1'**); 72.0 (1C, **C1''**); 128.6 (2C, **C2**); 129.9 (2C, **C1**); 133.3 (1C, **C3**).

ESI-MS (C₂₆H₄₄O₄): Calc'd 443.3 [M + Na⁺], Found 443.3 ;Calc'd 863.6 [2M+Na⁺], Found 863.8.

3-(hexadecyloxy)-2-((tetrahydro-2H-pyran-2-yl)oxy)propyl benzoate (5)



3-(hexadecyloxy)-2-hydroxypropyl benzoate (325 mg, 0.77 mmol, 1.0 eq) was dissolved in 10 mL dichloromethane. PPTS (19 mg, 0.077 mmol, 0.1 eq) and 3,4-dihydro-2H-pyran (97.5 mg, 1.2 mmol, 1.5 eq) was added and stirred

at rt for 4 hours. The solvent was removed and the resulting oily solid was purified by silica gel column chromatography Cyclohexane:Ethylacetate (95:5) to obtain the title compound (369 mg, 0.73 mmol, 95 %, yellowish oil) as a 1:1 mixture of two diastereoisomers. The separate assignment of the two diastereoisomers was impossible due to small differences in carbon and proton frequency. The ones which show differences are therefore stated twice in the assignment.¹³

Rf.: Cyclohexane/ethylacetate (95:5) = 0.27

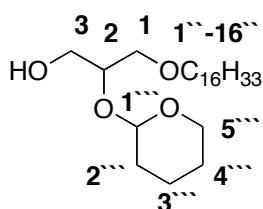
¹H-NMR (600 MHz, CD₂Cl₂, δ/ppm): 0.88 (t, ³J_{HH} = 8 Hz, 3H, **H16''**); 1.22-1.34 (m, 26H, **H3''-H15''**); 1.49-1.61 (m, 6H, **H2''**, **H2'''**, **H3'''**, **H4'''**); 1.64-1.76 (m, 1H, **H2'''**); 1.78-1.88 (m, 1H, **H4'''**); 3.42-3.55 (m, 3H, **H1''**, **H5'''**); 3.56-3.70 (m, 2H, **H1'**); 3.85 – 4.02 (m, 1H, **H5'''**); 4.14-4.23 (m, 1H, **H2**); 4.34 (dd, ³J_{HH} = 11.6 Hz, ³J_{HH} = 6.1 Hz, 0.5H, **H3**); 4.46 (d, ³J_{HH} = 5.3 Hz, 1H, **H3**); 4.58 (dd, ³J_{HH} = 11.6 Hz, ³J_{HH} = 6.1 Hz, 0.5H, **H3**); 4.85-4.87 (m, 1H, **H1'''**); 4.87-4.89 (m, 1H, **H1'''**); 7.43-7.46 (m, 2H, **H4'**); 7.55-7.59 (m, 1H, **H5'**); 8.04-8.06 (m, 2H, **H3'**).

¹³C-NMR (151 MHz, CDCl₃, δ/ppm): 14.3 (1C, **C16''**); 19.3 (1C, **C4'''**); 22.9 (1C, **C15'**); 25.5 (1C, **C3'''**); 26.2 (1C, **C14''**); 29.7-31.0 (9C, **C12''-C4''**, **C2''**); 30.8 (1C, **C2'''**); 32.1 (1C, **C3''**); 62.0 (1C, **C5'''**); 62.4 (1C, **C5'''**); 64.7 (1C, **C3**); 65.4 (1C, **C3**); 70.5 (1C, **C1**); 70.8 (1C, **C1**); 71.8 (1C, **C1''**); 73.3 (1C, **C2**); 98.0 (1C, **C1'''**);

98.3 (1C, **C1''**); 128.5 (2C, **C4'**); 129.7 (2C, **C3'**); 130.2 (1C, **C2'**); 133.1 (1C, **C5'**); 166.35 (1C, **C1'**).

ESI-MS ($C_{31}H_{52}O_5$): Calc'd 527.4 [M + Na⁺], Found 527.4 ;Calc'd 1031.8 [2M+Na⁺], Found 1032.

3-(hexadecyloxy)-2-((tetrahydro-2H-pyran-2-yl)oxy)propan-1-ol (6)



Freshly prepared sodium methanolate (2 mL) in methanol (3 mL) was added to 3-(hexadecyloxy)-2-((tetrahydro-2H-pyran-2-yl)oxy)propyl benzoate at 0 °C and stirred for 10 minutes. The solution was then allowed to warm to rt and stirred for additional 20 minutes. The solvent was removed and the resulting oily solid was purified by silica gel column chromatography cyclohexane/ethyl acetate 9:1 to obtain HG-31 (269 mg, 0.67 mmol, 92 %) as yellowish oil.¹⁴

There are two sets of NMR signals resulting from the two stereo centers, which are both racemic. The two diastereotopic forms, which vary a lot in the geometry, deliver therefore different shifts in the carbon and proton frequencies on the THP-ether and on the glycerine backbone. The alkyl chain is not influenced.

Rf.: Cyclohexane/ethyl acetate (95:5) = 0.06

Diastereoisomer 1: **¹H-NMR** (600 MHz, CD₂Cl₂, δ/ppm): 0.88 (t, ³J_{HH} = 8 Hz, 3H, **H16''**); 1.22-1.34 (m, 26H, **H3''-H15''**); 1.49-1.61 (m, 5H, **H2''**, **H2**, **H3**, **H4**); 1.64-1.84 (m, 3H, **H2**, **H3**, **H4**); 3.42-3.55 (m, 4H, **H1''**, **H5**, **H1'**); 3.56-3.70 (m, 2H, **H1'**, **H3'**); 3.85-4.02 (m, 2H, **H5**, **H2'**); 4.52-4.53 (m, 1H, **H1**).

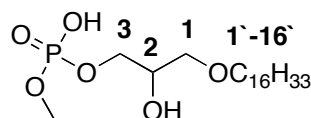
Diastereoisomer 2: **¹H-NMR** (600 MHz, CD₂Cl₂, δ/ppm): 0.88 (t, ³J_{HH} = 8 Hz, 3H, **H16''**); 1.22-1.34 (m, 26H, **H3''-H15''**); 1.49-1.61 (m, 6H, **H2''**, **H3**, **H4**); 1.64-1.84 (m, 2H, **H2**); 3.42-3.55 (m, 4H, **H1''**, **H5**, **H1'**); 3.56-3.70 (m, 2H, **H3'**); 3.85-4.02 (m, 2H, **H5**, **H2'**); 4.55-4.62 (m, 1H, **H1**).

Diastereoisomer 1: **¹³C-NMR** (151 MHz, CDCl₃, δ/ppm): 14.2 (1C, **C16''**); 19.9 (1C, **C4**); 21.0 (1C, **C3**); 22.7 (1C, **C15''**); 26.1 (1C, **C14''**); 29.7-31.0 (10C, **C13''-C4''**, **C2''**); 30.9 (1C, **C2**); 31.9 (1C, **C3''**); 63.2 (1C, **C3'**); 71.7 (1C, **C1'**); 71.9 (1C, **C1''**); 75.6 (1C, **C2'**); 98.5 (1C, **C1**).

Diastereoisomer 2: **¹³C-NMR** (151 MHz, CDCl₃, δ/ppm): 14.2 (1C, **C16''**); 22.7 (1C, **C15''**); 25.3 (1C, **C4**); 26.1 (1C, **C14''**); 29.7-31.0 (10C, **C13''-C4''**, **C2''**); 31.4 (2C, **C2**, **C3**); 31.9 (1C, **C3''**); 63.8 (1C, **C3'**); 70.9 (1C, **C1'**); 71.9 (1C, **C1''**); 80.3 (1C, **C2'**); 101.0 (1C, **C1**).

ESI-MS ($C_{24}H_{48}O_4$): Calc'd 423.4 [$M + Na^+$], Found 423.4 ; Calc'd 823.8 [$2M+Na^+$], Found 823.9.

3-(hexadecyloxy)-2-hydroxypropyl methyl hydrogen phosphate (A)



To a solution of $POCl_3$ (0.02 mL, 0.25 mmol, 1.0 eq) and NEt_3 (0.04 mL, 0.25 mmol, 1.0 eq) in $CHCl_3$ (1 mL) was added a solution of 3-(hexadecyloxy)-2-((tetrahydro-2H-pyran-2-yl)oxy)propan-1-ol (0.501g, 1.6 mmol, 0.8 eq) in $CHCl_3$ (8 mL) at $-10^\circ C$ over a period of 30 minutes. The mixture was warmed to rt and stirred for additional 16 h. Pyridine (1.1 mL, 13.8 mmol, 7.0 eq) and MeOH (0.09 mL, 2.4 mmol, 1.2 eq) were added and stirred for 30 min at rt. The solvent was removed and the resulting precipitate was redissolved in DCM:Toluene (1:1, 10 mL) and filtered. The solvent was removed and dried at high vacuum.¹⁵

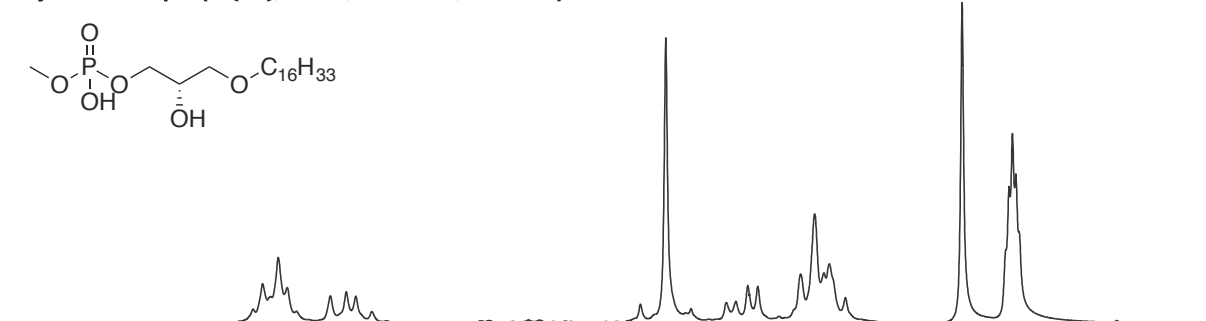
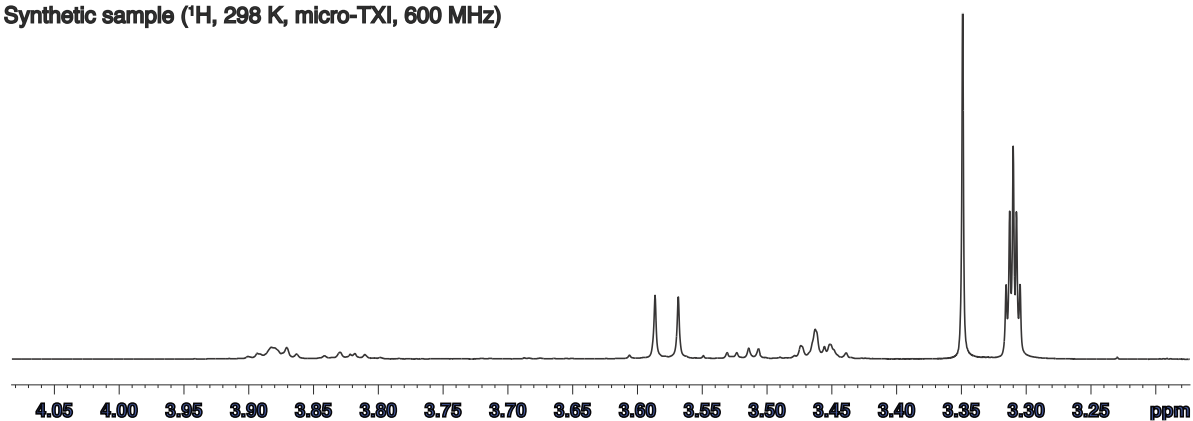
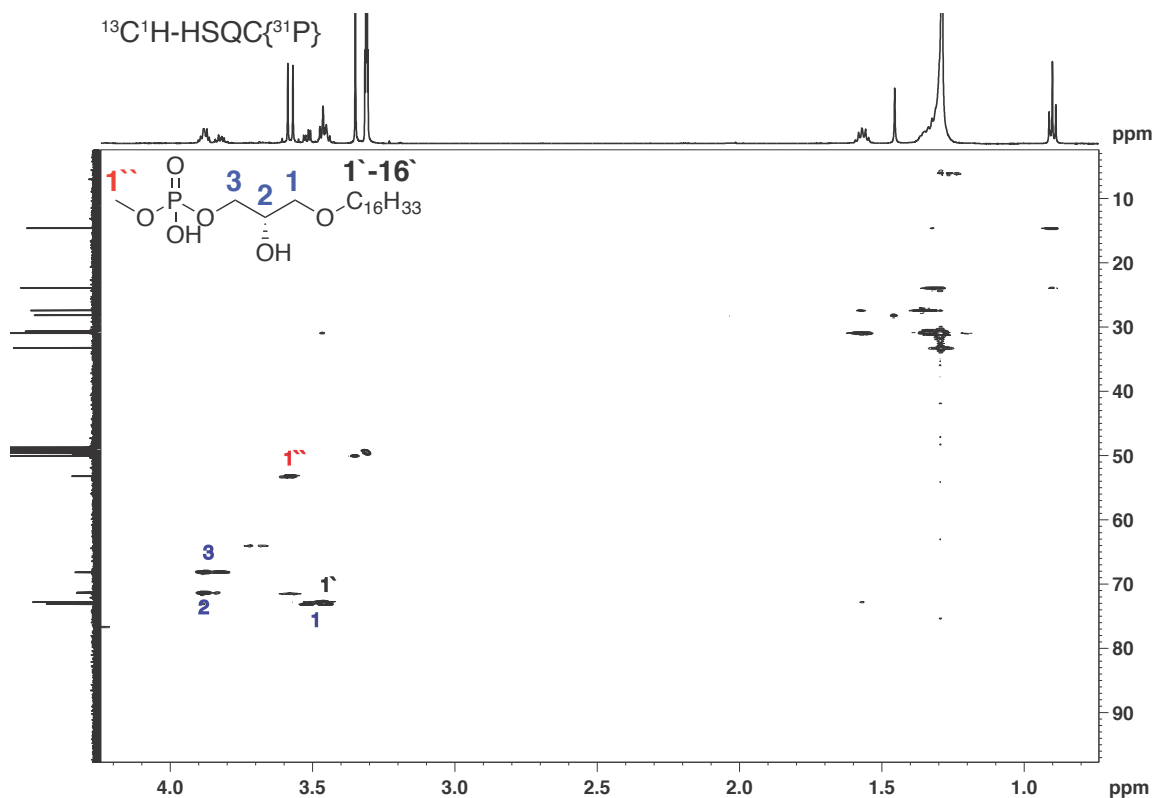
The resulting solid was tried to purify by silica gel column chromatography (chloroform/methanol/water 65:35:4). In this case the product stacked on the column. An effort to tune the pH to 2 and further purification with preparative TLC (chloroform/methanol 99:1) failed because most of the product was already destroyed during the acidic workup. The purification strategy was then changed to preparative TLC under basic condition (without acidifying of the compound) with chloroform/methanol (8:2) as eluent. This purification was done twice to obtain a more pure sample of HG-22. Purification with alox (aluminium oxide) column chromatography failed. The change to preparative HPTLC (reversed phase preparative TLC) allowed the removal of different by-products. Basic, acidic and neutral extraction failed as well as the salt formation. The most pure sample could be obtained after purification with HPLC using the same conditions as for the purification of the natural sample.

1H -NMR (600 MHz, CD_2Cl_2 , δ /ppm): 0.88 (t, $^3J_{HH} = 8$ Hz, 3H, **H16'**); 1.21-1.35 (m, 26H, **H3'-H15'**); 1.57 (q, $^3J_{HH} = 8$ Hz, 2H, **H2'**); 3.41 (m, 1H, **H1**); 3.46 (m, 2H, **H1'**); 3.47 (m, 1H, **H1**); 3.51 (m, 1H, **H3**); 3.55 (m, 3H, **OMe**); 3.58 (m, 1H, **H3**); 3.72 (m, 1H, **H2**).

^{13}C -NMR (151 MHz, $CDCl_3$, δ /ppm): 14.4 (1C, **C16'**); 26.4 (1C, **C15'**); 27.2 (1C, **C14'**); {29.4 – 30.5, **C3'-C13'**}; 30.6 (1C, **C2'**); 52.8 (1C, **OMe**); 64.9 (1C, **C1**); 72.2 (1C, **C2**); 72.5 (1C, **C1'**); 73.1 (1C, **C3**).

ESI-MS ($C_{20}H_{43}O_6P$): Calc'd 409.5 [$M - 1$], Found 409.5.

C.8.3 NMR spectra of synthetic mLPA

Synthetic sample ($^1\text{H}\{^{31}\text{P}\}$, 298 K, micro-TXI, 600 MHz)Synthetic sample (^1H , 298 K, micro-TXI, 600 MHz)Figure C-20: Comparison of $^1\text{H}\{^{31}\text{P}\}$ decoupled and ^1H NMR spectra in MeOD- d_4 at 298 K recorded on a micro-TXI probe head.Figure C-21: $^{13}\text{C}\{^1\text{H}\}$ -HSQC $\{^{31}\text{P}\}$ spectrum showing the $^1J_{\text{CH}}$ -correlations.

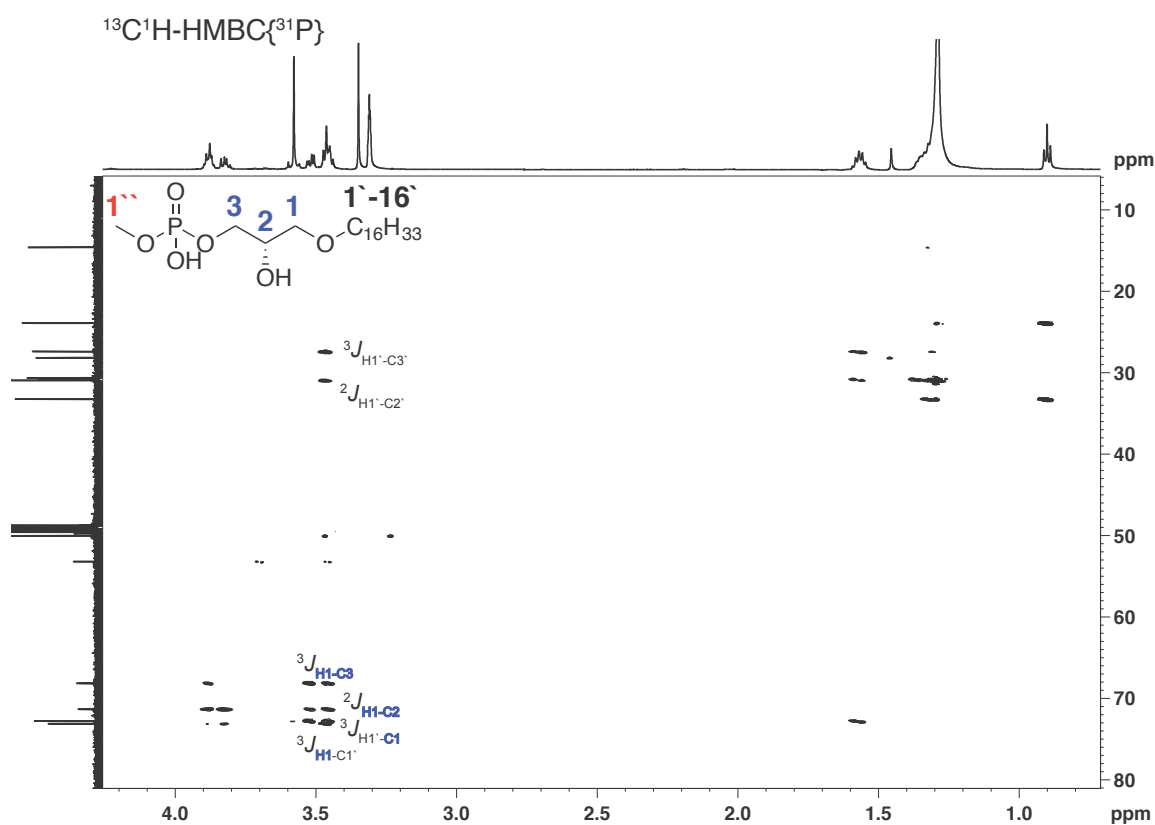


Figure C-22: $^{13}\text{C}\{^1\text{H}\}\text{-HMBC}\{^{31}\text{P}\}$ spectrum for the synthetic mLPA sample.

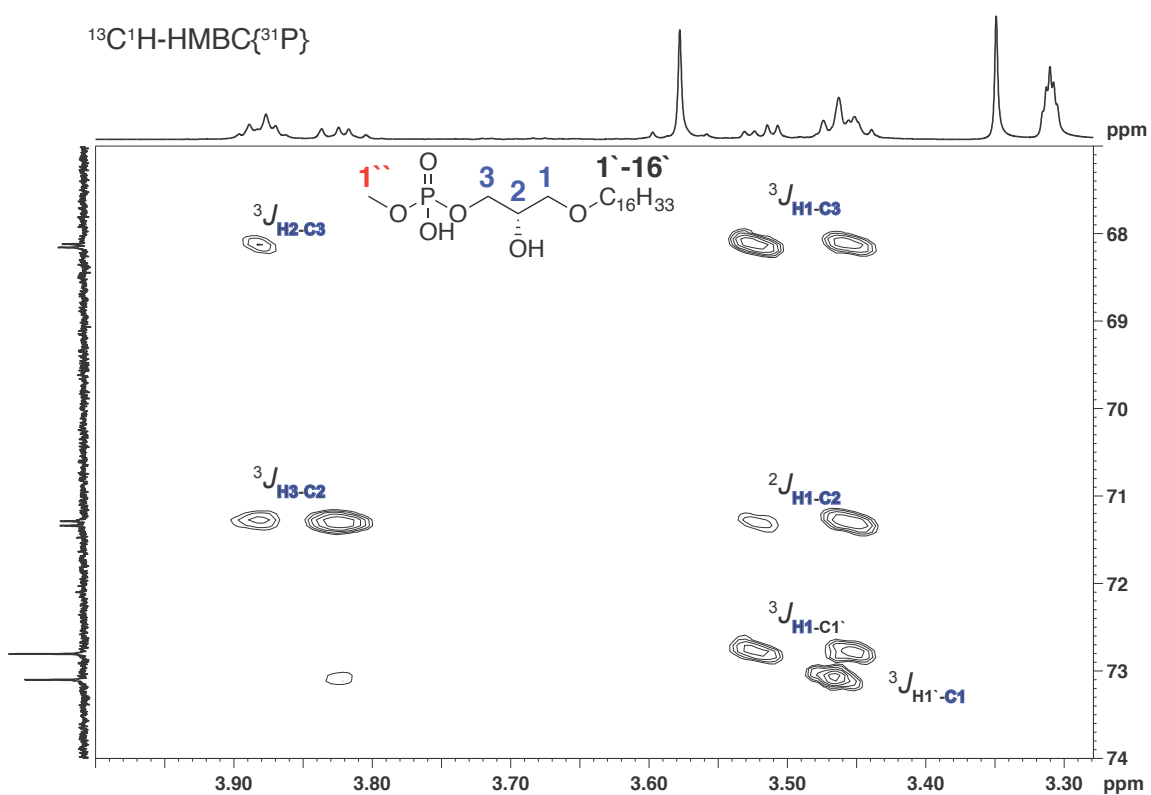


Figure C-23: Selection of the $^{13}\text{C}\{^1\text{H}\}\text{-HMBC}\{^{31}\text{P}\}$ spectrum delivering the connection between the aliphatic side chain and the glycerine backbone.

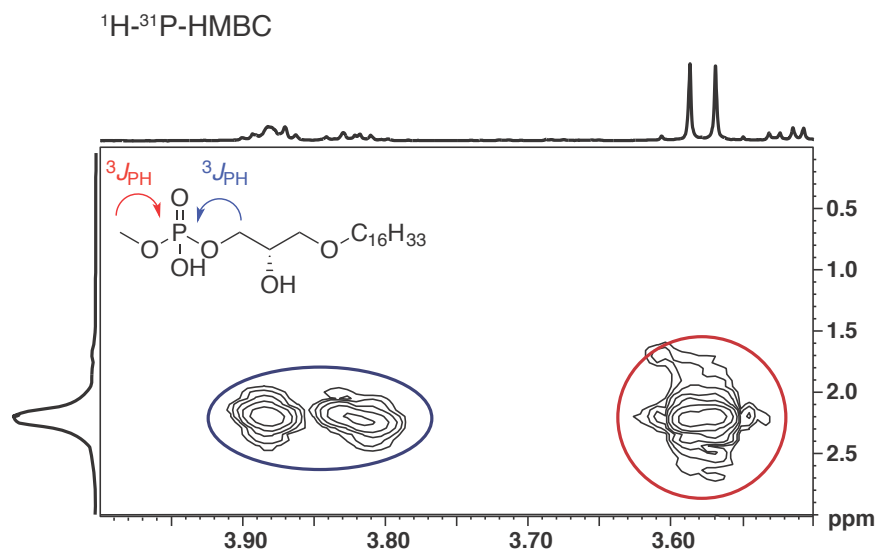


Figure C-24: ^1H - ^{31}P -HMBC spectra confirming that the CH_2 -group from the glycerine backbone and the OMe-group are connected to the same phosphorous.

C.8.4 LC-MS-data for the natural C-18 sample eluting at 19.9 min.

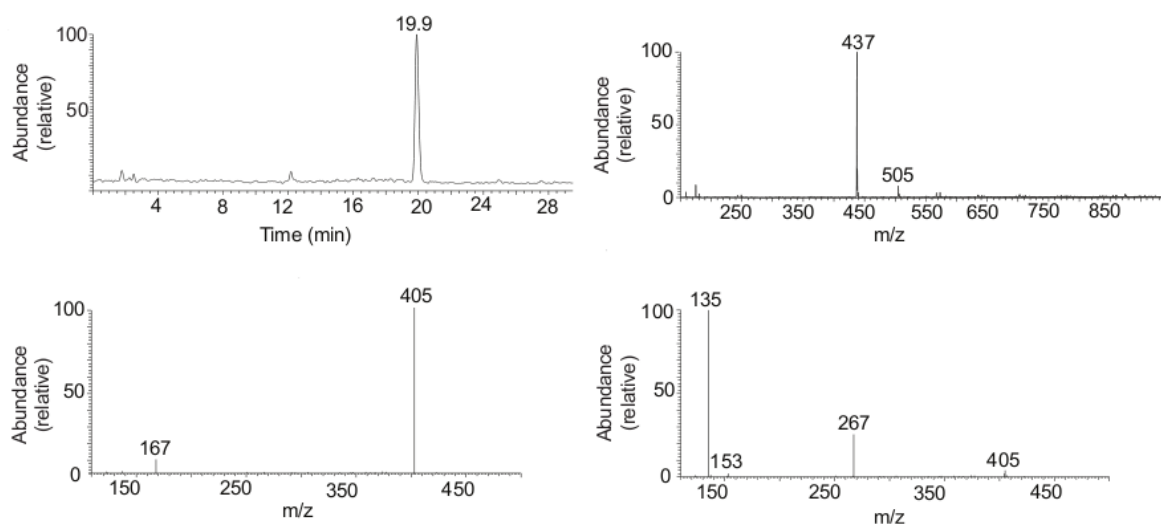


Figure C-25: On top left: HPLC trace of the purified natural mLPA sample. On top right: ESI-MS spectra of the mLPA sample measured in the negative mode. On bottom left: ESI- MS^2 of the mass 437 $^-$. On bottom right: ESI- MS^3 of the mass 405 $^-$.

C.9 References

1. Finton, K. A. & Strong, R. K. Structural insights into activation of antiviral NK cell responses. *Immunol. Rev.* **250**, 239–257 (2012).
2. De Libero, G. *et al.* Bacterial Infections Promote T Cell Recognition of Self-Glycolipids. *Immunity* **22**, 763–772 (2005).
3. Lepore, M. *et al.* A novel self-lipid antigen targets human T cells against CD1c+ leukemias. *J. Exp. Med.* jem.20140410 (2014). doi:10.1084/jem.20140410
4. Tourne, S. Structure and immunological functions of human CD1 molecules. *Hématologie* **12**, 412 (2006).
5. Berzofsky, J. & Terabe, M. The Contrasting Roles of NKT Cells in Tumor Immunity. *Curr. Mol. Med.* **9**, 667–672 (2009).
6. Dhodapkar, M. V. & Richter, J. Harnessing natural killer T (NKT) cells in human myeloma: Progress and challenges. *Clin. Immunol.* **140**, 160–166 (2011).
7. Israël, M. A possible primary cause of cancer: deficient cellular interactions in endocrine pancreas. *Mol. Cancer* **11**, 63 (2012).
8. [43_09TcellsAndMHC_L.jpg](http://bio1152.nicerweb.com/Locked/media/ch43/43_09TcellsAndMHC_L.jpg) (JPEG-Grafik, 624 × 376 Pixel) - Skaliert (0%). at <http://bio1152.nicerweb.com/Locked/media/ch43/43_09TcellsAndMHC_L.jpg>
9. Kertscher. Synthesis of some acid structure analogues of the plateket-activating factor. *Pharmazie* **38**, 792–792 (1983).
10. Schwetlick, K. *Organikum, 22. vollst. überarb. u. aktualis. Auflage.* (Wiley-VCH, 2004).
11. Dumoulin, F. *et al.* Self-Organizing Properties of Natural and Related Synthetic Glycolipids. *J. Am. Chem. Soc.* **124**, 13737–13748 (2002).
12. Avetisyan, A. A., Alvandzhyan, A. G. & Avetisyan, K. S. New syntheses on the basis of 4-hydroxy-2H-chromen-2-ones. *Russ. J. Org. Chem.* **45**, 1086–1090 (2009).
13. Miyashita, M., Yoshikoshi, A. & Grieco, P. A. Pyridinium p-toluenesulfonate. A mild and efficient catalyst for the tetrahydropyranylation of alcohols. *J. Org. Chem.* **42**, 3772–3774 (1977).
14. Dransfield, P. J., Moutel, S., Shipman, M. & Sik, V. Stereocontrolled synthesis of polyhydroxylated hexahydro-1H-cyclopent[c]isoxazoles by intramolecular oxime olefin cycloadditions: an approach to aminocyclopentitols. *J. Chem. Soc. [Perkin 1]* 3349–3355 (1999). doi:10.1039/A905706D

15. Guivisdalsky, P. N. & Bittman, R. An efficient stereocontrolled route to both enantiomers of platelet activating factor and analogs with long-chain esters at C-2: saturated and unsaturated ether glycerolipids by opening of glycidyl arenesulfonates. *J. Org. Chem.* **54**, 4643–4648 (1989).

Curriculum vitae

Personal Data Heiko Gsellinger
Date/Place of birth July 11th 1985, Lörrach, Germany
Nationality: German

Diploma

2010 Master of Science in Chemistry, University of Basel
2009 Bachelor of Science in Chemistry
2005 Certificate of having passed the "Abitur" majoring in Maths,
Chemistry and BWL

Education

2010-Okt 2014: Ph.D in Chemistry, "*Combining NMR spectroscopy and
organic synthesis: From small building blocks to large
biomolecules*"
Advisor: Prof. Dr. Andreas Pfaltz, Supervisor: Pd. Dr.
Daniel Häußinger, University of Basel
2009-2010 University of Basel
Master thesis: "*Synthesis and NMR characterization of T-
cell activating phospho-lipids*"
Supervisor: PD. Dr. Daniel Häußinger
2006-2009 University of Basel
Bachelor in Chemistry

Experience

2005-2006 Civilian service, Red Cross of Müllheim
2002-2010 Holiday job, Industriereinigung Dieter Wagner

Language German native, English B2, French A1

Teaching

2012-2014 Tutorial lectures in analytical Chemistry
2006-2010 Private lessons in Math and Chemistry

2000-Present Drum instructor at "Musikverein Freundschaft Wies e.V."

Posters

2014, 2013 "Investigations of asymmetric lanthanide chelating tags" H. Gsellinger, D. Häussinger, 9th Euromar, Hersonisos, Crete; 12th Swiss Snow Symposium, Sass Fee, Switzerland

2012 "*Atropisomerization of torsion-angle-restricted propyl-bridged biphenyl cyclophanes*" H. Gsellinger, J. Rotzler, A. Bihlmeier, W. Klopper, M. Mayor, D. Häussinger, EMBO practical course, Berlin, Germany

2012 "*Atropisomerization of para di substituted propyl bridged biphenyl cyclophanes*" H. Gsellinger, J. Rotzler, M. Mayor, D. Häussinger, 8th Euromar, Dublin, Ireland

Publications

2014 M. Lepore et. al. A novel self-lipid antigen targets human T-cells against CD1c+ leukemias. *J. of Exp. Medicine*, **2014**, 211 (7), 1363-1377.

2013 H. Gsellinger et. al. Atropisomerization of di-para-substitutedpropyl-bridged biphenyl cyclophanes, *Org. Biomol. Chem.*, **2013**, 11 (1), 110-118.

2011 J. Rotzler, H.Gsellinger, M. Neuburger, D. Häussinger and M. Mayor, Racemisation dynamics of torsion angle restricted biphenyl push-pull cyclophanes, *Org. Biomol. Chem.*, **2011**,9,86-91